
Effective One-Dimensional Models Including Two-Particle Interaction From Matrix Product States

Dissertation
zur Erlangung des akademischen Grades
Dr. rer. nat.

vorgelegt von
Frederik Keim
geboren in Tett nang

Lehrstuhl für Theoretische Physik I
Fakultät Physik
Technische Universität Dortmund
2018

1. Gutachter : Prof. Dr. Götz S. Uhrig
2. Gutachter : Prof. Dr. Frithjof Anders

Datum des Einreichens der Arbeit: 15. Februar 2018

Abstract

In this thesis a method for deriving effective models for one-dimensional spin systems is introduced. It is based on matrix product state (MPS) and exploits translation invariance to efficiently work in the thermodynamic limit. It is tested on two analytically solvable models: The ferromagnetic spin- $\frac{1}{2}$ Heisenberg chain in an external field, and the transverse magnetic field Ising model (TFIM). The previously developed ansatz for one-particle states is extended to the description of two-particle states. The challenges of this extension and different choices for a basis of the two-particle space are discussed. Results for the two-particle spectral weight in the TFIM and for quasi-particle scattering in both models are provided.

Contents

Contents	V
1 Introduction	1
1.1 Motivation	1
1.2 Effective models in second quantization	2
1.3 The approach	3
1.4 Structure of the thesis	4
2 The models	5
2.1 Ferromagnetic Heisenberg chain	5
2.1.1 Bound state	8
2.2 The transverse field Ising model	8
2.2.1 Exact solution	10
2.2.2 Solution by CUT	11
2.2.3 Ground state magnetization	12
2.2.4 Correlation function	13
3 The framework: Matrix product states	15
3.1 The tools	15
3.2 Why matrix product states?	18
3.3 Definition of MPS	21
3.4 Construction of canonical MPS	21
3.5 Matrix product operators	26
3.6 The thermodynamic limit: iMPS	28
3.6.1 Limitations of iMPS	28
3.6.2 Definitions: uMPS and iMPS	29
3.6.3 Operators in the thermodynamic limit	33
3.6.4 Canonical gauge of uMPS	35
3.7 Chapter summary	37
4 Ground state properties	39
4.1 Ground state search	39
4.1.1 Iterative search algorithm	39
4.1.2 Notes on implementation	43
4.2 Transfer operator	45
4.3 Ground state energy	48
4.3.1 Results for the FMHC	48
4.3.2 Results for the TFIM	49
4.4 Von Neumann entropy	49
4.5 TFIM ground state magnetization	50
4.6 Chapter summary	53
5 One-particle properties	55

5.1	One-QP excited states and dispersion	55
5.1.1	Describing excited states	56
5.1.2	Canonical gauge for excitation tensors	56
5.1.3	Momentum space variation	59
5.2	Tensor network calculations	61
5.2.1	TN topology	62
5.2.2	TN factorization	63
5.2.3	Matrix element TN evaluation	63
5.2.4	Complexity analysis	67
5.3	Momentum discretization	68
5.4	Dispersion results	69
5.4.1	Results for the FMHC	69
5.4.2	Results for the TFIM	71
5.5	The effective model	74
5.5.1	Definition of the creation operator	74
5.5.2	Analysis of the quasi-particle representation	75
5.5.3	Error estimation	76
5.5.4	Notes on implementation	78
5.6	One-particle spectral weight	81
5.6.1	Results for TFIM	81
5.7	Efficient computation	82
5.8	Chapter summary	85
6	Two-particle properties	87
6.1	Definition of two-particle states	87
6.1.1	Real space basis	87
6.1.2	Momentum space basis	90
6.1.3	Hybrid basis	91
6.1.4	Metric tensor	92
6.2	Results for the metric tensor of the TFIM	94
6.3	Two-particle spectral weight in the TFIM	96
6.3.1	Reference result from uMPS	97
6.3.2	Results	98
6.4	Efficient computation of two-particle quantities	101
6.4.1	2QP-ground state matrix element	102
6.4.2	Complexity analysis	105
6.5	Quasi-particle decay amplitude	106
6.6	Scattering matrix	109
6.6.1	Matrix element computation	110
6.6.2	Results for the FMHC	111
6.6.3	Results for the TFIM	112
6.7	Chapter summary	116
7	Conclusion and outlook	117
7.1	Summary of the method	117
7.2	Summary of results	119
7.2.1	Ground state results	119
7.2.2	One-particle results	120
7.2.3	Two-particle results	121
7.3	Outlook	122
A	Supplementary material	125

A.1	The Kronecker identity	125
A.2	Hamiltonian of the FMHC in the 2QP sector	126
A.3	2QP interaction matrix of the TFIM	127
A.4	Properties of transfer operator T	129
A.4.1	Largest eigenvalue	129
A.4.2	Properties of eigenmatrices	130
A.4.3	TN boundaries in the thermodynamic limit	133
A.4.4	uMPS and iMPS	135
A.5	Ground state degeneracy	135
A.5.1	Working with degenerate ground states	136
A.5.2	Transformation for ground state uMPS in the TFIM	136
A.5.3	Dispersion for degenerate ground states	137
A.6	Orthogonality of Wannier states	138
A.7	Occupation-number and Hilbert space dimensions	139
A.8	Gram-Schmidt orthonormalization without vectors	142
A.9	2QP basis transformations	145
A.10	Hard-core bosons in momentum space	149
A.10.1	Hard-core bosonic metric tensor in momentum space	149
A.10.2	Hard-core corrections for bilinear Hamiltonians	150
B	Efficient computation of 2QP quantities	153
B.1	General approach	153
B.2	Metric tensor	155
B.2.1	2QP overlap	155
B.2.2	2QP-1QP overlap	161
B.3	2QP matrix element	161
B.3.1	1QP contributions	162
B.3.2	Ground state-1quasi-particle (QP) matrix element corrections	165
B.3.3	Different tensor network (TN) types	167
B.3.4	Case i)	168
B.3.5	Case ii)	171
B.3.6	Case iii)	175
B.3.7	Case iv)	179
B.3.8	Case v)	185
B.4	2QP-1QP matrix element	192
B.4.1	1QP-ground state matrix element correction	192
B.4.2	Different TN types	193
B.4.3	Case i)	194
B.4.4	Case ii)	195
B.4.5	Case iii)	195
B.4.6	Case iv)	196
B.4.7	Case v)	198
C	Summary of TN calculation results	201
C.1	Shorthand definitions	201
C.1.1	Scalars	201
C.1.2	Summed left boundary matrices	201
C.1.3	Summed right boundary matrices	202
C.2	Summary of 2QP matrix element contributions	203
C.3	Summary of 2QP-1QP matrix element contributions	205
	Bibliography	207

List of Figures	213
List of Tables	214
List of Acronyms	215

Chapter 1

Introduction

What we know is a drop, what we don't know is an ocean.

Isaac Newton

1.1 Motivation

For many decades, the field of quantum magnetism has been an extremely active field of research. Quantum magnets show a vast variety of interesting phenomena. For instance a widely discussed hypothesis is that the Cooper pairing of electrons responsible for high-temperature superconductivity observed in the so-called cuprates and other quasi-two-dimensional materials is mediated by magnetic excitations [1, 2].

But also beyond the field of high temperature superconductivity quantum magnetism has gained visibility. The 2016 Nobel prize in physics went to Haldane, Kosterlitz and Thouless “for theoretical discoveries of topological phase transitions and topological phases of matter” [3]. Kosterlitz and Thouless showed theoretically that the unbinding of vortex-antivortex pairs in a two-dimensional magnet leads to a previously unknown type of transition between phases that are not distinguished by their symmetry breaking [4, 5]. Since vortices and antivortices are topological defects in the magnetic order, this new type of phase transition is now known as topological phase transition. Later, concepts of topology helped to explain the robustness of the quantization in the conductance of the integer quantum Hall effect [6] in 1982. One year later, Haldane included topological effects into the treatment of anti-ferromagnetic Heisenberg spin chains, which led him to the formulation of the famous “Haldane conjecture”. It predicts that half-integer spin chains are gapless, while chains of integer spins show a finite excitation gap [7, 8]. This Haldane gap could later be observed in experiments with ultracold atomic gases [9].

Moreover, the idea of quantum computing has sparked much interest since Feynman introduced it in the 1980s [10]. Unlike in a classical computer, the units of information or quantum-bits (qubits), can not only take the values 0 and 1 but also any quantum mechanical superposition of these two states. This allows the quantum computer to tackle certain problems much more efficiently than a classical computer, most notably the simulation of other quantum systems. Although to the present day no viable realization of a scalable quantum computer exists, many theoretical models use an effective (or even physical) spin- $\frac{1}{2}$ degree of freedom for the qubits [11]. Therefore this, too, is a possible field of application of quantum magnets or at least of the theoretical framework used to describe them.

All this interest shows that there is ample need to learn as much as possible about the dynamics of quantum magnets. In this thesis, a method is presented that can help on the

way towards this goal by providing an approach to derive an effective low-energy model for quantum magnets.

1.2 Effective models in second quantization

Many quantum magnets display some sort of order in the ground state. Excitations above the ground state are then disturbances of this magnetic order. In most cases several spins are involved in such an excitation, wherefore they are often termed collective excitations. Spin waves are a simple example of such excitations. As the name suggests, these are wave-like modulations of the magnetic order. Sound waves, wave like modulations of the lattice structure, are quantized into phonons. Analogously spin waves are quantized into so-called magnons. Another easy-to-imagine excitation is a flipped spin in an otherwise ferromagnetically (or antiferromagnetically) ordered system. Domain walls are a third common type of excitations in low-dimensional quantum magnets with degenerate ground states. They separate regions of different ground states from one another. In one dimension, the size of these regions does not change the energy cost of a domain wall. There are many other and exotic types of magnetic excitations, but this thesis focuses on spin-flips and domain walls.

All these excitations have in common, that they are emergent phenomena, i.e., they only exist on the background of a many body system. But, in many aspects they behave like elementary particles. Therefore, another common term to describe them is quasi-particle (QP). Often, understanding how a single one of these collective excitations behaves and how a few of them interact with each other goes a long way in understanding the physics in the system at low excitation density.

As quanta of the excitation field, they can be described using standard second quantization techniques. A generic low-energy model in second quantization is given by the Hamiltonian [97]

$$\begin{aligned}
 H_{\text{eff}} = & E_0 + \sum_q \omega_q a_q^\dagger a_q + \frac{1}{\sqrt{L}} \sum_{q_1, q_2, q_3} \left(D_{q_3}^{q_1, q_2} a_{q_1}^\dagger a_{q_2}^\dagger a_{q_3} + \text{h.c.} \right) \\
 & + \frac{1}{L} \sum_{q_1, q_2, q_3, q_4} V_{q_3, q_4}^{q_1, q_2} a_{q_1}^\dagger a_{q_2}^\dagger a_{q_3} a_{q_4} + \dots \quad (1.1)
 \end{aligned}$$

The symbols in Eq. (1.1) are defined as follows: The constant E_0 is the ground state energy. It is an extensive quantity in the thermodynamic limit and one therefore commonly looks at the ground state energy per lattice site ϵ_0 instead. The prefactor ω_q of the bilinear term is the single particle dispersion relation. The operators a_q^\dagger and a_q create and annihilate a (quasi-) particle, respectively. The matrix elements $D_{q_3}^{q_1, q_2}$ and their Hermitian conjugates describe the amplitudes for the decay of one QP into two and the fusion of two QPs into one, respectively. Such processes can occur, if the quasi-particles have a finite life time. They can be identified by the single-particle dispersion entering the two-particle continuum [47] at a critical momentum, beyond which the quasi-particles cease to exist as stable excitations. In a particle number conserving picture, these decay processes and the associated matrix elements $D_{q_3}^{q_1, q_2}$ do not appear. If they do, conservation of total momentum requires $q_3 = q_1 + q_2$. The $V_{q_3, q_4}^{q_1, q_2}$ are the scattering matrix elements of two-QP states. They are of great interest, because they are the stepstone towards any kind of interacting theory which can, for instance, describe the formation of bound states. This thesis is mainly concerned with constructing the 2QP states from which these scattering elements can be determined. Lastly, the dots represent interaction terms involving higher

numbers of QPs. These are beyond the scope of the current work.

This type of second quantized model does not only give an intuitive understanding of how the quasi-particles behave and how they interact. On the level outlined above, it also allows to obtain further one- and two-particle properties. This includes dynamic properties such as the spectral function [12, 13]. Although being a zero temperature result, it can also serve as the starting point for calculations at finite temperature, for instance by means of diagrammatic perturbation theory [14, 15] or approximate Bethe ansatz techniques [13].

1.3 The approach

In the case of quantum magnetism, the natural language to write down a Hamiltonian is the spin-language. In terms of these elementary magnets, it is easy to formulate interactions, like nearest or next-nearest neighbor spin-spin coupling with different coupling constants etc. While this description is easy to define, it does not say anything about what the collective magnetic excitations or even the ground state will look like or how the excitations behave. An effective second quantization model, as described in section 1.2, offers a much more accessible way to understand the properties of interacting magnetic systems.

This thesis presents a way to derive an effective second quantization model from a spin Hamiltonian. It is based on the framework of matrix product states (MPSs), more precisely the infinite system variant thereof.

The concept of MPS was introduced in various ways and contexts, for instance by Baxter in Ref. [16] to tackle spin dimerization in a plane. However, it is most successfully applied to one-dimensional systems. This is best understood in context of the close relation to the well-known density matrix renormalization group (DMRG). S.R. White introduced the DMRG method in 1992 [17] as an improvement to K. Wilson's numerical renormalization group (NRG) method [18] for quantum lattice models.

In renormalization group methods, the lattice system is built by adding successively more lattice sites. When the computing capacity for exact description is reached after adding a new site, a part of the Hilbert space is discarded. In contrast to NRG, the criterion for keeping states in the reduced basis are the eigenvalues of a density matrix (hence the name). The key idea of DMRG is that the states with the largest eigenvalues of the density matrix are most important and should therefore be kept, regardless of their energy, which is the criterion in NRG. This approach proved to be highly successful for a vast variety of problems.

Östlund and Rommer showed that MPS naturally appear when the infinite system DMRG algorithm converges [19, 20]. Since then, a considerable amount of research has been performed in the field. In the context of quantum spin chains, MPS received much attention through the work of Fannes et al. [21, 22]. U. Schollwöck's excellent review [23] shows how the DMRG can be formulated very elegantly in the language of MPS. This close connection to the DMRG is the reason for the success of the MPS formalism. In the original formulation of Ref. [17] the DMRG was a method to compute equilibrium properties of one-dimensional systems at zero temperature. The method presented in this thesis works in the same setting. As a variational method, the DMRG and thus the MPS formalism has the advantage of being largely unbiased. Therefore, it can be applied to a broad variety of problems where other, more specialized methods may not.

Inspired by the great success of DMRG, many extensions to the original formulation have been developed. There is time-dependent DMRG (tDMRG) [24, 25], momentum space

DMRG [26, 27] and DMRG for finite temperature [28]. All these extensions can also be formulated for MPS. Using the Liouville operator instead of the Hamiltonian, frequency resolved results at finite temperatures can be obtained [29]. There was limited success extending the original DMRG to higher dimensions, due to the intrinsic way it works. Only ribbons of finite (and rather small) width or cylinders of limited circumference can be handled [30]. Here, the concept of tensor network states (TNS) with tensors of higher dimension represent a promising development. The natural extension of MPS to two dimensions are projected entangled pair states (PEPS) [31, 32], which can also be adapted to treat infinite systems (iPEPS) [33]. There are ongoing efforts to extend the framework and improve the description of long-range entangled states such as critical systems and quantum spin liquids [34, 35, 36, 37]. So far, TNS calculations in two dimensions are still limited mainly to ground state properties due to the necessary larger tensor dimension which makes the calculations numerically costly.

As mentioned above, another way to obtain finite temperature results is by means of effective models and diagrammatic perturbation theory, for example. A powerful method to derive effective models is that of continuous unitary transformations (CUTs), also known as the flow equation method [38, 39]. CUTs have been applied successfully to a wide variety of problems and there are different variants [40, 41, 42]. The Dyson-Maleev representation [43, 44], which maps spins to bosons, can be very useful but results in a non-Hermitian Hamiltonian. For this case, the CUT can be generalized to a continuous similarity transformation (CST) that can yield very accurate results [45, 46].

While applicable to many problems, flow equation methods tend to run into numerical problems, if level crossings occur during the flow [47]. Another problem that can occur, especially for perturbative CUTs is that the ground state of the unperturbed Hamiltonian has to be adiabatically connected to the ground state of the full Hamiltonian. If this is not the case, the transformation may not converge or produce unpredictable or unphysical results. Here, MPS as a variational method can potentially be more successful.

1.4 Structure of the thesis

The remainder of the thesis is structured as follows: Chapter 2 introduces the models on which the method is tested. Some analytical results are derived, more involved results are briefly presented. In chapter 3 the framework of MPS is introduced. It is intended as an overview for novices in the field and will briefly cover the concepts needed to implement the presented method. Chapters 4 and 5 show how a ground state approximation can be found and how the one-QP dispersion and the creation operator of the effective model are constructed. Chapter 6 contains the main results of the thesis, the two-QP interaction algorithms and results. In chapter 7 the results are summarized and an outlook on possible future research is given.

Appendices A and B contain some more detailed calculations which would interrupt the main text too much, but can be helpful in understanding how the method is implemented. Their sections are referenced in the main text where appropriate. Appendix C contains a summary of the tensor network calculation results. These are essential in efficiently implementing the method.

Chapter 2

The models

*Truth ... is much too complicated to
allow anything but approximations.*
John von Neumann

This section offers a detailed description of the models which the presented method is tested on. Along with some analytical calculations, the reference results are given to which the numerical results are compared later on. For convenience, in all calculations the convention

$$\hbar = 1 \tag{2.1}$$

is used. All models are investigated on one-dimensional chains with equidistant lattice spacing. Therefore, all lattices constants a are set to unity. Consequently, the unit of crystal momentum is π .

2.1 Ferromagnetic Heisenberg chain

Consider as a simple test case the ferromagnetic spin- $\frac{1}{2}$ Heisenberg chain (FMHC) in an external field given by the Hamiltonian

$$H = \sum_j -J\vec{S}_j\vec{S}_{j+1} + \Gamma S_j^z, \quad J, \Gamma > 0. \tag{2.2}$$

The Heisenberg interaction $\sum_j -J\vec{S}_j\vec{S}_{j+1}$ aligns all spins parallel and is $SU(2)$ symmetric. The external field $\sum_j \Gamma S_j^z$ does not compete with the Heisenberg interaction. It just breaks the $SU(2)$ symmetry and favors the spins to point downwards, so the ground state is simply the fully polarized state with all spins pointing down.

$$|\downarrow\downarrow\cdots\downarrow\downarrow\rangle = |\downarrow\rangle|\downarrow\rangle\cdots|\downarrow\rangle|\downarrow\rangle. \tag{2.3}$$

Note that this polarized state is a product state. Excitations on top of this ground state are completely localized spin-flips. Rewriting the Hamiltonian in terms of the spin ladder operators

$$S^\pm = S^x \pm iS^y \quad \Leftrightarrow \quad S^x = \frac{1}{2}(S^+ + S^-), \quad S^y = \frac{1}{2i}(S^+ - S^-) \tag{2.4a}$$

$$S^z = S^+S^- - \frac{1}{2} \tag{2.4b}$$

yields

$$H = \sum_j -\frac{J}{2} \underbrace{\left(S_j^+ S_{j+1}^- + S_{j+1}^+ S_j^- \right)}_{H_{\text{kin}}} - \underbrace{(J + \Gamma) S_j^+ S_j^-}_{H_{\text{field}}} - \underbrace{J S_j^+ S_j^- S_{j+1}^+ S_{j+1}^-}_{H_{\text{int}}} - \underbrace{\left(\frac{J}{4} + \frac{\Gamma}{2} \right)}_{E_0}. \quad (2.5)$$

The formulation in Eq. (2.5) shows clearly that the state Eq. (2.3) is an eigenstate of H on top of which the spin raising operator S_j^+ creates a local excitation and the lowering operator S_j^- annihilates one. The kinetic term H_{kin} can be diagonalized by the Fourier transformation

$$S_q^+ := \frac{1}{\sqrt{L}} \sum_j S_j^+ e^{+iqj} \quad S_q^- := \frac{1}{\sqrt{L}} \sum_j S_j^- e^{-iqj} \quad (2.6a)$$

$$S_j^+ = \frac{1}{\sqrt{L}} \sum_q S_q^+ e^{-iqj} \quad S_j^- = \frac{1}{\sqrt{L}} \sum_q S_q^- e^{+iqj}, \quad (2.6b)$$

where L denotes the number of lattice sites. By inserting Eq. (2.6b) into the kinetic term H_{kin} and the field term H_{field} from Eq. (2.5), these transform as

$$H_{\text{kin}} = \sum_j -\frac{J}{2} \frac{1}{L} \left[\sum_q e^{-iqj} S_q^+ \sum_{q'} e^{+iq'(j+1)} S_{q'}^- + \sum_{q'} e^{-iq'(j+1)} S_{q'}^+ \sum_q e^{+iqj} S_q^- \right] \quad (2.7a)$$

$$= \sum_j -\frac{J}{2} \frac{1}{L} \sum_{q,q'} S_q^+ S_{q'}^- e^{i(q-q')j} \left(e^{+iq'} + e^{-iq'} \right) \quad (2.7b)$$

$$= \sum_q -J \cos(q) S_q^+ S_q^- \quad (2.7c)$$

and

$$H_{\text{field}} = \sum_j -(J + \Gamma) \frac{1}{L} \sum_{q,q'} e^{i(q-q')j} S_{q'}^+ S_q^- \quad (2.8a)$$

$$= \sum_q -(J + \Gamma) S_q^+ S_q^-, \quad (2.8b)$$

where the Kronecker identity Eq. (A.1.1) was used. The field term can be absorbed into the now diagonal kinetic part and renormalizes the dispersion relation. It is convenient to symmetrize the interaction term and also take into account interaction with the neighboring site to the left, because then the prefactor is real.

$$H_{\text{int}} = \sum_j -\frac{J}{2} \left(S_j^+ S_{j+1}^+ S_j^- S_{j+1}^- + S_j^+ S_{j-1}^+ S_j^- S_{j-1}^- \right) \quad (2.9a)$$

$$= \sum_j -\frac{J}{2L^2} \sum_{q_1, q_2, q_3, q_4} S_{q_1}^+ S_{q_2}^+ S_{q_3}^- S_{q_4}^- \times \left(e^{-iq_1 j - iq_2(j+1) + iq_3 j + iq_4(j+1)} + e^{-iq_1 j - iq_2(j-1) + iq_3 j + iq_4(j-1)} \right) \quad (2.9b)$$

$$= -\frac{J}{2L} \sum_{q_1, q_2, q_3, q_4} \frac{1}{L} \sum_j S_{q_1}^+ S_{q_2}^+ S_{q_3}^- S_{q_4}^- \times e^{-i(q_1 + q_2 - q_3 - q_4)j} \left(e^{-i(q_2 - q_4)} + e^{+i(q_2 - q_4)} \right) \quad (2.9c)$$

$$= -\frac{J}{2L} \sum_{q_1, q_2, q_3} S_{q_1}^+ S_{q_2}^+ S_{q_3}^- S_{q_1+q_2-q_3}^- \left(e^{-i(q_2 - q_1 - q_2 + q_3)} + e^{+i(q_2 - q_1 - q_2 + q_3)} \right) \quad (2.9d)$$

$$= \sum_{q_1, q_2, q_3} -\frac{J}{L} \cos(q_1 - q_3) S_{q_1}^+ S_{q_2}^+ S_{q_3}^- S_{q_1+q_2-q_3}^-. \quad (2.9e)$$

The summation over q_4 disappears, since the conservation of total momentum implied in Eq. (2.9c) requires

$$q_1 + q_2 = q_3 + q_4 = Q . \quad (2.10)$$

The spin ladder operators on different sites commute, which is a bosonic property. However, since a spin can be flipped only once, there can only be one excitation on each lattice site, which is fermionic behavior. A second flip takes the system back to the ground state. In other words, the excitations are so-called hard-core bosons, following the algebra

$$[S_i^+, S_j^+] = [S_i^-, S_j^-] = 0 \quad \forall i, j; \quad [S_i^-, S_j^+] = 0, \quad j \neq i; \quad \{S_i^-, S_i^+\} = 1 \quad (2.11)$$

which implies

$$S_i^+ S_i^+ = S_i^- S_i^- = 0 . \quad (2.12)$$

The commutation and anti-commutation relations can be expressed by a single commutator

$$[S_i^-, S_j^+] = \delta_{i,j} (1 - 2S_j^+ S_j^-) \quad (2.13)$$

which translates to momentum space as

$$[S_q^-, S_{q'}^+] = \delta_{q,q'} - \frac{2}{L} \sum_j e^{i(q'-q)j} S_j^+ S_j^- . \quad (2.14)$$

Identifying the spin raising and lowering operators as hard-core bosonic creation and annihilation operators

$$a_q^\dagger := S_q^+, \quad a_q := S_q^- , \quad (2.15)$$

the Hamiltonian can directly be interpreted as a second quantization effective model of hard-core bosonic quasi-particles

$$H = E_0 + \sum_q \omega_q a_q^\dagger a_q + \frac{1}{L} \sum_{q_1, q_2, q_3} V_{q_1 q_2 q_3} a_{q_1}^\dagger a_{q_2}^\dagger a_{q_3} a_{q_1+q_2-q_3} \quad (2.16a)$$

$$\text{with } E_0 = -L \left(\frac{J}{4} + \frac{\Gamma}{2} \right) \quad (2.16b)$$

$$\omega_q = \Gamma + J(1 - \cos(q)) \quad (2.16c)$$

$$V_{q_1 q_2 q_3} = -J \cos(q_1 - q_3) . \quad (2.16d)$$

Introducing a next nearest neighbor interaction term

$$H_{\text{NNN}} = \sum_j -J_2 \vec{S}_j \vec{S}_{j+2} \quad (2.17)$$

adds another Fourier component to the dispersion relation and the interaction, which then become

$$\omega_q = \Gamma + J(1 - \cos(q)) + J_2(1 - \cos(2q)) \quad (2.18)$$

and

$$V_{q_1 q_2 q_3} = -J \cos(q_1 - q_3) - J_2 \cos(2(q_1 - q_3)) , \quad (2.19)$$

respectively. The ground state energy is also shifted to

$$E_0 = -L \left(\frac{J}{4} + \frac{J_2}{4} + \frac{\Gamma}{2} \right) . \quad (2.20)$$

The calculations are completely analogous to those for the nearest neighbor interaction.

2.1.1 Bound state

The model also shows a bound state of two quasi-particles (QPs). Its formation can be understood very easily on a cartoon level. In a 2QP state where the two particles are far apart

$$|i,j\rangle := |\downarrow \cdots \downarrow \uparrow_i \downarrow \cdots \downarrow \uparrow_j \downarrow \cdots \downarrow\rangle, \quad (2.21)$$

there is a total of four unsatisfied ferromagnetic bonds. However, if the excitations are next to each other

$$|i,i+1\rangle = |\downarrow \cdots \downarrow \uparrow_i \uparrow_{i+1} \downarrow \cdots \downarrow\rangle, \quad (2.22)$$

there are only two broken bonds. This leads to an attraction of the quasi-particles and the formation of a bound state.

For $J_2 = 0$, i.e., without next-nearest neighbor interaction, the energy of the bound state E_B is given by [48, 49]

$$E_B = 2\Gamma + \frac{1}{2}(1 - \cos Q), \quad (2.23)$$

where $Q = q_1 + q_2$ denotes total momentum. With $J_2 > 0$, the energy of this bound state is hard to obtain analytically, but straight forward to compute numerically by diagonalizing the Hamiltonian in the 2QP subspace, where it takes the matrix form

$$\begin{aligned} & \langle Q,q' | (H - E_0) | Q,q \rangle \\ &= \omega_q \delta_{q'q} - \frac{2}{L} \left(\omega_{\frac{Q+q}{2}} + \omega_{\frac{Q-q}{2}} + \omega_{\frac{Q+q'}{2}} + \omega_{\frac{Q-q'}{2}} - 2t_0 \right) \\ & \quad - \frac{2J}{L} \left[\cos\left(\frac{q'-q}{2}\right) + \cos\left(\frac{q'+q}{2}\right) \right] - \frac{2J_2}{L} [\cos(q'-q) + \cos(q'+q)]. \end{aligned} \quad (2.24)$$

In Eq. (2.24) $q = q_1 - q_2$ is the relative momentum of the two particles, and t_0 the one-particle on-site energy. The condition $q \geq 0$ makes the basis unique. See App. A.2 for details.

2.2 The transverse field Ising model

The method will also be tested on the transverse field Ising model (TFIM). It was used, for example, by P. G. De Gennes to describe tunneling in ferroelectric crystals [50] and has since been studied extensively, see for instance Refs. [51, 52]. It shows many interesting phenomena including a quantum phase transition, ground state degeneracy, and therefore, domain wall excitations.

In this thesis, the one-dimensional ferromagnetic case is considered, in which the model is described by the Hamiltonian

$$H = \Gamma \sum_j S_j^z - J \sum_j S_j^x S_{j+1}^x, \quad \Gamma, J > 0 \quad (2.25)$$

where S^z and S^x are the common spin- $\frac{1}{2}$ operators. It describes a chain of spin- $\frac{1}{2}$ degrees of freedom that interact only in x -direction. Such spins are often referred to as Ising spins, hence the name Ising model. Adding an external field perpendicular to the interaction (here the z -axis is chosen) adds quantum fluctuations, since the field term does not commute with the Ising interaction.

The dimensionless parameter

$$\lambda := \frac{J}{2\Gamma}, \quad \lambda \in [0, \infty) \quad (2.26)$$

controls the behavior of the system. In terms of this parameter, the Hamiltonian can be written as

$$\frac{H}{\Gamma} = \sum_j S_j^z - 2\lambda \sum_j S_j^x S_{j+1}^x. \quad (2.27)$$

In this notation, all energies are measured in units of Γ , which for convenience is set to 1.

In the strong-field limit $\lambda = 0$, the ground state is fully polarized along the z -axis. The elementary excitations are spin-flips, and one can think of them as quasi-particles. These excitations are immobile, since there is no interaction between neighboring spins.

For $0 < \lambda < 1$, the external field still dominates. This phase is called the strong-field phase or disordered phase, since the external field suppresses long-range order along the Ising coupling direction. If a small amount of Ising coupling is added, the spin-flips become mobile and also “dressed”. This means that a flipped spin on one site acquires a polarization cloud of a certain spatial extension which is considered part of the quasi-particle. As for the ferromagnetic Heisenberg chain (FMHC), these QPs are hard-core bosons.

At $\lambda = 1$, the external field is as strong as the Ising coupling, giving rise to a quantum critical point (QCP). The excitation gap closes at momentum $q = 0$, meaning arbitrarily many spin-flips can be created at zero energy cost.

For $\lambda > 1$, the Ising coupling dominates, and the spins align along the x -direction. The Hamiltonian Eq. (2.25) shows a \mathbb{Z}_2 symmetry for $S^x \rightarrow -S^x$, giving rise to a two-fold ground state degeneracy. The spins can point either in positive or in negative x -direction and both configurations have the same energy. Spontaneous symmetry breaking occurs, but since \mathbb{Z}_2 is a discrete symmetry, no Goldstone modes appear. This phase is referred to as the ordered phase or Ising phase, since it is dominated by the Ising interaction, and long-range order forms along the direction of this interaction. Since a spin pointing in x -direction in presence of a field along the quantization axis, i.e., the z axis, can be interpreted as fluctuating between the up and down states, the phase transition can also be viewed as a condensation of the spin-flip excitations. In this regime, the elementary excitations are domain walls between regions of the two ground state realizations. In the Ising limit $\lambda \rightarrow \infty$ (i.e. $\Gamma \rightarrow 0$) they are again exact. Away from the limit, the domain walls, too, acquire a dressing, i.e. get “smeared out” over a certain spatial region.

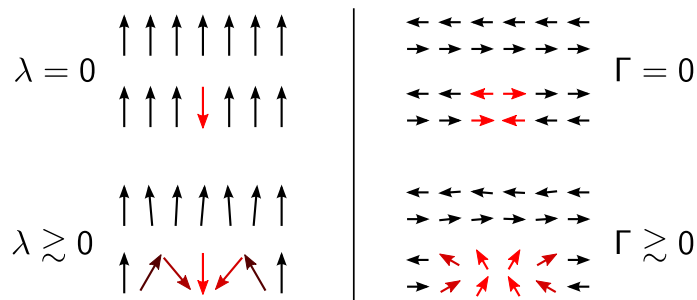


Figure 2.1: Illustration of the ground states and quasi-particles in the TFIM. Left side: disordered phase; ground state and spin-flip excitation in the weak coupling limit $\lambda = 0$ (top) and away from the limit (bottom). Right side: ordered phase; ground state and domain wall excitation in the strong coupling limit $\Gamma = 0$ (top) and away from the limit (bottom).

Figure 2.1 illustrates these quasi-particles. In the left panel, ground state and the spin-flip excitations of the disordered phase are sketched, and in the right panel the ground states and domain walls of the ordered phase.

2.2.1 Exact solution

This section provides a short review of the analytic solution and states the closed expressions for ground state energy and the dispersion relation.

In Ref. [53] Pfeuty showed, that the model can be solved analytically by a sequence of Jordan-Wigner, Fourier and Bogolyubov transformations [54].

As a first step, the Hamiltonian Eq. (2.27) is rewritten in spin ladder operators Eq. (2.4)

$$H = \sum_j S_j^+ S_j^- - \frac{1}{2} - \frac{\lambda}{2} \sum_j \left(S_j^+ + S_j^- \right) \left(S_{j+1}^+ + S_{j+1}^- \right) \quad (2.28a)$$

$$= \sum_j S_j^+ S_j^- - \frac{1}{2} - \frac{\lambda}{2} \sum_j S_j^+ S_{j+1}^- + S_{j+1}^+ S_j^- + S_j^+ S_{j+1}^+ + S_j^- S_{j+1}^- \quad (2.28b)$$

which illustrates the effective model interpretation when viewing the ladder operators S^+ (S^-) to create (annihilate) a quasi-particle. Again, these operators follow the hard-core algebra Eq. (2.11).

The Jordan-Wigner transformation

$$c_j = \exp \left(i\pi \sum_{i<j} S_i^+ S_i^- \right) S_j^- \quad c_j^\dagger = S_j^+ \exp \left(-i\pi \sum_{i<j} S_i^+ S_i^- \right) \quad (2.29a)$$

$$S_j^- = \exp \left(-i\pi \sum_{i<j} c_i^\dagger c_i \right) c_j \quad S_j^+ = c_j^\dagger \exp \left(i\pi \sum_{i<j} c_i^\dagger c_i \right) \quad (2.29b)$$

can be used to map the hardcore bosons to spinless fermions. The c_j then satisfy the canonical anticommutation relations [55]

$$\{c_i^\dagger, c_j\} = \delta_{ij}, \quad \{c_i^\dagger, c_j^\dagger\} = \{c_i, c_j\} = 0. \quad (2.30)$$

Note that these fermionic operators c_j are highly non-local objects in terms of real space lattice sites. In the exponential, the number of spin-flips to the left of c_j is counted, giving it a positive sign if that number is even and a negative sign if it is odd.

Consider a chain of L sites. For open boundary conditions (OBC), the second sum in the Hamiltonian runs from $j = 1$ to $j = L - 1$, whereas for periodic boundary conditions (PBC) it runs to $j = L$ with $L + 1 = 1$. However, in the limit $L \rightarrow \infty$, the error in letting both sums run to L , and neglecting the coupling between the first and last site is small. Thus, in the thermodynamic limit (TDL), the Hamiltonian reads

$$H = \frac{L}{2} - \sum_j c_j^\dagger c_j - \frac{\lambda}{2} \sum_j \left(c_j^\dagger c_{j+1} + c_{j+1}^\dagger c_j + c_j^\dagger c_{j+1}^\dagger - c_j c_{j+1} \right). \quad (2.31)$$

The bilinear terms containing one creation and one annihilation operator can be diagonalized by Fourier transformation. The so called Bogolyubov terms that create and annihilate *two* particles couple momenta $+q$ and $-q$. They can be diagonalized by a Bogolyubov transformation [56]

$$\eta_q := u_q c_q + v_q c_q^\dagger \quad (2.32a)$$

$$\eta_q^\dagger := u_q^* c_q^\dagger + v_q^* c_q \quad (2.32b)$$

where c_q is the Fourier transform of c_j and u_q and v_q are complex numbers. This yields the Hamiltonian in diagonal form

$$H = E_0 + \sum_q \omega_q \eta_q^\dagger \eta_q \quad (2.33)$$

with the one-particle energy dispersion and the ground state energy per lattice site in the TDL, cf. Ref. [53]:

$$\omega_q = \Gamma \sqrt{1 + \lambda^2 - 2\lambda \cos q} \quad (2.34a)$$

$$\epsilon_0 = \frac{E_0}{L} = -\frac{1}{2L} \sum_q \omega_q = -\frac{1}{2\pi} \int_0^\pi \omega_q dq \quad (2.34b)$$

The ground state energy is an elliptic integral and it has a non-analyticity at $\lambda = 1$. It is easy to see that the excitation energy gap Δ follows as

$$\Delta = \min_q \omega_q = \Gamma |1 - \lambda| \quad (2.35)$$

and vanishes at the quantum critical point $\lambda = 1$.

The excitations created by η_q^\dagger are linear combinations of Jordan-Wigner fermions and therefore highly non-local in terms of the original spin-flip excitations.

2.2.2 Solution by CUT

In Ref. [57] Fauszeweh applied the method of CUTs to the TFIM to derive an effective model. He showed that the Hamiltonian can be written in terms of so-called string operators $T_{n,j}$ as

$$H_{\text{CUT}} = \sum_j t_0 T_{0,j} + \sum_{n=1}^{\infty} (-1)^{n-1} t_n (T_{n,j} + \text{h.c.}) \quad (2.36)$$

with the string operators

$$T_{0,j} := 2a_j^\dagger a_j - \mathbf{1} \quad (2.37a)$$

$$T_{n,j} := a_j^\dagger T_{0,j+1} \cdots T_{0,j+n-1} a_{j+n} \quad (2.37b)$$

and the Fourier coefficients t_n of the one-particle dispersion Eq. (2.34a)

$$t_n = \frac{1}{2\pi} \int_{-\pi}^{\pi} e^{iqn} \omega_q dq = \frac{\Gamma}{2\pi} \int_{-\pi}^{\pi} e^{iqn} \sqrt{1 + \lambda^2 - 2\lambda \cos q} dq. \quad (2.38)$$

Unlike Pfeuty's exact quasi-particles, the quasi-particles created (annihilated) by a^\dagger (a) have a localized character by construction¹. However, from Eq. (2.29) it is apparent that in the operator product $c_i^\dagger c_i$ the phase tails cancel out. Therefore, the quasi-particles from Ref. [57] have the same energy dispersion ω_q , but the effective Hamiltonian is not bilinear. In contrast to Eq. (2.33) it contains interaction terms that conserve the particle number, but involve any number of particles.

From Eq. (2.36) one can see that the multi-particle interaction matrix elements are entirely determined by the one-particle dispersion through the hopping elements t_n .

The aim of this thesis is to derive the two-particle interaction part of the Hamiltonian. Equation (2.36) also shows that for the TFIM, any 2QP interaction term with a non-zero amplitude is necessarily of the form

$$h_{n,k}^j \propto a_j^\dagger (-\mathbf{1}_{j+1}) \cdots (-\mathbf{1}_{j+k-1}) (a_{j+k}^\dagger a_{j+k}) (-\mathbf{1}_{j+k+1}) \cdots (-\mathbf{1}_{j+n-1}) a_{j+n} \quad (2.39a)$$

$$= (-1)^{n-2} a_j^\dagger a_{j+k}^\dagger a_{j+k} a_{j+n}, \quad \text{with } n \geq 2, \quad 1 \leq k < n. \quad (2.39b)$$

¹If Ref. [57] the operators are called σ^\pm and $\sigma^z = 2\sigma^+ \sigma^- - 1$. In the beginning, these are identical to the Pauli matrices, i.e. $\sigma^i = 2S^i$. However, during the flow of the CUT they become increasingly non-local and are then termed "effective observables". It is important to note, though, that they retain a *finite* spatial extension, in contrast to the Jordan-Wigner fermions.

Combining the powers of -1 from Eqs. (2.36) and (2.39) yields a prefactor of

$$V_{n,k}^j = -2t_n \quad (2.40)$$

so that the complete irreducible 2QP-part of the Hamiltonian is given by

$$H_{2P} = -2 \sum_j \sum_{n \geq 2} \sum_{k=1}^{n-1} t_n (a_j^\dagger a_{j+k}^\dagger a_{j+k} a_{j+n} + \text{h.c.}) . \quad (2.41)$$

To compare to MPS results, the interaction matrix in the basis $|Q, q_1\rangle$ of total momentum Q and first particle momentum q_1 is used

$$\begin{aligned} \langle Q, q_1' | H_{2P} | Q, q_1 \rangle = & -\frac{4}{L} \sum_{d', d > 0} t_{d'+d} [\cos(q_1' d' + q_1 d) + \cos(q_2' d' + q_2 d) \\ & + \cos(q_1' d' + q_2 d) + \cos(q_2' d' + q_1 d)] \end{aligned} \quad (2.42)$$

where conservation of total momentum implies $q_1' + q_2' = q_1 + q_2 = Q$. See App. A.3 for details.

2.2.3 Ground state magnetization

The ground state magnetization M_x along the direction of the Ising coupling is the order parameter in the Ising phase. In the strong-field phase, it is always zero. It was found in Ref. [53] to be

$$|M_x| := \langle GS | S^x | GS \rangle = \begin{cases} 0, & \text{for } \lambda < 1 \\ \frac{1}{2} \left(1 - \frac{1}{\lambda^2}\right)^{\frac{1}{8}}, & \text{for } \lambda \geq 1 \end{cases} . \quad (2.43)$$

Due to the spontaneously broken \mathbb{Z}_2 symmetry, the magnetization can be either positive or negative, and its sign can be used to distinguish the degenerate ground states.

At $\lambda = 1$, the function has a kink, where the ground state energy is non-analytic. The phase transition is of the continuous type, and the critical exponent for M_x is given by

$$\beta = \frac{1}{8} \quad \Rightarrow \quad |M_x| \propto (\lambda - \lambda_c)^{\frac{1}{8}} \quad (2.44)$$

close to the QCP $\lambda_c = 1$ in the ordered phase [58].

The magnetization in z -direction was also derived in Ref. [53] and is given by another integral expression²

$$M_z = -\frac{1}{2\pi} \int_0^\pi \frac{1 + \lambda \cos(q)}{\omega_q} dq . \quad (2.45)$$

Limit value analysis shows the value at $\lambda = 1$ to be $M_z = -\frac{1}{\pi}$. In Fig. 2.2 both M_x and M_z are plotted.

²In Ref. [53], M_z has the opposite sign because the Hamiltonian is defined with $-T$.

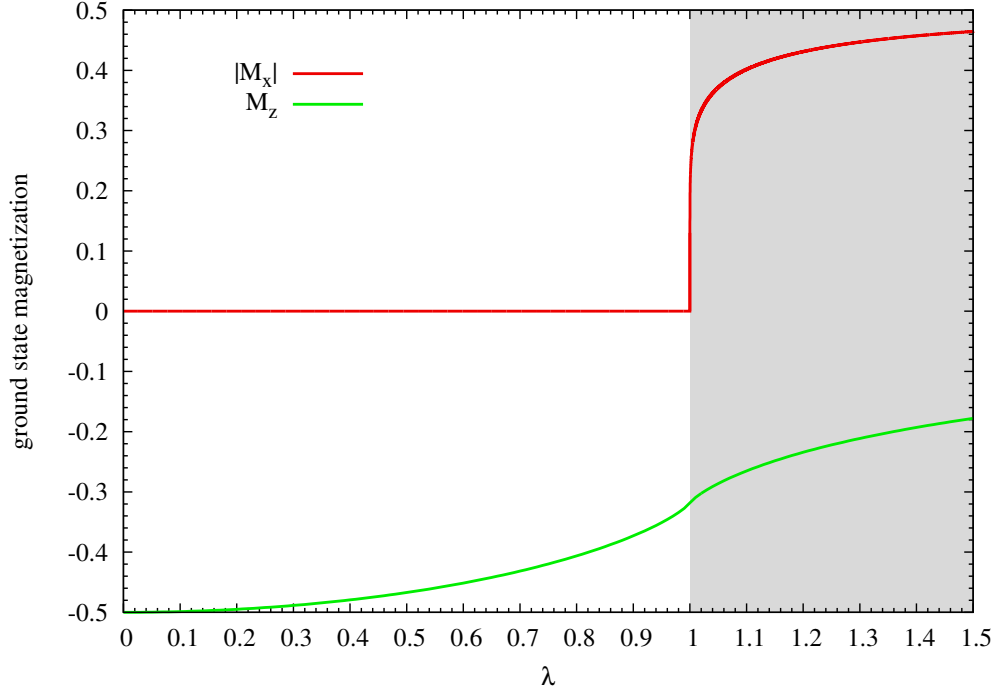


Figure 2.2: Exact ground state magnetizations M_x and M_z of the TFIM

2.2.4 Correlation function

An important quantity when dealing with magnetic phenomena is the spin-spin correlation function in the ground state

$$G_j^{\alpha\beta} := \langle S_0^\alpha S_j^\beta \rangle = \langle GS | S_0^\alpha S_j^\beta | GS \rangle \quad (2.46)$$

where $\alpha, \beta \in \{x, y, z, +, -\}$ and $|GS\rangle$ denotes the ground state. For translation invariant, one-dimensional systems with local interactions and an excitation gap, this ground state correlation function Eq. (2.46) is known to show exponential behavior [59]

$$G_j \propto \exp\left(-\frac{|r_j|}{\xi}\right) \quad (2.47)$$

where ξ is the correlation length. For the 1D TFIM it can be calculated analytically [60] to be

$$\xi = \frac{1}{|\ln \lambda|}. \quad (2.48)$$

An often used approximation for the correlation length in lattice models is $\xi \approx \frac{v}{\Delta}$, where v is obtained by fitting $\omega_q \approx \sqrt{\Delta^2 + (2v \sin(\frac{q}{2}))^2}$ to the minimum and maximum of the dispersion. It is found to be in very good agreement with Eq. (2.48) for $\lambda \gtrsim 0.2$.

The correlation function is also important, as it relates theory to experiment via the dynamic structure factor (DSF) [61]. The DSF is defined as

$$S^{\alpha\beta}(\omega, Q) = \frac{1}{2\pi L} \sum_{i,j} \int_{-\infty}^{\infty} dt e^{i[\omega t + Q(r_i - r_j)]} \langle S_j^\alpha(t) S_i^\beta(0) \rangle \quad (2.49)$$

and describes the measured intensity in neutron scattering experiments. It represents the Fourier transform in space and time of the spin-spin correlation function, of which

Eq. (2.46) is the special case for equal time and zero temperature, where the angular brackets denote the ground state expectation value.

Integrating Eq. (2.49) over frequency yields the static structure factor (SSF)

$$S^{\alpha\beta}(Q) = \frac{1}{L} \sum_{i,j} e^{iQ(r_i-r_j)} \langle S_j^\alpha S_i^\beta \rangle, \quad (2.50)$$

which is the Fourier transform of Eq. (2.46). If the subspaces with different numbers of particles are well separated, the n -particle spectral weight $S_{nP}^{\alpha\beta}(Q)$ can be defined by projecting the SSF onto the n -particles subspace

$$S_{nP}^{\alpha\beta}(Q) = \langle GS | S_{-Q}^\alpha P_{nP}^Q S_Q^\beta | GS \rangle. \quad (2.51)$$

Here S_Q^α is the Fourier transform of the spin operator S_j^α and P_{nP}^Q is the projector on the n -particle subspace with total momentum Q . For the one-particle subspace, the projector is simply

$$P_{1P}^Q = |Q\rangle\langle Q|, \quad (2.52)$$

i.e., the projector on the one-particle state with momentum Q . For the two-particle subspace, the projector is given by

$$P_{2P}^Q = \sum_{\Lambda} |Q,\Lambda\rangle\langle Q,\Lambda| \quad (2.53)$$

where Λ is a quantum number that enumerates the two-particle states with total momentum Q , e.g. relative momentum.

These n -particle spectral weights indicate how much of the integrated intensity $S^{\alpha\beta}(Q)$ at total momentum Q falls into the n -particle sector.

Analytic formulae for the one-particle spectral weights of the TFIM in the disordered phase are given by Hamer et al. in Ref. [52], where they were conjectured from high order series expansions. Their Fourier transforms were derived exactly earlier by Vaidya and Tracy in Ref. [51]. The expression for the spectral weight in the xx -channel reads

$$S_{1P}^{xx}(Q) = \frac{(1-\lambda^2)^{\frac{1}{4}}}{4\omega(Q,\lambda)}, \quad \lambda < 1. \quad (2.54)$$

Reference [51] also states that there is no spectral weight in this channel for $\lambda > 1$.

In the formulation of the TFIM in Jordan-Wigner fermions, the structure factor in the zz -channel can be calculated analytically [62], too. From that it can be shown that all the spectral weight in the zz -channel is contained in the 0QP and 2QP subspaces. Therefore, the 2QP spectral weight can be written down exactly as the complete spectral function minus the projection onto the 0QP sector (i.e. the ground state)

$$S_{2P}^{xx}(Q) = \langle GS | S_{-Q}^z S_Q^z | GS \rangle - \langle GS | S_{-Q}^z | GS \rangle \langle GS | S_Q^z | GS \rangle \quad (2.55a)$$

$$= \frac{1}{L} \sum_{j,k} e^{iQ(j-k)} (\langle GS | S_j^z S_k^z | GS \rangle - \langle GS | S_j^z | GS \rangle \langle GS | S_k^z | GS \rangle) \quad (2.55b)$$

$$= \frac{1}{L} \sum_{j,k} e^{iQ(j-k)} (\langle GS | S_{j-k}^z S_0^z | GS \rangle - \langle GS | S_0^z | GS \rangle^2) \quad (2.55c)$$

$$= \sum_j e^{iQj} (\langle GS | S_j^z S_0^z | GS \rangle - M_z^2) \quad (2.55d)$$

where M_z is the ground state magnetization defined in Eq. (2.45).

Chapter 3

The framework: Matrix product states

*Hilbert space is big. You just won't believe how vastly,
hugely, mind-bogglingly big it is.*

Ashley Milsted et al. after Douglas Adams

This chapter provides an introduction to the method of matrix product states (MPSs). Section 3.2 considers typical applications of the method and shows why it is such a powerful tool. It also examines limitations, where and why it may fail to produce reliable results, and concludes that MPSs are indeed a good choice for the purposes of this thesis. Sections 3.3 through 3.5 introduce the basic concepts of MPSs and matrix product operators (MPOs). These sections are based on the excellent review articles by U. Schollwöck [23] and R. Orús [63]. Readers familiar with the concepts of finite system MPS can skip these sections. In section 3.6 it is shown how the idea of transfer matrices can be adopted to work very efficiently in the thermodynamic limit with MPS. This variant is known as infinite system matrix product state (iMPS). The contents of this chapter are also partly contained in my master's thesis [64] and a condensed version of them was published in Ref. [65].

Remark on the notation: throughout this and all subsequent chapters, the following notation convention will be used. Vectors are typeset using the vector arrow symbol \vec{v} and mostly lowercase Latin letters. Matrices are typeset using plain uppercase Latin letters M . Tensors of higher rank are denoted using uppercase Latin letters in a sans serif font \mathbf{A} . Note that fixing one index of a rank-3 tensor \mathbf{A} , or two indices of a rank-4 tensor \mathbf{W} , yields a rank-2 tensor, which is a matrix and is thus denoted as A^s and $W^{s's}$, respectively.

3.1 The tools

This section contains a number of theorems and definitions which will be referenced frequently throughout this and the following chapters. It also introduces the tensor network (TN) notation, which provides a graphical and intuitive representation of mathematical expressions, somewhat similar to Feynman diagrams.

The key to understanding MPS is the singular value decomposition (SVD) of a matrix.

Theorem 3.1 (Singular value decomposition) For every $m \times n$ complex matrix Ψ there is a decomposition

$$\Psi = USV^\dagger, \quad (3.1)$$

such that U is a $m \times k$ column-orthogonal matrix, V is a $n \times k$ column-orthogonal matrix and S is a $k \times k$ real diagonal matrix with $s_i := S_{ii} \geq 0$, where $k := \min(m, n)$. The diagonal elements of S are called the singular values of Ψ . If they are ordered $s_i \geq s_j$ for $i > j$, S is uniquely determined by Ψ .

Note that $U^\dagger U = \mathbb{1}$ and $V^\dagger V = \mathbb{1}$. Either U or V is a square matrix and therefore unitary. If Ψ is square, then both U and V are unitary and $U^\dagger U = UU^\dagger = V^\dagger V = VV^\dagger = \mathbb{1}$.

The Schmidt decomposition is a restatement of the SVD commonly found in quantum mechanics in connection with entanglement.

Theorem 3.2 (Schmidt decomposition) Let \mathcal{H}_1 and \mathcal{H}_2 be two Hilbert spaces of dimensions m and n , respectively (assume $m \geq n$). Then for every element \vec{w} of the tensor product space $\mathcal{H}_1 \otimes \mathcal{H}_2$ there is a representation

$$\vec{w} = \sum_{i=1}^n s_i \vec{u}_i \otimes \vec{v}_i \quad (3.2)$$

such that the s_i are real and non-negative and as a set uniquely determined by \vec{w} . The sets $\{\vec{u}_i\}$ and $\{\vec{v}_i\}$ are orthonormal bases of \mathcal{H}_1 and \mathcal{H}_2 . The numbers s_i are called Schmidt coefficients of \vec{w} .

The existence of this representation of elements in the tensor product space immediately follows from the existence of the SVD with $s_i = S_{ii}$ and $\{\vec{u}_i\}$ and $\{\vec{v}_i\}$ the columns of the matrices U and V respectively. Without loss of generality, it is assumed that $s_i \geq s_j$ if $j > i$, i.e. the Schmidt coefficients are sorted in descending order. An important quantity in this context is the Schmidt rank.

Definition 3.1 (Schmidt rank) The Schmidt rank of a Schmidt decomposition is defined as the number of non-zero Schmidt coefficients, and the upper bound is the dimension of the smaller of the Hilbert spaces \mathcal{H}_1 and \mathcal{H}_2

$$K := \max_{s_i > 0} i, \quad K \leq \min(\dim(\mathcal{H}_1), \dim(\mathcal{H}_2)). \quad (3.3)$$

Especially in the treatment of MPS for infinite systems, it is often helpful to switch between matrix and vector representations of the same object. For this, the vectorization operator is used.

Definition 3.2 (Vectorization of a matrix) The vectorization of a $m \times n$ matrix A is the mn -dimensional column vector obtained by stacking all columns of the matrix on top of each other, starting from the left

$$\text{vec}(A) = \vec{A} := \begin{pmatrix} \vec{a}_1 \\ \vdots \\ \vec{a}_n \end{pmatrix} \quad (3.4)$$

where \vec{a}_i are the m -dimensional columns of A . The vector $\text{vec}(A)$ can also be interpreted as a $n \times 1$ block matrix of $m \times 1$ blocks. A useful indexing scheme in this context is a

double index (α, α') where α designates the block (i.e. column of A) and α' the element within the block

$$\text{vec}(A)_{(\alpha, \alpha')} = A_{\alpha' \alpha} = A_{\alpha \alpha'}^T. \quad (3.5)$$

By this definition, an element of the Hermitian conjugate vector is given by

$$\text{vec}(A)_{(\alpha, \alpha')}^\dagger = A_{\alpha' \alpha}^*. \quad (3.6)$$

The second notation in Eq. (3.4) with the vector arrow symbol is used when it is clear from context that the object is the vectorization of a matrix. From the vector $\text{vec}(A)$ alone, the dimensions of the matrix A cannot generally be determined. But if $\text{vec}(\cdot)$ is defined as a linear map

$$\text{vec} : \mathbb{C}^{m \times n} \rightarrow \mathbb{C}^{mn}, \quad A \mapsto \text{vec}(A) \quad (3.7)$$

from a matrix space of fixed dimension $m \times n$, it is a bijection and the inverse is given by

$$\text{vec}^{-1} : \mathbb{C}^{mn} \rightarrow \mathbb{C}^{m \times n}, \quad \text{vec}(A) \mapsto A. \quad (3.8)$$

Using the vectorization, a linear map on a matrix space $B : \mathbb{C}^{m \times n} \rightarrow \mathbb{C}^{m \times n}$ can itself be represented as a $n \times n$ block matrix of $m \times m$ blocks. An indexing scheme compatible with Eq. (3.5) is given by $B_{(\alpha, \alpha')(\beta, \beta')}$

$$(B \text{vec}(A))_{(\alpha, \alpha')} = \sum_{\beta=1}^n \sum_{\beta'=1}^m B_{(\alpha, \alpha')(\beta, \beta')} \text{vec}(A)_{(\beta, \beta')} \quad (3.9a)$$

$$= \left(\sum_{\beta=1}^n B_{\alpha\beta} \vec{a}_\beta \right)_{\alpha'} \quad (3.9b)$$

$$\text{with } B = \begin{pmatrix} B_{11} & \cdots & B_{1n} \\ \vdots & \ddots & \vdots \\ B_{n1} & \cdots & B_{nn} \end{pmatrix} \text{ and } \text{vec}(A) = \begin{pmatrix} \vec{a}_1 \\ \vdots \\ \vec{a}_n \end{pmatrix} \quad (3.9c)$$

$$\text{where } B_{\alpha\beta} \in \mathbb{C}^{m \times m} \text{ and } \vec{a}_\beta \in \mathbb{C}^m. \quad (3.9d)$$

For two $m \times n$ matrices A and B the following relation holds

$$\text{vec}(A)^\dagger \text{vec}(B) = \sum_{\alpha=1}^n \sum_{\alpha'=1}^m \text{vec}(A)_{(\alpha, \alpha')}^\dagger \text{vec}(B)_{(\alpha, \alpha')} \quad (3.10a)$$

$$= \sum_{\alpha, \alpha'} A_{\alpha' \alpha}^* B_{\alpha' \alpha} \quad (3.10b)$$

$$= \sum_{\alpha, \alpha'} A_{\alpha \alpha'}^\dagger B_{\alpha' \alpha} \quad (3.10c)$$

$$= \sum_{\alpha} (A^\dagger B)_{\alpha\alpha} \quad (3.10d)$$

$$= \text{Tr}(A^\dagger B). \quad (3.10e)$$

This series of equalities defines a scalar product for $m \times n$ matrices, since $\text{vec}(\cdot)$ is bijective. This scalar product is equivalent to the standard inner product of \mathbb{C}^{nm} and induces the Frobenius norm of matrices.

The tensor network (TN) notation is another important tool in handling MPS. It provides a graphical, intuitive representation of mathematical expressions such as the expansion coefficients in Eq. (3.17) below. In TN notation, each index of a tensor is represented as

a line or “leg” coming out of an icon representing the object. Therefore, a scalar has zero legs, a vector has one, a matrix has two etc. A line connecting two tensors denotes the contraction of (i.e. summation over) one index. Table 3.1 shows some examples of tensor network notation.

Table 3.1: Examples of tensor network notation

$v_i : \bullet -$	Vector (1 leg)
$U_{ij}, S_{jk} : \blacklozenge -$	Matrix (2 legs)
$(US)_{ik} = \sum_j U_{ij} S_{jk} : \blacklozenge - \blacklozenge -$	Matrix (2 legs)
$\text{Tr}(US) = \sum_i (US)_{ii} : \text{---} \text{---} \text{---} \text{---}$	Scalar (0 legs)

3.2 Why matrix product states?

As mentioned above, the DMRG introduced by S.R. White in Ref. [17] is *the* reference method for one-dimensional lattice systems today. Östlund and Rommer showed [19, 20] that in the thermodynamic limit a formulation in the MPS language naturally presents itself. Therefore, we expect very accurate results for one-dimensional systems from MPS calculations. An excellent overview of the formulation of the DMRG, not only for infinite systems, in MPS is given by Schollwöck in Ref. [23].

The reason behind the success of DMRG and subsequently MPS are the so called area laws of entanglement (entropy) [66, 67, 68, 69, 70]. Consider a system that can be divided into two subsystems A and B as seen in Fig. 3.1, where $A \cup B$ is in the thermodynamic limit (TDL).

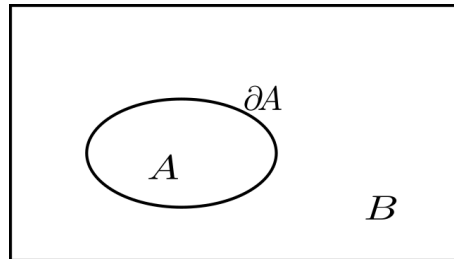


Figure 3.1: Bipartition $A|B$ of a 2D system.

In the one-dimensional case this means that a chain or ribbon is cut at one point or a ring is cut at two points. Let \mathcal{H}_A and \mathcal{H}_B be the Hilbert spaces of subsystems A and B , respectively.

By virtue of the Schmidt decomposition Eq. (3.2), a state of the entire system can be written as

$$|\psi\rangle = \sum_i^K s_i |a_i\rangle \otimes |b_i\rangle \quad (3.11)$$

where $\{|a_i\rangle\}$ and $\{|b_i\rangle\}$ are orthonormal bases of \mathcal{H}_A and \mathcal{H}_B , one of which is incomplete if the dimensions differ, and K is the Schmidt rank of the bipartition $A|B$. Note that

normalization of the state $|\psi\rangle$ implies

$$1 = \langle\psi|\psi\rangle = \sum_{i,i'} s_{i'} s_i \langle b_{i'} | \otimes \langle a_{i'} | a_i \rangle \otimes |b_i\rangle \quad (3.12a)$$

$$= \sum_{i,i'} s_{i'} s_i \langle b_{i'} | b_i \rangle \langle a_{i'} | a_i \rangle \quad (3.12b)$$

$$= \sum_i s_i^2 . \quad (3.12c)$$

The main idea behind DMRG and MPS is to perform a Schmidt decomposition on every bond of a one-dimensional system and to store the Schmidt coefficients and the Schmidt bases for each decomposition. When the limits of computational resources are reached, the Schmidt vectors corresponding to the smallest coefficients s_i are dropped, which leads to truncation errors. Due to the exponential growth of the Hilbert space, truncation becomes necessary already at relatively small system sizes. However, in typical applications the truncation errors are very small, so that systems of several thousands of sites can be treated. Note that these truncations do not reduce the dimension of the physical Hilbert space. An approximate MPS is still a linear combination of all basis states [23]. However, due to the limited number of states in the Schmidt basis, interdependencies of the coefficients for each basis state are generated, which puts restrictions on the forms of the linear combinations that can be expressed.

The quantity

$$S_{\text{vN}} := - \sum_{i \leq K} s_i^2 \ln s_i^2 \quad (3.13)$$

is the so called von Neumann or entanglement entropy [71] of the bipartition $A|B$. In a sense it is a measure of “how quantum” a state is. For a pure (classical) product state, the Schmidt rank of any bipartition is $K = 1$ leading to a von Neumann entropy of

$$S_{\text{vN}} = -1 \ln 1 = 0 . \quad (3.14)$$

Such a state can be described exactly by a MPS, since every Schmidt basis contains only one element. The other extreme is the maximally entangled state, also known as $T = \infty$ state. Here, the Schmidt rank is always maximal and all Schmidt coefficients are equal

$$s_i = \frac{1}{\sqrt{K}} \quad \forall i \quad \text{with } K = \dim(\mathcal{H}) . \quad (3.15)$$

The entanglement entropy is

$$S_{\text{vN}} = - \sum_{i \leq K} \frac{1}{K} \ln \frac{1}{K} = \ln K \propto L . \quad (3.16)$$

This means that even in 1D the maximum entropy still diverges linearly with system size L , i.e., proportional to the volume. Therefore, such a state cannot be described well as MPS, since all Schmidt vectors are equally important. Any truncation is equally bad and will result in relatively large errors.

However, the area laws for entanglement entropy [66, 67, 68, 69, 70] state that for the *low-energy states* of gapped, short ranged Hamiltonians in the TDL, S_{vN} does not grow as the volume of A , but only as the *area* of the boundary. Especially in one dimension, this implies that the entanglement is bounded by a constant. In two dimensions, it is proportional to the boundary ∂A , i.e. the linear extension L of A as seen in Eq. (3.16). Consequently, the

spectrum of the Schmidt decomposition cannot have the form of Eq. (3.15). Rather, the s_i must converge to zero sufficiently fast to yield a constant sum, although the Hilbert space dimension diverges. However, this behavior is a highly exceptional property of the low-energy states. The region of Hilbert space with states that obey an area law is exponentially small [63]. A generic quantum state does therefore indeed exhibit entanglement entropy proportional to the volume of A , as seen for instance in Eq. (3.16).

Analyses on a variety of models show [72, 73, 74, 75] that for the low energy states of gapped 1D systems, the Schmidt coefficients s_i generically decay roughly as $s_i \propto e^{-c \ln^2 i}$. Therefore, truncation errors are small in these cases. This is why the DMRG and subsequently the MPS formalism is so successful in describing the low energy physics of 1D systems. In a 2D system of width W , however, $c \propto \frac{1}{W}$, i.e., the decay becomes slower with growing width, and therefore DMRG becomes inefficient for truly two-dimensional systems. Stripes of finite width or cylinders of finite circumference can be treated rather successfully though [30, 76]. Truly two-dimensional systems require an extension of the ansatz, like, for instance, the PEPS [31, 32] and iPEPS [33] methods. Even time evolution can be implemented rather efficiently [24, 25]. It can be shown [77] that the part of the Hilbert space which can be reached under the time evolution generated by a local Hamiltonian is exponentially small. Therefore, a state that starts in the region of the Hilbert space with exponentially decaying s_i is highly unlikely to leave this region in polynomial time. Often, long time behavior can be accessed analytically, and one is then interested in numerically simulating short time behavior, for which polynomial time scales are sufficient. Because DMRG can be formulated in the MPS language, MPSs share the strengths and weaknesses of DMRG. Since this thesis is concerned with the low-energy physics of spin-chain models, i.e., 1D systems, MPSs indeed provide an excellent framework.

The DMRG was originally developed to overcome the problems that arise when applying Wilson’s numerical renormalization group method [18] to quantum lattice systems [78]. While the derivation is straight forward in this context, it somewhat obscures a very important fact that is much easier to see in the reformulation through MPS: that it is a *variational ansatz* over the class of states that can be described with a fixed maximum Schmidt rank K_{\max} on each bond. The variational parameters are essentially the Schmidt vectors. The quality of the result depends on how close or far the target state is from this class of states. As stated above, product states can be described very well, whereas maximally entangled states can lead to dramatic errors if $\dim(\mathcal{H}) \gg K_{\max}$.

This is the reason why MPS “favor product states”. If, for instance, the ground state is twofold degenerate, the variational algorithm converges to one realization instead of a superposition of both, because the Schmidt coefficients of each single state decay faster than those of a superposition.

Note that in DMRG literature the maximal Schmidt rank K_{\max} is called m , and is identified with the number of eigenvectors of the density matrix ρ that is kept in the description. In newer MPS literature, it is called the “bond dimension” and denoted as D or χ . In this thesis, the symbol D will be used following the notation of Ref. [23].

As a variational method, the MPS framework has two inherent strengths. First, in a ground state search, it is guaranteed to yield an upper bound for the ground state energy (up to machine precision) by virtue of Ritz’ variation principle. Secondly, it is largely unbiased; this means no knowledge of the system required. Although exploiting known quantum symmetries in the code can lead to substantial speedups, doing so is not a necessity. This avoids biasing the result by starting from possibly incorrect assumptions on the physical behavior of the system, or getting stuck in a certain symmetry sector by choosing disadvantageous initial conditions.

3.3 Definition of MPS

The concept of MPS presents a formulation of quantum mechanics in the Schrödinger picture that proves to be particularly well suited for variational approaches. A MPS for a quantum system with L degrees of freedom is defined as

$$|\psi\rangle = \sum_{s_1, s_2, \dots, s_L} \text{Tr}(A^{s_1} A^{s_2} \dots A^{s_L}) |s_1, s_2, \dots, s_L\rangle \quad (3.17)$$

where A^{s_i} are matrices, s_i enumerates the i -th quantum number and $|s_1, s_2, \dots, s_L\rangle$ is an orthonormal basis (ONB) of the Hilbert space. This means the state $|\psi\rangle$ is expanded in some ONB and the expansion coefficients are given by the trace of products of matrices. The next sections explain why this is a useful definition.

3.4 Construction of canonical MPS

Consider an arbitrary pure state $|\psi\rangle$ of a quantum system with L quantum numbers

$$|\psi\rangle = \sum_{s_1, \dots, s_L} c_{s_1, \dots, s_L} |s_1, \dots, s_L\rangle \quad (3.18)$$

which is assumed to be normalized. The s_i can be any quantum numbers characterizing a state of the system. Because this thesis deals with one-dimensional spin models on spatially fixed lattices, from here on the s_i will mostly be the z -component of spin i . In a multi-site unit cell, for instance in a dimer or ladder model, s_i labels the states of each unit cell. Therefore, only the case where all s_i take d possible values is considered. Here d is the dimension of the local Hilbert space of a single spin or a unit cell, respectively. For the sake of simplicity, the unit cells will just be called *sites* or *lattice sites*. Keep in mind though that a site can be a site of a super-lattice.

The states $|s_1, \dots, s_L\rangle$ denote an ONB of the Hilbert space. For the lattice systems under consideration, the most intuitive choice is the tensor product of the bases of the local Hilbert spaces

$$|s_1, \dots, s_L\rangle = |s_1\rangle \otimes |s_2\rangle \otimes \dots \otimes |s_L\rangle. \quad (3.19)$$

Such an ONB always exists, and the actual form of the $\{|s_i\rangle\}$ enters the calculation only through the choice of the matrix representation of operators in the local Hilbert space of one unit cell. For instance, by representing the spin- $\frac{1}{2}$ operators in Eq. (2.25) with the usual Pauli matrices, the eigenbasis of the S^z operator is chosen as local basis.

Thus, for a chain of length L , there are d^L coefficients c_{s_1, \dots, s_L} in Eq. (3.18). As these coefficients are (possibly time-dependent) \mathbb{C} -numbers, they can be understood as the components of a d^L -dimensional vector or, equivalently, as the elements of a $d \times d^{L-1}$ matrix Ψ

$$c_{s_1, \dots, s_L} = \Psi_{(s_1), (s_2, \dots, s_L)}. \quad (3.20)$$

Now the SVD is applied to this Ψ , yielding

$$c_{s_1, \dots, s_L} = \Psi_{(s_1), (s_2, \dots, s_L)}^{[1]} = \left(U^{[1]} S^{[1]} V^{[1]\dagger} \right)_{(s_1), (s_2, \dots, s_L)} \quad (3.21a)$$

$$= \sum_{\alpha_1=1}^{K_1} U_{s_1, \alpha_1}^{[1]} S_{\alpha_1, \alpha_1}^{[1]} V_{\alpha_1, (s_2, \dots, s_L)}^{[1]\dagger}, \quad (3.21b)$$

where $K_1 \leq d$ is the Schmidt rank of the decomposition across the bond 1 – 2. In the following calculations, it will be assumed that the Schmidt ranks K_i take the maximum

value, which is the lesser of the dimensions of $\Psi^{[i]}$. Then theorem 3.1 states that $U^{[1]}$ and $S^{[1]}$ are of dimension $d \times d$ and $V^{[1]\dagger}$ is of dimension $d \times d^{L-1}$.

The matrix $U^{[1]}$ has d rows addressed by the index s_1 , each row corresponding to a physical state of lattice site 1. The index s_1 is therefore called the physical index. Hence, one can also interpret $U^{[1]}$ as a set of d matrices of dimension $1 \times d$

$$U^{[1]} = \begin{pmatrix} U_{1,1}^{[1]} & \cdots & U_{1,d}^{[1]} \\ \vdots & & \vdots \\ U_{d,1}^{[1]} & \cdots & U_{d,d}^{[1]} \end{pmatrix} \rightarrow \left\{ \begin{pmatrix} U_{1,1}^{[1]}, \dots, U_{1,d}^{[1]} \\ \vdots \\ U_{d,1}^{[1]}, \dots, U_{d,d}^{[1]} \end{pmatrix} \right\} =: \left\{ \begin{matrix} A^{s_1=1} \\ \vdots \\ A^{s_1=d} \end{matrix} \right\}. \quad (3.22)$$

Next, a new matrix $\Psi^{[2]}$ is defined by reshaping the product $S^{[1]}V^{[1]\dagger}$ into a $d^2 \times d^{L-2}$ matrix

$$\Psi_{(s_2, \alpha_1), (s_3, \dots, s_L)}^{[2]} := (S^{[1]}V^{[1]\dagger})_{\alpha_1, (s_2, \dots, s_L)}. \quad (3.23)$$

Applying the SVD again yields

$$\Psi_{(s_2, \alpha_1), (s_3, \dots, s_L)}^{[2]} = (U^{[2]}S^{[2]}V^{[2]\dagger})_{(s_2, \alpha_1), (s_3, \dots, s_L)} \quad (3.24a)$$

$$= \sum_{\alpha_2=1}^{d^2} U_{(s_1, \alpha_1), \alpha_2}^{[2]} S_{\alpha_2, \alpha_2}^{[2]} V_{\alpha_2, (s_3, \dots, s_L)}^{[2]\dagger}. \quad (3.24b)$$

Again, the matrix $U^{[2]}$ has a block structure

$$U^{[2]} = \begin{pmatrix} U_{(1,1),1}^{[2]} & \cdots & U_{(1,1),d^2}^{[2]} \\ \vdots & & \vdots \\ U_{(1,d),1}^{[2]} & \cdots & U_{(1,2),d^2}^{[2]} \\ U_{(2,1),1}^{[2]} & \cdots & U_{(2,1),d^2}^{[2]} \\ \vdots & & \vdots \\ U_{(d,d),1}^{[2]} & \cdots & U_{(d,d),d^2}^{[2]} \end{pmatrix} \rightarrow \left\{ \begin{pmatrix} U_{(1,\alpha_1),1}^{[2]}, \dots, U_{(1,\alpha_1),d}^{[2]} \\ \vdots \\ U_{(d,\alpha_1),1}^{[2]}, \dots, U_{(d,\alpha_1),d}^{[2]} \end{pmatrix} \right\} =: \left\{ \begin{matrix} A^{s_2=1} \\ \vdots \\ A^{s_2=d} \end{matrix} \right\} \quad (3.25)$$

where the blocks are now indexed by s_2 and each block is of dimension $d \times d^2$ with indices α_1 and α_2 . This can also be interpreted as a rank-3 tensor $\mathbf{A}^{[2]}$ with elements

$$\mathbf{A}_{\alpha_1, \alpha_2}^{s_2} := U_{(s_2, \alpha_1), \alpha_2}. \quad (3.26)$$

In TN notation, this is represented by an object with three legs

$$\mathbf{A}_{\alpha_{i-1}, \alpha_i}^{s_i} = \begin{array}{c} | \\ \bullet \\ \text{---} \end{array}, \quad \mathbf{A}_{\alpha_{i-1}, \alpha_i}^{s_i *} = \begin{array}{c} \text{---} \\ \bullet \\ | \end{array} \quad (3.27)$$

where the ‘‘physical’’ index, i.e. the one enumerating the local quantum states, is taken to be the vertical leg. For the complex conjugate of the tensor, the physical index leg is drawn upside down. The reason for this will become clear later. Although a three-leg object strictly speaking denotes a rank-3 tensor, from here on it will often be identified with a matrix A^{s_i} that depends on the site i and its physical state s_i .

The procedure of taking the product $S^{[i-1]}V^{[i-1]\dagger}$, which is of dimension $d^m \times d^{L-(i-1)}$, reshaping it to a matrix $\Psi^{[i]}$ of dimension $d^{m+1} \times d^{L-i}$, and applying the SVD can be repeated until $i = L$ is reached. In each step, a matrix $U^{[i]}$ of dimension $d^{m+1} \times d^k$ is

obtained, which can be reinterpreted as a rank-3 tensor $\mathbf{A}^{[i]}$ of dimension $d \times d^m \times d^k$. A short calculation reveals that for L even

$$m = \begin{cases} i-1, & \text{if } i \leq \frac{L}{2} + 1 \\ L - (i-1), & \text{if } i > \frac{L}{2} + 1 \end{cases} \quad \text{and} \quad k = \begin{cases} i, & \text{if } i \leq \frac{L}{2} \\ L - i, & \text{if } i > \frac{L}{2} \end{cases} \quad (3.28)$$

and for L odd

$$m = \begin{cases} i-1, & \text{if } i \leq \lceil \frac{L}{2} \rceil \\ L - (i-1), & \text{if } i > \lceil \frac{L}{2} \rceil \end{cases} \quad \text{and} \quad k = \begin{cases} i, & \text{if } i \leq \lfloor \frac{L}{2} \rfloor \\ L - i, & \text{if } i > \lfloor \frac{L}{2} \rfloor \end{cases} \quad (3.29)$$

where $\lceil \cdot \rceil$ and $\lfloor \cdot \rfloor$ denote rounding to the nearest higher and lower integer, respectively. Fixing the physical index s_i of this tensor reduces it to a $d^m \times d^k$ matrix A^{s_i} . For these matrices, the above dimension analysis yields the maximum dimensions

$$(1 \times d)(d \times d^2) \dots (d^{L/2-1} \times d^{L/2})(d^{L/2} \times d^{L/2-1}) \dots (d^2 \times d)(d \times 1) \quad (3.30)$$

for even L and

$$(1 \times d)(d \times d^2) \dots (d^{L/2-1} \times d^{L/2})(d^{L/2} \times d^{L/2})(d^{L/2} \times d^{L/2-1})(d^2 \times d)(d \times 1) \quad (3.31)$$

for odd L . From the SVD there are leftover matrices $S^{[L]}$ and $V^{[L]\dagger}$, both of dimension 1×1 . Since $V^{[L]\dagger}$ must be unitary, it must have absolute value 1. The non-negative number $S^{[L]}$ is the norm of the state $|\psi\rangle$. If it is not 1, it can be reabsorbed into A^{s_L} along with $V^{[L]\dagger}$.

Thus, one can now identify

$$c_{s_1, \dots, s_L} = A^{s_1} A^{s_2} \dots A^{s_L} . \quad (3.32)$$

This means that for each coefficient c_{s_1, \dots, s_L} , the physical indices on all the $\mathbf{A}^{[i]}$ tensors are fixed, leaving a product of L matrices. This already looks very much like the coefficients in Eq. (3.17), except for the trace. Note that in the construction described above, the matrix indices α_1 on A^{s_1} and α_{L+1} on A^{s_L} are ‘‘dummy’’ indices. They can only take the value 1, i.e., A^{s_1} is a row vector and A^{s_L} is a column vector. Therefore, the matrix product in Eq. (3.32) is a scalar, and the trace operation could be added without changing anything.

The MPS constructed in this way is called *left-normalized*, since by construction on every lattice site i (except possibly the last), the matrices A^{s_i} fulfill the relation

$$\sum_{s_i} A^{s_i \dagger} A^{s_i} = U^{[i]\dagger} U^{[i]} = \mathbf{1} \quad \forall i (< L) , \quad (3.33)$$

i.e., the sum over A^{s_i} multiplied with its Hermitian conjugate from the left yields the identity, hence left-normalized. However, this is not always true for multiplication of A^{s_i} with $A^{s_i \dagger}$ from the *right*

$$\sum_{s_i} A^{s_i} A^{s_i \dagger} = U^{[i]} U^{[i]\dagger} \neq \mathbf{1} , \quad (3.34)$$

because for $i > \frac{L}{2}$ the matrix $U^{[i]}$ is no longer square and therefore not unitary. The matrices A^{s_L} must account for the norm of the state, and therefore fulfill Eq. (3.33) only if $|\psi\rangle$ is normalized.

To see that Eq. (3.33) implies normalization, consider the norm

$$\langle \psi | \psi \rangle = \sum_{s_{1'}, \dots, s_{L'}} \sum_{s_1, \dots, s_L} c_{s_{1'}, \dots, s_{L'}}^* c_{s_1, \dots, s_L} \langle s_{1'}, \dots, s_{L'} | s_1, \dots, s_L \rangle \quad (3.35a)$$

$$= \sum_{s_1, \dots, s_L} c_{s_1, \dots, s_L}^* c_{s_1, \dots, s_L} \quad (3.35b)$$

$$= \sum_{s_1, \dots, s_L} (A^{s_L \dagger} \dots A^{s_1 \dagger})(A^{s_1} \dots A^{s_L}) \quad (3.35c)$$

$$= \sum_{s_L} A^{s_L \dagger} \dots \underbrace{\left(\sum_{s_1} A^{s_1 \dagger} A^{s_1} \right)}_{=1} \dots A^{s_L} = 1 \quad (3.35d)$$

which relies on the fact that for scalars, complex conjugation equals Hermitian conjugation, and $(AB)^\dagger = B^\dagger A^\dagger$. An MPS where all A^{s_i} are left normalized is referred to as *left-canonical*.

While the SVD construction starting from the left is an obvious choice, it is not the only possibility. A SVD construction starting from the right side is just as valid. Here the matrices $U^{[i]}$ and $V^{[i]\dagger}$ interchange their roles, and the matrix $\tilde{\Psi}^{[i]}$ is formed by reshaping the product $U^{[i]} S^{[i]}$ accordingly. This results in *different* tensors $\tilde{\mathbf{A}}^{[i]}$ of the same dimensions as $\mathbf{A}^{[i]}$ which still describe the expansion coefficients as

$$c_{s_1, \dots, s_L} = \tilde{A}^{s_1} \dots \tilde{A}^{s_{L-1}} \tilde{A}^{s_L}. \quad (3.36)$$

By construction, these \tilde{A}^{s_i} are then *right-normalized*

$$\sum_{s_i} \tilde{A}^{s_i} \tilde{A}^{s_i \dagger} = V^{[i]\dagger} V^{[i]} = \mathbb{1} \quad \forall i (> 1) \quad (3.37)$$

i.e. the sum over the matrices A^{s_i} multiplied from the *right* by their Hermitian conjugates yields the identity. Reversing the order of c^* and c , the argument in Eqs. (3.35) also holds true for this type of matrix assuming a normalized state. A MPS where all A^{s_i} are right normalized is called *right canonical* accordingly.

Mixed-canonical states, where the SVD construction is carried out from *both* ends, are a less obvious but sometimes useful choice. In this case, there is again a “left over” matrix of singular values $S^{[j]}$ at the point where the left and right canonical parts meet. Then, the norm is given by

$$\langle \psi | \psi \rangle = \text{Tr}(\langle \psi | \psi \rangle) \quad (3.38a)$$

$$= \text{Tr} \left[\sum_{s_1, \dots, s_L} (\tilde{A}^{s_L \dagger} \dots \tilde{A}^{s_{j+1} \dagger} S^{[j]\dagger} A^{s_{j-1} \dagger} \dots A^{s_1 \dagger})(A^{s_1} \dots A^{s_{j-1}} S^{[j]} \tilde{A}^{s_{j+1}} \dots \tilde{A}^{s_L}) \right] \quad (3.38b)$$

$$= \text{Tr} \left[\sum_{s_1, \dots, s_L} S^{[j]\dagger} (A^{s_{j-1} \dagger} \dots A^{s_1 \dagger} A^{s_1} \dots A^{s_{j-1}}) S^{[j]} (\tilde{A}^{s_{j+1}} \dots \tilde{A}^{s_L} \tilde{A}^{s_L \dagger} \dots \tilde{A}^{s_{j+1} \dagger}) \right] \quad (3.38c)$$

$$= \text{Tr} [S^{[j]\dagger} \mathbb{1} S^{[j]} \mathbb{1}] \quad (3.38d)$$

$$= \text{Tr}((S^{[j]})^2) \quad (3.38e)$$

$$\stackrel{!}{=} 1. \quad (3.38f)$$

This relates back to the Schmidt decomposition and the requirement of Eq. (3.12).

A fourth way to represent a MPS will be referred to as *composite canonical* representation. In the construction of left and right canonical MPS by SVD, the matrix of Schmidt coefficients $S^{[i]}$ is multiplied into either $V^{[i]\dagger}$ or $U^{[i]}$ in each step, and then the product is reshaped for the next step. However, one can just keep the matrices $S^{[i]}$ as separate entities which can be associated with the bonds. The remaining rank-3 tensors $\Gamma^{[i]}$ are then said to “live” on the sites only. In TN notation, a composite canonical MPS has the following form:

$$|\psi\rangle = \begin{array}{c} \bullet \quad \blacklozenge \quad \bullet \quad \blacklozenge \quad \cdots \quad \bullet \quad \blacklozenge \quad \bullet \\ \Gamma^{s_1} \quad S^{[1]} \quad \Gamma^{s_2} \quad S^{[2]} \quad \cdots \quad S^{[L-1]} \quad \Gamma^{s_L} \end{array} . \quad (3.39)$$

This representation is especially useful in the context of infinite systems and will be discussed in more detail in Sec. 3.6.4.

All these different MPS representations derived from the same coefficient vector show that a MPS is *not* uniquely determined by the coefficients c_{s_1, \dots, s_L} . Generally, there are many gauge degrees of freedom in the MPS representation. On every bond, an invertible matrix $X^{[i]}$ can be introduced such that

$$c_{s_1, \dots, s_L} = A^{s_1} A^{s_2} \dots A^{s_L} \quad (3.40a)$$

$$= A^{s_1} X^{[1]} (X^{[1]})^{-1} A^{s_2} X^{[2]} (X^{[2]})^{-1} \dots X^{[L-1]} (X^{[L-1]})^{-1} A^{s_L} \quad (3.40b)$$

$$= \bar{A}^{s_1} \bar{A}^{s_2} \dots \bar{A}^{s_L} , \quad (3.40c)$$

where the transformed matrices \bar{A}^{s_i} are given by $\bar{A}^{s_i} := (X^{[i-1]})^{-1} A^{s_i} X^{[i]}$, and the missing matrices at the the end are defined as $X^{[-1]} = X^{[L]} = 1$.

In TN notation, Eq. (3.32) is represented by

$$c_{s_1, \dots, s_L} \Big|_{\text{OBC}} = \begin{array}{c} \bullet \quad \bullet \quad \bullet \quad \bullet \quad \bullet \quad \bullet \\ A^{s_1} \quad A^{s_2} \quad \cdots \quad A^{s_L} \end{array} \quad (3.41)$$

The beauty of the TN notation is that if one draws what periodic boundary conditions mean, namely a connection between the first and the last lattice site

$$c_{s_1, \dots, s_L} \Big|_{\text{PBC}} = \begin{array}{c} \bullet \quad \bullet \quad \bullet \quad \bullet \quad \bullet \quad \bullet \\ A^{s_1} \quad A^{s_2} \quad \cdots \quad A^{s_L} \end{array} \quad (3.42a)$$

$$= \text{Tr}(A^{s_1} A^{s_2} \dots A^{s_L}) , \quad (3.42b)$$

it immediately translates into the correct mathematical description. The example in table 3.1 shows that connecting the two legs of a matrix corresponds to taking the trace. This means that Eq. (3.17) holds for both OBC and PBC.

Note that the coefficient vector c_{s_1, \dots, s_L} can describe a state with either OBC or PBC, therefore Eq. (3.32) technically holds for both cases, too. However, the distinct forms of the matrices at the boundaries of the MPS description are inconvenient for PBCs.

For a periodic system, the lattice sites are all equivalent. This means that in this case a description where all matrices A^{s_i} are of the same dimension is much more practical. An exact construction from a given coefficient vector c_{s_1, \dots, s_L} is not as straight forward in this case.

However, the SVD construction from a coefficient vector only serves to show that the MPS representation is indeed a valid formulation of quantum states. It does not represent, how computations in the MPS framework are done because generally the c_{s_1, \dots, s_L} are either unknown or cannot be represented on a classical computer, or both.

So far, only exact transformations were performed, so there is no gain compared to exact diagonalization. The true power of the method lies in the possibility to restrict the bond dimension, i.e. the matrix size, to a manageable number $D \ll d^{L/2}$. Especially for PBC, it is clear that this systematically affects *all* lattice sites in the same way. In the case of OBC, at least all sites in the bulk, i.e., with matrix dimension larger than D , are affected in the same way. This systematic truncation allows DMRG and MPS calculations on systems with several thousand sites in spite of their humongous Hilbert spaces.

3.5 Matrix product operators

Having defined MPSs as a way to handle quantum mechanical wavefunctions which is suited well for variational algorithms, a matching definition for operators is needed to carry out computations. This matching definition is that of matrix product operators (MPOs). In general, the framework of MPOs for finite systems is very powerful, but also rather involved. For a more detailed introduction to the topic, the reader is referred to Ref. [23].

However, since the method described in this thesis aims at the thermodynamic limit, only one class of operators needs to be discussed. This is the class of local operators which act on a finite and small number of sites n

$$\hat{O} = V_{i, \dots, i+n} \hat{O}_i \hat{O}_{i+1} \cdots \hat{O}_{i+n}, \quad \text{with } n \in \mathcal{O}(D), \quad (3.43)$$

where each factor \hat{O}_i in the product acts on a single site, and $V_{i, \dots, i+n} \in \mathbb{C}$ can be a coupling constant.

The Hamiltonians in Chapter 2 consist of this type of operator and also the observables of interest are of this form.

In a discrete and finite Hilbert space, a wavefunction can be described by the expansion coefficients with respect to a certain ONB c_{s_1, \dots, s_L} . Similarly, an operator is described by its matrix elements with respect to this ONB. Generically, a MPO can be expressed as a product of rank-4 tensors $W_{\alpha_{i-1} \alpha_i}^{s'_i, s_i}$

$$\hat{O} = \sum_{s'_1, \dots, s'_L} \sum_{s_1, \dots, s_L} W^{s'_1, s_1} W^{s'_2, s_2} \cdots W^{s'_L, s_L} |s'_1, \dots, s'_L\rangle \langle s_1, \dots, s_L|, \quad (3.44)$$

i.e., for fixed sets of physical indices $\{s'_i\}$ and $\{s_i\}$, the operator is represented as a product of L matrices $W^{s'_i, s_i}$ which are non-trivial to obtain.

However, for an operator that acts on a single site j , all tensors $W^{[i]}$ are identity tensors except for the one at site j . On this site j , the matrices $W^{s'_j, s_j}$ are of dimension 1×1 and are simply the matrix elements $O_{s'_j, s_j}$ of the operator with respect to the local basis $\{|s_j\rangle\}$ of site j .

Computing the matrix element of such a one-site MPO with respect to two MPSs $|\psi\rangle$ and

$|\tilde{\psi}\rangle$ corresponds to evaluating the following TN

$$\langle \tilde{\psi} | \hat{O}_j | \psi \rangle = \text{Diagram} \quad (3.45)$$

In the discussion of TNs such as the one in Eq. (3.45), it is often useful to put the result under a trace operation. This does not change the result, because it is a scalar

$$\text{Tr} z = z \quad \forall z \in \mathbb{C}, \quad (3.46)$$

but allows the use of the cyclic property of the trace to rearrange the involved matrix products. It also allows the use of the following identity for the traces of two matrices A and B

$$\text{Tr} A \cdot \text{Tr} B = \text{Tr}(A \otimes B) = \text{Tr}(B \otimes A) \quad (3.47)$$

where \otimes denotes the Kronecker product, i.e., the tensor product for matrices.

Using Eqs. (3.46) and (3.47), Eq. (3.45) translates to

$$\langle \tilde{\psi} | \hat{O}_i | \psi \rangle = \text{Tr} \left[\left(\sum_{s_1} \tilde{A}^{s_1*} \otimes A^{s_1} \right) \cdots \left(\sum_{s_i, s'_i} O_{s'_i, s_i} \tilde{A}^{s'_i*} \otimes A^{s_i} \right) \cdots \left(\sum_{s_L} \tilde{A}^{s_L*} \otimes A^{s_L} \right) \right]. \quad (3.48)$$

This also shows that the proper product to use when contracting physical indices is the Kronecker product \otimes . It is easy to see that for the matrix element of an operator which consists of a product of local operators, for instance

$$\hat{O}_i = \hat{S}_i^x \hat{S}_{i+1}^x \quad (3.49)$$

this scheme straight forwardly extends to

$$\langle \tilde{\psi} | \hat{O} | \psi \rangle = \text{Diagram} \quad (3.50a)$$

$$\begin{aligned} &= \text{Tr} \left[\left(\sum_{s_1} \tilde{A}^{s_1*} \otimes A^{s_1} \right) \cdots \left(\sum_{s_i, s'_i} S_{s'_i, s_i}^x \tilde{A}^{s'_i*} \otimes A^{s_i} \right) \right. \\ &\quad \left. \times \left(\sum_{s_{i+1}, s'_{i+1}} S_{s'_{i+1}, s_{i+1}}^x \tilde{A}^{s'_{i+1}*} \otimes A^{s_{i+1}} \right) \cdots \left(\sum_{s_L} \tilde{A}^{s_L*} \otimes A^{s_L} \right) \right]. \end{aligned} \quad (3.50b)$$

This “trick” of using the trace operation to write a matrix element or overlap as a matrix product of Kronecker products is especially useful in the thermodynamic limit, as will be shown in the next section.

Note that the “hat symbol” is used to distinguish operators \hat{O} from matrices for conceptual reasons. On finite, discrete Hilbert spaces, operators always have a matrix representation, so that the term *operator* is mostly interchangeable with *operator matrix*. The elements of an operator matrix are denoted using the same letter which is used for the operator without the hat symbol.

3.6 The thermodynamic limit: iMPS

So far, MPSs for finite systems have been discussed, since they arise intuitively from the introduction of the concept by SVD of the coefficient vector c_{s_1, \dots, s_L} . This section describes how the idea can be extended to the thermodynamic limit and which restrictions this extension imposes on the kind of systems that can be treated.

3.6.1 Limitations of iMPS

Starting from the MPS formulation for PBC with matrices of the same dimension for every site, the extension to the thermodynamic limit is quite straight forward. One can simply view the MPS as consisting of an infinite number of \mathbf{A} -tensors, one for each lattice site. Obviously, in general an infinite number of tensors cannot be treated numerically. But by sacrificing some of the universality of the MPS ansatz, the thermodynamic limit can be treated very efficiently.

Specifically, the first restriction which must be made is that to short ranged Hamiltonians. This means any Hamiltonian, that couples lattice sites only over finite distances¹. This is in contrast to finite systems, where long-range interactions such as the Coulomb interaction can also be treated [79]. While this is a substantial limitation in theory, most real many body systems exhibit short-ranged interactions due to shielding effects. The class of local Hamiltonians therefore holds a host of models that are both close to experiment and show all kinds of interesting physical properties.

Secondly, the approach is limited to translation invariant systems. This restriction is not very severe, since usually, when taking the thermodynamic limit, one is interested in the bulk properties of periodic structures. It also does not mean that only one-site periodicity can be treated. Any finite size unit cell is possible in principle, as long as it is repeated periodically. The physical dimension d of the tensor \mathbf{A} describing each unit cell then grows as the size of the unit cell increases.

The final restriction and the key to the treatment of the thermodynamic limit is the assumption that the ground state does not spontaneously break translation symmetry, i.e., *all* unit cells can be described by the *same* \mathbf{A} -tensor. This type of MPS is referred to as uniform matrix product state (uMPS). In many cases this is true. However, this implies that the boundary conditions are irrelevant. This condition is fulfilled if the ground state shows finite or exponentially decaying correlations. Then, there are only a few sites that are influenced by boundary effects and the bulk properties are independent of them.

As a counter example, one think of a spin chain that shows Peierls type behavior, i.e., spontaneous dimerization. The dimers can form on the odd bonds or on the even bonds, making the sites distinguishable between even and odd. The ground state which the system actually chooses may very well depend on the boundary conditions. In the bulk, a lattice translation by one site (which is *half* a dimer) transforms one ground state into the other. Therefore, a uMPS still captures the bulk properties of either ground state realization. However, it does *not* generally account for the twofold degeneracy. But this degeneracy is of great physical importance, as it means the lowest excitations are domain walls between sections of the two different ground states, and they cannot be created by a local operation. That being said, some types of ground state degeneracy can still be handled with iMPS. An explicit ansatz for domain wall excitations can be made if the ground state is known to be degenerate, and different realizations can be distinguished by an observable, for instance the magnetization in the ordered phase of the TFIM. See App. A.5 for details.

¹In practice, this also includes exponentially decaying interactions, as the coupling strength then quickly approaches machine precision as function of site distance.

3.6.2 Definitions: uMPS and iMPS

If the conditions outlined in 3.6.1 are met, a new ansatz for the uniform matrix product state (uMPS) can be made

$$|\psi\rangle = \sum_{s_1, \dots, s_L} \text{Tr}(QA^{s_1} \cdots A^{s_L}) |s_1, \dots, s_L\rangle. \quad (3.51)$$

This ansatz still contains infinitely many A tensors of equal size. The handling of the boundary conditions is moved to the *boundary operator* Q , and the trace is required to make the coefficients scalar. For PBC, the boundary operator is just the $D \times D$ identity matrix, as can readily be seen from Eq. (3.42). In the case of OBC, the actual form of Q is less clear. For the moment, assume that it contains information on all lattice sites which are influenced by boundary effects. Since these sites differ from the bulk in their properties, they cannot be adequately described by the uMPS tensor. As discussed above there are, however, only a finite number of these sites, and it will be shown that the specific form of Q does not matter in the TDL.

The key to handling uMPS is the idea of transfer matrices, which is famous at least since L. Onsager's solution of the 2D Ising model [80]. To see how transfer matrices arise in the context of uMPS, consider the norm of the state in Eq. (3.51)

$$\langle \psi | \psi \rangle = \sum_{s_1, \dots, s_L, s'_1, \dots, s'_L} \text{Tr}(Q^* A^{s'_1} \cdots A^{s'_L}) \text{Tr}(QA^{s_1} \cdots A^{s_L}) \underbrace{\langle s'_1, \dots, s'_L | s_1, \dots, s_L \rangle}_{\delta_{s'_1 s_1} \cdots \delta_{s'_L s_L}} \quad (3.52a)$$

$$= \text{Tr} \left[(Q^* \otimes Q) \left(\sum_s A^{s_1*} \otimes A^{s_1} \right) \cdots \left(\sum_s A^{s_L*} \otimes A^{s_L} \right) \right]. \quad (3.52b)$$

Since the A tensors are the same on all lattice sites, this can be written concisely as

$$\langle \psi | \psi \rangle = \text{Tr}(\tilde{Q} T^L) \quad (3.53)$$

where $\tilde{Q} := Q^* \otimes Q$ and the object T , which is a matrix of dimension $D^2 \times D^2$, is defined by

$$T := \sum_s A^{s*} \otimes A^s = \begin{array}{c} \bullet \\ | \\ \bullet \end{array}. \quad (3.54)$$

It is called the transfer matrix or transfer operator. The name derives from the notion that an application of T which corresponds to one “rung” in a TN as shown in Eq. (3.45) transfers the properties of the TN “ladder” by one lattice site to the left or to the right.

To further analyze the expression in Eq. (3.53), T is decomposed into the spectral representation

$$T = \sum_i \Lambda_i \vec{v}_i \vec{u}_i^\dagger \quad (3.55)$$

where Λ_i are the eigenvalues and \vec{u}_i and \vec{v}_i the corresponding left and right eigenvectors of T fulfilling the following equations

$$\vec{u}_i^\dagger T = \Lambda_i \vec{u}_i^\dagger \quad \text{and} \quad T \vec{v}_i = \Lambda_i \vec{v}_i. \quad (3.56)$$

Generally, T is not Hermitian and thus $\vec{u}_i \neq \vec{v}_i$. The left and right eigenvectors are still pairwise orthogonal though, and are assumed to be normalized, i.e.,

$$\vec{u}_i^\dagger \vec{v}_j = \vec{v}_j^\dagger \vec{u}_i = \delta_{ij}. \quad (3.57)$$

The matrix T not being Hermitian also means that the eigenvalues are not necessarily real. For the complete spectral representation to exist, T must be diagonalizable, which is not guaranteed. However, this is not necessary. If T is not diagonalizable, a generalized spectral representation can be constructed using generalized eigenvectors, and the arguments below still hold. The only assumption that must be made is that the largest modulus eigenvalue (EV) Λ_0 of T is real, positive and unique, i.e.,

$$\Lambda_0 \in \mathbb{R}^+, |\Lambda_i| < \Lambda_0 \quad \forall i \neq 0. \quad (3.58)$$

The dyadic products $\vec{v}_i \vec{u}_i^\dagger =: P_i$ are projectors onto the eigenspace of T corresponding to eigenvalue Λ_i . As such, they have the projector properties $P_i^2 = P_i$ and $P_i P_j = 0$ for $j \neq i$. From these follows that

$$T^L = \sum_i \Lambda_i^L P_i = \sum_i \Lambda_i^L \vec{v}_i \vec{u}_i^\dagger. \quad (3.59)$$

Therefore, for the norm in Eq. (3.53) to be well-defined in the thermodynamic limit $L \rightarrow \infty$, two conditions must be met. The first is stated in (3.58). In this case, Λ_0 can be renormalized to 1 by setting

$$A^s \rightarrow \frac{A^s}{\sqrt{\Lambda_0}} \quad \Rightarrow \quad T \rightarrow \frac{T}{\Lambda_0} \quad (3.60)$$

so that

$$\lim_{L \rightarrow \infty} \Lambda_0^L = 1 \quad (3.61)$$

which is the only finite and well-defined value for this limit. This condition is fulfilled by all models considered in this thesis, and it is therefore assumed to hold. However, there is no rigorous mathematical statement that ensures that this is always possible. For a more detailed discussion, see Appendix A.4.1.

Assuming (3.58) and subsequently Eq. (3.61), the limit of Eq. (3.59) is

$$\lim_{L \rightarrow \infty} T^L = \vec{v}_0 \vec{u}_0^\dagger \quad (3.62)$$

since all other eigenvalues $\Lambda_{i>0}$ are of modulus smaller than unity and thus

$$\lim_{L \rightarrow \infty} \left(\frac{\Lambda_i}{\Lambda_0} \right)^L = \lim_{L \rightarrow \infty} \Lambda_i^L = 0 \quad \forall i > 0. \quad (3.63)$$

Then the norm takes the form

$$\langle \psi | \psi \rangle = \text{Tr}(\tilde{Q} \vec{v}_0 \vec{u}_0^\dagger) = \vec{u}_0^\dagger \tilde{Q} \vec{v}_0 \quad (3.64)$$

which leads to the second condition, namely that the product $\nu := \vec{u}_0^\dagger \tilde{Q} \vec{v}_0$ must be finite and positive. This allows the rescaling

$$Q \rightarrow \frac{Q}{\sqrt{\nu}} \quad \Rightarrow \quad \tilde{Q} \rightarrow \frac{\tilde{Q}}{\nu} \quad (3.65)$$

which normalizes $|\psi\rangle$. For PBC, $\tilde{Q} = \mathbb{1}$ so this is trivially true, and the state $|\psi\rangle$ is also normalized given $\Lambda_0 = 1$. For general boundary conditions, some more work is required.

The Kronecker product $A^{s*} \otimes A^s$ has the block matrix structure of Eq. (3.9), with $D \times D$ blocks of size $D \times D$, where each block $T_{\alpha\beta}$ is given by $\sum_s A_{\alpha\beta}^{s*} A^s$. Since the eigenvectors \vec{u}_0 and \vec{v}_0 are of dimension D^2 , they can be interpreted as vectorizations of $D \times D$ matrices

u and v . Using the double index scheme of Eq. (3.9), an element of the matrix-vector product $T\vec{v}$ is given by

$$(T\vec{v})_{(\alpha,\alpha')} = \sum_{\beta,\beta'} T_{(\alpha,\alpha')(\beta,\beta')} \vec{v}_{(\beta,\beta')} \quad (3.66a)$$

$$= \sum_s \sum_{\beta,\beta'} A_{\alpha\beta}^{s*} A_{\alpha'\beta'} v_{\beta'\beta} \quad (3.66b)$$

$$= \sum_s \sum_{\beta,\beta'} A_{\alpha'\beta'} v_{\beta'\beta} A_{\beta\alpha}^{s\dagger} \quad (3.66c)$$

$$= \sum_s (A^s v A^{s\dagger})_{\alpha'\alpha} . \quad (3.66d)$$

This allows to define T as a superoperator acting on matrices with

$$T[v] := \sum_s A^s v A^{s\dagger} . \quad (3.67)$$

The application of T as a superoperator to a $D \times D$ matrix v will be denoted with square brackets.

Especially in numerical application, using the matrix form of \vec{v}_0 and \vec{u}_0 is advantageous, since the matrix-vector product $T\vec{v}_0$ takes $\mathcal{O}(D^4)$ operations, whereas the application scheme in Eq. (3.67) takes $\mathcal{O}(2dD^3)$ operations. This is a clear speedup, if $2d < D$. Since the local Hilbert space dimension d is usually much smaller than the bond dimension, this is mostly the case. At very low bond dimensions computations are very fast, so that a possible small loss in performance is negligible.

Using Eq. (3.67) and the definition of the matrix scalar product Eq. (3.10), the application of the Hermitian adjointed superoperator T^\dagger can easily be defined

$$(u, T[v]) \stackrel{!}{=} (T^\dagger[u], v) \quad (3.68a)$$

$$\text{Tr} \left(u^\dagger \left(\sum_s A^s v A^{s\dagger} \right) \right) = \sum_s \text{Tr} \left(u^\dagger A^s v A^{s\dagger} \right) \quad (3.68b)$$

$$= \sum_s \text{Tr} \left(A^{s\dagger} u^\dagger A^s v \right) \quad (3.68c)$$

$$= \text{Tr} \left(\left(\sum_s A^{s\dagger} u A^s \right)^\dagger v \right) \quad (3.68d)$$

$$\Rightarrow T^\dagger[u] = \sum_s A^{s\dagger} u A^s . \quad (3.68e)$$

Interpreted as $D \times D$ matrices, the eigenvectors v_0 and u_0 are Hermitian and can be chosen such that they are positive definite, see App. A.4.2 for a proof. This choice is assumed from here on and, together with the normalization constraint $(u_0, v_0) = 1$, uniquely defines the eigenmatrices.

In the remainder the index 0 is dropped, and the matrices are labeled u and v for convenience, and are referred to as *boundary matrices*, as they describe the boundaries of the iMPS *tensor networks*. See App. A.4.3 for a discussion of TN boundaries in the TDL. They are not to be confused with the *boundary operator* Q , which describes the boundaries (or lack thereof) of the *physical system*.

Let $\{v_\alpha\}$ and $\{u_\beta\}$ be the sets of EVs of v and u , respectively, and $\{\vec{\alpha}\}$ and $\{\vec{\beta}\}$ the sets of the corresponding eigenvectors. Since u and v are positive definite, the 2-form

$$(\mathbf{A}, \mathbf{B})_{vu} := \text{Tr} \left(\sum_s u^\dagger B^s v A^{s\dagger} \right) = \vec{u}^\dagger \left(\sum_s A^{s*} \otimes B^s \right) \vec{v} \quad (3.69)$$

then defines a scalar product for two tensors \mathbf{A} and \mathbf{B} . Sesqui-linearity, i.e. linearity in the second and anti-linearity in the first argument, is immediately apparent from the linearity of the trace and the matrix product. Positive semi-definiteness follows from

$$(\mathbf{A}, \mathbf{A})_{vu} = \text{Tr} \left(\sum_s u^\dagger A^s v A^{s\dagger} \right) \quad (3.70a)$$

$$= \text{Tr} \left(\sum_s \sum_{\alpha, \beta} u_\beta \vec{\beta} \vec{\beta}^\dagger A^s v_\alpha \vec{\alpha} \vec{\alpha}^\dagger A^{s\dagger} \right) \quad (3.70b)$$

$$= \text{Tr} \left(\sum_s \sum_{\alpha, \beta} u_\beta v_\alpha \vec{\beta}^\dagger A^s \vec{\alpha} \vec{\alpha}^\dagger A^{s\dagger} \vec{\beta} \right) \quad (3.70c)$$

$$= \sum_s \sum_{\alpha, \beta} v_\alpha u_\beta |\vec{\beta}^\dagger A^s \vec{\alpha}|^2 \quad (3.70d)$$

$$\geq 0 \quad (3.70e)$$

with equality if and only if \mathbf{A} is the null-tensor.

The norm as given in Eq. (3.64) is a special case of the scalar product with $\mathbf{A} = \mathbf{B} = Q$, where the boundary operator Q can be seen as a rank-3 tensor with a physical “dummy” index, i.e. the sum over s only contains one term. Therefore, the renormalization Eq. (3.65) is always possible. Moreover, the actual form of Q and therefore the boundary conditions it describes do not matter. This can be understood from a physical point of view, since it is expected that the bulk of an infinite system is not influenced by boundary effects. Again, there are systems for which this is not true. Because the ansatz inherently renormalizes any boundary effects, such systems cannot be adequately described by this type of uMPS. See App. A.5 for more details.

The sub-leading term in the spectral decomposition Eq. (3.55) is also of great importance, as it determines the rate at which T^L converges to $\vec{v}_0 \vec{u}_0^\dagger$. For the sake of simplicity, Λ_1 will be assumed to be unique; however, this is not a requirement and the following arguments can be made just as well if there are multiple EVs of second-largest absolute value. The prefactor in T^L of the projector onto the eigenspace of Λ_1 is given by

$$\left(\frac{\Lambda_1}{\Lambda_0} \right)^L = \Lambda_1^L \propto |\Lambda_1|^L. \quad (3.71)$$

Consider for instance a correlation function

$$G(\ell) := \langle \psi | S_\ell^x S_0^x | \psi \rangle \quad (3.72a)$$

$$= \vec{u}^\dagger \left(\sum_{ss'} S_{ss'}^x A^{s'*} \otimes A^s \right) T^{\ell-1} \left(\sum_{ss'} S_{ss'}^x A^{s'*} \otimes A^s \right) \vec{v} \quad (3.72b)$$

$$=: \vec{u}^\dagger S^x T^{\ell-1} S^x \vec{v}. \quad (3.72c)$$

In the TDL, this expression decomposes into the product of two scalars

$$G_\infty := G(\ell \rightarrow \infty) = \vec{u}^\dagger S^x \vec{v} \cdot \vec{u}^\dagger S^x \vec{v} = M_x^2 \quad (3.73)$$

namely the magnetization squared. For finite ℓ , the difference $G(\ell) - G_\infty$ is dominated by

$$G(\ell) - G_\infty \approx \Lambda_1^\ell \vec{u}_0^\dagger S^x \vec{v}_1 \vec{u}_1^\dagger S^x \vec{v}_0 \propto |\Lambda_1|^\ell. \quad (3.74)$$

This shows that in the framework of iMPS, any correlation is always expanded in a series of exponentials, the leading term of which is given by $|\Lambda_1|^\ell$. Therefore, a state with diverging or even algebraic correlations can never be described exactly by a uMPS, which ties into the requirement that the state must not be explicitly dependent on the boundary conditions. By Eq. (3.74) the second largest EV Λ_1 defines a correlation length [63]

$$\xi_T := -\frac{1}{\ln \frac{|\Lambda_1|}{\Lambda_0}}, \quad (3.75)$$

which defines the correlations that *are described* by the transfer operator T . Obviously, if ξ_T is smaller than the physical correlation length ξ of, for instance, the ground state, then the state cannot be exactly represented by an uMPS of the given bond dimension.

The states defined in Eq. (3.51) form the set of *uniform* iMPS (uMPS). In many cases, they can be used to describe a ground state of a translation invariant system in the TDL. Therefore, they form a subset of the iMPS class that holds all MPSs of given bond dimension for infinite systems.

However, the goal is to derive an effective model of excitations that have particle-like properties, including a certain degree of localization. Such an excited state can clearly not be a uMPS. The simplest generalization from uMPS to less restricted iMPS is replacing the uniform tensor \mathbf{A} by some other tensor \mathbf{B} on a single site. This type of iMPS describes localized elementary excitations and is discussed in more detail in Sec. 5.1.1. Some mathematical background is given in App. A.4.4.

In the following, the circle shape of Eq. (3.27) will be used to denote the uMPS ground state tensor \mathbf{A} , and a triangular shape

$$\begin{array}{c} \blacktriangle \\ \hline \end{array} = \mathbf{B}, \quad \begin{array}{c} \hline \blacktriangledown \end{array} = \mathbf{B}^* \quad (3.76)$$

will be used to represent those other tensors inserted on single sites.

3.6.3 Operators in the thermodynamic limit

While the concept of uMPS is very efficient in the sense that an infinite system is described by a single tensor, this efficiency comes at a price. Most notably, there is no representation of “the state” in memory. This means an expression like

$$|\phi\rangle = \hat{O} |\psi\rangle \quad (3.77)$$

cannot be computed except in some very special cases. This also makes it very challenging, in most cases even impossible, to define powers of operators unless they act on a single site.

However, in practice, most quantities of interest are overlaps and especially matrix elements of local operators that act on a finite number of sites, or sums thereof. Both can be computed in the iMPS framework. The corresponding TNs take the following form (cf. Sec. 3.6.4 and App. A.4.3)

$$\langle \psi' | \hat{O} | \psi \rangle = \begin{array}{c} \bullet \quad \bullet \quad // \quad \bullet \quad \bullet \quad \blacktriangledown \quad \bullet \quad // \quad \bullet \quad \bullet \\ \bullet \quad \bullet \quad // \quad \blacksquare \quad \blacksquare \quad \bullet \quad // \quad \bullet \quad \bullet \\ \bullet \quad \bullet \quad // \quad \blacktriangle \quad \bullet \quad // \quad \bullet \quad \bullet \end{array}, \quad (3.78)$$

with

$$\left[= u^\dagger, \quad \right] = v, \quad \begin{array}{c} \bullet \\ | \\ \bullet \end{array} = T, \quad (3.79)$$

and the triangular shape represents some tensor \mathbf{B} other than \mathbf{A} . The symbol \llcorner denotes that an arbitrary number of transfer operators T are left out. Since u and v are eigenmatrices of T to the eigenvalue $\Lambda_0 = 1$, it is easy to see that any number of T -“rungs” on both ends of the ladder do not change anything, and the TN collapses to

$$\langle \psi' | \hat{O} | \psi \rangle = \begin{array}{c} \bullet \quad \bullet \\ | \quad | \\ \blacktriangle \quad \bullet \\ | \quad | \\ \bullet \quad \bullet \end{array} \llcorner. \quad (3.80)$$

The rightmost rung in the TN above is an object very similar to T , but with the bra-side tensor being \mathbf{B} instead of \mathbf{A} . The right end of the TN is therefore given by

$$\begin{array}{c} \blacktriangle \\ | \\ \bullet \end{array} \llcorner = \left(\sum_s B^{s*} \otimes A^s \right) \vec{v}. \quad (3.81)$$

Equation (3.50) then shows that rungs containing local operators naturally lead to

$$\begin{array}{c} \bullet \\ | \\ \blacksquare \\ | \\ \blacktriangle \end{array} \llcorner = \left(\sum_{s,s'} O_{s's} A^{s'*} \otimes B^s \right) \vec{v} \quad \text{and} \quad (3.82a)$$

$$\llcorner \begin{array}{c} \bullet \\ | \\ \blacksquare \\ | \\ \blacktriangle \end{array} = \left(\left(\sum_{s,s'} O_{s's}^\dagger (A^{s'*})^\dagger \otimes B^{s\dagger} \right) \vec{u} \right)^\dagger. \quad (3.82b)$$

The calculation in (3.66) readily extends to rungs with operators, and the application of the Hermitian adjointed operator can be defined analogous to Eq. (3.68).

This yields the following schemes for the application of local operators to $D \times D$ boundary matrices, which generalize Eqs. (3.67) and (3.68)

$$\hat{O}^{(\mathbf{A};\mathbf{B})}[v] := \sum_{s,s'} O_{s's} B^s v A^{s'\dagger} \quad (3.83a)$$

$$\hat{O}^{\dagger(\mathbf{A};\mathbf{B})}[u] := \sum_{s,s'} O_{s's}^\dagger A^{s'\dagger} u B^s. \quad (3.83b)$$

Therefore, in the superoperator picture, Eq. (3.81) can also be written as

$$\sum_s A^s v B^{s\dagger} = \sum_{s',s} \delta_{s's} A^s v B^{s'\dagger} = \mathbb{1}^{(\mathbf{B};\mathbf{A})}[v]. \quad (3.84)$$

Consequently, the transfer operator T can also be interpreted as an identity operator on the given site.

3.6.4 Canonical gauge of uMPS

The result of the ground state search algorithms described in section 4.1 is a uniform iMPS (uMPS). By construction it does not have a canonical form. Note that in the context of uMPS, the term canonical is used synonymously with the term *normalized* as defined in section 3.4, since there is only one tensor. This means a left-canonical uMPS fulfills the condition

$$\sum_s A_\ell^{s\dagger} A_\ell^s = \mathbb{1} , \quad (3.85)$$

while for a right-canonical uMPS the equation

$$\sum_s A_r^s A_r^{s\dagger} = \mathbb{1} \quad (3.86)$$

holds.

Having a uMPS in a canonical form has certain advantages. In the left canonical form, the boundary matrix u is the $D \times D$ identity, while v is a real diagonal matrix with positive elements and unit trace. It is also identical to the density matrix ρ appearing in DMRG calculations. In the right-canonical form, the forms of u and v are reversed. Throughout this thesis the left canonical form will be used.

In order to bring the uMPS matrices A^s into canonical form an algorithm presented in Ref. [81] is used. Recall the composite canonical representation of a MPS introduced in section 3.4

$$c_{\sigma_1, \sigma_2, \dots, \sigma_N} = \text{Tr} \left(\begin{array}{c} \text{---} \blacklozenge \text{---} \bullet \text{---} \blacklozenge \text{---} \blacklozenge \text{---} \dots \text{---} \bullet \text{---} \blacklozenge \text{---} \\ \lambda^{[1]} \quad \Gamma^{[1]} \quad \lambda^{[2]} \quad \lambda^{[L]} \quad \Gamma^{[L]} \quad \lambda^{[L+1]} \end{array} \right) , \quad (3.87)$$

where the $\Gamma^{[i]}$ are rank-3 tensors that live on the lattice sites and the $\lambda^{[i]}$ are the Schmidt coefficients on the bonds. Note that either $\lambda^{[1]}$ or $\lambda^{[L+1]}$ is just the identity in some gauge of Γ , as can be seen by assuming periodic boundary conditions, where there must be exactly one bond matrix on the bond $L + 1 \leftrightarrow 1$. It is introduced only to emphasize that the situation is indeed symmetric and the choices of left or right canonical representation are equivalent. The left and right canonical forms are obtained as follows

$$A_\ell^s = \lambda \Gamma^s \quad (3.88)$$

$$A_r^s = \Gamma^s \lambda . \quad (3.89)$$

From this representation, two transfer matrices can be defined, which occur when tensor networks involving such a state are contracted

$$T_r := \begin{array}{c} \Gamma^* \quad \lambda^* \\ \bullet \text{---} \blacklozenge \\ | \\ \bullet \text{---} \blacklozenge \\ \Gamma \quad \lambda \end{array} = \sum_s A_r^{s*} \otimes A_r^s \quad (3.90a)$$

$$T_\ell := \begin{array}{c} \lambda^* \quad \Gamma^* \\ \blacklozenge \text{---} \bullet \\ | \\ \blacklozenge \text{---} \bullet \\ \lambda \quad \Gamma \end{array} = \sum_s A_\ell^{s*} \otimes A_\ell^s . \quad (3.90b)$$

If $\{\Gamma, \lambda\}$ is a canonical iMPS representation, the identity is a left or right eigenvector of T_ℓ and T_r , respectively

$$T_r \mathbf{1} = \Lambda \mathbf{1} \quad (3.91a)$$

$$\mathbf{1}^\dagger T_\ell = \Lambda \mathbf{1}^\dagger \quad (3.91b)$$

where $\mathbf{1}$ is to be understood as the vectorization of the $D \times D$ identity matrix and normalization implies the corresponding eigenvalue Λ must be 1.

To get a canonical composite representation from a given uMPS A^s , one must first decompose it into some $\{\tilde{\Gamma}, \tilde{\lambda}\}$ by SVD and then bring this newly found representation into canonical form. To carry out the SVD, all A^s are put into a single $dD \times D$ matrix A (cf. matrix U in Sec. 3.4). Then

$$A = \begin{pmatrix} A^1 \\ \vdots \\ A^d \end{pmatrix} = U \tilde{\lambda} V^\dagger = \begin{pmatrix} U^1 \\ \vdots \\ U^d \end{pmatrix} \tilde{\lambda} V^\dagger, \quad (3.92)$$

where U is a $dD \times D$ column-orthogonal matrix, $\tilde{\lambda}$ is the $D \times D$ diagonal matrix of singular values, and V^\dagger is a $D \times D$ unitary matrix. The site tensor $\tilde{\Gamma}$ is obtained by setting

$$\tilde{\Gamma}^s := V^\dagger U^s \quad (3.93)$$

since

$$\text{Tr}(A^s \dots A^s) = \text{Tr}(U^s \tilde{\lambda} V^\dagger \dots U^s \tilde{\lambda} V^\dagger) = \text{Tr}(\tilde{\lambda} V^\dagger U^s \dots \tilde{\lambda} V^\dagger U^s) \quad (3.94a)$$

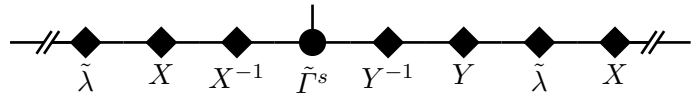
$$= \text{Tr}(\tilde{\lambda} \tilde{\Gamma}^s \dots \tilde{\lambda} \tilde{\Gamma}^s) = \text{Tr}(\tilde{\Gamma}^s \tilde{\lambda} \dots \tilde{\Gamma}^s \tilde{\lambda}). \quad (3.94b)$$

Now $\tilde{\Gamma}$ needs to be transformed such that the identity is an eigenvector of T_r and T_ℓ , respectively. To this end, the left eigenvector \tilde{u}_ℓ of \tilde{T}_ℓ and the right eigenvector \tilde{v}_r of \tilde{T}_r corresponding to the largest magnitude eigenvalue Λ are computed. Reinterpreted as $D \times D$ matrices, \tilde{u}_ℓ and \tilde{v}_r are then decomposed into their respective eigenbasis and eigenvalues

$$\tilde{v}_r = M \sqrt{D_r} \sqrt{D_r} M^\dagger = X X^\dagger \quad (3.95a)$$

$$\tilde{u}_\ell = W \sqrt{D_\ell} \sqrt{D_\ell} W^\dagger = Y^\dagger Y, \quad (3.95b)$$

where the matrices of eigenvectors M and W are unitary, since u_ℓ and v_r are hermitian and positive definite. The matrices X and Y defined in Eq. (3.95) are therefore invertible. Now, an identity matrix can be inserted on the bonds between each $\tilde{\lambda}$ and $\tilde{\Gamma}^s$ yielding



$$\text{---} // \blacklozenge_{\tilde{\lambda}} \blacklozenge_X \blacklozenge_{X^{-1}} \bullet_{\tilde{\Gamma}^s} \blacklozenge_{Y^{-1}} \blacklozenge_Y \blacklozenge_{\tilde{\lambda}} \blacklozenge_X \text{---} // \quad (3.96)$$

With another SVD of the matrix product

$$Y \tilde{\lambda} X = U \lambda V^\dagger \quad (3.97)$$

where both U and V are square and therefore unitary the composite canonical representation is finally obtained as

$$\{\Gamma, \lambda\}, \quad \text{with} \quad \Gamma^s = V^\dagger X^{-1} \tilde{\Gamma}^s Y^{-1} U. \quad (3.98)$$

The left and right canonical A^s follow according to Eq. (3.88).

The fact that this representation is indeed canonical is not quite obvious. However, it can be verified by reversing all the transformations applied to achieve it. Here, it will only be shown that $A_\ell^s = \lambda \Gamma^s$ is left-canonical, as this gauge is used throughout the thesis. First, Eq. (3.97) implies that

$$\lambda = U^\dagger Y \tilde{\lambda} X V . \quad (3.99)$$

Also, in the matrix interpretation of \tilde{u}_ℓ , being a left eigenvector of \tilde{T}_ℓ means

$$T_\ell^\dagger[\tilde{u}_\ell] = \sum_s A_\ell^{s\dagger} \tilde{u}_\ell A_\ell^s = \sum_s \tilde{\Gamma}^{s\dagger} \tilde{\lambda}^\dagger \tilde{u}_\ell \tilde{\lambda} \tilde{\Gamma}^s = \Lambda \tilde{u}_\ell . \quad (3.100)$$

The condition for a left-canonical iMPS is (cf Eq. (3.85))

$$\mathbb{1} \stackrel{!}{=} \sum_s A_\ell^{s\dagger} A_\ell^s \quad (3.101a)$$

$$= \sum_s (\lambda V^\dagger X^{-1} \tilde{\Gamma}^s Y^{-1} U)^\dagger \lambda V^\dagger X^{-1} \tilde{\Gamma}^s Y^{-1} U \quad (3.101b)$$

$$= \sum_s U^\dagger Y^{-1\dagger} \tilde{\Gamma}^{s\dagger} X^{-1\dagger} V (V X^\dagger \tilde{\lambda}^\dagger Y^\dagger U) (U^\dagger Y \tilde{\lambda} X V) V^\dagger X^{-1} \tilde{\Gamma}^s Y^{-1} U \quad (3.101c)$$

$$= U^\dagger Y^{-1\dagger} \underbrace{\left(\sum_s \tilde{\Gamma}^{s\dagger} \tilde{\lambda}^\dagger \tilde{u}_\ell \tilde{\lambda} \tilde{\Gamma}^s \right)}_{\Lambda \tilde{u}_\ell = Y^\dagger Y} Y^\dagger U \quad (3.101d)$$

$$= U^\dagger (Y^\dagger)^{-1} Y^\dagger Y Y^{-1} U \quad (3.101e)$$

$$= \mathbb{1} \quad (3.101f)$$

is thus fulfilled, since U is unitary, $(Y^{-1})^\dagger = (Y^\dagger)^{-1}$, and $\tilde{\Gamma}^s$ can be scaled such that $\Lambda = 1$, which is assumed to be the case. This also proves that the identity is a left eigenvector of T_ℓ to the eigenvalue 1

$$\mathbb{1} = \sum_s A_\ell^{s\dagger} A_\ell^s = \sum_s A_\ell^{s\dagger} \mathbb{1} A_\ell^s = T_\ell^\dagger[\mathbb{1}] \quad (3.102)$$

which is true for any left-canonical uMPS. That A_r^s is right-canonical can be shown analogously.

3.7 Chapter summary

In this chapter, the framework of matrix product state (MPS) was introduced. Its origins in the DMRG were discussed, and why subsequently MPS are a very powerful method for 1D systems.

The extension from finite systems to the thermodynamic limit was discussed in some detail, because it is the foundation of the presented method. The special class of uniform matrix product state (uMPS) was introduced, which is well-suited to describe the ground states of translation invariant systems, if translation symmetry is not broken spontaneously. It was shown how transfer matrices arise from the use of uMPS and how they allow for very efficient treatment of the thermodynamic limit. Some of the mathematical details were left out and the inclined reader is referred to the respective appendices.

In the next chapter, an iterative algorithm to find an approximative ground state uMPS is presented, and some results for ground state properties of the TFIM and FMHC are provided.

Chapter 4

Ground state properties

Give me a place to stand, and I shall move the world.
Archimedes

4.1 Ground state search

Finding the best possible ground state approximation is a crucial step in the process of deriving the effective model. If an exact iMPS representation of the ground state exists at finite bond dimension D (as it is the case e.g. for the AKLT model, [82, 21, 23]), it is obviously also an exact eigenstate of the Hamiltonian. In iMPS language this means that the boundary matrices u and v are eigenmatrices of the Hamiltonian MPO. However, if the ground state is known only approximately, this is *not* the case. Therefore, an erroneous matrix element of the Hamiltonian appears, that couples the ground state to excited states

$$\eta := \langle j | H | GS \rangle \neq 0 . \quad (4.1)$$

This error fundamentally limits the accuracy that can be reached in any subsequent steps. This kind of error is the smaller, the closer the approximation \mathbf{A} is to the true ground state.

4.1.1 Iterative search algorithm

This section describes the algorithm used to obtain the results presented in this thesis. It has been featured in my Master's thesis [64] and in Ref. [65]. It is reiterated here for completeness and because it constitutes the basis of the description of excited states in chapter 5.

As mentioned above, a *conditio sine qua non* for the presented method is translation invariance. In a translation invariant system, the global Hamiltonian H is a sum of sub-Hamiltonians h_i

$$H = \sum_i h_i \quad (4.2)$$

where the summands h_i describe the physics of site i and its coupling to the rest of the lattice. The h_i are identical but for the site index i ¹. The second prerequisite is that h_i couples only a *finite* number of sites n . Therefore, h_i will be referred to as *local Hamiltonian* from here on.

¹A “site” can also be a unit cell consisting of multiple physical lattice sites, e.g. in a ladder system.

Under the assumption that the ground state is a uMPS, finding it is a variational problem in the elements of \mathbf{A} . Starting from the Rayleigh-Ritz equation

$$E_0 \leq \frac{\langle \psi(\mathbf{A}) | H | \psi(\mathbf{A}) \rangle}{\langle \psi(\mathbf{A}) | \psi(\mathbf{A}) \rangle} \quad (4.3)$$

the objective is to find a uMPS tensor \mathbf{A} that minimizes the energy, or rather the energy per lattice site ϵ , as much as possible. As described in Sec. 3.6, computing the energy expectation value $\langle \psi(\mathbf{A}) | H | \psi(\mathbf{A}) \rangle$ and the norm $\langle \psi(\mathbf{A}) | \psi(\mathbf{A}) \rangle$ in Eq. (4.3) requires the (at least partial) diagonalization of the transfer operator T . The energy ϵ is thus a highly non-linear function of the elements in \mathbf{A} .

As such, any generic multidimensional minimization scheme can be used to minimize it. Examples are simulated annealing [83] or the conjugate direction method. More specific methods to obtain a uMPS ground state approximation include imaginary time evolution (iTEBD) [84], other algorithms based on the time-dependent variational principle [85], or the recently proposed VUMPS algorithm [86].

In the following, an iterative algorithm developed in [64] is presented, which is inspired by DMRG and already makes use of many of the techniques used in describing excitations. The basic idea is to keep the uMPS tensor \mathbf{A} everywhere, but at one lattice site that is labeled site 0. On this site, the elements of the local tensor \mathbf{B} are varied to reduce the energy. The newly found \mathbf{B} is then adopted as new guess for \mathbf{A} until convergence is reached, i.e.,

$$|E(\mathbf{B}) - E(\mathbf{A})| < \theta \quad (4.4)$$

holds for a tolerance parameter θ . The optimal value for θ would be machine precision, but for higher bond dimensions and close to criticality this needs to be relaxed in order to achieve convergence in reasonable time. Typical values for $D > 10$ are 10^{-8} to 10^{-6} , in units of the system's energy scale.

Since the ground state energy is extensive, it diverges in the TDL. Equation (4.3) is therefore reformulated as function of \mathbf{A} and \mathbf{B} as

$$0 \leq \frac{\langle \psi(\mathbf{A}, \mathbf{B}) | (H - E_0(\mathbf{A})) | \psi(\mathbf{A}, \mathbf{B}) \rangle}{\langle \psi(\mathbf{A}, \mathbf{B}) | \psi(\mathbf{A}, \mathbf{B}) \rangle} = \sum_i \frac{\langle \psi(\mathbf{A}, \mathbf{B}) | (h_i - \epsilon_0(\mathbf{A})) | \psi(\mathbf{A}, \mathbf{B}) \rangle}{\langle \psi(\mathbf{A}, \mathbf{B}) | \psi(\mathbf{A}, \mathbf{B}) \rangle}, \quad (4.5)$$

where in each iteration $\epsilon_0(\mathbf{A})$ is the current estimate for the ground state energy per lattice site. The tensor \mathbf{B} , which is varied to lower the energy is placed at site 0. There are three types of matrix elements that occur in Eq. (4.5), depending on where h_i acts relatively to the \mathbf{B} tensors. The respective TNs are of the forms

$$\langle h_{i < -n} \rangle(\mathbf{A}, \mathbf{B}) = \begin{array}{c} \text{---} \bullet \text{---} \bullet \text{---} \bullet \text{---} \text{---} \blacktriangledown \text{---} \\ \text{---} \blacksquare \text{---} \blacksquare \text{---} \blacksquare \text{---} h_i \text{---} \blacktriangle \text{---} \\ \text{---} \bullet \text{---} \bullet \text{---} \bullet \text{---} \text{---} \blacktriangle \text{---} \end{array} \quad (4.6a)$$

$$\langle h_{i = -n, \dots, 0} \rangle(\mathbf{A}, \mathbf{B}) = \begin{array}{c} \text{---} \bullet \text{---} \blacktriangledown \text{---} \bullet \text{---} \text{---} \blacklozenge \\ \text{---} \blacksquare \text{---} \blacksquare \text{---} \blacksquare \text{---} h_i \text{---} \blacklozenge \\ \text{---} \bullet \text{---} \blacktriangle \text{---} \bullet \text{---} \text{---} \blacklozenge \end{array}, \quad (4.6b)$$

$$\langle h_{i > 0} \rangle(\mathbf{A}, \mathbf{B}) = \begin{array}{c} \text{---} \blacktriangledown \text{---} \text{---} \bullet \text{---} \bullet \text{---} \bullet \text{---} \text{---} \blacklozenge \\ \text{---} \blacktriangle \text{---} \text{---} \blacksquare \text{---} \blacksquare \text{---} \blacksquare \text{---} h_i \text{---} \blacklozenge \\ \text{---} \bullet \text{---} \text{---} \bullet \text{---} \bullet \text{---} \text{---} \blacklozenge \end{array}, \quad (4.6c)$$

where again the symbol $//$ denotes that a number of transfer operator rungs is left out.

The TN for the norm is simply the TN representation of the scalar product Eq. (3.69)

$$\langle \psi(\mathbf{A}, \mathbf{B}) | \psi(\mathbf{A}, \mathbf{B}) \rangle = \text{Diagram} . \quad (4.7)$$

Each of the TNs in Eq. (4.6) can be written as a 2-form in \mathbf{B}

$$\langle \psi(\mathbf{A}, \mathbf{B}) | h_i - \epsilon_0(\mathbf{A}) | \psi(\mathbf{A}, \mathbf{B}) \rangle = \text{vec}(\mathbf{B})^\dagger M^{[i]} \text{vec}(\mathbf{B}) , \quad (4.8)$$

and the same holds for the normalization constraint Eq. (4.7)

$$\langle \psi(\mathbf{A}, \mathbf{B}) | \psi(\mathbf{A}, \mathbf{B}) \rangle = \text{vec}(\mathbf{B})^\dagger N \text{vec}(\mathbf{B}) = \sum_s \text{Tr}(u^\dagger B^s v B^{s\dagger}) . \quad (4.9)$$

The vectorization of a rank-3 iMPS tensor is defined by stacking the vectorizations of the matrices B^s for each local physical state on top of each other, i.e.,

$$\vec{\mathbf{B}} = \text{vec}(\mathbf{B}) := \begin{pmatrix} \text{vec}(B^1) \\ \vdots \\ \text{vec}(B^d) \end{pmatrix} = \begin{pmatrix} \vec{B}^1 \\ \vdots \\ \vec{B}^d \end{pmatrix} . \quad (4.10)$$

This adds another block level to the indexing scheme in Eq. (3.5), and can be expressed by a triple index

$$(\vec{\mathbf{B}})_{(s, \alpha, \alpha')} = B_{\alpha' \alpha}^s . \quad (4.11)$$

To understand the structure of the matrices $M^{[i]}$ and N from Eqs. (4.8) and (4.9), we start with the expression for the normalization constraint

$$\sum_s \text{Tr}(u^\dagger B^s v B^{s\dagger}) = \sum_s \sum_{\alpha, \beta, \mu, \nu} u_{\alpha\beta}^\dagger B_{\beta\mu}^s v_{\mu\nu} B_{\nu\alpha}^{s\dagger} \quad (4.12a)$$

$$= \sum_{s, s'} \delta_{s' s} \sum_{\alpha, \beta, \mu, \nu} B_{\alpha\nu}^{s'*} u_{\alpha\beta}^\dagger v_{\nu\mu}^T B_{\beta\mu}^s \quad (4.12b)$$

$$= \sum_{s, s'} \sum_{\alpha, \beta, \mu, \nu} \vec{\mathbf{B}}_{(s', \nu, \alpha)}^\dagger \delta_{s' s} v_{\nu\mu}^T u_{\alpha\beta}^\dagger \vec{\mathbf{B}}_{(s, \mu, \beta)} \quad (4.12c)$$

$$= \sum_{s, s'} \sum_{\alpha, \beta, \mu, \nu} \vec{\mathbf{B}}_{(s', \nu, \alpha)}^\dagger N_{(s', \nu, \alpha), (s, \mu, \beta)} \vec{\mathbf{B}}_{(s, \mu, \beta)} \quad (4.12d)$$

$$= \vec{\mathbf{B}}^\dagger N \vec{\mathbf{B}} . \quad (4.12e)$$

Comparison to Eq. (3.9) reveals that the matrix N is given by the Kronecker product

$$N = \mathbb{1}_d \otimes v^T \otimes u^\dagger , \quad (4.13)$$

where v^T is the transpose of v . The $d \times d$ identity was introduced in (4.12b) to obtain the structure of a vector-matrix-vector product in a $d \cdot D^2$ dimensional vector space.

By inspecting the TNs, one can easily see that the matrices $M^{[i]}$ in Eqs. (4.6a) and (4.6c) are of the same structure as N . The only difference lies in the boundary matrices used to build them. For $i < -n$, the left boundary matrix is of a different form

$$u_{\text{eff}}^i := (T^\dagger)^{|i-n|} [h_i^{\dagger(\mathbf{A}; \mathbf{A})} [u]] . \quad (4.14)$$

Accordingly, for $i > 0$ the right boundary matrix has the form

$$v_{\text{eff}}^i := T^{i-1} [h_i^{(\mathbf{A}; \mathbf{A})} [v]] . \quad (4.15)$$

Theoretically, the index i runs from $-\infty$ to ∞ . However, as shown in Sec. 3.6.2, the matrix v_{eff} converges to $\epsilon_0 \cdot v$ as $|\Lambda_1|^{i-1}$, since for large i

$$T^{i-1} H_i \vec{v} \approx (\vec{v} \vec{u}^\dagger + \Lambda_1^{i-1} \vec{v}_1 \vec{u}_1^\dagger) H_i \vec{v} \quad (4.16a)$$

$$= \vec{v} (\vec{u}^\dagger H_i \vec{v}) + \Lambda_1^{i-1} \vec{v}_1 (\vec{u}_1^\dagger H_i \vec{v}) \quad (4.16b)$$

$$= \epsilon_0 \vec{v} + \mathcal{O}(\Lambda_1^{i-1}), \quad (4.16c)$$

where H_i is a $D^2 \times D^2$ operator matrix defined analogous to S^x in Eq. (3.72). Note that ϵ_0 is just the expectation value of h_i in the current ground state estimate \mathbf{A} , given by

$$\epsilon_0 = \langle \psi(\mathbf{A}) | h_i | \psi(\mathbf{A}) \rangle = \vec{u}^\dagger H_i \vec{v} = \left(u, h_i^{(\mathbf{A};\mathbf{A})} [v] \right), \quad (4.17)$$

where (\cdot, \cdot) denotes the matrix scalar product defined in Eq. (3.10).

The same also holds true for the right boundary matrix u_{eff} . Therefore, in numerics, the sum over all lattice sites i can be cut once $|\Lambda_1|^i$ is sufficiently small. This corresponds to the distance between h_i and \mathbf{B} being so large that they do not “see” each other within the limits of the intrinsic correlation length ξ_T of the uMPS \mathbf{A} . In order for the sum to have a finite value, or in the numerical case, to be independent from the cutoff, each matrix element has to be corrected by

$$\epsilon_0 \langle \psi(\mathbf{A}, \mathbf{B}) | \psi(\mathbf{A}, \mathbf{B}) \rangle = \epsilon_0 \vec{\mathbf{B}}^\dagger N \vec{\mathbf{B}} \quad (4.18)$$

as stated in Eq. (4.5). This can be achieved by setting

$$u_{\text{eff}}^i \rightarrow u_{\text{eff}}^i - \epsilon_0 u \quad \text{or} \quad v_{\text{eff}}^i \rightarrow v_{\text{eff}}^i - \epsilon_0 v, \quad (4.19)$$

respectively, since the Kronecker product is linear in both arguments.

This leaves to show how to compute the matrix $M^{[i]}$ for the case in Eq. (4.6b), i.e., where one of the operators in h_i acts on site 0, where \mathbf{A} is exchanged for \mathbf{B} . Assume the rather general case where h_i is a product of $n = 3$ local operators

$$h_i = \hat{O}_i \hat{O}_{i+1} \hat{O}_{i+2} \quad (4.20)$$

and acts on site $i = -1$, which is exactly the case shown in the TN in Eq. (4.6b). Then, it is clear that there are now *two* effective boundary matrices

$$u_{\text{eff}} = \hat{O}_i^{\dagger(\mathbf{A};\mathbf{A})} [u] - \epsilon_0 u, \quad v_{\text{eff}} = \hat{O}_{i+2}^{(\mathbf{A};\mathbf{A})} [v]. \quad (4.21)$$

The ground state energy correction can be subtracted from either boundary matrix. A calculation analogous to Eq. (4.12) shows that

$$\begin{aligned} & \langle \psi(\mathbf{A}, \mathbf{B}) | h_i - \epsilon_0(\mathbf{A}) | \psi(\mathbf{A}, \mathbf{B}) \rangle \\ &= \text{Tr} \left(u_{\text{eff}}^\dagger \left(\sum_{s, s'} (O_{i+1})_{s' s} B^s v_{\text{eff}} B^{s' \dagger} \right) \right) \end{aligned} \quad (4.22a)$$

$$= \sum_{s, s'} \sum_{\alpha, \beta, \mu, \nu} (O_{i+1})_{s' s} (u_{\text{eff}}^\dagger)_{\alpha \beta} B_{\beta \mu}^s (v_{\text{eff}})_{\mu \nu} B_{\nu \alpha}^{s' \dagger} \quad (4.22b)$$

$$= \sum_{s, s'} \sum_{\alpha, \beta, \mu, \nu} (B^{s' *})_{\alpha \nu} (O_{i+1})_{s' s} \sum_{s, s'} \sum_{\alpha, \beta, \mu, \nu} B_{\beta \mu}^s \quad (4.22c)$$

$$= \sum_{s, s'} \sum_{\alpha, \beta, \mu, \nu} \vec{\mathbf{B}}_{(s', \nu, \alpha)}^\dagger \left((O_{i+1})_{s' s} \sum_{s, s'} \sum_{\alpha, \beta, \mu, \nu} \right) \vec{\mathbf{B}}_{(s, \mu, \beta)} \quad (4.22d)$$

$$= \vec{\mathbf{B}}^\dagger M^{[-1]} \vec{\mathbf{B}} \quad (4.22e)$$

from which follows that

$$M^{[-1]} = O_{i+1} \otimes v_{\text{eff}}^T \otimes u_{\text{eff}}^\dagger. \quad (4.23)$$

This means, the matrix is built just as any other $M^{[i]}$, but the $d \times d$ identity in the Kronecker product is replaced by the matrix representation of the local operator \hat{O}_{i+1} which acts on site 0 where the tensor \mathbf{B} sits.

In this way Eq. (4.5) can be expressed by

$$0 \leq \sum_i \frac{\vec{\mathbf{B}}^\dagger M^{[i]} \vec{\mathbf{B}}}{\vec{\mathbf{B}}^\dagger N \vec{\mathbf{B}}}. \quad (4.24)$$

Defining $M = \sum_i M^{[i]}$ and introducing the Lagrange parameter ϵ , this is a minimization problem with constraint

$$f(\vec{\mathbf{B}}) = \vec{\mathbf{B}}^\dagger M \vec{\mathbf{B}} - \epsilon \vec{\mathbf{B}}^\dagger N \vec{\mathbf{B}}. \quad (4.25)$$

Taking the derivative of $f(\vec{\mathbf{B}})$ with respect to $\vec{\mathbf{B}}^\dagger$ and requiring it to be zero yields a generalized eigenvalue problem (EVP)

$$M(H, \mathbf{A}) \vec{\mathbf{B}} = \epsilon N(\mathbf{A}) \vec{\mathbf{B}}. \quad (4.26)$$

The iterative ground state search algorithm can now be formulated as summarized in table 4.1.

A fixed point in the iteration does not necessarily mean a global minimum in energy. It is also possible that the algorithm only finds a local minimum, or, since $\mathbf{B}_0 = \mathbf{A}$ can only be achieved within some tolerance, gets stuck on a very slow descent towards the global minimum. However, in practice the results are mostly very convincing.

Table 4.1: Ground state search algorithm

1	Make an initial guess for \mathbf{A}
2	Construct the matrices M and N
3	Solve the generalized EVP Eq. (4.26)
4	If $\mathbf{B}_0 = \mathbf{A}$ within tolerance, stop
5	Otherwise, take the eigenvector $\vec{\mathbf{B}}_0$ with lowest EV ϵ as new \mathbf{A} and go to step 2

4.1.2 Notes on implementation

In order for a generalized EVP such as the one in Eq. (4.26) to be solvable, the matrix N must be Hermitian and positive definite. From the definition in Eq. (4.13) it is obvious that this condition is fulfilled, since u and v are Hermitian and positive definite. A generalized EVP can be solved by mapping it to a standard EVP. This is achieved by diagonalizing the matrix N first

$$M \vec{v} = \epsilon N \vec{v} \quad (4.27a)$$

$$\Leftrightarrow M \vec{v} = \epsilon P^\dagger \sqrt{D_N} \underbrace{\sqrt{D_N} P \vec{v}}_{=: \vec{v}'} \quad (4.27b)$$

$$\Leftrightarrow \underbrace{\sqrt{D_N}^{-1} P M P^\dagger \sqrt{D_N}^{-1}}_{=: M'} \vec{v}' = \epsilon \vec{v}' \quad (4.27c)$$

$$\Leftrightarrow M' \vec{v}' = \epsilon \vec{v}' \quad (4.27d)$$

$$\Rightarrow \vec{v} = P^\dagger \sqrt{D_N}^{-1} \vec{v}' \quad (4.27e)$$

where D_N is the diagonal matrix of EVs of N and the unitary matrix P holds the eigenvectors.

As can be seen from the definition in Eq. (4.13), the matrix N is already diagonal in the left-canonical gauge of \mathbf{A} and consists of $d \cdot D$ copies of the boundary matrix v . Each EV is thus $d \cdot D$ -fold degenerate. As described in the previous chapter, in the left-canonical gauge, v holds the squared singular values of \mathbf{A} . Therefore, if the ground state is well described by a uMPS, the EVs of N can become very small. This leads to large errors in the computation of M' , where M is multiplied by the inverse of $\sqrt{D_N}$. To work around this, the columns of P corresponding to such very small EVs are considered to span the null-space (kernel) of N , which is then omitted from the transformation, which corresponds to projecting M onto the non-zero eigenspace of N . Note that actually bringing \mathbf{A} into canonical form in each iteration is numerically more costly than diagonalizing N , and is therefore not done in practice.

While the above procedure is easy to implement using standard LAPACK [87] routines, it is still not the most numerically stable as the results in the following sections show. Since only the lowest EV of the problem is relevant for the ground state search, a Krylov subspace method like the Lanczos algorithm could also be used and may prove numerically more stable.

Finally, to ensure that the energy decreases in each iteration, a linear minimization of the function

$$\epsilon_0(\varphi) := \epsilon_0(\cos(\varphi)\mathbf{A} + \sin(\varphi)\mathbf{B}_0) \quad (4.28)$$

with respect to φ is performed.

If no better alternative is available, the initial guess for \mathbf{A} is filled with random numbers. Significantly faster convergence can often be achieved if the converged result for a slightly different set of system parameters is used as initial input. Close to criticality this approach is less reliable, as the system properties may change rapidly over a comparably small parameter interval. The converged result for close-by parameters can still be used as input, but often does not prove to be better than a random guess. Also, close to a phase transition, it may be necessary to relax the tolerances a bit to reach convergence in reasonable time. Unfortunately, although the idea seems obvious, using the converged result for a smaller bond dimension D does not help. This is because of the truncation of very small eigenvalues of the norm matrix N in Eq. (4.26). To make use of the result with, for instance, bond dimension $D - 1$, the ground state tensor \mathbf{A}_{D-1} needs to be padded with zeros. That just increases the dimension of the null-space of N , which is projected out before M' is diagonalized. Therefore, the convergence is indeed faster, but the accuracy of the result does not improve, since the algorithm stays in the subspace of bond dimension $D - 1$.

Initializing the increased \mathbf{A}_D tensor with random numbers large enough not to fall into the nullspace of N leads to a loss of the information in \mathbf{A}_{D-1} within a few iterations and thus defeats the purpose of the whole undertaking.

4.2 Transfer operator

The first quantity of interest which can be obtained from the ground state uMPS tensor is the correlation length ξ_T , determined by the second largest EV of T . For a pure product state with bond dimension $D = 1$ it is by definition zero, wherefore this section only shows results for the TFIM. Figure 4.1 compares ξ_T as defined in Eq. (3.75) to the analytical expression for the physical correlation length Eq. (2.48) for various bond dimensions D .

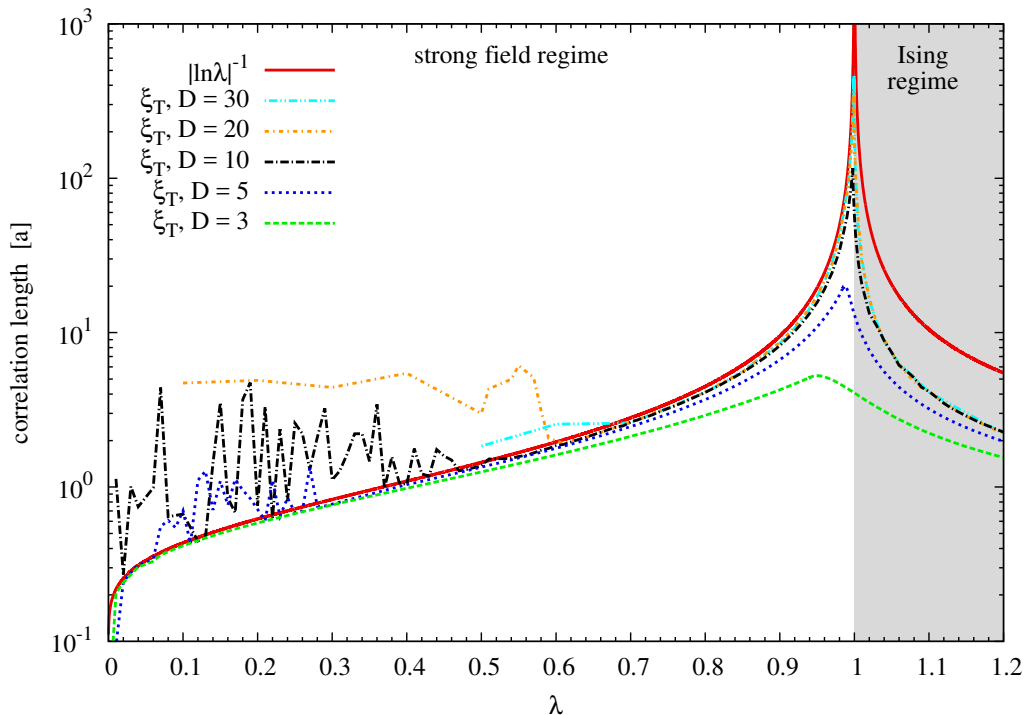


Figure 4.1: Correlation length ξ_T of the TFIM uMPS results for different bond dimensions D compared to the exact solution from Eq. (2.48).

It is apparent that the correlation length grows for increasing Ising interaction as expected. Therefore, for $\lambda \rightarrow 1$, increasingly large bond dimensions are required, or equivalently, a fixed bond dimension leads to increasing deviation from the exact result. However, for larger bond dimensions and small λ , the iMPS results are partially *larger* than the exact value, and the curves show erratic oscillations. Close to criticality, the curves are much smoother. This surprising finding can easily be understood by considering the weak coupling regime $J \rightarrow 0$. When there is no Ising interaction at all, the ground state is simply a product state where all spins point along the external field. This state can be exactly described by a uMPS of bond dimension $D = 1$. Increasing the bond dimension beyond $D = 3$ leads to numerical instability of the ground state search EVP Eq. (4.26) and subsequently to larger errors. Since the ground state develops adiabatically for increasing Ising coupling, small values of λ require only small bond dimensions. If D is much larger than is required to describe the system to machine precision, this results in numerical noise.

Figure 4.2 shows the diagonal elements of the right boundary matrix v at $\lambda = 0.1$ for various bond dimensions. As mentioned in Chap. 3, in the left-canonical gauge of a uMPS this matrix is diagonal and holds the squares of the Schmidt coefficients for a decomposition on any bond. For $D = 3$, the smallest element is of the order 10^{-10} , which can be considered numerically stable. Also, this bond dimension is sufficient to describe the system very accurately, which is confirmed by the result for the ground state energy, cf. Fig. 4.5 below.

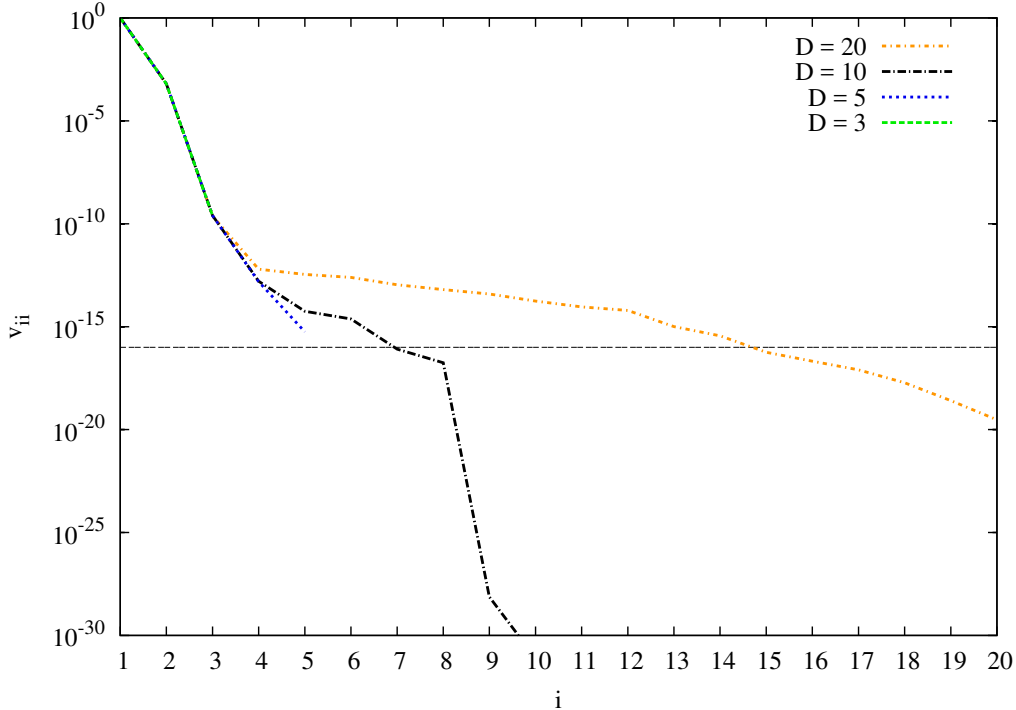


Figure 4.2: Diagonal elements of the right boundary matrix v for the TFIM uMPS at $\lambda = 0.1$ for different bond dimensions D . The thin horizontal line marks machine precision for 64-bit double computations.

The smallest value $v_{55} = s_5^2$ for $D = 5$ is already of the order of the machine precision. For $D = 10$, v_{ii} first shows the same decrease as for $D = 3$ and $D = 5$, then an area of reduced decay. In the last elements there is a sudden drop far below machine precision, which is rather surprising. Lastly, for $D = 20$, the decrease of v_{ii} becomes rather flat for $i > 4$. For $D = 30$, no convergence could be reached within reasonable tolerance at this parameter value.

The problem with entries in v close to or below machine precision is, that their significand (mantissa) can change arbitrarily due to rounding errors and thus has essentially no meaning. However, to obtain the canonical form of a uMPS, the square root of v is computed and inverted. In this process, the ill defined near-zero values can have a large impact on the result.

This is seen in Fig. 4.1. All results for ξ_T computed with bond dimension $D > 3$ are larger than the exact physical value. This corroborates the connection between very small elements in v and subsequently small EVs of the norm matrix N in Eq. (4.26), and unphysical results.

Note that in Fig. 4.1 the exact solution is plotted for qualitative comparison, and the peaks show up independently of it, as opposed to, for instance, the corresponding peaks in the deviation of the ground state energy in Fig. 4.5. Therefore, the onset of numerical instability and subsequently parameter regions where a certain bond dimension is unsuitable can be determined without an exact solution available.

Interestingly, for small bond dimensions the peak in the curves which indicates the critical point is located at a parameter value $\lambda < 1$. This means that the phase transition is not detected at the exact critical parameter value. However, with increasing D , the peak position moves towards $\lambda = 1$.

In the Ising regime the deviation from the exact solution is much larger. The reason for this

is probably as follows. The correlation length ξ_T plotted in Fig. 4.1 is determined from the second largest EV Λ_1 of the transfer operator T of a *single* ground state using Eq. (3.75). However, the true correlation length is related to the elementary excitations by $\xi \approx \frac{v}{\Delta}$ with the energy gap Δ and the QP velocity v . In the ordered phase, the elementary excitations are domain walls, i.e., they involve *two* ground states. Therefore, these correlations cannot be expected to be described properly by the transfer operator of a single ground state.

To analyze the dependence of the implicit correlation length ξ_T on the bond dimension, Fig. 4.3 depicts ξ_T as function of $\frac{1}{D}$ for several values of λ . The lines are least squares fits to the data points. Table 4.2 shows the extrapolated results for ξ obtained from the fits. In the disordered phase, the extrapolation to $D \rightarrow \infty$ allows a quite precise prediction of the results to the exact value. For all tested values of λ , the exact results are contained within the error brackets of the extrapolation, which are of the order of 1%. In spite of this good agreement, the distribution of the data points does not allow us to conclusively establish a linear relation $\xi_T \propto \frac{1}{D}$. In the Ising phase at $\lambda = 1.2$, the error bracket of the fit is still rather small at 2.1%. However, the extrapolated value differs greatly from the exact one, which is in agreement with the general behavior observed for $\lambda > 1$.

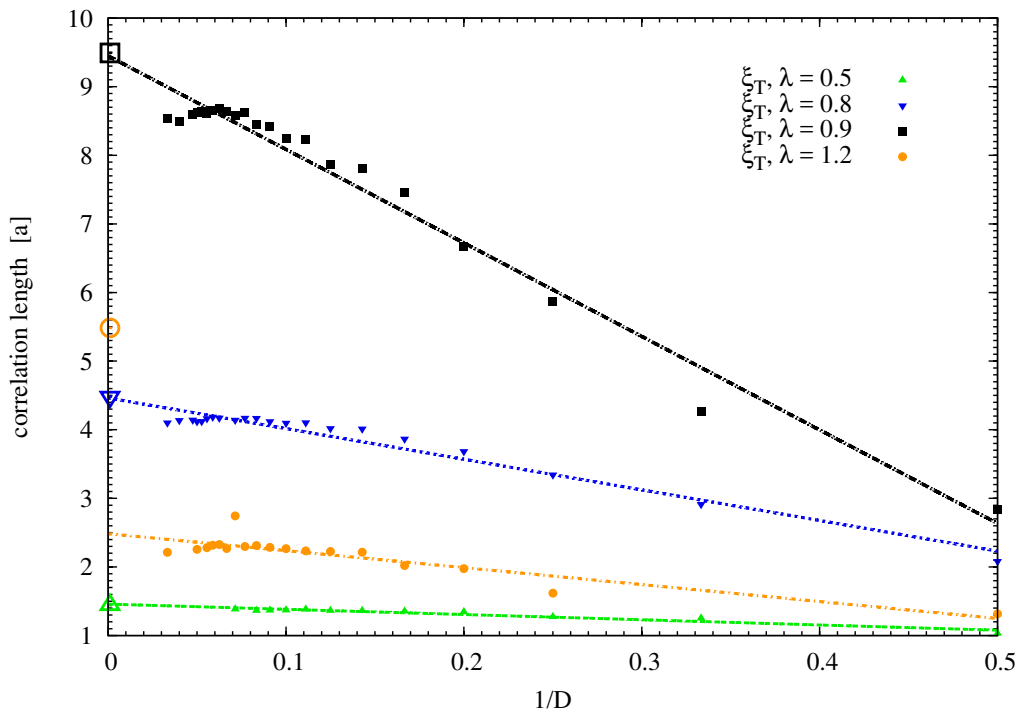


Figure 4.3: Correlation length ξ_T for the TFIM as function of the inverse bond dimension $\frac{1}{D}$ for various values of λ . The larger, open symbols of the same shape on the ordinate axis mark the exact values computed from Eq. (2.48). The lines are linear least squares fits to the data points. Refer to Tab. 4.2 for the numerical values of the extrapolations.

Table 4.2: Extrapolated results for TFIM correlation length

λ	ξ_{ex}	$\xi_{T,D \rightarrow \infty}$
0.5	1.44	1.46 ± 0.02 (1.04%)
0.8	4.48	4.46 ± 0.04 (0.85%)
0.9	9.49	9.45 ± 0.08 (0.89%)
1.2	5.48	2.48 ± 0.05 (2.09%)

4.3 Ground state energy

For both the FMHC and the TFIM, exact solutions for the ground state energy are available. The deviation

$$\Delta\epsilon_0 := |\epsilon_{0,\text{ex}} - \epsilon_{0,\text{uMPS}}| \quad (4.29)$$

is a good indicator for the quality of the uMPS result.

4.3.1 Results for the FMHC

Since the ground state of the model is a product state, it can be described exactly by a uMPS of bond dimension $D = 1$. Figure 4.4 shows the ground state energy and the deviation $\Delta\epsilon_0$ as function of Γ for several values of the next-nearest neighbor coupling J_2 . As the plot shows it is captured to machine precision by the algorithm. Increasing the bond dimension beyond the requirements can have adverse effects, since the norm matrix N in Eq. (4.26) becomes singular as discussed in Sec. 4.1.2.

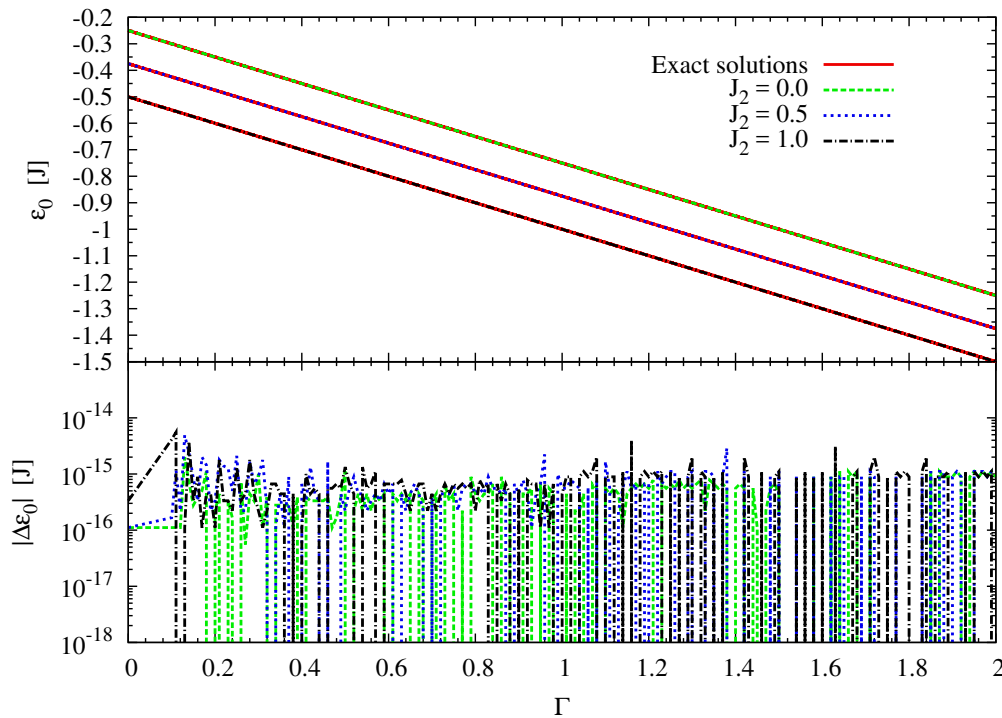


Figure 4.4: Ground state energy of the FMHC as function of the magnetic field Γ for various values of the next-nearest neighbor coupling J_2 . All data is computed with bond dimension $D = 1$. The upper part shows the energy itself, and the lower part the deviation of the uMPS result from the exact solution on a logarithmic scale. All energies are measured in units of the nearest neighbor coupling J which is set to unity.

4.3.2 Results for the TFIM

For the TFIM, too, the ground state energy can be obtained to very high precision. Figure 4.5 shows the energy and the deviation of the iMPS result from the exact solution Eq. (2.34b) as function of λ for various bond dimensions D .

It is apparent that the algorithm works just as well in the Ising phase with degenerate ground state as it does in the strong field phase. The same unstable behavior for small λ and large bond dimensions can be observed as in the correlation length ξ_T , however somewhat less pronounced. The deviation curves also show a maximum which is again located at some $\lambda \lesssim 1$ for small D , consistent with the results in Fig. 4.1.

The error dimensions are fairly consistent with DMRG results for finite chains of length $L = 300$ [88].

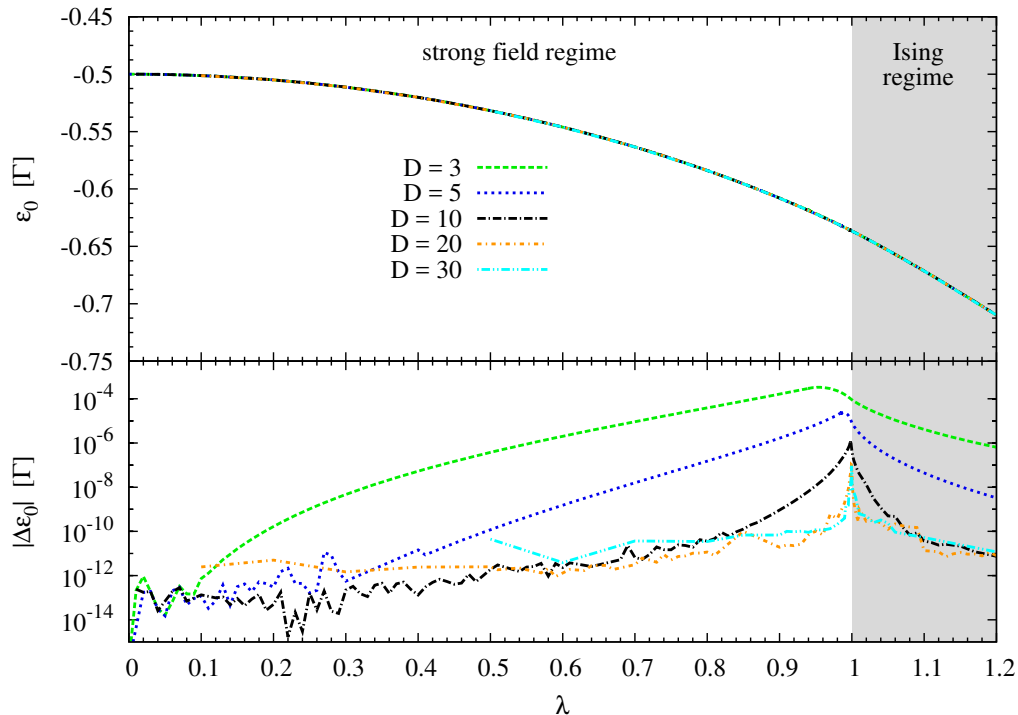


Figure 4.5: Ground state energy of the TFIM as function of λ for various bond dimension D . The upper part shows the energy itself, and the lower part the deviation of the iMPS result from the exact solution on a logarithmic scale.

4.4 Von Neumann entropy

Another quantity of interest which can be obtained from the ground state uMPS is the von Neumann or entanglement entropy S_{vN} , as defined in Eq. (3.13). As a measure of quantum entanglement across each bond, it is by definition zero for product states i.e. $D = 1$. Therefore, this section only contains results for the TFIM.

For a left-canonical uMPS as defined in Sec. 3.6.4, the left boundary matrix u is the $D \times D$ identity. As discussed in App. A.4.2, the right boundary matrix v is the reduced density matrix of either side of the bipartition of the chain across *any* bond in the ground state [23]. Therefore, for a uMPS, the von Neumann entropy is simply given by

$$S_{\text{vN}} = - \sum_{i=1}^D v_{ii} \ln v_{ii} . \quad (4.30)$$

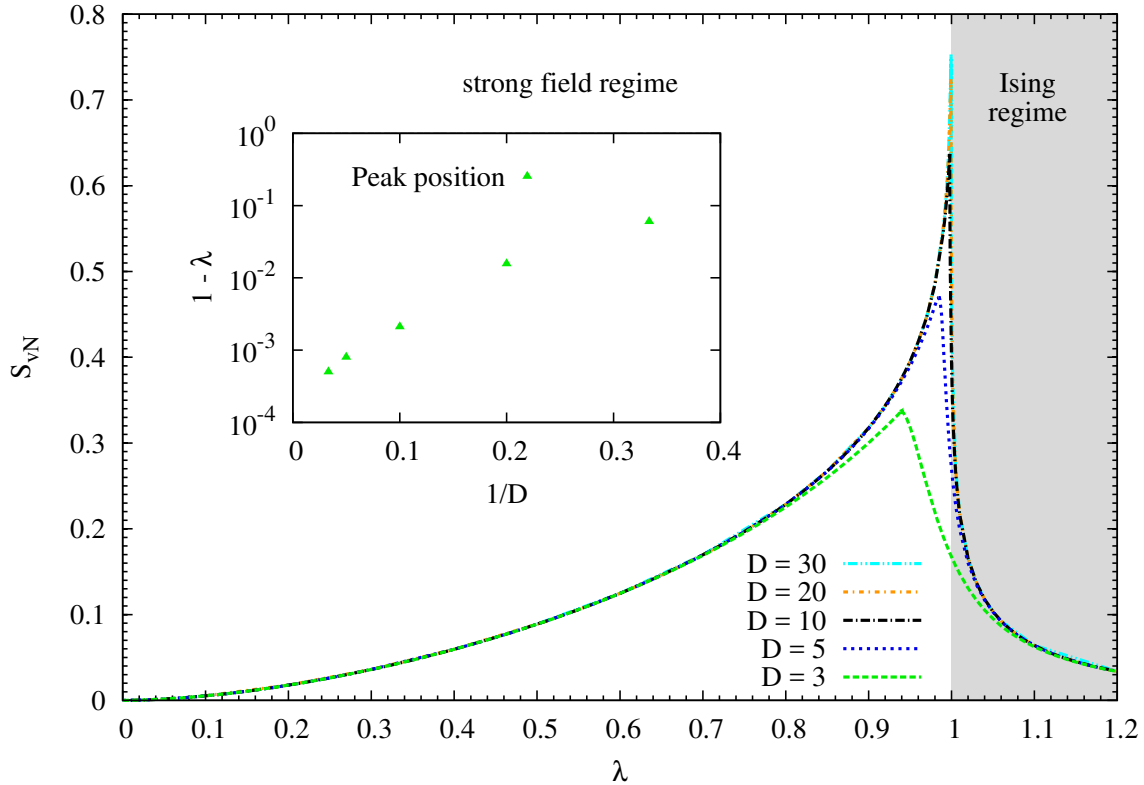


Figure 4.6: Von Neumann entropy S_{vN} of the ground state uMPS for the TFIM as function of λ for several bond dimensions D . The inset shows the deviation of the position of the peak in S_{vN} from the QCP $\lambda = 1$ as function of inverse bond dimension $\frac{1}{D}$.

Figure 4.6 shows S_{vN} for several bond dimensions D . The entanglement entropy is known to diverge logarithmically at $\lambda = 1$ [89]. This can again not be captured at finite bond dimension, but there is a clear and very sharp peak in each of the curves, located close to the value of λ , where the deviation of the uMPS result from the exact ground state energy in Fig. 4.5 has its maximum. However, in contrast to the latter, the von Neumann entropy can be computed without the exact solution, which normally is not available. Analyzing the entropy can therefore also help to find quantum phase transitions in models for which no exact solution exists.

The inset in Fig. 4.6 shows the deviation of the peak position in S_{vN} from the exact value $\lambda = 1$ as function of the inverse bond dimension $\frac{1}{D}$ on a logarithmic scale. There are only few data points, but the scaling seems neither linear, nor a power law nor exponential. However, a clear tendency towards the exact value is visible.

4.5 TFIM ground state magnetization

The ground state magnetization M_x in x -direction is the order parameter in the Ising phase. It decreases as λ approaches the critical point and vanishes in the strong field regime, where there is only magnetization in z -direction. Figure 4.7 shows the absolute value of the magnetization as function of the parameter λ . The left inset shows a magnification of the area around the critical point. As the plot shows the non-analytic onset of M_x at $\lambda = 1$ is not captured entirely by the MPS results. Instead, a smooth but rapid increase is observed. Again, for smaller bond dimensions it occurs at $\lambda \lesssim 1$.

The right inset shows the signed value of M_x for $D = 5$ and $\lambda > 1$. The occurrence of different signs is a clear indication of the ground state degeneracy. It also shows that as mentioned in Sec. 3.2, the algorithm converges to either one of the ground state realizations, not to a superposition which could be identified by a magnetization value somewhere between the positive and negative envelopes.

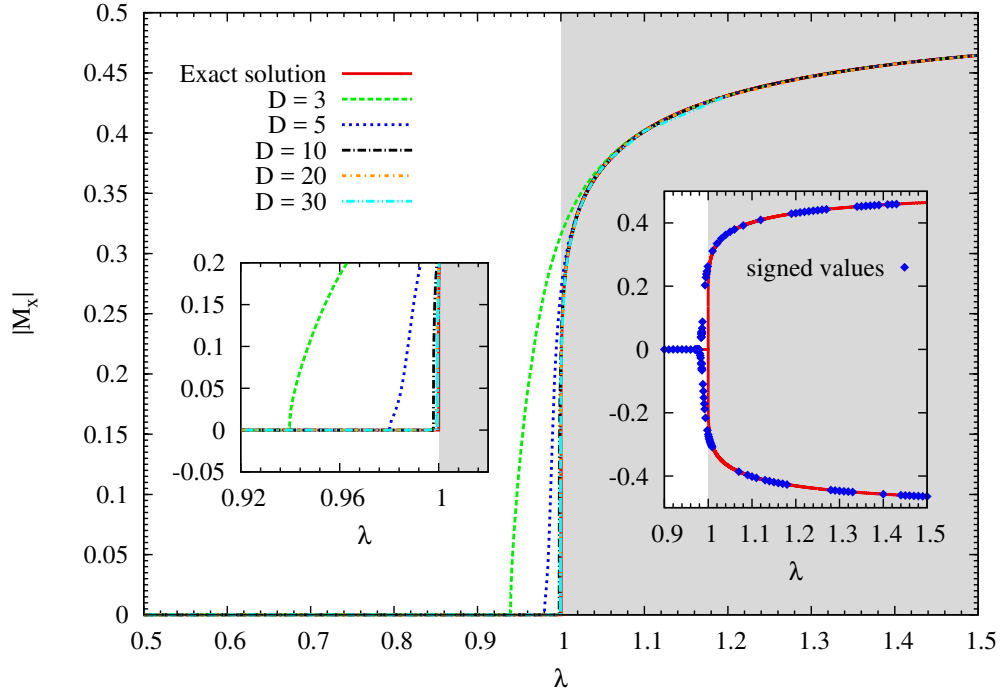


Figure 4.7: Ground state magnetization M_x as function of the parameter λ for various bond dimensions D . The exact curve is taken from Eq. (2.43). The left inset is a magnification of the parameter region around the QCP. The right inset shows the signed values of M_x at $D = 5$ as found by the ground state search algorithm.

In general, one can thus run the ground state search algorithm several times and check the value of an observable that distinguishes between degenerate ground states to obtain uMPS approximations for each of them. However, for the TFIM in the Ising phase, there is an analytical transformation that transforms one ground state into the other. It is in fact one of the rare cases, where an operator can be applied to a uMPS. This makes it possible to obtain the other ground state easily from the one that was found by the ground state search algorithm, see App. A.5 for details.

As stated in Chap. 2, the critical exponent for the longitudinal magnetization is given by $\beta = \frac{1}{8}$, i.e., M_x shows power law behavior

$$M_x \propto (\lambda - \lambda_c)^\beta = (\lambda - \lambda_c)^{\frac{1}{8}} \quad (4.31)$$

close to the phase transition at $\lambda_c = 1$.

Figure 4.8 shows the magnetization in a double logarithmic plot as function of $\lambda - \lambda_c$, where in this scaling $\lambda = 1$ corresponds to 0 on the x -axis. The plot focuses on parameters close to the critical point, therefore data is only plotted up to $\lambda = 1.2$. One can clearly

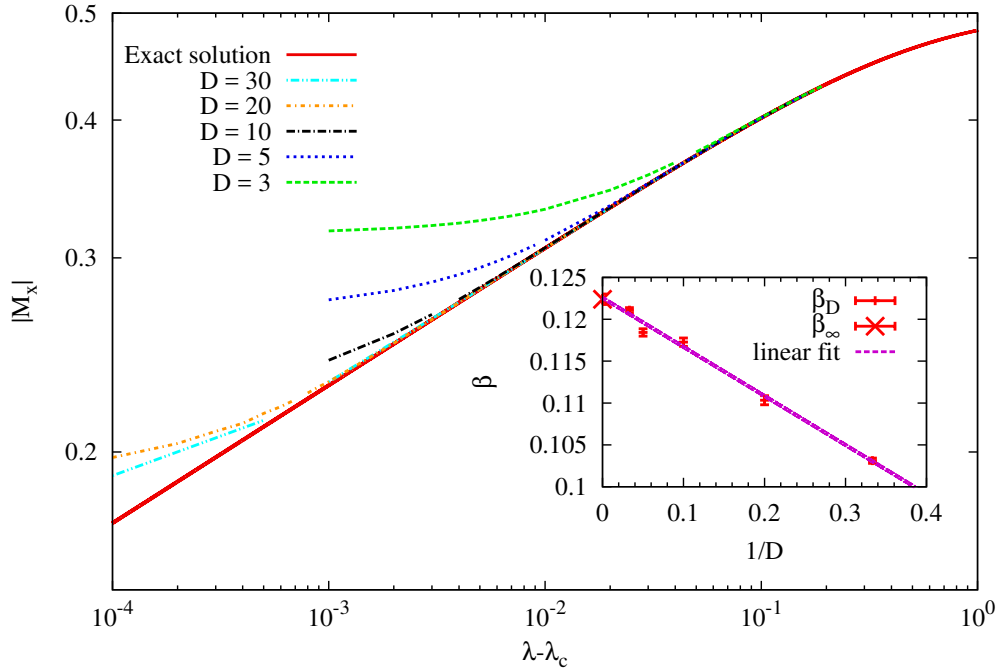


Figure 4.8: Double logarithmic plot of the ground state magnetization M_x as function of $\lambda - \lambda_c$ for various bond dimensions D . In this scaling, the critical parameter $\lambda_c = 1$ corresponds to 0 on the x -axis, and all data curves end at $\lambda = 1.2$. The gaps in the data indicate the assumed parameter where the power law behavior ends for $\lambda \rightarrow \lambda_c$ in the numerical description. The inset shows the critical exponent β as function of inverse bond dimension $\frac{1}{D}$, which was obtained by linear fits to the linear (right) parts of the curves. The straight line in the inset is another linear fit to extrapolate β for $D \rightarrow \infty$.

see a linear regime in all data sets that extends to increasingly small parameter values for growing bond dimension.

By fitting linear functions of the type

$$\ln(M_{x,D}) = \beta_D(\lambda - 1) + C \quad (4.32)$$

to the linear portion of each data set, the critical exponent β_D for each bond dimension can be estimated.

The estimates obtained for β_D are shown in the inset of Fig. 4.8, including the least squares fit error. As the plot shows, for the available data the error brackets are extremely small (less than 1%). By another linear fit to β_D as function of inverse bond dimension, the critical exponent can be extrapolated for $D \rightarrow \infty$. The extrapolated value of β is

$$\beta_\infty = 0.1226 \pm 0.0005, \quad (4.33)$$

again with an extremely small error bracket due to the small number of bond dimensions available. Notably, the error bracket does not include the exact value. The relative error is

$$\Delta\beta_{\text{rel}} = \frac{\beta - \beta_\infty}{\beta} \approx 0.019 = 1.9\%, \quad (4.34)$$

which is still quite small, given the number of data points.

Even better agreement with the exact value could be achieved by increasing the resolution in λ and D .

4.6 Chapter summary

In this chapter an iterative algorithm to find a ground state uMPS was presented, followed by results for some ground state properties for both the FMHC and the TFIM.

The FMHC was found to be described to machine precision by a ground state uMPS of bond dimension $d = 1$, i.e., a product state.

For the TFIM, the correlation length ξ_T defined by the second largest EV Λ_1 of the transfer operator T was examined as a first result and compared to the exact solution. It was found that in the disordered phase close to the QCP an increase in bond dimension leads to a systematic improvement of the results. For small parameters and larger bond dimensions, results exceeding the physical correlation length, as well as wild oscillations as function of the parameter were found. This could be traced back to the Schmidt coefficients of the ground state uMPS becoming very small in these cases. As a consequence, the norm matrix in the ground state search EVP becomes singular, which leads to numerical instability. The algorithm to bring the uMPS into canonical form becomes unstable as well. The maximum in the correlation length which indicates a phase transition was found to occur at parameter values $\lambda \lesssim 1$ slightly smaller than the exact value for low bond dimensions.

For the ground state energy ϵ_0 the same behavior could be observed in the deviation from the exact result.

The von Neumann entropy S_{vN} is easily obtained from the canonical form of the uMPS. It showed very pronounced peaks, the positions of which were also found to approach the exact value for the critical parameter with increasing bond dimension.

Finally, the longitudinal ground state magnetization M_x was examined, and an attempt was made to extrapolate its critical exponent β . Although the relative error in β was found to be as small as 2%, the exact value is not included in the error brackets of the extrapolation. However, it is expected that the result improves if more values of the bond dimension D are included.

In the next chapter, it is shown, how excited states are described in the framework of iMPS. Results for the one-particle dispersion for the FMHC and the TFIM are provided. Further, it is shown how the creation operator of the quasi-particles is represented in the iMPS formalism, and it is tested by computing the spectral weight in the xx -channel for the TFIM.

Chapter 5

One-particle properties

A journey of a thousand miles begins with a single step.

Lao Tse

This chapter shows how the dispersion relation and other, low-lying EVs of the Hamiltonian are obtained along with a representation of the creation operator, which is the key to the derivation of an effective model. Results for dispersion relation and bound states are given. Properties of the creation operator are discussed and it is validated by computing some one-particle spectral weights.

Most of the contents of this chapter can also be found in Refs. [65, 90]. However, the concepts presented here are essential, because they constitute the foundation of the more complex two-particle calculations in chapter 6.

5.1 One-QP excited states and dispersion

The next step towards the effective model in Eq. (1.1) is to construct 1QP excited states and to obtain their dispersion relation ω_q . There are many ways to do this for a one-dimensional model. Most of the methods mentioned in Sec. 1.3 can achieve the dispersion for specific cases. For the presented method this step is different insofar as it does not only yield the dispersion relation, but the entire 1QP part of the Hamiltonian, i.e. *including* the creation operator. Also, one is not limited to just the dispersion of one type of quasi-particles (QPs). The algorithm also yields higher lying eigenvalues (EVs) of the Hamiltonian. For instance, on a dimerized spin- $\frac{1}{2}$ chain, excitations are so-called triplons, spin-1 triplet excitations formed from two spin- $\frac{1}{2}$ [91]. These excitations can be mobile and hop from one dimer to another. Without an external field, they are degenerate in the magnetic quantum number. This can be seen in the spectrum produced by the algorithm by the occurrence of threefold degenerate lowest eigenvalue. Also, bound states, e.g., the ones of the FMHC from Sec. 2.1, can be detected as energy levels appearing between the one-particle dispersion and the lower boundary of the 2QP continuum.

As mentioned above, the ground state energy E_0 is an extensive quantity and therefore divergent in the TDL. For this reason, the ground state energy per lattice site ϵ_0 was defined. In contrast, energies of a finite number of excitations are always finite, even in the TDL, since they are defined *relative* to the ground state energy. To calculate them, the *reduced Hamiltonian* is defined as

$$\tilde{H} = \sum_i \tilde{h}_i := H - E_0 = \sum_i (h_i - \epsilon_0) . \quad (5.1)$$

5.1.1 Describing excited states

To understand how excited states are described in the iMPS formalism, we turn to the ground state search EVP Eq. (4.26). At the point of convergence, the eigenvector \vec{B}_0 corresponding to the lowest EV is the ground state tensor \mathbf{A} that was put in. The eigenvectors $\vec{B}_{\alpha>0}$ corresponding to higher EVs describe excited states. Let therefore

$$|\mathbf{B}_{\alpha,j}\rangle := \sum_{s_1, \dots, s_L} \text{Tr}(A^{s_1} \dots A^{s_{j-1}} B_{\alpha}^{s_j} \tilde{A}^{s_{j+1}} \dots \tilde{A}^{s_L}) |s_1, \dots, s_L\rangle \quad (5.2)$$

be an iMPS that is taken to have ground state tensors \mathbf{A} (and $\tilde{\mathbf{A}}$) everywhere except at site j , where one of the eigentensors \mathbf{B}_{α} of Eq. (4.26) is inserted instead. For a unique ground state, $\tilde{\mathbf{A}} = \mathbf{A}$, i.e., the ground states are the same on both sides of the excitation. In the case of a degenerate ground state, the excitations have domain wall character, i.e., there is one ground state to the left, and another ground state to the right of it. In this case, $\tilde{\mathbf{A}} \neq \mathbf{A}$, refer to App. A.5 for details on how to deal with domain wall excitations.

Following Ref. [92], the set of uMPS can be seen as a manifold. The states in Eq. (5.2) then span the tangent space of this manifold.

5.1.2 Canonical gauge for excitation tensors

The matrices M and N in Eq. (4.26) are of dimension $d \cdot D^2 \times d \cdot D^2$. Therefore, there are $d \cdot D^2 - 1$ eigenstates \mathbf{B}_{α} with $\alpha > 0$ if the ground state is unique. If it is not, another EVP needs to be solved, where there is one ground state to the left of \mathbf{B} and another to the right. This EVP has $d \cdot D^2$ eigenstates that are different from \mathbf{A} . However, although states constructed from these \mathbf{B}_{α} according to Eq. (5.2) are orthogonal on the same site by construction, they do not form a good basis since

$$\langle \mathbf{B}_{\alpha,j} | \mathbf{B}_{\beta,j} \rangle = \delta_{\alpha\beta} \quad (5.3a)$$

$$\langle \mathbf{B}_{\alpha,j} | \mathbf{B}_{\beta,j'} \rangle \neq 0 \text{ for } j' \neq j. \quad (5.3b)$$

The reason is that this basis is overcomplete as will be shown in the next section.

5.1.2.1 Nullspace of the excitation parametrization

Like the ground state tensor \mathbf{A} , any tensor \mathbf{B} describing a local excitation has $d \cdot D^2$ parameters. However, not all of them are independent as was shown in Ref. [90]. Let $B^s = X A^s - e^{-iq} \tilde{A}^s X$ with some matrix $X \in \mathbb{C}^{D \times D}$. Due to translational invariance and the gauge freedom Eq. (3.40), the resulting momentum superposition yields

$$|\mathbf{B},q\rangle := \frac{1}{\sqrt{L}} \sum_j e^{-iqj} |\mathbf{B},j\rangle \quad (5.4a)$$

$$= \frac{1}{\sqrt{L}} \sum_j e^{-iqj} \sum_{s_1, \dots, s_L} \text{Tr} \left(\dots A^{s_{j-1}} (X A^{s_j} - e^{-iq} A^{s_j} X) \tilde{A}^{s_{j+1}} \dots \right) |s_1, \dots, s_L\rangle \quad (5.4b)$$

$$= \frac{1}{\sqrt{L}} \sum_j e^{-iqj} \left[\sum_{s_1, \dots, s_L} \text{Tr} \left(\dots A^{s_{j-1}} X \tilde{A}^{s_j} \tilde{A}^{s_{j+1}} \dots \right) |s_1, \dots, s_L\rangle \right. \\ \left. - \sum_{s_1, \dots, s_L} e^{-iq} \text{Tr} \left(\dots A^{s_{j-1}} A^{s_j} X \tilde{A}^{s_{j+1}} \right) |s_1, \dots, s_L\rangle \right] \quad (5.4c)$$

$$= \frac{1}{\sqrt{L}} \sum_j e^{-iqj} |X\tilde{A}_j\rangle - \frac{1}{\sqrt{L}} \sum_j e^{-iq(j+1)} |X\tilde{A}_{j+1}\rangle \quad (5.4d)$$

$$= \frac{1}{\sqrt{L}} \sum_j e^{-iqj} |X\tilde{A}_j\rangle - \frac{1}{\sqrt{L}} \sum_j e^{-iqj} |X\tilde{A}_j\rangle \quad (5.4e)$$

$$= 0 \quad (5.4f)$$

where from line (5.4d) to line (5.4e) the index of the second sum was shifted from $j \rightarrow j-1$, which is always allowed in the TDL. Since the matrix X has D^2 elements, for any $q \neq 0$ a \mathbf{B} tensor has a D^2 dimensional null-space and therefore only $(d-1) \cdot D^2$ free parameters. The same holds true for $q = 0$ and $\tilde{\mathbf{A}} \neq \mathbf{A}$. For $q = 0$ and $\tilde{\mathbf{A}} = \mathbf{A}$, the choices of $X = \mathbb{1}$ and $X = 0$ both result in $B^s = 0$. Therefore, the number of linearly independent null-vectors is reduced by one, thus giving $(d-1)D^2 + 1$ free parameters. However, in practice it is better to sacrifice the additional degree of freedom for the benefit of having the same \mathbf{B} tensors for all q .

The next section shows an algorithm to find a representation of \mathbf{B} as $(d-1)D \times D$ matrix which also has the property

$$\langle \mathbf{B}_{\alpha,j} | \mathbf{B}_{\beta,j'} \rangle = \delta_{jj'} \delta_{\alpha\beta} . \quad (5.5)$$

5.1.2.2 Definition of the reduced excitation parametrization

In Ref. [92] J. Haegeman et al. also showed a parametrization scheme for the excitation tensors \mathbf{B}_{α} , that takes the reduced number of parameters into account. First we state that \mathbf{A} has column-rank D when seen as a $d \cdot D \times D$ matrix, and therefore a $(d-1)D$ -dimensional null-space in $\mathbb{C}^{d \cdot D}$. Define the matrix

$$L_{\mathbf{A}} := \left[A^{1\dagger} \sqrt{u} \ \dots \ A^{d\dagger} \sqrt{u} \right] = \left[A^{1\dagger} \ \dots \ A^{d\dagger} \right] \quad (5.6)$$

where the second equality holds if \mathbf{A} describes a left-canonical uMPS since then $\sqrt{u} = u = \mathbb{1}$. The null space of this matrix can be found by means of the Gram-Schmidt orthonormalization algorithm. To this end, first the rows of $L_{\mathbf{A}}$ are orthogonalized. Then, new vectors that are orthogonal to them are generated successively by applying the Gram-Schmidt method to the Cartesian basis vectors of the remaining subspace of $\mathbb{C}^{d \cdot D}$. In the end, these vectors form an orthonormal basis of the null-space of $L_{\mathbf{A}}$ and therefore of \mathbf{A} . The resulting matrix V_L , which contains the null-space basis vectors as columns, is of dimension $dD \times (d-1)D$ and fulfills the equation

$$L_{\mathbf{A}} V_L = 0_{D \times D(d-1)} \quad (5.7a)$$

$$\Leftrightarrow \left(A^{1\dagger} \sqrt{u} \ \dots \ A^{d\dagger} \sqrt{u} \right) \cdot \begin{pmatrix} V_L^1 \\ \vdots \\ V_L^d \end{pmatrix} = 0_{D \times D(d-1)} \quad (5.7b)$$

$$\Leftrightarrow \sum_s (A^{s\dagger} \sqrt{u}) V_L^s = 0_{D \times D(d-1)} \quad (5.7c)$$

where the second and third lines are just a reformulation in terms of block matrices. Each block V_L^s defined above is of dimension $D \times (d-1)D$. These matrices V_L^s also fulfill the identity

$$\sum_s V_L^s V_L^{s\dagger} = V_L V_L^\dagger = \mathbb{1}_D \quad (5.8)$$

by virtue of their construction from orthonormal basis vectors. Define

$$B^s := \sqrt{u}^{-1} V_L^s X \sqrt{v}^{-1} \quad (5.9)$$

where X is some matrix of dimension $(d-1)D \times D$. It follows that

$$\mathbb{1}^{\dagger(\mathbf{B};\mathbf{A})}[u] = \sum_s A^{s\dagger} u B^s \quad (5.10a)$$

$$= \sum_s A^{s\dagger} \underbrace{u \sqrt{u}^{-1}}_{\sqrt{u}} V_L^s X \sqrt{v}^{-1} \quad (5.10b)$$

$$= \left(\sum_s (A^{s\dagger} \sqrt{u}) V_L^s \right) X \sqrt{v}^{-1} \quad (5.10c)$$

$$= 0_{D \times D} \quad (5.10d)$$

$$= \mathbb{1}^{\dagger(\mathbf{A};\mathbf{B})}[u] \quad (5.10e)$$

regardless of X . Therefore, this formulation reduces the parameter space for an excitation tensor \mathbf{B} from dD^2 to the above mentioned true number of relevant parameters, $(d-1)D^2$. At the same time, this gauge ensures orthogonality of the states $|\mathbf{B}_{\alpha,j}\rangle$ for different j . Note, however, that since $v \neq \mathbb{1}$ this only holds if u is the left boundary matrix. This leads to an asymmetric behavior of matrix elements

$$\langle \mathbf{B}_{\alpha,j} | \hat{O}_k | \mathbf{B}_{\beta,j'} \rangle \begin{cases} = 0, & \text{if } k > \min(i,j) \\ \neq 0, & \text{if } k \leq \min(i,j) \end{cases} \quad (5.11)$$

for $j' \neq j$.

5.1.2.3 Finding the reduced parametrization

In order to find the reduced parametrization X_{α} , the generalized EVP Eq. (4.26) has to be reformulated in terms of their vectorizations \vec{X}_{α}

$$M \vec{X} = \epsilon N \vec{X} . \quad (5.12)$$

It is instructive to start by inspecting the normalization matrix N , by examining its elements with respect to the \vec{X}_{α}

$$\langle \mathbf{B}_{\alpha,j} | \mathbf{B}_{\beta,j} \rangle = \vec{X}_{\alpha}^{\dagger} N \vec{X}_{\beta} = (u, \mathbb{1}^{(\mathbf{B}_{\alpha}, \mathbf{B}_{\beta})}[v]) \quad (5.13a)$$

$$= \text{Tr} \left[u^{\dagger} \sum_s B_{\beta}^s v B_{\alpha}^{s\dagger} \right] \quad (5.13b)$$

$$= \sum_s \text{Tr} \left[u^{\dagger} (\sqrt{u}^{-1} V_L^s X_{\beta} \sqrt{v}^{-1}) v (\sqrt{u}^{-1} V_L^s X_{\alpha} \sqrt{v}^{-1})^{\dagger} \right] \quad (5.13c)$$

$$= \sum_s \text{Tr} \left[\underbrace{\sqrt{u}^{-1} u \sqrt{u}^{-1}}_{\mathbb{1}} V_L^s X_{\beta} \underbrace{\sqrt{v}^{-1} v \sqrt{v}^{-1}}_{\mathbb{1}} X_{\alpha}^{\dagger} V_L^{s\dagger} \right] \quad (5.13d)$$

$$= \text{Tr} \left[\underbrace{\sum_s V_L^{s\dagger} V_L^s}_{\mathbb{1}} X_{\alpha}^{\dagger} X_{\beta} \right] \quad (5.13e)$$

$$= \text{Tr}(X_{\alpha}^{\dagger} X_{\beta}) \quad (5.13f)$$

$$\Rightarrow N = \mathbb{1}_{(d-1)D^2} \quad (5.13g)$$

where the cyclic property of the trace operation was used. This means the choice of parametrizing \mathbf{B}_{α} also reduces the generalized EVP to a standard EVP without the need

to diagonalize the matrix N . It remains to be shown how the matrix M is to be constructed. In close analogy to the case described in section 4.1, it is given by a sum

$$M = \sum_i M^{[i]} \quad (5.14)$$

where $M^{[i]}$ is determined by

$$\langle \mathbf{B}_\alpha, 0 | h_i | \mathbf{B}_\beta, 0 \rangle \stackrel{!}{=} \vec{X}_\alpha^\dagger M^{[i]} \vec{X}_\beta. \quad (5.15)$$

Generally, this results in a calculation similar to Eq. (5.13), however, with the effective boundary matrices u_{eff} and v_{eff} from Sec. 4.1.1 with

$$\sqrt{u}^{-1} u_{\text{eff}} \sqrt{u}^{-1} =: \tilde{u}_{\text{eff}} \neq \mathbb{1} \quad \text{and} \quad (5.16a)$$

$$\sqrt{v}^{-1} v_{\text{eff}} \sqrt{v}^{-1} =: \tilde{v}_{\text{eff}} \neq \mathbb{1}. \quad (5.16b)$$

The matrix element with respect to the \vec{X}_α is thus

$$\langle \mathbf{B}_\alpha, 0 | h_i | \mathbf{B}_\beta, 0 \rangle = (u_{\text{eff}}, O_0^{\mathbf{B}_\alpha; \mathbf{B}_\beta}) [v_{\text{eff}}] \quad (5.17a)$$

$$= \text{Tr} \left[u_{\text{eff}}^\dagger \sum_{s,s'} O_{s's} B_\beta^s v_{\text{eff}} B_\alpha^{s'\dagger} \right] \quad (5.17b)$$

$$= \text{Tr} \left[(\sqrt{u}^{-1} u_{\text{eff}}^\dagger \sqrt{u}^{-1}) \sum_{s,s'} O_{s's} V_L^s X_\beta (\sqrt{v}^{-1} v_{\text{eff}}^\dagger \sqrt{v}^{-1}) X_\alpha^\dagger V_L^{s'\dagger} \right] \quad (5.17c)$$

$$= \text{Tr} \left[\tilde{u}_{\text{eff}}^\dagger \sum_{s,s'} O_{s's} V_L^s X_\beta \tilde{v}_{\text{eff}} X_\alpha^\dagger V_L^{s'\dagger} \right] \quad (5.17d)$$

$$= \sum_a \sum_{b,c,d,e,f} \sum_{s,s'} O_{s's} (\tilde{u}_{\text{eff}}^\dagger)_{ab} (V_L^s)_{bc} (X_\beta)_{cd} (\tilde{v}_{\text{eff}})_{de} (X_\alpha^\dagger)_{ef} (V_L^{s'\dagger})_{fa} \quad (5.17e)$$

$$= \sum_{c,d,e,f} (X_\alpha^\dagger)_{ef} \left[\sum_{s,s'} O_{s's} \sum_{a,b} (V_L^{s'\dagger})_{fa} (\tilde{u}_{\text{eff}}^\dagger)_{ab} (V_L^s)_{bc} \right] (\tilde{v}_{\text{eff}})_{de} (X_\beta)_{cd} \quad (5.17f)$$

$$= \sum_{c,d,e,f} \underbrace{(X_\alpha^\dagger)_{ef}}_{=(X_\alpha^*)_{fe}} \left[\underbrace{\sum_{s,s'} O_{s's} V_L^{s'\dagger} \tilde{u}_{\text{eff}} V_L^s}_{=: O_{\text{eff},i}^\dagger} \right]_{fc} (\tilde{v}_{\text{eff}})_{de} (X_\beta)_{cd} \quad (5.17g)$$

$$= \vec{X}_\alpha^\dagger (\tilde{v}_{\text{eff}}^T \otimes O_{\text{eff},i}^\dagger) \vec{X}_\beta. \quad (5.17h)$$

Here it was assumed that h_i is a product of local operators that acts on site 0 as well as on at least sites -1 and 1 . If O_i does not act on site 0, the operator matrix elements in Eq. (5.17) are simply given by $O_{s's} = \delta_{s's}$. Also, one of the effective boundary matrices in Eq. (5.16) is then the identity. This scheme for computing $M^{[i]}$ still holds though. The matrix $O_{\text{eff},i}$ has to be computed anew for each operator position i .

5.1.3 Momentum space variation

The procedure outlined above yields a $(d-1)D^2$ -dimensional standard EVP, from which the full excitation tensors \mathbf{B}_α are obtained according to Eq. (5.9). Note that the number of

\mathbf{B} tensors is $(d-1)D^2$ for both a unique and for a degenerate ground state in the reduced parametrization.

In general, the state $|\mathbf{B}_{\alpha},j\rangle$ is *not* a true one-particle eigenstate of the Hamiltonian. This is so for two reasons: First, because excitations are normally not strictly local, and second, because a single \mathbf{B} tensor is not enough to describe an excitation completely. A better description can be achieved by using a linear combination of all \mathbf{B} s. For translational invariant systems in the TDL this is best done in momentum space. Working in momentum space also provides an easy workaround for the gauge induced asymmetry of matrix elements mentioned in Eq. (5.11).

The basis states in momentum space are the Fourier transform of Eq. (5.2)

$$|\mathbf{B}_{\alpha},q\rangle := \frac{1}{\sqrt{L}} \sum_j e^{-iqj} |\mathbf{B}_{\alpha},j\rangle \quad (5.18)$$

as already introduced in Eq. (5.4). These states are known as Wannier states and are orthogonal with respect to momentum

$$\langle \mathbf{B}_{\alpha},q | \mathbf{B}_{\beta},q' \rangle \propto \delta_{q,q'} , \quad (5.19)$$

see App. A.6 for details. Orthogonality with respect to the index α is ensured by construction, cf. Eq. (5.13). Therefore, the norm matrix for each q in momentum space is simply the identity

$$N_{\alpha\beta}^q := \langle \mathbf{B}_{\alpha},q | \mathbf{B}_{\beta},q \rangle \quad (5.20a)$$

$$= \frac{1}{L} \sum_{j',j} e^{iq(j'-j)} \langle \mathbf{B}_{\alpha},j' | \mathbf{B}_{\beta},j \rangle \quad (5.20b)$$

$$= \frac{1}{L} \sum_{j',j} e^{iq(j'-j)} \delta_{j',j} \delta_{\alpha,\beta} \quad (5.20c)$$

$$= \delta_{\alpha,\beta} . \quad (5.20d)$$

Now, the dispersion relation is determined by variation of the coefficients v_{α}^q of the linear combination of the states $|\mathbf{B}_{\alpha},q\rangle$. This leads to another EVP

$$H^q \vec{v}^q = \omega_q N^q \vec{v}^q = \omega_q \vec{v}^q \quad (5.21)$$

where the elements of the Hamiltonian matrix H^q are given by

$$H_{\alpha\beta}^q = \langle \mathbf{B}_{\alpha},q | \tilde{H} | \mathbf{B}_{\beta},q \rangle . \quad (5.22)$$

Due to the orthogonality with respect to momentum, this EVP can be solved for each desired point in momentum space independently. The lowest EV ω_q of Eq. (5.21) is the best variational estimate for the dispersion relation.

The matrix elements $H_{\alpha\beta}^q$ are computed as follows

$$H_{\alpha\beta}^q = \langle \mathbf{B}_{\alpha},q | \tilde{H} | \mathbf{B}_{\beta},q \rangle \quad (5.23a)$$

$$= \frac{1}{L} \sum_{j',j} e^{iq(j'-j)} \langle \mathbf{B}_{\alpha},j' | \tilde{H} | \mathbf{B}_{\beta},j \rangle \quad (5.23b)$$

$$= \frac{1}{L} \sum_{j',j} \sum_i e^{iq(j'-j)} \langle \mathbf{B}_{\alpha},j' - j | \tilde{H} | \mathbf{B}_{\beta},0 \rangle \quad (5.23c)$$

$$= \sum_j e^{iqj} \langle \mathbf{B}_{\alpha},j | \tilde{H} | \mathbf{B}_{\beta},0 \rangle \quad (5.23d)$$

$$=: \sum_j e^{iqj} H_{\alpha\beta}^j . \quad (5.23e)$$

The index shift $j' \rightarrow j' - j$ in step (5.23b) to (5.23c) is allowed, since the matrix element does not depend on the absolute positions due to translation invariance (TI), but only on the relative distances. In the last step, the index was renamed again $j' - j \rightarrow j$, which is possible in the TDL since all sums run from $-\infty$ to ∞ . Then, the expression does no longer depend on j' at all, and the summation can be carried out, canceling out the normalization factor $\frac{1}{L}$.

The matrix element $H_{\alpha\beta}^j$ in Eq. (5.23e) is a matrix element of the full Hamiltonian, i.e., it contains the theoretically infinite sum over all lattice sites i . Note that generically the relation

$$\langle \psi | \hat{O} | \phi \rangle = \langle \phi | \hat{O}^\dagger | \psi \rangle^* \quad (5.24)$$

holds. Since the Hamiltonian is Hermitian, from Eq. (5.24) and TI follows that only matrix elements with $j \geq 0$ need to be computed because

$$H_{\alpha\beta}^{-j} = \langle \mathbf{B}_\alpha, -j | \tilde{H} | \mathbf{B}_\beta, 0 \rangle \quad (5.25a)$$

$$= \langle \mathbf{B}_\beta, 0 | \tilde{H} | \mathbf{B}_\alpha, -j \rangle^* \quad (5.25b)$$

$$= \langle \mathbf{B}_\beta, +j | \tilde{H} | \mathbf{B}_\alpha, 0 \rangle^* \quad (5.25c)$$

$$= (H_{\beta\alpha}^{+j})^* . \quad (5.25d)$$

For $j \geq 0$ the matrix element $H_{\alpha\beta}^j$ can then be computed as

$$H_{\alpha\beta}^j = \sum_i \langle \mathbf{B}_\alpha, j | \tilde{h}_i | \mathbf{B}_\beta, 0 \rangle \quad (5.26a)$$

$$= \sum_i \langle \mathbf{B}_\alpha, j - i | \tilde{h}_0 | \mathbf{B}_\beta, -i \rangle . \quad (5.26b)$$

Due to TI, matrix elements do not depend on absolute positions, but only on relative distances between the operator and the \mathbf{B} tensors. Therefore, as done in Eq. (5.26), all positions are shifted such that the first operator in a product of local operators acts on site $i = 0$. This is adopted as a convention throughout the remainder of this thesis.

The computation of matrix elements is generically linear; therefore, the matrix element for an operator that consists of a sum results in a sum of matrix elements, for instance

$$\langle \mathbf{B}_\alpha, j - i | \tilde{h}_0 | \mathbf{B}_\beta, -i \rangle = \langle \mathbf{B}_\alpha, j - i | (S_0^z - 2\lambda S_0^x S_1^x - \mathbb{1}\epsilon_0) | \mathbf{B}_\beta, -i \rangle \quad (5.27a)$$

$$= \langle \mathbf{B}_\alpha, j - i | S_0^z | \mathbf{B}_\beta, -i \rangle - 2\lambda \langle \mathbf{B}_\alpha, j - i | S_0^x S_1^x | \mathbf{B}_\beta, -i \rangle - \epsilon_0 \langle \mathbf{B}_\alpha, j - i | \mathbb{1} | \mathbf{B}_\beta, -i \rangle , \quad (5.27b)$$

each of which is represented by its own TN. The next section shows how these matrix elements are computed in practice.

5.2 Tensor network calculations

As stated in Chap. 3, the tensor network (TN) notation is a very powerful tool in MPS calculations in general, and for iMPS in particular. This section shows, how the intuitively drawn network diagrams translate into mathematical expressions.

5.2.1 TN topology

The matrix elements in Eq. (5.27) can all be drawn as tensor networks. For instance, for $i = -3$ and $j = 2$, the matrix element of the Ising interaction becomes

$$\langle B_{\alpha,2+3} | S_0^x S_1^x | B_{\beta,3} \rangle = \text{Diagram} \quad (5.28)$$

where the ground state tensors **A** are drawn as circles as always, and the **B** tensors are represented by triangles for easy distinction.

In the previous chapter, the symbol --- was used as a placeholder for an arbitrary number of transfer operators T , and to denote that a given TN is to be considered as an example.

To make this even simpler, the concept of TN topology is now defined. Two TNs are considered topologically equivalent if they can be transformed into each other by adding or removing transfer operators only. For example, the following TN is topologically equivalent to the one in Eq. (5.28)

$$\text{Diagram} \quad (5.29)$$

because it can be transformed into it by adding one transfer operator between S_1^x and B_{β} , and removing one between B_{β} and B_{α} . In contrast, the following TN not *not* topologically equivalent to Eq. (5.28)

$$\text{Diagram} \quad (5.30)$$

because a), the relative positions of B_{β} and B_{α} are changed, and b), B_{α} is on the same site as an operator, which is not the case in Eq. (5.28).

From here on, every TN is considered as a representative for *all* TNs that are topologically equivalent to it, unless explicitly stated otherwise.

Also, the notation

$$\text{Diagram} := T^{\delta_i} \quad (5.31)$$

is used to denote a block of transfer operators of variable width δ_i , including zero. Therefore, T^0 is defined as not applying any transfer operators, i.e.

$$T^0[v_{\text{eff}}] := v_{\text{eff}} \quad \forall v_{\text{eff}}. \quad (5.32)$$

As will be shown in Sec. 5.2.3, all topologically equivalent TNs with the same operator (including no operator at all) and the same **B** tensors are evaluated in the same way.

5.2.2 TN factorization

A second important concept is that of TN factorization. As discussed in Sec. 3.6, for the transfer operator T , the following relation holds

$$\lim_{j \rightarrow \infty} T^j = \Lambda_0^j \vec{v} \vec{u}^\dagger. \quad (5.33)$$

In numerical calculations, for practical purposes the limit is reached for $j = \Xi_T$ with

$$\left| \frac{\Lambda_1}{\Lambda_0} \right|^{\Xi_T} < \theta \quad (5.34)$$

where θ is either machine precision or some larger tolerance value that one is willing to accept. With $\Lambda_0 = 1$, this translates to TN notation as

$$\underbrace{\begin{array}{c} \bullet \quad \bullet \\ | \quad | \\ \bullet \quad \bullet \end{array}}_{\delta_i} \stackrel{\delta_i > \Xi_T}{\approx} \left. \begin{array}{c} \bullet \\ | \\ \bullet \end{array} \right\} \times \left[\begin{array}{c} \bullet \\ | \\ \bullet \end{array} \right]. \quad (5.35)$$

Therefore, if it contains a sufficiently large power of T , a TN factorizes into a product of smaller networks. For instance

$$\begin{array}{c} \begin{array}{c} \bullet \quad \bullet \quad \bullet \quad \bullet \quad \bullet \quad \bullet \quad \bullet \\ | \quad | \quad | \quad | \quad | \quad | \quad | \\ \bullet \quad \bullet \quad \bullet \quad \bullet \quad \bullet \quad \bullet \quad \bullet \end{array} \\ \underbrace{\hspace{10em}}_{\delta_0} \\ \begin{array}{c} \square S_0^x \quad \square S_1^x \\ | \quad | \\ \bullet \quad \bullet \end{array} \end{array} \times \begin{array}{c} \begin{array}{c} \bullet \quad \bullet \quad \bullet \\ | \quad | \quad | \\ \bullet \quad \bullet \quad \bullet \end{array} \\ \begin{array}{c} \blacktriangledown B_\alpha \\ \blacktriangle B_\beta \end{array} \end{array} \stackrel{\delta_0 > \Xi_T}{\approx} \begin{array}{c} \begin{array}{c} \bullet \quad \bullet \quad \bullet \\ | \quad | \quad | \\ \bullet \quad \bullet \end{array} \\ \begin{array}{c} \square S_0^x \quad \square S_1^x \\ | \quad | \\ \bullet \quad \bullet \end{array} \end{array} \times \begin{array}{c} \begin{array}{c} \bullet \quad \bullet \quad \bullet \\ | \quad | \quad | \\ \bullet \quad \bullet \quad \bullet \end{array} \\ \begin{array}{c} \blacktriangledown B_\alpha \\ \blacktriangle B_\beta \end{array} \end{array}. \quad (5.36)$$

This helps to quickly assess what a given TN converges to. For instance, for $\delta_0 > \Xi_T$ the above TN converges to zero, since the right factor is zero in canonical gauge due to Eq. (5.10).

Note that a factorization can also be made for a TN that does not include a power T^{Ξ_T} of the transfer operator. The value of such a factorization is generally *not* equal to value of the original TN. However, this is still an important tool in determining the 1QP content of 2QP TNs, as will be discussed in Chap. 6.

5.2.3 Matrix element TN evaluation

As seen already in the construction of the EVPs in the ground state search and in the search for excitations, all TNs are ultimately evaluated as a scalar product of two $D \times D$ matrices u_{eff} and v_{eff} , using the matrix scalar product defined in Eq. (3.10). The matrix u_{eff} represents the left half-infinite part of the system, and v_{eff} represents the right half-infinite part, respectively.

Using the convention, that the operator always acts on site 0, and with $j \geq 0$, there are three different cases of TNs which occur in the computation of $H_{\alpha\beta}^j$ in Eq. (5.23e), depending on the summation index i

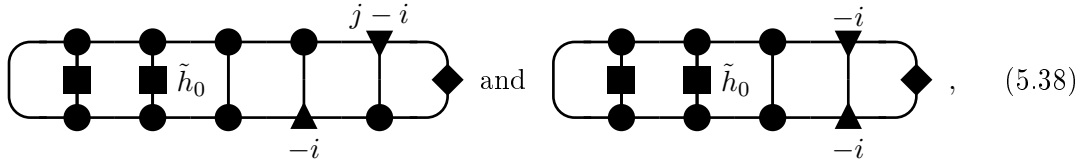
$$H_{\alpha\beta}^j = \sum_i \langle \mathbf{B}_{\alpha, j-i} | \tilde{h}_0 | \mathbf{B}_{\beta, -i} \rangle \quad (5.37a)$$

$$\begin{aligned} &= \sum_{i \leq -n} \langle \mathbf{B}_{\alpha, j-i} | \tilde{h}_0 | \mathbf{B}_{\beta, -i} \rangle + \sum_{i=-n+1}^j \langle \mathbf{B}_{\alpha, j-i} | \tilde{h}_0 | \mathbf{B}_{\beta, -i} \rangle \\ &\quad + \sum_{i > j} \langle \mathbf{B}_{\alpha, j-i} | \tilde{h}_0 | \mathbf{B}_{\beta, -i} \rangle . \end{aligned} \quad (5.37b)$$

Here n is the number of lattice sites the operator acts on. For the local Hamiltonian \tilde{h} , in case of the TFIM $n = 2$, and for the FMHC with next-nearest neighbor interaction, $n = 3$.

Case i): $i \leq -n$

Due to the index shift by $-i$ in Eq. (5.26), this means that the operator acts to the left of both \mathbf{B} tensors. This results in two topologically distinct classes of TNs



for $j > 0$ and $j = 0$, respectively. In this case, an effective right boundary matrix $v_{\alpha\beta}^j$ can be defined

$$v_{\alpha\beta}^j := \begin{cases} \mathbb{1}^{(\mathbf{B}_{\alpha}; \mathbf{B}_{\beta})}[v], & \text{if } j = 0 \\ \mathbb{1}^{(\mathbf{A}; \mathbf{B}_{\beta})}[T^{j-1}[\mathbb{1}^{(\mathbf{B}_{\alpha}; \mathbf{A})}[v]]], & \text{if } j > 0 \end{cases} . \quad (5.39)$$

Note the different handling for the topologically distinct cases $j = 0$ and $j > 0$. Then, each contribution to the sum is given by

$$\langle \mathbf{B}_{\alpha, j-i} | \tilde{h}_0 | \mathbf{B}_{\beta, -i} \rangle = \left((T^\dagger)^{|i|-n} [\tilde{h}_i^\dagger^{(\mathbf{A}; \mathbf{A})}[u]], v_{\alpha\beta}^j \right) . \quad (5.40)$$

In case of the TFIM, every TN with an operator \tilde{h}_0 actually stands for *three* TNs, as seen in Eq. (5.27). However, due to the sesquilinearity of the scalar product, the expression $\tilde{h}_0^\dagger^{(\mathbf{A}; \mathbf{A})}[u]$ can be defined as

$$\tilde{h}_0^\dagger^{(\mathbf{A}; \mathbf{A})}[u] := \mathbb{1}_1^\dagger^{(\mathbf{A}; \mathbf{A})}[S_0^{z\dagger(\mathbf{A}; \mathbf{A})}[u]] - 2\lambda S_1^{x\dagger(\mathbf{A}; \mathbf{A})}[S_0^{x\dagger(\mathbf{A}; \mathbf{A})}[u]] - \epsilon_0 \mathbb{1}_1^\dagger^{(\mathbf{A}; \mathbf{A})}[S_0^{x\dagger(\mathbf{A}; \mathbf{A})}[u]] \quad (5.41a)$$

$$\begin{aligned} &= \sum_{s'_1, s_1} \mathbb{1}_{s'_1 s_1}^\dagger A^{s'_1 \dagger} \left(\sum_{s'_0, s_0} S_{s'_0 s_0}^{z\dagger} A^{s'_0 \dagger} u A^{s_0} \right) A^{s_1} \\ &\quad - 2\lambda \sum_{s'_1, s_1} S_{s'_1 s_1}^{x\dagger} A^{s'_1 \dagger} \left(\sum_{s'_0, s_0} S_{s'_0 s_0}^{x\dagger} A^{s'_0 \dagger} u A^{s_0} \right) A^{s_1} \\ &\quad - \epsilon_0 \sum_{s'_1, s_1} \mathbb{1}_{s'_1 s_1}^\dagger A^{s'_1 \dagger} \left(\sum_{s'_0, s_0} \mathbb{1}_{s'_0 s_0}^\dagger A^{s'_0 \dagger} u A^{s_0} \right) A^{s_1} , \end{aligned} \quad (5.41b)$$

which allows to treat all three TNs at the same time as one.

Note the order in which the operators are applied to the boundary matrix u . First the operator on site 0 is applied, then the operator on site 1, just as depicted in the TN. Also note that for correct alignment the field term S_0^z needs to be padded with an identity operator on the right side, so that this summand in \tilde{h}_0 acts on $n = 2$ sites, too. For the ground state energy correction term $-\epsilon_0 \mathbb{1}_0$ this is not strictly necessary, but also does not change the result. Therefore, for consistent handling it is easiest to pad all terms with identities from the right so that they act on n sites.

Using the sesquilinearity of the scalar product again, the sum over i in Eq. (5.40) can also be carried out on the level of left boundary matrices. Therefore, the contribution for $i < -n$ can be expressed as

$$H_{\alpha\beta}^j \Big|_{i < -n} = \sum_{i < -n} \left((T^\dagger)^{|i-n|} [\tilde{h}_i^{\dagger(A;A)}[u]], v_{\alpha\beta}^j \right) \quad (5.42a)$$

$$= \left(\sum_{i=0}^{\infty} (T^\dagger)^i [\tilde{h}^{\dagger(A;A)}[u]], v_{\alpha\beta}^j \right) \quad (5.42b)$$

$$=: \left(u_{\tilde{h}}, v_{\alpha\beta}^j \right). \quad (5.42c)$$

The matrix

$$u_{\tilde{h}} := \sum_{i=0}^{\infty} (T^\dagger)^i [\tilde{h}^{\dagger(A;A)}[u]] \quad (5.43)$$

can be computed very efficiently by noting that each summand is obtained by just applying the Hermitian conjugate T^\dagger of the transfer operator once to the previous one. See Sec. 5.7 for a more detailed analysis of the numerical effort.

In Eq. (5.42) the sum theoretically still runs to infinity. However, for $|i-n| > \Xi_T$, the TN factorizes as seen in Eq. (5.36)

$$\langle \mathbf{B}_{\alpha,j-i} | \tilde{h}_0 | \mathbf{B}_{\beta,-i} \rangle \stackrel{|i-n| > \Xi_T}{\approx} \langle GS | \tilde{h}_0 | GS \rangle \times \langle \mathbf{B}_{\alpha,j-i} | \mathbb{1} | \mathbf{B}_{\beta,-i} \rangle. \quad (5.44)$$

The first factor is always zero since that is the ground state expectation value of $\tilde{h}_0 = h_0 - \epsilon_0$. Thus, in numerics the sum only needs to be computed for $i \leq \Xi_T$. Due to the orthogonality of the \mathbf{B}_α tensors to the ground state, the second factor is also zero if $j \neq 0$.

There is one important thing to keep in mind about TNs for excited states. Although there is a strong appearance of locality in the iMPS formulation, since every tensor \mathbf{A} or \mathbf{B} is associated with one local site, and operators can also be attributed to a local site. However, this can be misleading. For non-trivial bond dimensions, i.e., $D > 1$, a TN such as

$$\langle \mathbf{B}_{\alpha,\ell} | O_0 | \mathbf{B}_{\beta,\ell} \rangle = \text{Diagram} \quad (5.45)$$

evaluates to

$$\langle \mathbf{B}_{\alpha,\ell} | O_0 | \mathbf{B}_{\beta,\ell} \rangle = \text{Diagram 1} \times \text{Diagram 2} \quad (5.46)$$

only for $|\ell| > \Xi_T$. For smaller distances, due to the entanglement encoded in the site tensors, the tensor \mathbf{B} “sees” the operator, even if it acts on a site at a distance of up to Ξ_T .

Case ii): $i > j$

The second type of TN from Eq. (5.26) is the case $i > j$, i.e. the operator acts to the *right* of all \mathbf{B} tensors. This case can be handled very similarly to the first one. Again, there are two topologically distinct TN classes depending on j

$$(5.47)$$

Here, an effective left boundary matrix $u_{\alpha\beta}^j$ can be defined

$$u_{\alpha\beta}^j := \begin{cases} \mathbb{1}^{\dagger(\mathbf{B}_\alpha; \mathbf{B}_\beta)}[u], & \text{if } j = 0 \\ 0, & \text{if } j > 0, \end{cases} \quad (5.48)$$

where again the topologically different cases $j = 0$ and $j > 0$ need to be handled differently. The vanishing of this matrix for $j \neq 0$ follows from the left-canonical gauge of \mathbf{B}_β . Taking this into account, the contribution from this type of TN is given by

$$\langle \mathbf{B}_\alpha, j - i | \tilde{h}_0 | \mathbf{B}_\beta, -i \rangle = \left(u_{\alpha\beta}^j, T^{i-1}[\tilde{h}^{(\mathbf{A}; \mathbf{A})}[v]] \right). \quad (5.49)$$

The expression $\tilde{h}_0^{(\mathbf{A}; \mathbf{A})}[v]$ is defined analogously to Eq. (5.41), with the difference that the operator at site 1 is applied to v first, and then the operator at site 0. Again, this is exactly as depicted in the TN.

As in the previous case, the sum can be carried out on the level of boundary matrices, in this case the right one, v . The summed contribution reads

$$H_{\alpha\beta}^j \Big|_{i>j} = \sum_{i>j} \left(u_{\alpha\beta}^j, T^{i-1}[\tilde{h}^{(\mathbf{A}; \mathbf{A})}[v]] \right) \quad (5.50a)$$

$$= \left(u_{\alpha\beta}^j, \sum_{i=0}^{\infty} T^i[\tilde{h}^{(\mathbf{A}; \mathbf{A})}[v]] \right) \quad (5.50b)$$

$$=: \left(u_{\alpha\beta}^j, v_{\tilde{h}} \right) \quad (5.50c)$$

with a summed right boundary matrix defined analogously to $u_{\tilde{h}}$ as

$$v_{\tilde{h}} := \sum_{i=0}^{\infty} T^i[\tilde{h}^{(\mathbf{A}; \mathbf{A})}[v]] = \sum_{i=0}^{\Xi_T} T^i[\tilde{h}^{(\mathbf{A}; \mathbf{A})}[v]] + \mathcal{O}(|\Lambda_1|^{\Xi_T}), \quad (5.51)$$

which can be computed in the same efficient manner. Again, the TN factorizes for $i > \Xi_T$, and the second factor $\langle GS | \tilde{h}_0 | GS \rangle$ is always zero, so that the sum can be cut at $i = \Xi_T$.

Case iii): $-n < i \leq j$

The intermediate case with $-n < i \leq j$ is the most difficult one. One simplification is that the sum actually only runs to $i = 0$. In left-canonical gauge, all TNs with $i > 0$ are zero except for those with $j = 0$, which are already covered in case ii) above. Unfortunately, this is the only simplification that can be made.

Like in the other two cases, there are two topologically distinct TN types, depending on j

$$(5.52)$$

where the second type can only occur if $j < n$.

The first TN type, where the operator acts on only one site with a \mathbf{B} tensor, evaluates to

$$= \left(\hat{O}_{-i}^{\dagger(\mathbf{A};\mathbf{B}_\beta)}[u], T^{j-2}[\mathbb{1}^{(\mathbf{B}_\alpha;\mathbf{A})}[v]] \right). \quad (5.53)$$

For an n -site operator $\hat{O} = \hat{O}_0 \hat{O}_1 \cdots \hat{O}_{n-1}$, the expression $\hat{O}_{-i}^{\dagger(\mathbf{A};\mathbf{B}_\beta)}[u]$ is defined as

$$\hat{O}_{-i}^{\dagger(\mathbf{A};\mathbf{B}_\beta)}[u] := \begin{cases} \hat{O}_{n-1}^{\dagger(\mathbf{A};\mathbf{A})}[\cdots \hat{O}_1^{\dagger(\mathbf{A};\mathbf{A})}[\hat{O}_0^{\dagger(\mathbf{A};\mathbf{B}_\beta)}[u]]], & \text{if } -i = 0 \\ \hat{O}_{n-1}^{\dagger(\mathbf{A};\mathbf{A})}[\cdots \hat{O}_1^{\dagger(\mathbf{A};\mathbf{B}_\beta)}[\hat{O}_0^{\dagger(\mathbf{A};\mathbf{A})}[u]]], & \text{if } -i = 1 \\ \vdots \\ \hat{O}_{n-1}^{\dagger(\mathbf{A};\mathbf{B}_\beta)}[\cdots \hat{O}_1^{\dagger(\mathbf{A};\mathbf{A})}[\hat{O}_0^{\dagger(\mathbf{A};\mathbf{A})}[u]]], & \text{if } -i = n-1 \end{cases}. \quad (5.54)$$

The second TN type, where the operator acts on two sites with a \mathbf{B} tensor, evaluates to

$$= \left(\hat{O}_{j-i;-i}^{\dagger(\mathbf{B}_\alpha;\mathbf{B}_\beta)}[u], v \right). \quad (5.55)$$

The expression $\hat{O}_{j-i;-i}^{\dagger(\mathbf{B}_\alpha;\mathbf{B}_\beta)}[u]$ is defined analogously to Eq. (5.54) as

$$\hat{O}_{j-i;-i}^{\dagger(\mathbf{B}_\alpha;\mathbf{B}_\beta)}[u] := \hat{O}_{n-1}^{\dagger(\mathbf{B}_\alpha;\mathbf{A})}[\cdots \hat{O}_1^{\dagger(\mathbf{A};\mathbf{A})}[\hat{O}_0^{\dagger(\mathbf{A};\mathbf{B}_\beta)}[u]]], \quad \text{if } -i = 0 \text{ and } j-i = n-1 \quad (5.56)$$

and so forth. Both Eq. (5.54) and Eq. (5.56) imply that there is a ground state tensor \mathbf{A} on any site which does not explicitly have a \mathbf{B} tensor assigned to it.

This type of expression must be evaluated for each summand in a multi-term operator like \tilde{h} individually, and the results are summed up.

5.2.4 Complexity analysis

The computational cost of evaluating a TN scales linearly with its width, i.e., the number of non-trivial rungs. Non-trivial in this context means that the rung is not a transfer operator, or it is a transfer operator which is not directly adjacent to a pure left or right boundary matrix u or v . For instance, the width of the TNs in Eq. (5.47) is 4, and the width of the TN in Eq. (5.55) is 2.

The cost of applying a transfer operator T or an identity $\mathbb{1}^{(\mathbf{B};\mathbf{A})}$ to a boundary matrix is in $\mathcal{O}(dD^3)$, which can be seen from Eq. (3.67). The cost of applying a non-trivial operator to a boundary matrix scales as $\mathcal{O}(d^2D^3)$, as seen in Eq. (3.83).

In $H_{\alpha\beta}^j$, the average TN width is $\frac{\Xi_T}{2}$. Therefore, the overall computation cost scales as

$$\tau_c = \mathcal{O}(\Xi_T D^3(\Xi_T d + d^2)). \quad (5.57)$$

5.3 Momentum discretization

In the TDL, the momentum q is actually a continuous variable. However, in order to carry out numerical computations, such as solving the EVP for the dispersion, momentum must be discretized. This means the Brillouin zone is sampled with a finite number $L_q \in \mathbb{N}$ of momentum values. Due to the properties of the discrete Fourier transformation, this means that the model is evaluated on a *finite* system of length L_q . Using the standard definition of the discrete Fourier transformation used throughout this thesis, this implies *periodic boundary conditions*. In principle, the iMPS framework allows to choose L_q arbitrarily. In practice, some important considerations need to be made.

First, real space quantities which are derived from momentum space results will also be L_q -periodic. For instance, the hopping element

$$t_j := \frac{1}{L_q} \sum_q e^{+iqj} \omega_q \quad (5.58)$$

cannot be determined for $|j| > \frac{L_q}{2}$, since this is the periodicity of the finite lattice implied by the choice of L_q . Therefore, if some real space quantity is to be computed as Fourier transform of a momentum space result, and a certain spatial extent is needed, this determines the minimum value for L_q that can be used.

Second, there is a difference between L_q being even or odd. In this thesis, it is chosen odd. The reason for this is the choice of the 2QP basis, refer to App. A.7 for details. With an odd number of sampling points or, equivalently, momentum intervals

$$\Delta q := \frac{2\pi}{L_q}, \quad (5.59)$$

one can either sample $q = 0$ or $q = \pi$ exactly, but not both. Since for both the TFIM and the FMHC the gap is located at $q = 0$, the sampling points are chosen such that they include $q = 0$, and neither of the boundaries $q = \pm\pi$. In this choice, $q = \pm\pi$ cannot be sampled exactly, but approximated to arbitrary precision by increasing L_q , thereby decreasing Δq . Thus, all momentum points are contained in the open interval

$$q \in (-\pi, \pi) \quad (5.60)$$

and the momentum points accessible by the discrete sampling are given by

$$q = n_q \Delta q \quad \text{with} \quad n_q \in \left\{ -\left\lfloor \frac{L_q}{2} \right\rfloor, \dots, \left\lfloor \frac{L_q}{2} \right\rfloor \right\}. \quad (5.61)$$

The momentum q is therefore referred to as being odd or even depending on the integer n_q being odd or even.

If critical behavior is expected at $q = \pm\pi$, the interval can simply be shifted by π , yielding samples for instance from the open interval $(0, 2\pi)$, where $q = \pi$ is one of the sampling points.

5.4 Dispersion results

In this section, some results for the dispersion relations of the FMHC and the TFIM are given.

5.4.1 Results for the FMHC

As mentioned above, the ground state of the model is a product state and can therefore be described exactly by a MPS with $D = 1$. For this bond dimension, there is only one excitation tensor \mathbf{B} in the reduced parametrization, since $(d-1)D^2 = 1$. This tensor is of dimension $d \times D \times D = 2 \times 1 \times 1$. Since the momentum space EVP Eq. (5.21) is of dimension 1×1 , there are no higher energy EVs to capture the bound state. This can be remedied by increasing the bond dimension beyond $D = 1$, which is more than is needed for the ground state, but has the capacity to produce EVs at higher energies.

In general, these higher EVs lie somewhere in a multiparticle continuum. The lower and upper boundaries of the 2QP continuum are given by

$$\Omega_Q^{\ell} = \min_q (\omega_q + \omega_{Q-q}) \quad (5.62a)$$

$$\Omega_Q^h = \max_q (\omega_q + \omega_{Q-q}), \quad (5.62b)$$

respectively.

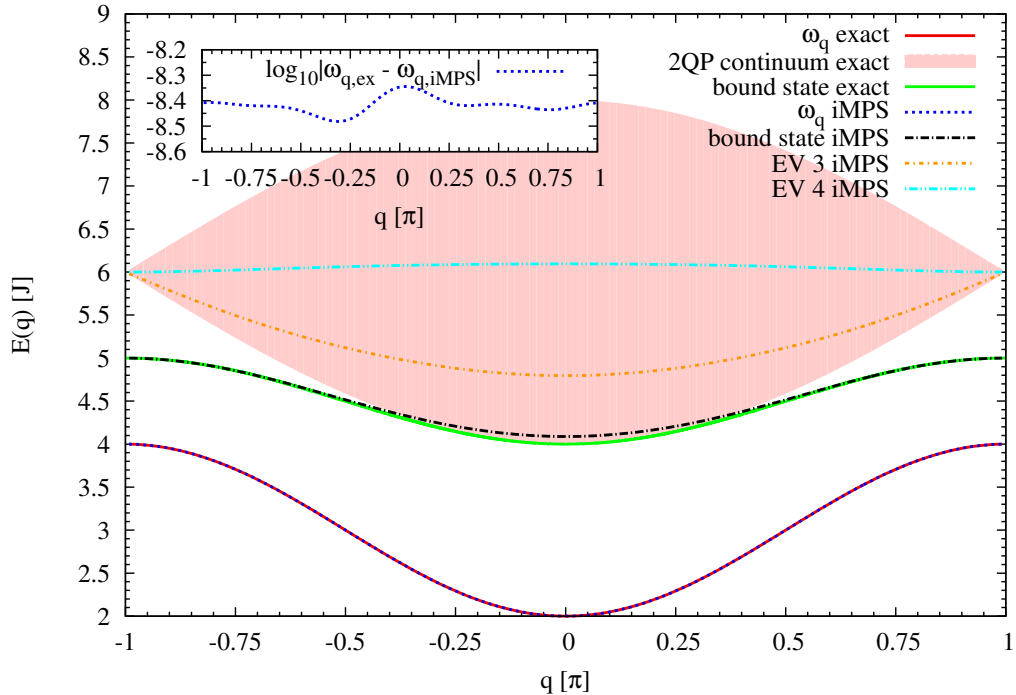


Figure 5.1: Energy spectrum of the FMHC for the parameters $\Gamma = 2$ and $J_2 = 0$, computed with bond dimension $D = 3$. The figure shows both the exact solution and the iMPS results. The one-particle dispersion ω_q is reproduced perfectly. The bound state result from the iMPS computation protrudes slightly into the two-particle continuum, and the other EVs lie inside it. The inset shows the base 10 logarithm of the deviation of the iMPS dispersion from the exact solution.

Figure 5.1 shows the energy spectrum of the FMHC for the parameters $\Gamma = 2$ and $J_2 = 0$, i.e., without next-nearest neighbor interaction, computed with $D = 3$.

The dispersion is clearly reproduced perfectly, as can be seen in the inset, which shows the deviation of the iMPS result from the exact solution. This deviation is by roughly 8 orders of magnitude larger than the deviations in the ground state energy shown in Fig. 4.4. However, 10^{-8} is still very small, especially given the excess bond dimension. The accurate result for the dispersion allows us to establish the boundaries of the 2QP continuum with very high precision as well, using (5.62). Therefore, they are not shown in Fig. 5.1. Of the overall nine EVs from the iMPS result, seven lie inside the 2QP continuum, as expected. Five of them were omitted in order not to clutter the plot too much.

The remaining EV is the second lowest, and it lies *below* the boundary of the 2QP continuum, at least at the edges of the Brillouin zone. This is a clear indication of a bound state. The agreement with the exact bound state energy from Eq. (2.23) is quite remarkable, since the bound state is not really a one-particle state. Around the center of the Brillouin zone the iMPS results protrudes slightly into the 2QP continuum. For a true 2QP result this would mean that the bound state becomes unstable in this region and only exists as a resonance.

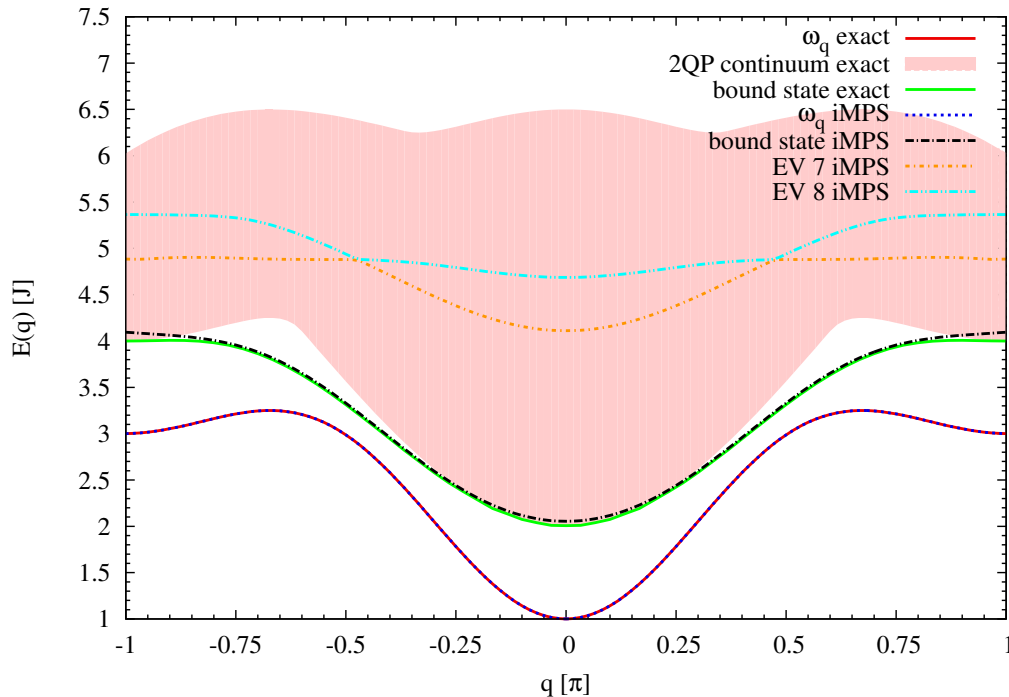


Figure 5.2: Energy spectrum of the FMHC for the parameters $\Gamma = 1.0$ and $J_2 = 0.5$, computed with bond dimension $D = 3$. The figure shows both the exact solution and the iMPS results. The one-particle dispersion ω_q is reproduced perfectly. The bound state result from the iMPS computation protrudes slightly into the two-particle continuum, and the other EVs lie inside of it.

Figure 5.2 shows the same data as Fig. 5.1, but for a different set of parameters, $\Gamma = 1$ and $J_2 = 0.5$, i.e., *with* next-nearest neighbor interaction. Due to this interaction, the spectrum displays more features. However, the basic observations remain unchanged. Only the bound state enters the continuum at the edges of the Brillouin zone, too. It is still clearly identifiable a such, though. The exact result was obtained by diagonalizing the 2QP Hamiltonian in Eq. (2.24).

Again, five of the nine EVs are omitted from the plot. The two that are chosen show one important fact: in variational algorithms, energies are usually ordered simply by their value. If a level crossing occurs as function of momentum, individual EVs may exhibit kinks. This can also affect the lowest EV, if there are multiple, non-degenerate flavors of elementary excitations. In this case, human revision of the dispersion results is required.

For bond dimension $D = 3$, the Schmidt coefficients $s_{i>1}$ of \mathbf{A} are of the order of machine precision. Therefore, the fact that any accurate results can be obtained is rather surprising. For $D > 3$, no sensible excitation energies can be obtained. This is due to the excess number of parameters in the ground state tensor \mathbf{A} , which makes the EVP Eq. (5.12) numerically unstable and is expected.

5.4.2 Results for the TFIM

As described in Sec. 2.2, the elementary excitations of the TFIM are dressed spin-flips in the disordered phase and dressed domain walls in the ordered phase. The spin flips are clearly non-degenerate. The domain walls come in two types, $\leftarrow\rightarrow$ and $\rightarrow\leftarrow$. However, these are equivalent. Also, the ansatz in Eq. (5.2) only allows one type to occur in the computation. Therefore, the only EV of interest of Eq. (5.21) is the lowest one, which yields the one-particle dispersion ω_q .

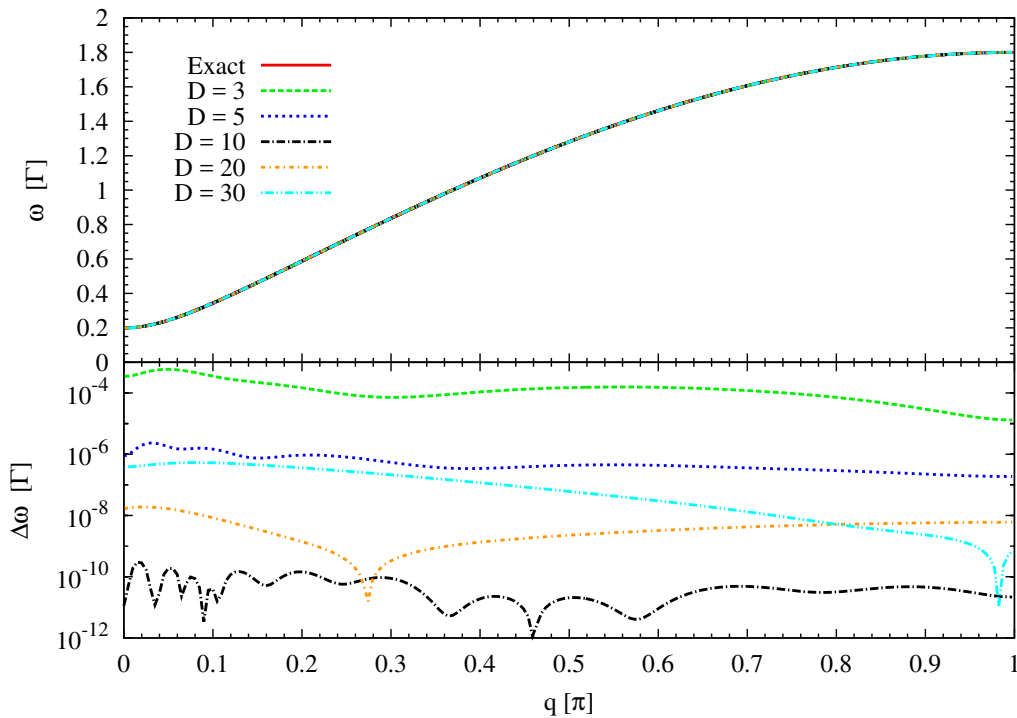


Figure 5.3: Dispersion relation of the TFIM for $\lambda = 0.8$.

Figures 5.3 through 5.5 show the dispersion relation for various values of λ and several bond dimensions. It is apparent from Fig. 5.3 and Fig. 5.4 that the algorithm works equally well in the ordered and in the disordered phase. Away from criticality, the dispersion can be obtained to extremely high precision with very moderate effort¹. Note that the deviation

$$\Delta\omega_q := |\omega_{q,\text{iMPS}} - \omega_{q,\text{ex}}| \quad (5.63)$$

¹Using parallelization, computing the dispersion from a known ground state \mathbf{A} at bond dimension $D = 10$ takes less than two minutes on a quad-core workstation computer.

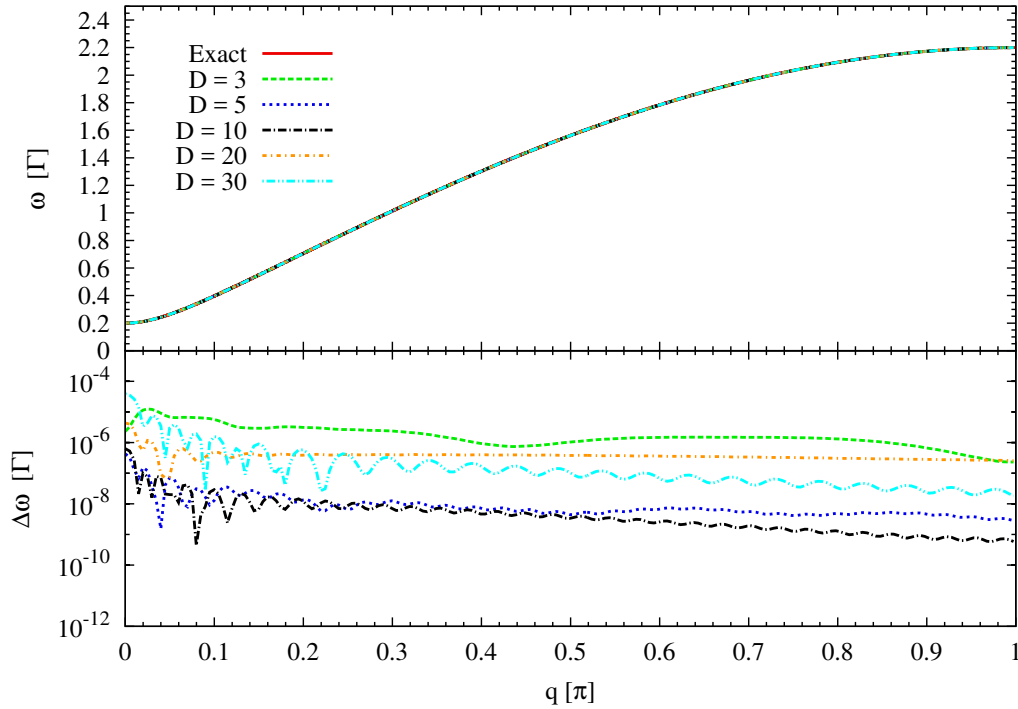


Figure 5.4: Dispersion relation of the TFIM for $\lambda = 1.2$.

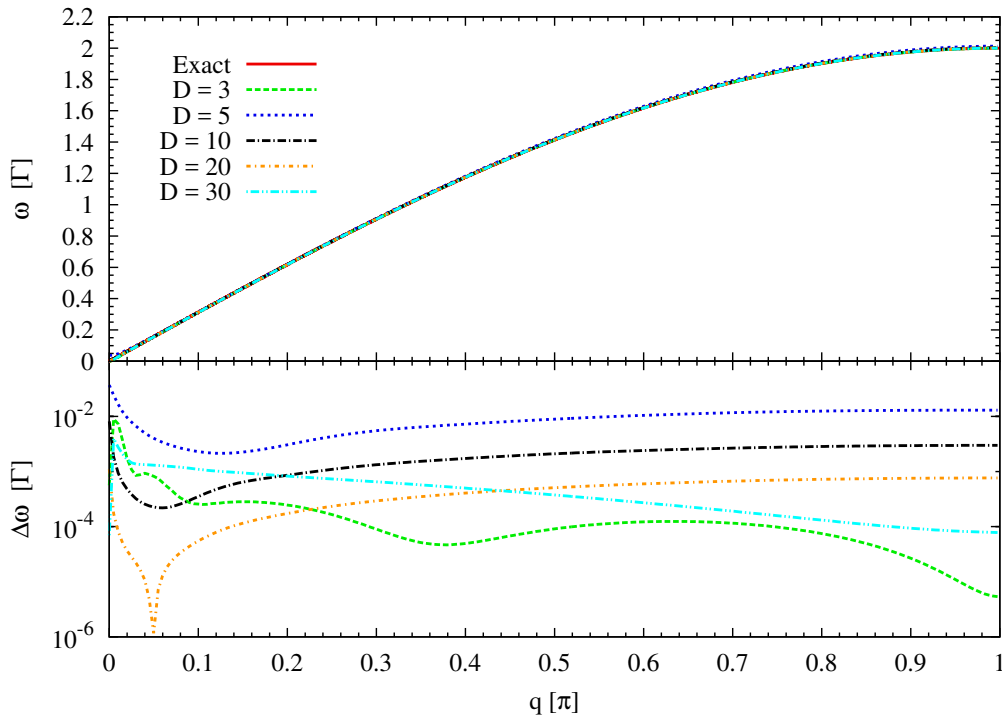


Figure 5.5: Dispersion relation of the TFIM at the QCP, i.e. for $\lambda = 1.0$.

is shown on a logarithmic scale. The “dips” in the curves are caused by the deviation changing the sign. For the ground state energy ϵ_0 , this cannot happen due to the variational principle. However, the dispersion is the difference of the energy of the excited state and the ground state energy. Therefore, if E_0 is known only approximately, ω_q can no longer be guaranteed to be an upper bound for the true excitation energy.

The plots also show, that there is a minimum in the deviation as function of bond di-

mension. Using bond dimensions $D = 20$ and $D = 30$ does not improve the accuracy of the result for these parameter values. On the contrary, the adverse effects of too many variational parameters are visible in the one-particle computations, too.

In Fig. 5.5 the dispersion at the critical point is plotted. One can clearly see that the deviations are several orders of magnitude larger than for $\lambda = 0.8$ and $\lambda = 1.2$. This is no surprise, since the correlation length diverges, which cannot be captured with finite D . Also, the relative improvement for increasing bond dimension is considerably smaller, which originates from the same fact.

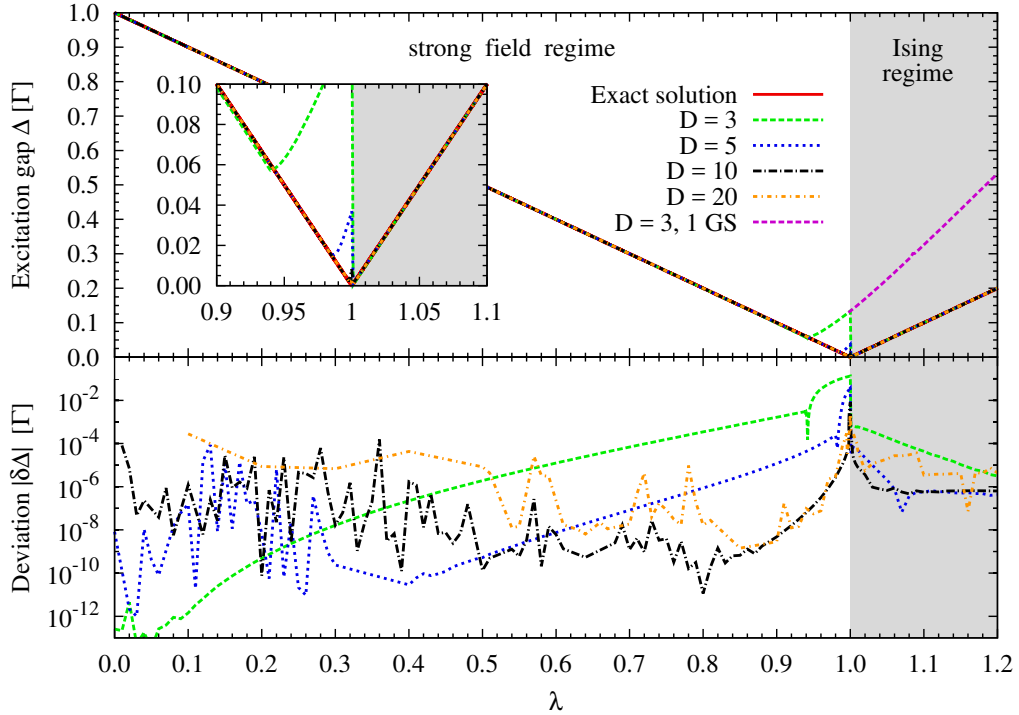


Figure 5.6: Excitation gap Δ of the TFIM as function of λ for various bond dimensions D . The upper panel shows the gap itself in comparison to the exact solution. The curve labeled “ $D = 3$, 1 GS” was computed using a unique ground state in the Ising regime, where this does not correctly reflect the physical behavior. The inset is focusing on the QCP. The lower panel shows the deviation from the exact result on a logarithmic scale.

Figure 5.6 shows the gap Δ as function of λ , with the inset being a magnification of the vicinity of the critical point. As expected, the gap can be obtained very accurately away from criticality, with some numerical noise for small λ . The closing of the gap at the QCP is again notoriously hard to capture at finite bond dimension.

The data for $D = 3$ shows an interesting behavior. Two curves are plotted for this bond dimension. The first (green) curve was obtained using a single ground state for $\lambda < 1$, and the domain wall ansatz for excitations for $\lambda > 1$. As already observed for the ground state energy (cf. Fig. 4.5), the critical point appears to be at a value $\lambda < 1$. Beyond this point, the gap increases again linearly. At $\lambda = 1$, there is a sudden jump in when the excitation ansatz changes. Interestingly, the results are surprisingly accurate compared to those with higher bond dimensions.

The second curve, labeled “ $D = 3$, 1 GS” was obtained by using the spin-flip ansatz for excitations also in the Ising phase. This leads to a further increase of the slope of the gap

to roughly 2. This is easy to understand, since the correct excitations are domain walls in the Ising regime. Assuming a unique ground state and therefore changing only a single tensor \mathbf{B} and keeping the *same* \mathbf{A} everywhere else means that \mathbf{B} must describe *two* domain walls. Thus, the minimum energy is twice that of the exact excitation.

5.5 The effective model

5.5.1 Definition of the creation operator a^\dagger

Consider the eigenvector \vec{v}^q of the momentum space EVP Eq. (5.21). It describes how the states $|\mathbf{B}_{\alpha,q}\rangle$ are superposed to describe a state that satisfies the eigenvalue equation

$$\tilde{H}|q\rangle = \omega_q|q\rangle \quad (5.64)$$

where the momentum eigenstate $|q\rangle$ is given by

$$|q\rangle := a_q^\dagger|GS\rangle = \sum_{\alpha} v_{\alpha}^q |\mathbf{B}_{\alpha,q}\rangle, \quad (5.65)$$

with the components v_{α}^q of the eigenvector \vec{v}^q . Therefore, \vec{v}^q represents a definition for the creation operator a^\dagger . Since this is a single particle state, no statements on the algebraic properties of a_q can be made at this point.

The representation Eq. (5.65) can be transformed into real space by Fourier transformation

$$|j\rangle := a_j^\dagger|GS\rangle = \sum_{\alpha,\ell} v_{\alpha,\ell} |\mathbf{B}_{\alpha,j+\ell}\rangle \quad (5.66a)$$

$$\text{with } v_{\alpha,\ell} := \sum_q e^{iq\ell} v_{\alpha}^q. \quad (5.66b)$$

Since the states $|\mathbf{B}_{\alpha,j}\rangle$ form a vector space, the sum over α can be carried out on the level of the \mathbf{B} tensors, yielding a distinct new tensor for each distance ℓ from the site j , where the particle is created

$$\mathbf{C}_{\ell} := \sum_{\alpha} v_{\alpha,\ell} \mathbf{B}_{\alpha}. \quad (5.67)$$

This makes it possible to define the real space representation of the creation operator a^\dagger as the set

$$a_j^\dagger \mapsto \{\mathbf{C}_{\ell}, \ell = -\Xi_T, \dots, \Xi_T\} \quad (5.68)$$

where Ξ_T is the maximum distance from the site j where the particle is created, which is defined by the correlation length of the transfer operator T , cf. Eq. (5.34)

$$\left| \frac{\Lambda_1}{\Lambda_0} \right|^{\Xi_T} < \theta. \quad (5.69)$$

In principle, the tolerance value θ should be same one which was used to determine the convergence of the ground state search for consistency, cf. Eq. (4.4). In practice, a larger value is often sufficient, as will be discussed in Sec. 5.5.3.

5.5.2 Analysis of the quasi-particle representation

A completely local excitation such as the spin-flips found in the FMHC can be described by a single tensor \mathbf{B}_1 . The components of the eigenvector \vec{v}^q of the EVP Eq. (5.21) are then given by

$$v_\alpha^q = \delta_{\alpha,1} \quad \forall q, \quad (5.70)$$

and the Fourier transform

$$v_{\alpha,\ell} = \delta_{\alpha,1} \delta_{\ell,0} \quad (5.71)$$

reflects the local character of the excitation. Excitations which are not completely local, such as the dressed spin-flips found in the TFIM, generally require more than one \mathbf{B} tensor. Also, the components of \vec{v}^q are not simply flat as function of q , so that Eq. (5.71) no longer holds.

As seen in Eq. (5.67), the tensor \mathbf{C}_ℓ is a linear combination of all \mathbf{B}_α tensors, weighted with the Fourier coefficients $v_{\alpha,\ell}$ of \vec{v}_α^q . It describes the polarization cloud of an excitation ℓ sites away from where it is created. The norm of the vector \vec{v}_ℓ

$$V_\ell := \|\vec{v}_\ell\| \quad (5.72)$$

can therefore be interpreted as a measure of the non-locality of the quasi-particle.

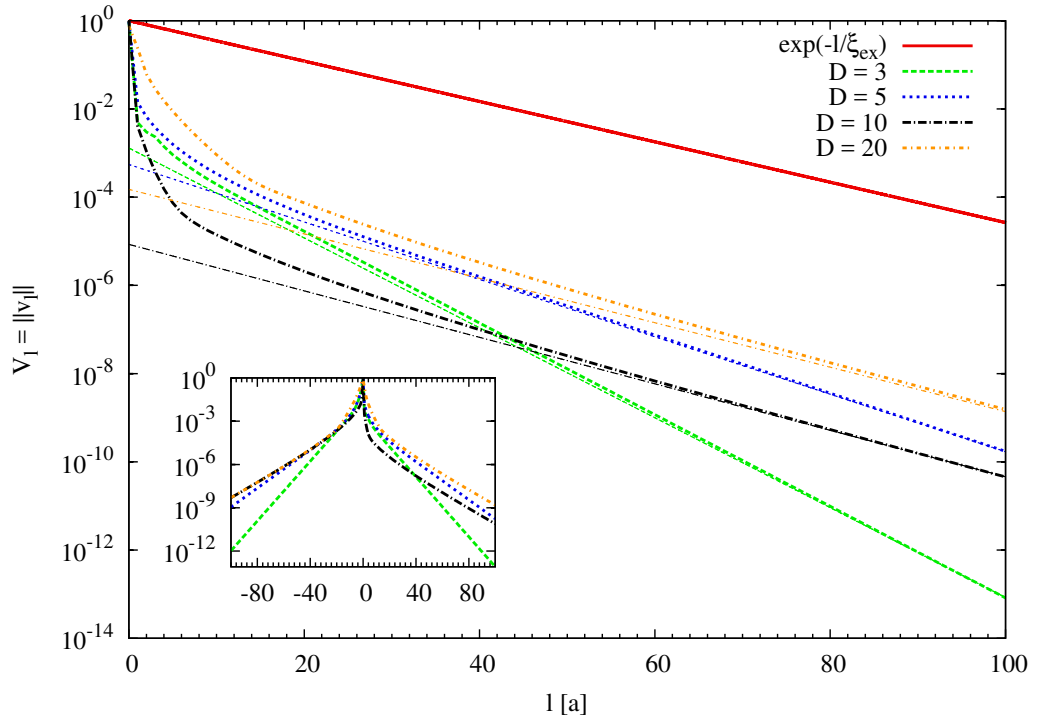


Figure 5.7: Norm V_ℓ of the real space representation of the creation operator \vec{v}_ℓ for the parameter value $\lambda = 0.9$ and various bond dimensions D . The red (solid) curve is the function $\exp(-\ell/\xi_{\text{ex}})$ with exact correlation length ξ_{ex} from Eq. (2.48). The thin lines are functions of the type $G_D(\ell) \propto \exp(-\ell/\xi_{T,D})$, where $\xi_{T,D}$ is the correlation length as determined by the transfer operator T for the given bond dimension D . The inset shows V_ℓ for both positive and negative ℓ .

In Fig. 5.7 V_j is plotted for $\lambda = 0.9$ and various bond dimensions D . The red (solid) line is the function $G_{\ell,\text{ex}} = \exp(-\ell/\xi_{\text{ex}})$ with the exact correlation length ξ_{ex} from Eq. (2.48). The thin lines are functions $G_{\ell,D} \propto \exp(-\ell/\xi_{T,D})$, where $\xi_{T,D}$ is the correlation length

determined by the transfer operator T for the given bond dimension D as defined in Eq. (3.75). The proportionality factors are chosen such that $G_{\ell,D}$ matches the long range behavior of V_ℓ for the respective bond dimension.

Figure 5.7 reveals several noteworthy things. Since by the definition of ξ_T Eq. (3.75)

$$\exp\left(-\frac{\ell}{\xi_T}\right) = |\Lambda_1|^\ell \quad \text{with} \quad |\Lambda_1| < 1, \quad (5.73)$$

the QP representation shows a long range behavior of $V_\ell \propto |\Lambda_1|^\ell$, which is exactly what is expected. Therefore, unsurprisingly, the slope of $G_{\ell,D}$ approaches that of $G_{\ell,\text{ex}}$, as $\xi_{T,D}$ converges to the exact value ξ_{ex} for increasing D . One can also see, that $\exp(-\ell/\xi_{\text{ex}})$ serves as an upper bound for any V_ℓ by several orders of magnitude.

Lastly, the inset shows V_ℓ for both positive and negative ℓ . The graph is not completely symmetric, which is a result of the asymmetric gauge of the uMPS. However, it shows the same decrease proportional to $|\Lambda_1|^\ell$ on both sides.

Figure 5.7 shows that even though V_j decreases exponentially, for it to reach machine precision, a distance of several hundred sites from the center of the quasi-particle may be required. Therefore, when computing quantities in real space using the representation Eq. (5.67), Ξ_T may be too large to obtain results in reasonable time. Even a cutoff based on the error estimate η may still be too large. Therefore, a cutoff parameter Θ is introduced which is an upper bound for the spatial extension of the particle which is tracked, and which has to be chosen according to available computational resources. The error introduced by this cutoff is of the order

$$\eta_\Theta = \mathcal{O}(|\Lambda_1|^\Theta). \quad (5.74)$$

5.5.3 Error estimation

As stated in Sec. 4.1, the uMPS found by the ground state search is generally not an exact eigenstate of the Hamiltonian. The usual estimate for the error is the standard deviation σ_H of the Hamiltonian

$$\sigma_H = \sqrt{\langle H^2 \rangle - \langle H \rangle^2}, \quad (5.75)$$

which is zero for eigenstates. However, in the framework of iMPS, this is very challenging to compute. Consider a Hamiltonian such as the one in Eq. (2.25). Squaring it, as required to compute the standard deviation from Eq. (5.75), produces products of local Hamiltonians $h_i \cdot h_j$ for all possible values of i and j including very large ones. This makes the quantity hard to compute in the iMPS framework compared to MPS for finite systems, where the MPO formalism allows one to calculate an exact MPO expression for H^2 which can be evaluated directly [23].

Therefore, the error matrix element η from Eq. (4.1) is used as an error estimate, since it is by far easier accessible.

Figure 5.8 shows η as function of λ for various bond dimensions. One can see that it fluctuates rather consistently around $1 \cdot 10^{-8}$ for bond dimensions up to $D = 10$. For $D = 20$, it is about one order of magnitude larger, which is a result of the higher tolerance value θ required in order for the ground state search algorithm to converge. The jump at the phase transition is due to the ground state degeneracy, which makes matrix elements coupling the ground state to the 1QP sector ill-defined. In the Ising phase, the matrix element η contains the overlap of the two ground states which is a problem in the uMPS formalism. Refer to App. A.4.4 for details.

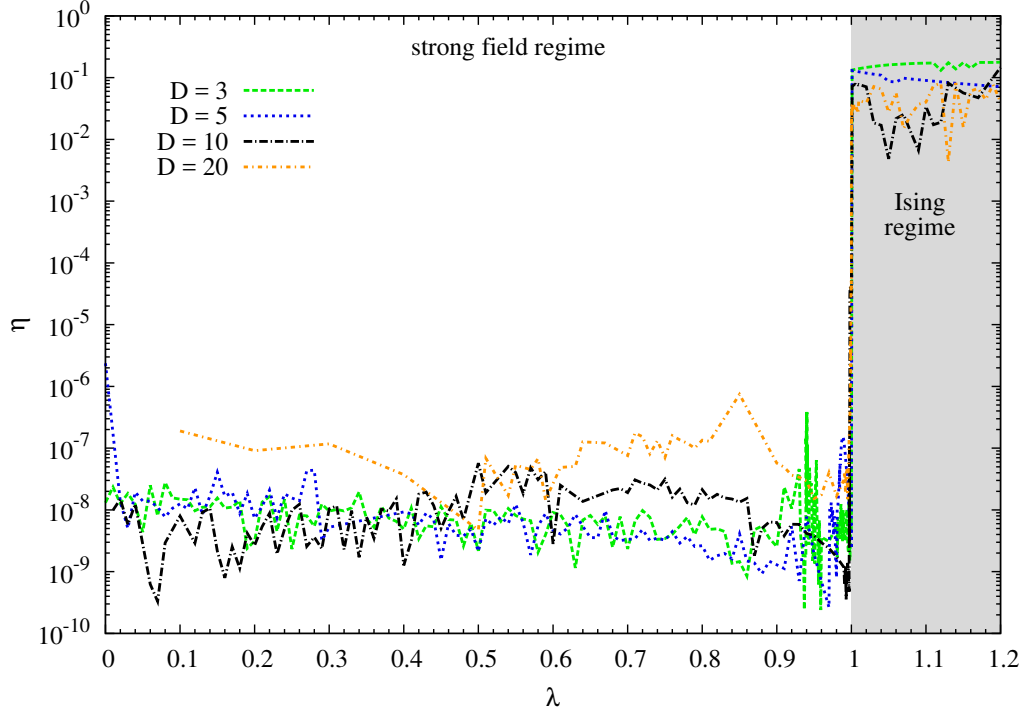


Figure 5.8: Error matrix element $\eta = \langle 0|(H - E_0)|GS\rangle$ as function of λ for various bond dimensions D .

To analyze the effect of truncating the creation operator representation Eq.(5.67), Fig. 5.9 shows the deviation of the gap Δ from the exact result as function of the cutoff length Θ at $\lambda = 0.5$. Since the minimum of the dispersion is at $q = 0$ for the TFIM, its energy value is simply given by

$$\Delta = \sum_{j=-\infty}^{\infty} t_j \quad (5.76a)$$

$$\approx \sum_{j=-\Theta}^{\Theta} \langle j|\tilde{H}|0\rangle \quad (5.76b)$$

$$= \sum_{j=-\Theta}^{\Theta} \sum_{i=-2\Theta}^{2\Theta} \sum_{\ell=-\Theta}^{\Theta} \langle C_{\ell}, j + \ell | \tilde{h}_i | C_{\ell}, \ell \rangle \quad (5.76c)$$

where the range for i was chosen such, that there is at least a distance of Θ between the operator and the nearest particle location at the boundaries.

Two types of errors can be discussed examining Fig. 5.9. The first is due to the cutoff Θ , but it reaches a minimum quickly. After that, the error increases again, which is due to the deviation changing the sign, and then converges to a constant value. The curves for each bond dimension end at the cutoff determined by Ξ_T . The vertical lines in corresponding line style (and color) show the cutoff determined by η as

$$|\Lambda_1|^\Theta < \eta. \quad (5.77)$$

As the plot shows, the error does not change significantly beyond these cutoffs any more. It can be expected, that other properties derived from the quasi-particle description Eq. (5.68) show a similar error scaling. This supports the choice of η to define the cutoff for performance reasons.

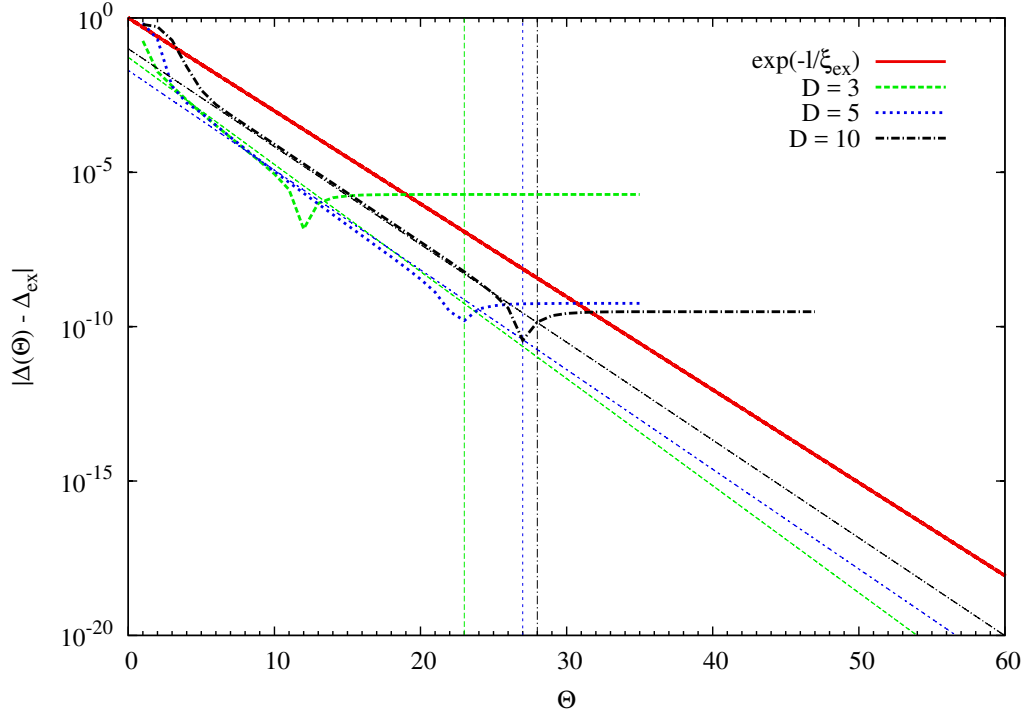


Figure 5.9: Deviation of the gap Δ from the exact solution as function of the cutoff length Θ at $\lambda = 0.5$ for various bond dimensions. The red (solid) line is the function $\exp(-\ell/\xi_{\text{ex}})$ with exact correlation length ξ_{ex} from Eq. (2.48). The thin lines are functions of the type $G_{\ell,D} \propto \exp(-\ell/\xi_{T,D})$ where $\xi_{T,D}$ is the correlation length as determined by the transfer operator T for the given bond dimension D . The vertical lines in corresponding line style (and color) show the position of the cutoff defined by η .

5.5.4 Notes on implementation

The EVP Eq. (5.21) not only can, but also has to be, solved for each momentum q independently. Since normalized eigenvectors are unique only up to multiplication by a phase factor, the components of \vec{v}^q are not necessarily smooth functions of q . Figure 5.10 shows some exemplary results. Fourier transforming a function like this requires considerably more coefficients than its smooth counterpart. Therefore, smoothing out the vector components is an integral part of efficient computation, if transformation to real space is intended.

The arbitrary phase between eigenvectors is a common problem one faces when diagonalizing a Hamiltonian for different momenta independently. In some cases, there are clearly just sign flips from one q -value to the next. Generally, a phase of the order of $\mathcal{O}(\Delta q)$ can occur from one momentum point to the next. Therefore, not only sign flips are possible, but also more general phase relations.

In fact, even after repairing phase jumps such as the ones seen in Fig. 5.10, a phase of $\pm\pi$ can occur between the boundaries of the Brillouin zone. This is known as Zak's phase [93] and is an indication of a topologically non-trivial band. However, in cases of the FMHC and the TFIM no such topological phases are observed, as expected.

Generically, there is one dominant component in \vec{v}^q which means that one tensor \mathbf{B}_α carries most of the information of the elementary excitation. In the Fourier transform Eq. (5.66b) this component produces most of the weight. For an adequate description of a quasi-local

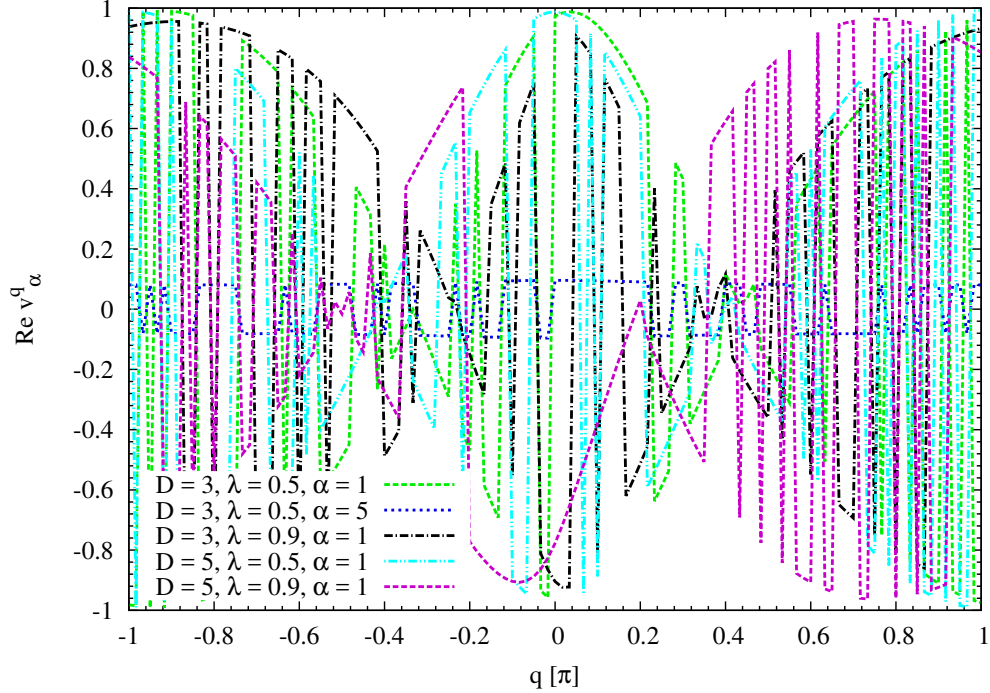


Figure 5.10: Real part of some exemplary components of the eigenvector \vec{v}^q corresponding to the dispersion EV of Eq. (5.21). The plotted data was chosen to illustrate generic behavior of the eigenvector.

excitation, this weight should be at position $\ell = 0$. However, due to the ambiguity of \vec{v}^q as an eigenvector of H^q ,

$$\vec{v}^{q'} := \vec{v}^q e^{-iq\ell} \quad (5.78)$$

is an eigenvector, too, and moreover also a smooth function of q if \vec{v}^q is one. But the largest weight in the Fourier transform is shifted to position ℓ . This example shows, that the phase relation between \vec{v}^q and $\vec{v}_{q+\Delta q}$ is largely arbitrary but may have great impact on the Fourier transform v_ℓ . Note that in a strict mathematical sense, any “gauge” of \vec{v}^q and also its Fourier transform holds the same information. However, as with any gauge, there are some gauges that are more convenient for practical application. In the case of \vec{v}^q , the most useful gauge is that where the component with largest absolute value is chosen real and positive

$$\vec{v}^{q'} := \frac{\vec{v}^q |v_{\alpha^*}^q|}{v_{\alpha^*}^q} \quad \text{with } v_{\alpha^*}^q = \max_{|\alpha|} v_\alpha^q. \quad (5.79)$$

This ensures that the largest weight in \vec{v}_ℓ is at position $\ell = 0$ which matches the physical intuition. We also find, that this gauge produces the fastest decay of V_ℓ as function of ℓ .

As with the ground state properties, numerical problems are observed if the number of variational parameters is a lot larger than is required to describe the physics in the system. In a reflection symmetric system such as the TFIM, the Hamiltonian is expected to be symmetric about $q = 0$, i.e., that

$$H^q = H^{-q} \quad (5.80)$$

holds. Then, after applying the gauge Eq. (5.79), the same must be true for the eigenvector \vec{v}^q . However, for smaller λ and higher bond dimension deviations from this symmetry occur.

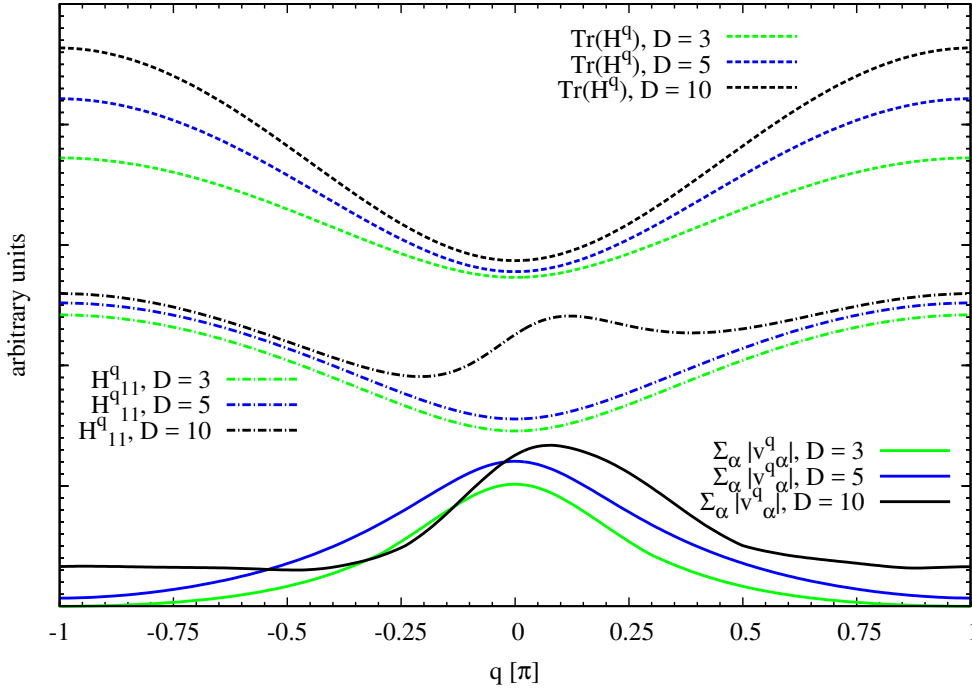


Figure 5.11: The “symmetry measure” V_q (solid lines) as defined in Eq. (5.81), the smallest diagonal element H_{11}^q (dashed-dotted lines) and the trace of H^q at $\lambda = 0.5$ (dashed lines) for several bond dimensions. The curves only serve to examine the symmetry in q and are shifted and scaled to fit the plot.

Figure 5.11 shows the sum of the absolute values of the components of \vec{v}^q

$$V_q := \sum_{\alpha} |v_{\alpha}^q|. \quad (5.81)$$

This quantity is sensitive to any asymmetries in \vec{v}^q , if they are randomly distributed and do not cancel each other out. It therefore allows us to quickly assess the symmetry or lack thereof of \vec{v}^q . Plotted alongside V_q is the smallest diagonal element of H^q , to represent the behavior of the matrix as function of momentum. Also included is the trace of H^q , since it is invariant under the diagonalization.

For bond dimensions $D = 3$ and $D = 5$, the diagonal element is symmetric in q , and so are the other matrix elements that are not shown. Consequently, the phase-gauged \vec{v}^q shows the same symmetry. But for $D = 10$, H_{11}^q shows an unphysical asymmetry, and so do other matrix elements. This asymmetry is visibly reflected in the resulting eigenvector \vec{v}^q .

The violation of Eq. (5.80) can be traced back to the real space hopping elements $H_{\alpha\beta}^j$ from Eq. (5.23e). In a reflection symmetric system, hopping in both directions should have the same amplitude, i.e.,

$$H_{\alpha\beta}^j = H_{\alpha\beta}^{-j}. \quad (5.82)$$

This is found to hold true for $D = 3$ and $D = 5$, but not for $D = 10$. The reason behind this is numerical instability in the computation of the excitation tensors \mathbf{B}_{α} . This happens when the singular values in v are too small. Indeed, different program runs for the same parameters yield different results for \mathbf{B} , as shown in Fig. 6.5 in Chap. 6. This is a strong indication of random rounding errors impacting the computation.

Therefore, a more stable algorithm to compute the \mathbf{B} is required in the future.

Interestingly, the trace of H^q is symmetric for all bond dimensions. This explains why the asymmetry is not observed in the dispersion.

5.6 One-particle spectral weight

To verify the QP representation Eq. (5.68), the one-particle spectral weight in the xx -channel

$$S_{\text{1P}}^{xx}(Q) := \langle GS | S_{-q}^x | q \rangle \langle q | S_q^x | GS \rangle \quad (5.83a)$$

$$= \langle GS | S_{-q}^x a_q^\dagger | GS \rangle \langle GS | a_q S_q^x | GS \rangle \quad (5.83b)$$

$$=: |\chi_q^x|^2 \quad (5.83c)$$

is computed. The matrix elements are given by

$$\chi_q^x := \langle GS | a_q S_q^x | GS \rangle \quad (5.84a)$$

$$= \frac{1}{L} \sum_{j,m} e^{iq(j-m)} \langle GS | a_j S_m^x | GS \rangle \quad (5.84b)$$

$$= \sum_j e^{iqj} \langle GS | a_j S_0^x | GS \rangle \quad (5.84c)$$

$$= \sum_{j,\ell} e^{iqj} \langle C_{\ell,j} + \ell | S_0^x | GS \rangle. \quad (5.84d)$$

5.6.1 Results for TFIM

Figures 5.12 and 5.13 show the spectral weight in the xx -channel for different values of λ and several bond dimensions each.

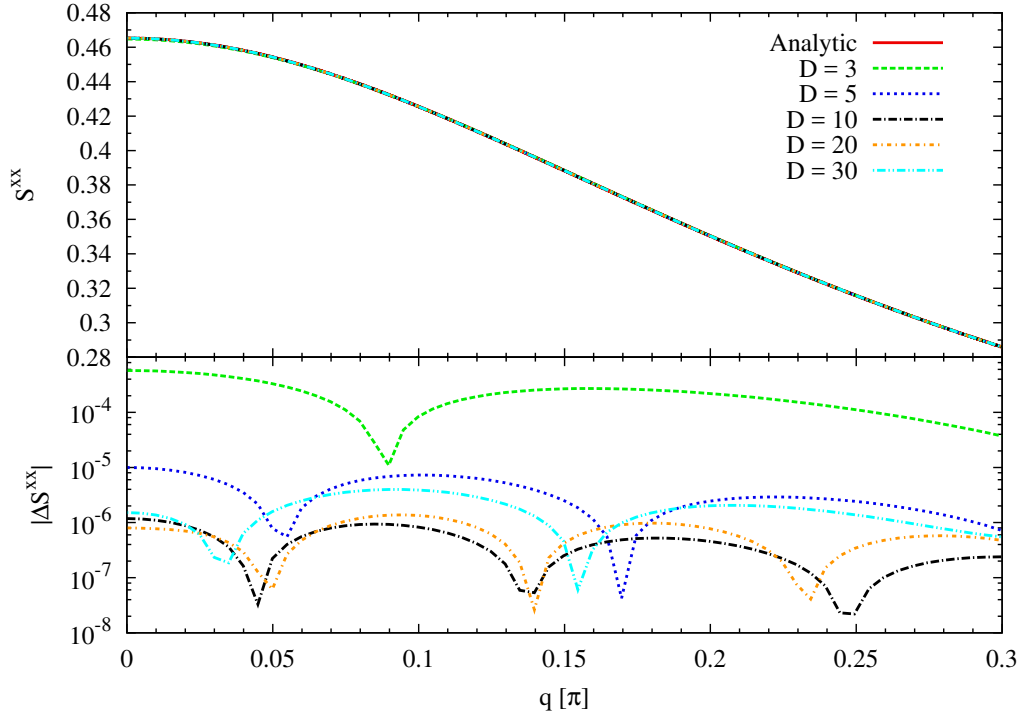


Figure 5.12: Spectral weight S^{xx} for the TFIM at $\lambda = 0.5$.

From Fig. 5.12 it is apparent that away from criticality, the spectral weight can be obtained to very high precision, even at low bond dimension. Again, as for the dispersion, the deviation from the analytical result is plotted on a logarithmic scale. Here, too, the appearance

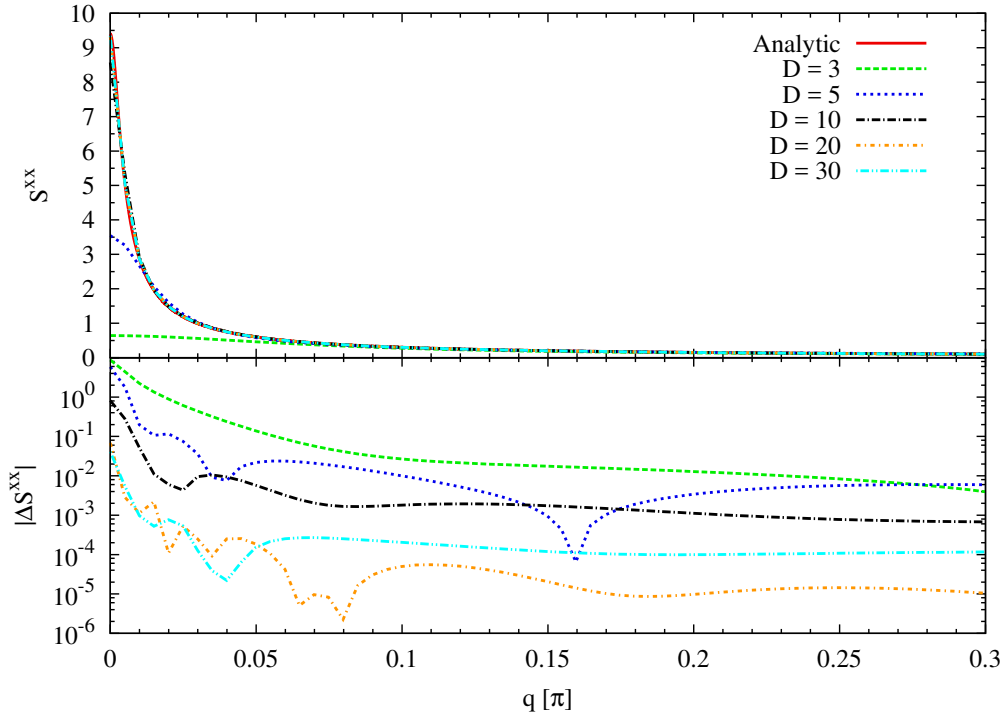


Figure 5.13: Spectral weight S^{xx} for the TFIM at $\lambda = 0.99$.

of dips shows that both positive and negative deviations occur. Directly at the critical point, the spectral weight diverges for $q \rightarrow 0$, because the gap closes (cf. Eq. (2.54)). Therefore, Fig. 5.13 shows the spectral weight for $\lambda = 0.99$, i.e., very close to, but not directly at the critical point. Clearly, the large peak at $q = 0$ is not captured perfectly at low bond dimensions. But for $D = 30$, the deviation is only around 1 %.

Interestingly, the asymmetry in \vec{v}^q observed in Sec. 5.5.4 does not seem to have adverse effects on the results for one-particle properties.

5.7 Efficient computation

While it is instructive to examine the real space representation of the quasi-particle Eq. (5.68), and the spectral weights can indeed be computed from real space matrix elements, it is far more efficient to work in momentum space. This section is intended to show why.

In the TDL, the real space matrix element in Eq. (5.84) converges to zero as function of the distance j from the operator position, which is assumed to be site 0. This convergence occurs on a length scale of Ξ_T , as explained in Sec. 5.2.3. Therefore, to obtain χ_q requires computing $2\Xi_T$ real space matrix elements $\langle j|S_0^x|GS\rangle$, each of which consists of $2\Xi_T$ contributions of the form $\langle C_{\ell,j+\ell}|S_0^x|GS\rangle$.

This amounts to evaluating $4\Xi_T^2$ TNs of the form

$$\langle C_{\ell,j+\ell}|S_0^x|GS\rangle = \text{Diagram} \quad (5.85)$$

Since the tensors \mathbf{C}_ℓ are distinct for each distance ℓ from the particle center j , none of these TNs appears more than once. This makes it extremely difficult to reuse partial results in the process.

However, the following observation from Ref. [92] permits it to compute momentum space matrix elements much more efficiently

$$|q\rangle = \frac{1}{\sqrt{L}} \sum_{j,\ell} e^{-iqj} |\mathbf{C}_{\ell,j+\ell}\rangle \quad (5.86a)$$

$$= \frac{1}{\sqrt{L}} \sum_{j,\ell} e^{-iq(j-\ell)} |\mathbf{C}_{\ell,j}\rangle \quad (5.86b)$$

$$= \frac{1}{\sqrt{L}} \sum_j e^{-iqj} \sum_\ell e^{+iq\ell} |\mathbf{C}_{\ell,j}\rangle \quad (5.86c)$$

$$=: \frac{1}{\sqrt{L}} \sum_j e^{-iqj} |\mathbf{C}_q,j\rangle \quad (5.86d)$$

where \mathbf{C}_q is defined as

$$\mathbf{C}_q := \sum_\ell e^{+iq\ell} \mathbf{C}_\ell. \quad (5.87)$$

The index shift $j \rightarrow j - \ell$ from line (5.86a) to line (5.86b) is possible, since in principle all sums run from $-\infty$ to ∞ . Restricting them to $\pm \Xi_T$ in numerics just means leaving out small numbers below machine precision. Note that the tensor \mathbf{C}_q defined in Eq. (5.87) is not the Fourier transform of \mathbf{C}_ℓ , but has the opposite sign in the phase factor.

The series of equalities in (5.86) shows that *under the Fourier transform* the QP representation Eq. (5.68) can be reduced to a single tensor \mathbf{C}_q which represents a particle with momentum q at site j . Performing the summation on the level of \mathbf{C} tensors is much faster than evaluating and summing TNs of type Eq. (5.85). The tensor \mathbf{C}_q can be computed directly from \vec{v}_q

$$\mathbf{C}_q = \sum_\ell e^{+iq\ell} \mathbf{C}_\ell = \sum_\ell e^{+iq\ell} \sum_\alpha v_{\alpha,\ell} \mathbf{B}_\alpha \quad (5.88a)$$

$$= \sum_\alpha \left(\sum_\ell e^{+iq\ell} v_{\alpha,\ell} \right) \mathbf{B}_\alpha \quad (5.88b)$$

$$= \sum_\alpha v_\alpha^{-q} \mathbf{B}_\alpha \quad (5.88c)$$

and is therefore independent of any cutoff made in \vec{v}_ℓ . We highlight that v^{-q} occurs in Eq. (5.88c) because of the opposite sign of the phase compared to the normal Fourier transformation mentioned above.

Using the momentum space representation Eq. (5.87), χ_q is computed as

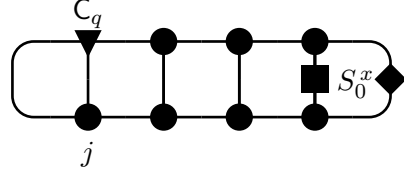
$$\chi_q = \frac{1}{L} \sum_{j,m} e^{iq(j-m)} \langle GS | a_j S_m^x | GS \rangle \quad (5.89a)$$

$$= \frac{1}{L} \sum_{j,m} e^{iq(j-m)} \langle \mathbf{C}_q,j | S_m^x | GS \rangle \quad (5.89b)$$

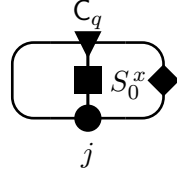
$$= \sum_j e^{iqj} \langle \mathbf{C}_q,j | S_0^x | GS \rangle. \quad (5.89c)$$

This requires only $\mathcal{O}(\Xi_T)$ TN evaluations in contrast to the real space computation in Eq. (5.84d), which needs $\mathcal{O}(\Xi_T^2)$ TN evaluations.

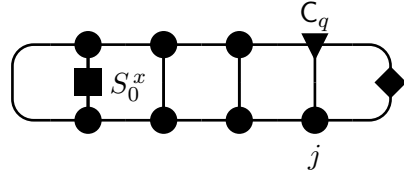
The second benefit of using C_q is that this tensor is the same for all sites j . This makes it possible to reuse already computed parts of the TN. In summing over all required positions j , the following topologically distinct TNs occur:



$$\text{for } j < 0 \quad (5.90a)$$



$$\text{for } j = 0 \quad (5.90b)$$

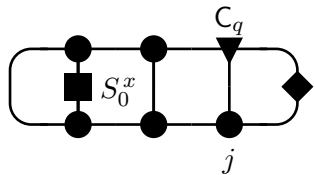


$$\text{for } j > 0 . \quad (5.90c)$$

They are generally evaluated as

$$\begin{aligned} \chi_q = \sum_{j < 0} e^{+iqj} \left((T^\dagger)^{|j|-1} [\mathbb{1}^{\dagger(C_q;A)}[u]], S^{x(A;A)}[v] \right) + \left(u, S^{x(C_q;A)}[v] \right) \\ + \sum_{j > 0} e^{+iqj} \left(S^{x\dagger(A;A)}[u], T^{j-1} [\mathbb{1}^{(C_q;A)}[v]] \right) . \quad (5.91) \end{aligned}$$

Note, however, that C_q is a linear combination of B_α tensors. Therefore, all TNs for $j < 0$ evaluate to zero in left-canonical gauge, since they contain the expression $\mathbb{1}^{\dagger(C;A)}[u] = 0_{D \times D}$ as seen in Eq. (5.10). Consider therefore, as an example, the case $j > 0$. For each distance j , the contribution of the TN to the matrix element χ_q is



$$= e^{+iqj} \left(S^{x\dagger(A;A)}[u], T^{j-1} [\mathbb{1}^{(C_q;A)}[v]] \right) \quad (5.92a)$$

$$= e^{iqj} \left(S^{x\dagger(A;A)}[u], T[v_{j-1}^q] \right) \quad (5.92b)$$

$$\text{with } v_{j-1}^q := T^{j-2} [\mathbb{1}^{(C_q;A)}[v]] . \quad (5.92c)$$

Reusing the left boundary matrix v_{j-1}^q from the last step $j-1$ is possible, since the tensor C_q is the same for all j , in contrast to C_ℓ , which is distinct.

The width of the TNs in Eq. (5.85) is on average of the order Ξ_T . Therefore, the computational cost for obtaining χ_q from real space matrix elements scales as $\mathcal{O}(\Xi_T^3)$. In contrast, the computation in momentum space scales only as $\mathcal{O}(\Xi_T^2)$ assuming a momentum discretization $L_q \propto \Xi_T$.

Of course, this speed up comes at a price. Once the real space matrix elements $\langle j | S^x | GS \rangle$ are computed, χ_q can be obtained for arbitrary q by Fourier transformation, which is very fast, without the need to recompute any matrix elements. In contrast, Eq. (5.89) must be

evaluated for each desired q value. Changing the resolution in momentum space requires either to discard the known results, or to exactly double the number of momentum samples by computing matrix elements in the middle between each pair of existing q -points. However, in practice there is hardly ever the need to compute results for arbitrary q , if a reasonably high resolution in momentum space is chosen from the start.

5.8 Chapter summary

In this chapter, the description of excited states in the framework of iMPS was introduced. It was shown that the tensors \mathbf{B}_α used to describe excitations have a reduced number of independent variational parameters, although they are of the same dimension as the ground state uMPS tensor \mathbf{A} . Following this observation, an algorithm was presented that restricts the search for excitation tensors to the relevant subspace. This canonical representation of \mathbf{B} tensors also proves convenient because it makes the iMPS orthogonal with respect to the location of the \mathbf{B} tensor. However, matrix elements show an asymmetry in their computation, depending on the operator position. Therefore, the momentum superposition of the excited states in real space was introduced. Using these Wannier states, the Hamiltonian matrix in momentum space was constructed and diagonalized to find the linear combination of excited states with lowest energy.

This lowest eigenvalue of H^q was seen to be a very accurate approximation to the one-particle dispersion. For the TFIM, the dispersion could be obtained equally well in the disordered phase and the ordered phase.

Next, the Fourier transform for the eigenvector \vec{v}^q corresponding to the dispersion eigenvalue was examined. The Fourier coefficients are a representation of the polarization cloud which the quasi-particles acquire away from the strong coupling and strong field limits. The coefficients were shown to decrease as $|\Lambda_1|^\ell$ with distance ℓ from the site where the particle is created, in full accordance with the expectations.

Further, some numerical details on the computation of \vec{v}^q were given, and it was observed that the components show an unphysical asymmetry for smaller λ and higher bond dimension.

To test the one-particle representation, the spectral weight in the xx -channel was computed. Sufficiently far away from criticality, it was found to be very accurate. Close to the phase transition, the agreement was not perfect, but for larger bond dimensions still quite good.

The asymmetry in \vec{v}^q was found not to have negative effects on the quality of these results.

In the next chapter, the ansatz is extended to two-particle states and the challenges of this extension are discussed. Results are provided for the two-particle spectral weight and the quasi-particle decay amplitude of the TFIM, as well as for the two-particle interaction matrix for both models.

Chapter 6

Two-particle properties

*Everything must be made as simple as possible.
But not simpler.*
Albert Einstein

In this chapter, algorithms to obtain two-particle (2QP) properties are presented, along with a number of results. This represents the main part of the original research of this thesis. Note that some two-particle results were also found by Verstraete et al. [94, 13, 95] using a different ansatz for 2QP states.

First, the definition of and various bases for 2QP states are discussed in Sec. 6.1. In Sec. 6.2, some results on the metric tensor of the TFIM are presented and discussed. Then, in Sec. 6.3, the two-particle spectral weight in the zz -channel is computed for the TFIM, for which an analytical result is available to compare the numerical results to. In Sec. 6.4, the concepts used in efficient 2QP computations are introduced. Section 6.5 presents and discusses results on the quasi-particle decay amplitude. Finally, Sec. 6.6 holds the main results, namely those on the 2QP interaction matrix.

6.1 Definition of two-particle states

Now that it is known how a state can be constructed that holds one QP, it seems natural to construct two-particle states by applying the creation operator found in Sec. 5.5 twice.

6.1.1 Real space basis

This leads to the following definition of a two-particle state in real space

$$|j,k\rangle := \sum_{\ell,m} |\mathbf{C}_\ell, j+\ell; \mathbf{C}_m, k+m\rangle, \quad (6.1)$$

where $|\mathbf{C}_\ell, j+\ell; \mathbf{C}_m, k+m\rangle$ is a state analogous to Eq. (5.2) which has ground state tensors everywhere except at sites $j+\ell$ and $k+m$, where \mathbf{A} is replaced by \mathbf{C}_ℓ and \mathbf{C}_m as defined in Eq. (5.67), respectively,

$$\begin{aligned} & |\mathbf{C}_\ell, j+\ell; \mathbf{C}_m, k+m\rangle \\ & := \sum_{s_1, \dots, s_L} \text{Tr}(A^{s_1} \dots A^{s_{j+\ell-1}} C_\ell^{s_{j+\ell}} A^{s_{j+\ell+1}} \dots A^{s_{k+m-1}} C_m^{s_{k+m}} A^{s_{k+m+1}} \dots A^{s_L}) \\ & \quad \times |s_1, \dots, s_L\rangle. \end{aligned} \quad (6.2)$$

Note that for small particle distances the case $j + \ell = k + m$ can occur, i.e., both \mathbf{C} tensors fall onto the *same* lattice site. These contributions are set to zero, which will be motivated below.

Often, the relative distance $d := k - j$ of the two particles is more useful and the state is written as

$$|j, j + d\rangle = |j, k\rangle . \quad (6.3)$$

On the level of iMPS as defined in Eq. (6.2), there is no concept of particle exchange. Interchanging the particle positions j and k produces the same state, i.e.

$$|j, k\rangle = |k, j\rangle . \quad (6.4)$$

In this respect, the quasi particles are therefore bosonic. As mentioned in Chap. 2, the excitations in spin systems are hard-core bosons. How and to what extent this can be described in the iMPS framework will be discussed later.

Unfortunately, the naïve definition in Eq. (6.1) does not generally yield an orthonormal basis (ONB). Instead, the following behavior is observed

$$\langle j, j + d | j, j + d \rangle \quad \begin{cases} = 1, & \text{if } d > 2\varepsilon_T \\ \neq 1, & \text{otherwise} \end{cases} \quad (6.5a)$$

$$\langle j', j' + d' | j, j + d \rangle \quad \begin{cases} = 0, & \text{if } d > 2\varepsilon_T \wedge d' > 2\varepsilon_T \text{ or } |j - j'| > 4\varepsilon_T \\ \neq 0, & \text{otherwise} \end{cases} , \quad (6.5b)$$

where ε_T is the cutoff defined by the second largest EV of the transfer operator, cf. Eq. (5.34). In summary, the states *are* orthonormal if the particles are so far apart that none of the involved representations overlap. If there is an overlap, deviations from orthonormality can occur. The deviations are larger for bigger overlaps.

This behavior can easily be understood by the following argument: For a particle distance larger than $2\varepsilon_T$, the \mathbf{C} -tensors cannot “see” each other within the iMPS class of that bond dimension. Therefore, such a state then describes a non-interacting system, which is captured already by the one-particle dynamics. Hence, the interesting part of the Hilbert space is also the difficult part which requires additional work.

As mentioned above, for $d < 2\varepsilon_T$, the case $j + \ell = j + d + m$ can occur, i.e., the two \mathbf{C} tensors would have to be on the same lattice site. In this case, it is not really clear how to proceed. Since in spin systems the elementary excitations are generically of hard-core bosonic type, all contributions of this type are set to zero. Although it may seem arbitrary in real space, it can be shown that under Fourier transformation omitting states with two \mathbf{C} on the same site can be interpreted as a form of hard-core constraint (cf. Sec. 6.4).

Figure 6.1 shows the squared norm and some overlaps of the states defined in Eq. (6.3), computed for bond dimension $D = 5$ at $\lambda = 0.6$. As can be seen, the state with particle distance $d' = 0$ does not have zero norm, even by numerical standards. This means the QP representation does not exactly reproduce the expected hard-core property, even if the contributions with both \mathbf{C} tensors on the same site are dropped. However, the norm of the $d' = 0$ state is considerably smaller than that of the $d' = 1$ state, and the $d' = 3$ state already has a norm of around 0.8. Since the particles still overlap considerably for small distances, this is by no means trivial, but rather a sign that the iMPS description, although not perfect, is quite close to hard-core bosons. The plot also shows that $2\varepsilon_T$ is really an upper limit for the 2QP basis to become orthonormal. In practice, $1\varepsilon_T$ is usually enough

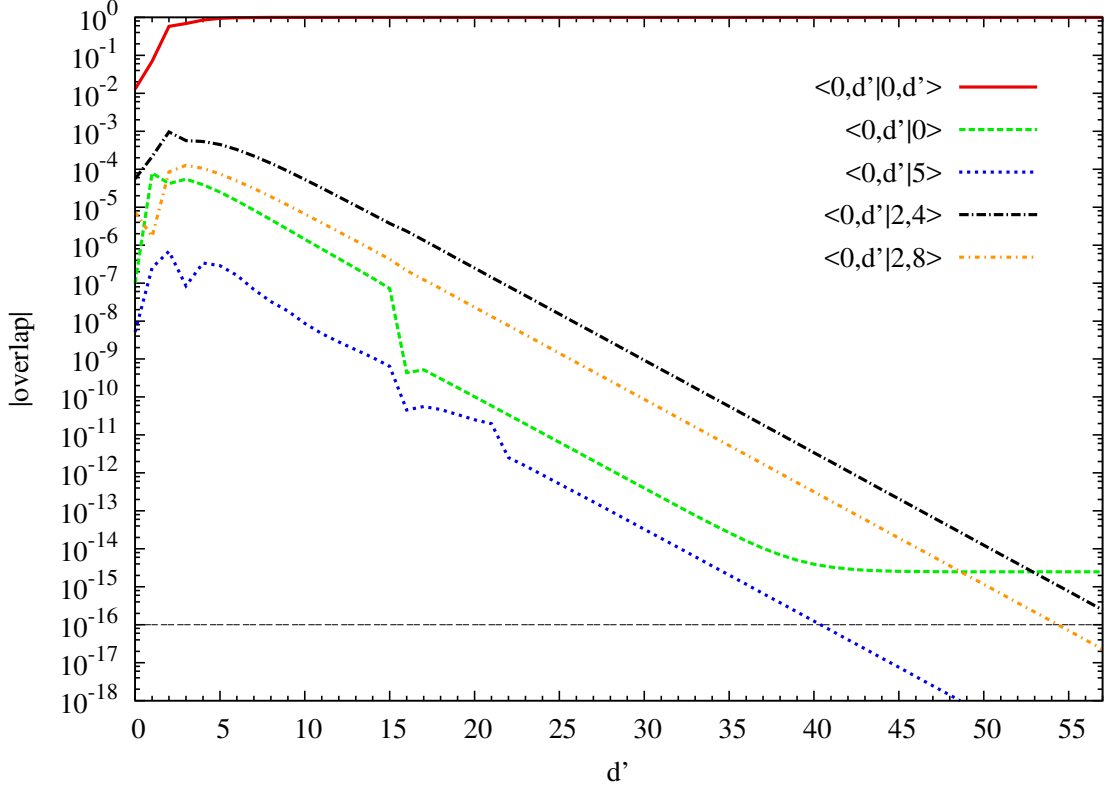


Figure 6.1: Exemplary overlaps of the 2QP real space states $|j, j + d\rangle$, also including overlaps with the 1QP sector $|j\rangle$. Computed for the TFIM at $\lambda = 0.6$ with bond dimension $D = 5$. The numerical tolerance value is 10^{-14} , for which $\Xi_T = 57$ as defined in Eq. (5.34). The thin horizontal line represents machine precision for 64-bit double computations.

to reach the tolerance value θ and even machine precision.

Unfortunately, for $d < \Xi_T$ the so defined 2QP states are also not always orthogonal to the 1QP sector. At least they are orthogonal to the ground state. The reason for this is that Eq. (5.10) is linear, and therefore holds for any linear combination of \mathbf{B} tensors, including \mathbf{C}_ℓ

$$\mathbf{1}^{(a;\mathbf{B}_\alpha;A)}[u] = a \cdot \mathbf{1}^{(\mathbf{B}_\alpha;A)}[u] = 0 \quad \forall \quad \mathbf{B}_\alpha \quad \Rightarrow \quad \mathbf{1}^{(\mathbf{C}_\ell;A)}[u] = 0 = \mathbf{1}^{(A;\mathbf{C}_\ell)}. \quad (6.6)$$

Note that as done in Eq. (6.5b), throughout this chapter primed letters like j' , d' , ℓ' etc. are always used to refer to the bra-state, whereas plain letters j , d , ℓ etc. refer to the ket-state.

6.1.2 Momentum space basis

To overcome the orthogonality problem, one can once more pass to momentum space by taking the Fourier transform in both real space coordinates

$$|q_1, q_2\rangle := \frac{1}{L} \sum_{j,k} e^{-iq_1 j} e^{-iq_2 k} |j, k\rangle \quad (6.7a)$$

$$= \frac{1}{L} \sum_{j,d} e^{-iq_1 j} e^{-iq_2(j+d)} |j, j+d\rangle \quad (6.7b)$$

$$= \frac{1}{L} \sum_{j,d} e^{-i(q_1+q_2)j} e^{-iq_2 d} |j, j+d\rangle \quad (6.7c)$$

where q_1 is the momentum of the particle at site j and q_2 that of the particle at site $k = j + d$. Unfortunately, the so defined states are not orthogonal with respect to q_1 and q_2 either.

However, the argument for one-particle Wannier states (cf. App. A.6) also applies in this case with respect to *total* momentum

$$Q := q_1 + q_2 . \quad (6.8)$$

The canonical choice of a second momentum coordinate is the relative momentum

$$q := q_2 - q_1 . \quad (6.9)$$

Then, the individual particle momenta can be written as

$$q_1 = \frac{Q - q}{2} \quad \text{and} \quad q_2 = \frac{Q + q}{2} . \quad (6.10)$$

Inserting these definitions into Eq. (6.7c), the two-particle state in momentum space reads

$$|Q, q\rangle := \frac{1}{L} \sum_{j,d} e^{-iQj} e^{-i\frac{Q+q}{2}d} |j, j+d\rangle \quad (6.11a)$$

$$= \frac{1}{L} \sum_{j,d} e^{-iQj} e^{-iQ\frac{d}{2}} e^{-iq\frac{d}{2}} |j, j+d\rangle . \quad (6.11b)$$

This shows that there are multiple equivalent definitions for a momentum space basis, just like there are for a real space basis as seen in Eq. (6.3). In order to make use of the relation $\langle Q', q' | Q, q \rangle \propto \delta_{Q', Q}$, total momentum Q has to be chosen as the primary quantum number. The choice of relative momentum q as second quantum number is viable, if it is actually a continuous variable. However, when momentum is discretized as described in Sec. 5.3, relative momentum becomes an inconvenient choice, because it is the difference of the two individual particle momenta. This is so for two reasons: First, q can take values in the interval $(-2\pi, 2\pi)$, half of which lies outside the first Brillouin zone, requiring different handling of Q and q . Second, if $Q = q_1 + q_2$ is even, then $q = q_1 - q_2$ must be even, too, and the same holds for odd Q . This requires different handling of odd and even Q -sectors. Therefore, the basis in Eq. (6.11) will *not* be used. Instead, one of the individual particle momenta, q_1 , is chosen as the second quantum number. The values are then contiguous and can be taken to sample the first Brillouin zone only. This resulting basis is defined as

$$|Q, q_1\rangle := \frac{1}{L} \sum_{j,d} e^{-iQj} e^{-iQd} e^{+iq_1 d} |j, j+d\rangle \quad (6.12)$$

which can easily be related to the basis of individual particle momenta $|q_1, q_2\rangle$ by Eq. (6.7). Note that conservation of total momentum Q is always considered implied. In this notation, the momentum of the second particle q_2 is therefore always fixed by Q and q_1 as

$$q_2 = Q - q_1 , \quad (6.13)$$

and is often used as a shorthand for this expression.

6.1.3 Hybrid basis

So far, two-particle bases in both real and momentum space have been defined, neither of which proves to be a proper ONB. Moreover, neither basis provides a distinguished state from which to start an orthogonalization.

Therefore, a hybrid basis of total momentum Q and relative particle distance d is chosen. It is defined as

$$|Q, d\rangle = \frac{1}{\sqrt{L}} e^{-iQ\frac{d}{2}} \sum_j e^{-iQj} |j, j+d\rangle , \quad (6.14)$$

i.e., it is formally obtained by dropping the Fourier transformation in the relative distance from Eq. (6.11).

Though this basis may seem uncommon, it combines the favorable properties of the real and momentum space bases. First, states with different total momentum Q are guaranteed to be orthogonal, and therefore each sector can be treated independently. Second, it is also clear that the 2QP states are orthogonal for relative distances $d > 2\varepsilon_T$ as well, and thus form an ONB in that part of Fock space. Therefore, the state $|Q, d = 2\varepsilon_T\rangle$ does provide a well-defined starting point for the Gram-Schmidt orthonormalization scheme. States with smaller d can then successively be orthogonalized. Since the Gram-Schmidt algorithm does not change the first vector, it is important to start from a well-defined 2QP state.

Once more, one faces the problem that a representation of the actual states does not exist in computer memory, and only overlaps and matrix elements are accessible. Appendix A.8 shows how to apply the Gram-Schmidt algorithm using the metric tensor consisting of the overlaps of a skew basis and operator matrices computed in that skew basis.

In the hybrid basis, each Q -sector holds $1 + \frac{L_q - 1}{2}$ unique states, determined by the relative distance $d = 0, \dots, \frac{L_q - 1}{2}$. Since the excitations in spin systems are hard-core bosons, the state with $d = 0$, i.e., both particles on the same site, has norm 0 in the limit that the iMPS representation is exact. Due to the real space periodicity implied by momentum discretization, the states are L_q -periodic in d and thus only the states with $d \leq \frac{L_q - 1}{2}$ are unique. It is also clear that for bosons the states with $+d$ and $-d$ are the same, see App. A.7.

Although the hybrid basis defined above is beneficial in terms of orthogonality and a necessary “detour” for using the Gram-Schmidt algorithm, quantities are not directly accessible in this basis. Overlaps and matrix elements have to be computed either in the real space basis $|j, j+d\rangle$ or in the momentum space basis $|Q, q_1\rangle$ and then Fourier transformed into the hybrid basis for orthogonalization. The orthogonalized results can then be transformed again, either into real space or momentum space as needed. See App. A.9 for a summary of 2QP basis transformations.

To distinguish it from the original, skew iMPS basis Eq. (6.14), the orthogonalized hybrid basis is denoted as $|\widetilde{Q}, d\rangle$ with a tilde.

6.1.4 Metric tensor

If the two-particle real space states defined in Eq. (6.3) did form a proper ONB, the metric tensor would simply be given by

$$\langle j', j' + d' | j, j + d \rangle = \delta_{j', j} \delta_{d', d} + \delta_{j'+d', j} \delta_{j', j+d} - 2\delta_{j', j} \delta_{d', d} \delta_{d, 0} \quad (6.15)$$

where the last term reflects the hard-core constraint. This would straight forwardly transform into momentum space as

$$\langle Q, q'_1 | Q, q_1 \rangle = \delta_{q'_1, q_1} + \delta_{q'_1, q_2} - \frac{2}{L}, \quad (6.16)$$

as shown in App. A.10. In fact, for pure product states at $D = 1$ this is true. However, as seen in Fig. 6.1, for non-trivial bond dimension the 2QP states do *not* form an ONB. For increasing bond dimension D , the overlaps of states with small particle distance get larger, since the site tensors are able to “see” more and more neighboring sites. Therefore, the metric tensor of this skew basis, or more precisely, its *deviation* ΔN from an orthonormal basis needs to be computed. Transformed into the hybrid basis, this metric tensor is needed to obtain operator matrices in an orthogonal basis.

As in the case of the matrix element in Sec. 5.7, computations can be done much more efficiently in momentum space. However, they are more involved and can therefore be found in App. B.2.

They result in the following metric tensor in the skew momentum space basis $|Q, q_1\rangle$

$$N_{q'_1, q_1}^Q = \frac{1}{L_q} \Delta N_{q'_1, q_1}^Q + \delta_{q'_1, q_1} + \delta_{q'_1, q_2} \quad (6.17)$$

consisting of a diagonal *bosonic* part $\delta_{q'_1, q_1} + \delta_{q'_1, q_2}$ and the deviation $\Delta N_{q'_1, q_1}^Q$. The hard-core property is included in $\Delta N_{q'_1, q_1}^Q$ to the extent to which it is captured by the iMPS description. In order to obtain operator matrices in a diagonal basis, Eq. (6.17) has to be transformed into the hybrid basis.

6.1.4.1 Metric tensor representation in the hybrid basis

The ground state uMPS is normalized and orthogonal to all excited states by construction. One-particle excited states are also normalized and orthogonal to each other; they can, however, have overlaps with two-particle states. After efficiently computing the overlaps in momentum space, they are transformed into the hybrid basis using the transformations in App. A.9. In each Q -sector, the metric tensor is then representable by a matrix

$$N^Q = \begin{pmatrix} \langle GS | GS \rangle & 0 & \dots & \dots & 0 \\ 0 & \langle Q | Q \rangle & \langle Q | Q, d \rangle & \dots & \langle Q | Q, d \rangle \\ \vdots & \langle Q, d' | Q \rangle & & & \\ \vdots & \vdots & & \langle Q, d' | Q, d \rangle & \\ 0 & \langle Q, d' | Q \rangle & & & \end{pmatrix}. \quad (6.18)$$

The Gram-Schmidt algorithm as described in App. A.8 is applied starting with the ground state, which is not changed, then to the 1QP state, which is not changed either, and then successively to the 2QP states. For consistency, this process begins with the 2QP state, which has its norm in the upper left corner of the sub-matrix $N_{d', d}^Q$. Since states with

sufficiently large particle distance are assumed correct, $N_{d',d}^Q$ should therefore be ordered beginning with the maximum distance $d_{\max} = \frac{L_q-1}{2}$. Then, the matrix N^Q takes the form

$$N^Q = \begin{pmatrix} 1 & 0 & 0 & \cdots & 0 \\ 0 & 1 & (N_{d_{\max}}^Q)^* & \cdots & (N_0^Q)^* \\ 0 & N_{d_{\max}}^Q & N_{d_{\max},d_{\max}}^Q & \cdots & N_{d_{\max},0}^Q \\ \vdots & \vdots & \vdots & \ddots & \vdots \\ 0 & N_0^Q & N_{0,d_{\max}}^Q & \cdots & N_{0,0}^Q \end{pmatrix}. \quad (6.19)$$

6.1.4.2 Note on the hard-core property

The state with $d = 0$ is included for two reasons. First, its squared norm $N_{0,0}^Q$ is an indicator of how close the iMPS description is to hard-core bosons.

If the metric tensor is ordered as in Eq. (6.19), $|Q, d = 0\rangle$ is the last state, to which the Gram-Schmidt algorithm is applied. Therefore, it does not influence any of the other states. If the element $N_{0,0}^Q$ is found to be smaller than a threshold value, the state can simply be excluded from orthonormalization.

Second, if there are significant deviations from hard-core bosons, the state may actually carry physically relevant information.

By definition (cf. Eq. (A.8.1)), the Gram-Schmidt algorithm normalizes all orthogonalized states to unity. This includes the state with particle distance $d = 0$, if no special treatment for it is implemented explicitly.

If $N_{0,0}^Q$ is very small in the skew basis, the normalization can result in spurious and very large matrix elements of the $d = 0$ state in the orthogonalized basis. Since they do not influence the computation of any other matrix elements, they can still be discarded before the operator matrix is transformed back to momentum space or real space. Although this is physically motivated, it is still somewhat arbitrary.

At this point it is not entirely clear, if the iMPS ansatz allows for a proper description of hard-core bosons. Even if the diagonal element $N_{0,0}^Q$ is significant, the metric tensor generically has an EV that is much smaller. Also, the overlap $\langle Q, \widetilde{d = 0} | Q, d = 0 \rangle$ between the $d = 0$ state in the skew basis and in the orthogonalized basis is much smaller than $N_{0,0}^Q$ in these cases. This suggests, that a hard-core bosonic quasi-particle picture should in principle be possible with iMPS. However, the results for the two-particle spectral weight in Sec. 6.3 below indicate, that the matrix elements of the $d = 0$ in the skew basis carry significant physical information.

Three alternatives to the generic Gram-Schmidt orthogonalization come to mind. All of them include a certain bias, since they assume that the quasi-particles are hard-core bosons and that the basis contains one state that should have norm zero.

First, the state with particle distance $d = 0$ can generally be excluded from the computations, regardless of its norm. As shown in Fig. 6.4 below, this can lead to significantly less accurate results.

Second, the information held by the state with $d = 0$ in the skew basis could be extracted during the computation of the operator matrix in the orthogonalized basis. If the state with $d = 0$ has a significant norm, it also shows significant overlaps with the 2QP states with small particle distance $d > 0$. By projecting the matrix elements of the $d = 0$ state

onto the orthogonalized 2QP states with $d > 0$, the unphysical state can be eliminated and problems due to division by a very small norm can be avoided.

Third, one could diagonalize the metric tensor and discard the eigenspace corresponding to the smallest eigenvalue, which is usually closer to zero than the diagonal element $N_{0,0}^Q$. Since the spectrum of N^Q is invariant under the Fourier transformation, this could be done directly in the momentum space basis without the “detour” through the hybrid basis. However, since the eigenvectors are linear combinations of the original states $|Q,d\rangle$ or $|Q,q_1\rangle$, the interpretation as 2QP states with definite momentum q_1 or definite particle distance d is lost.

As seen in Fig. 6.2 below, for bond dimension $D = 2$, the diagonal element $N_{0,0}^Q$ is so small that the state can be excluded without introducing significant additional errors. For bond dimension $D \geq 3$, other errors are by far predominant. Therefore, a comparison is only done between including and excluding the state with $d = 0$ from the Gram-Schmidt algorithm.

6.2 Results for the metric tensor of the TFIM

As a first result, the metric tensor $N_{d',d}^Q$ of the TFIM in the non-orthogonal hybrid basis is analyzed. This is done at the parameter value $\lambda = 0.5$, which is in the disordered phase, halfway between the trivial strong field limit at $\lambda = 0$ and the critical point at $\lambda = 1$. The focus is set on low bond dimensions $D = 2$ and $D = 3$, because these two data sets already show curiously diverse behavior.

Three quantities are examined in this context. The first is the deviation of the diagonal part of the metric tensor from exact hard-core bosons

$$\Delta_{\text{hcb}} := 1 - \frac{\left\| \text{diag}(N_{d',d}^Q) \right\|}{\|N_{\text{hcb}}\|} \quad (6.20)$$

where $\text{diag}(N_{d',d}^Q)$ denotes the main diagonal of the matrix $N_{d',d}^Q$, and N_{hcb} the metric tensor of exact hard-core bosons in the Fock space of the same dimension, i.e.,

$$N_{\text{hcb}} := \mathbb{1}_{\dim(N_{d',d}^Q)-1} \oplus \mathbb{0}_{1 \times 1} . \quad (6.21)$$

The second quantity is the off-diagonality OD_N of the metric tensor matrix, which is defined as

$$OD_N := \frac{\left\| N_{d',d}^Q - \text{diag}(N_{d',d}^Q) \right\|}{\|N_{\text{hcb}}\|} . \quad (6.22)$$

Both these quantities are defined relative to the norm of the exact hard-core bosonic metric tensor N_{hcb} in order to make them independent of the dimension of $N_{d',d}^Q$. By definition, Δ_{hcb} and OD_N both vanish in the limit that $N_{d',d}^Q$ describes exact hard-core bosons. The diagonal elements of $N_{d',d}^Q$, which for an exact iMPS representation should be

$$N_{d,d}^Q = \begin{cases} 0, & \text{for } d = 0 \\ 1, & \text{for } d > 0 \end{cases} , \quad (6.23)$$

are the third quantity of interest.

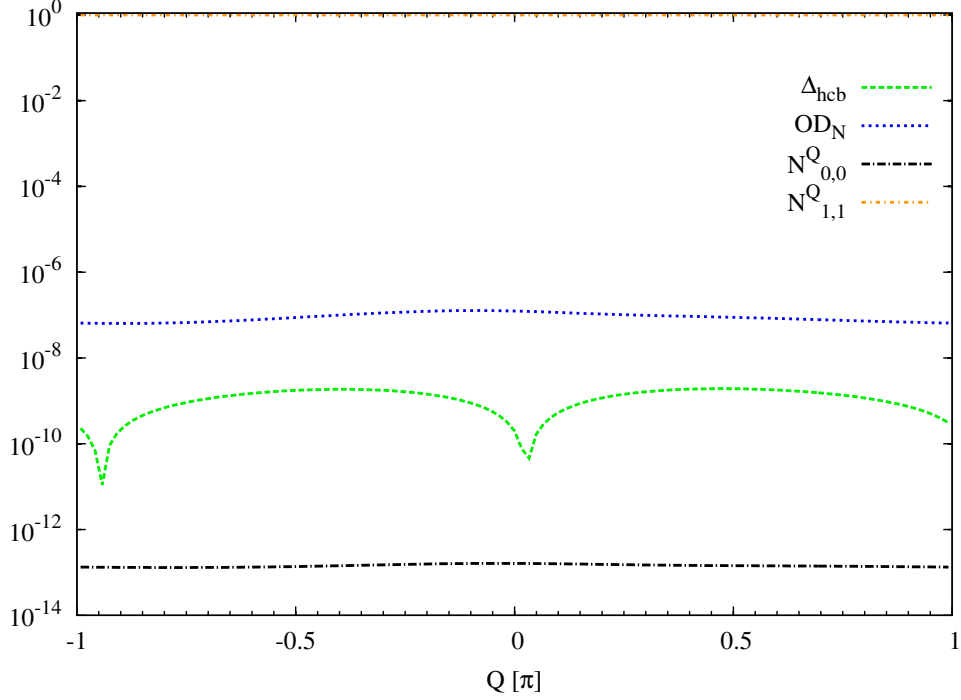


Figure 6.2: Characteristics of the metric tensor in the non-orthogonal hybrid basis $\{|Q, d\rangle\}$ for the TFIM at $\lambda = 0.5$, for bond dimensions $D = 2$ as function of total momentum Q . The quantity Δ_{hcb} is the deviation of the main diagonal from exact hard-core bosons as defined in Eq. (6.20). OD_N is the off-diagonality of the metric tensor as defined in Eq. (6.22). The curves labeled $N_{d,d}^Q$ are the diagonal elements of the metric tensor for different particle distances d , most importantly $d = 0$ and $d = 1$.

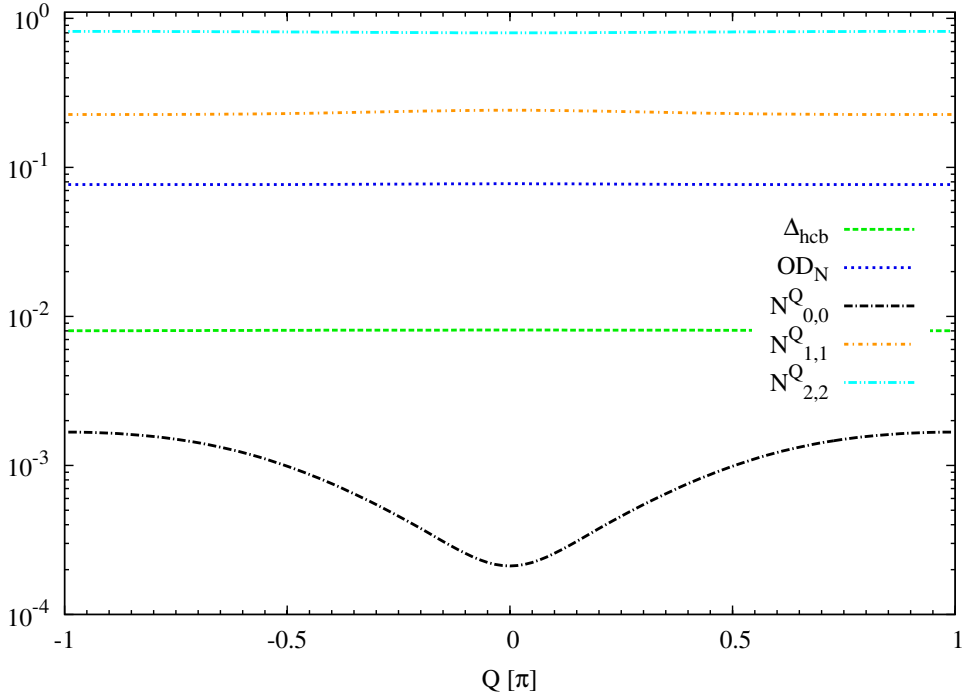


Figure 6.3: Same as Fig. 6.2 but for bond dimension $D = 3$.

Figures 6.2 and 6.3 show Δ_{hcb} , OD_N and some diagonal elements $N_{d,d}^Q$ for the TFIM at $\lambda = 0.5$. Strikingly, the results for $D = 2$ show very little deviation from exact hard-core bosons. Both the deviation quantities and the diagonal element $N_{0,0}^Q$ are very small, whereas $N_{1,1}^Q$ is very close to 1. In the Gram-Schmidt algorithm, all orthogonalized vectors are normalized to 1. This includes the $d = 0$ state if it is not excluded explicitly. Therefore, if $N_{0,0}^Q$ is very small, this will result in spurious and potentially large operator matrix element $\hat{O}_{0,0}^Q$ after orthonormalization. Because of that, the results for $D = 2$ are *not* subjected to the orthogonalization process.

For bond dimension $D = 3$, the situation is quite different. The deviation Δ_{hcb} is of the order of 10^{-2} (i.e. 1%), and the off-diagonality of the order 10^{-1} . The diagonal element $N_{1,1}^Q$ is also of the order 10^{-1} , and the following $N_{2,2}^Q$ almost reaches unity. The most critical element $N_{0,0}^Q$ shows some modulation as function of total momentum and is on average of the order 10^{-3} . At first glance, this is neither cause for concern about numerical instability, nor would it appear to be negligible. Therefore, although this is still rather close to exact hard-core bosons, one would expect quantitative improvements of operator matrices from applying the orthogonalization scheme.

6.3 Two-particle spectral weight in the TFIM

For the TFIM on a one-dimensional chain, it is known from analytic results [62] that in the strong field phase all spectral weight of the zz -channel lies in the 0QP and 2QP sectors. Therefore, the two-particle spectral weight is a good point to continue investigating the properties of our two-particle states.

The two-particle spectral weight is the projection of the spin-spin correlation function onto the 2QP subspace, i.e.

$$S_{2\text{p}}^{\alpha\beta}(Q) = \langle GS | S_{-Q}^\alpha P_{2\text{p}}^Q S_Q^\beta | GS \rangle \quad (6.24a)$$

$$\text{with } P_{2\text{p}}^Q = \sum_{q \in \text{BZ}} |Q, q\rangle \langle Q, q| = \sum_{d=0}^{d_{\text{max}}} |\widetilde{Q}, d\rangle \langle \widetilde{Q}, d| \quad (6.24b)$$

$$= \sum_d \langle GS | S_Q^{\alpha\dagger} |\widetilde{Q}, d\rangle \langle \widetilde{Q}, d| S_Q^\beta | GS \rangle \quad (6.24c)$$

$$=: \sum_d \Omega_d^\alpha(Q) \Omega_d^\beta(Q)^* \quad (6.24d)$$

$$\stackrel{\alpha=\beta}{=} \sum_d |\Omega_d^\alpha(Q)|^2 \quad (6.24e)$$

where, however, $|\widetilde{Q}, d\rangle$ must be an orthonormal basis of the 2QP subspace. Applying the Gram-Schmidt algorithm, with $\alpha = z$, the matrix element in the orthogonalized hybrid basis is given by (cf. Eq. (A.8.14))

$$\Omega_d^z(Q) := \langle GS | S_Q^{z\dagger} |\widetilde{Q}, d\rangle \quad (6.25a)$$

$$= \frac{1}{\sqrt{V_{dd}}} \left[\langle GS | S_Q^{z\dagger} |Q, d\rangle - \sum_{\ell > d} \frac{V_{\ell d}}{V_{\ell\ell}} \langle GS | S_Q^{z\dagger} |\widetilde{Q}, \ell\rangle \right] \quad (6.25b)$$

with $V_{ij} := \langle \widetilde{Q}, i | Q, j \rangle$ (cf. Eq. (A.8.4)). Note that this formulation assumes that the Gram-Schmidt algorithm is started at the maximal $d_{\text{max}} = \frac{L_q - 1}{2}$ and is then applied to states with successively smaller d .

This means that the only matrix elements required to compute the spectral weight are those between the ground state and the 2QP sector

$$\langle GS|S_Q^{z\dagger}|Q,d\rangle = \langle Q,d|S_Q^z|GS\rangle^* . \quad (6.26)$$

But to obtain the auxiliary matrix V , which is also needed, the entire metric tensor

$$N_{d'd}^Q := \langle Q,d'|Q,d\rangle \quad (6.27a)$$

$$N_{d'i}^Q := \langle Q,d'|Q\rangle \quad (6.27b)$$

of the skew basis including the spurious overlaps of the 1QP and 2QP sectors must be known.

To compute the matrix element Eq. (6.26), it must be expressed either in the real space basis or in the momentum space basis

$$\langle Q,d'|S_Q^z|GS\rangle = \frac{1}{L}e^{+iQ\frac{d'}{2}} \sum_{j',\ell} e^{+iQj'} e^{-iQ\ell} \langle j',j'+d'|S_\ell^z|GS\rangle \quad (6.28a)$$

$$= \frac{1}{L}e^{+iQ\frac{d'}{2}} \sum_{j',\ell} e^{iQ(j'-\ell)} \langle j'-\ell,j'-\ell+d'|S_0^z|GS\rangle \quad (6.28b)$$

$$= e^{iQ\frac{d'}{2}} \sum_{j'} e^{iQj'} \langle j',j'+d'|S_0^z|GS\rangle \quad (6.28c)$$

$$= \frac{1}{\sqrt{L}}e^{+iQ\frac{d'}{2}} \sum_{q'_1} e^{+iq'_1 d'} \langle Q,q'_1|S_Q^z|GS\rangle \quad (6.28d)$$

$$= e^{+iQ\frac{d'}{2}} \sum_{q'_1} \langle Q,q'_1|S_{\ell=0}^z|GS\rangle \quad (6.28e)$$

where the last equality holds true due to TI.

6.3.1 Reference result from uMPS

The 2QP spectral weight in the zz -channel for the TFIM in the strong field phase is given by Eq. (2.55). The ground state correlation function can be computed from the uMPS representation

$$S^{zz}(Q) = \langle GS|S_{-Q}^z S_Q^z|GS\rangle \quad (6.29a)$$

$$= \sum_j e^{iQj} \langle GS|S_j^z S_0^z|GS\rangle \quad (6.29b)$$

$$=: \sum_j e^{iQj} S_j^{zz} \quad (6.29c)$$

with

$$S_j^{zz} = \begin{cases} \left(S^{z\dagger(\mathbf{A};\mathbf{A})}[u], T^{|j|-1}[S^{z(\mathbf{A};\mathbf{A})}[v]] \right), & \text{if } j \neq 0 \\ \left(u, (S^z)^{2(\mathbf{A};\mathbf{A})}[v] \right) = \frac{1}{4} \left(u, \mathbb{1}^{(\mathbf{A};\mathbf{A})}[v] \right) = \frac{1}{4}, & \text{if } j = 0 \end{cases} . \quad (6.30)$$

Note, that S_j^{zz} converges to

$$\langle GS|S_j^z|GS\rangle \langle GS|S_0^z|GS\rangle = \langle GS|S_0^z|GS\rangle^2 = M_z^2 \quad (6.31)$$

for $|j| > \Xi_T$. It is therefore numerically favorable, to compute the deviation of the correlation function from the ground state magnetization directly and then take the Fourier

transform to avoid loss of significance. The reference result for the two-particle spectral weight is given by

$$S_{\text{ref}}^{zz}(Q) = \sum_j e^{iQj} (S_j^{zz} - M_z^2) \quad (6.32)$$

where the uMPS result for the ground state magnetization is used for consistency.

6.3.2 Results

Despite the efficient momentum space algorithms outlined in the next section, 2QP calculations are generically more challenging and CPU intensive than those for 1QP. Therefore, results are only shown for bond dimensions up to $D = 10$. Since the method is in a proof-of-concept stage, this is sufficient to assess its advantages and disadvantages.

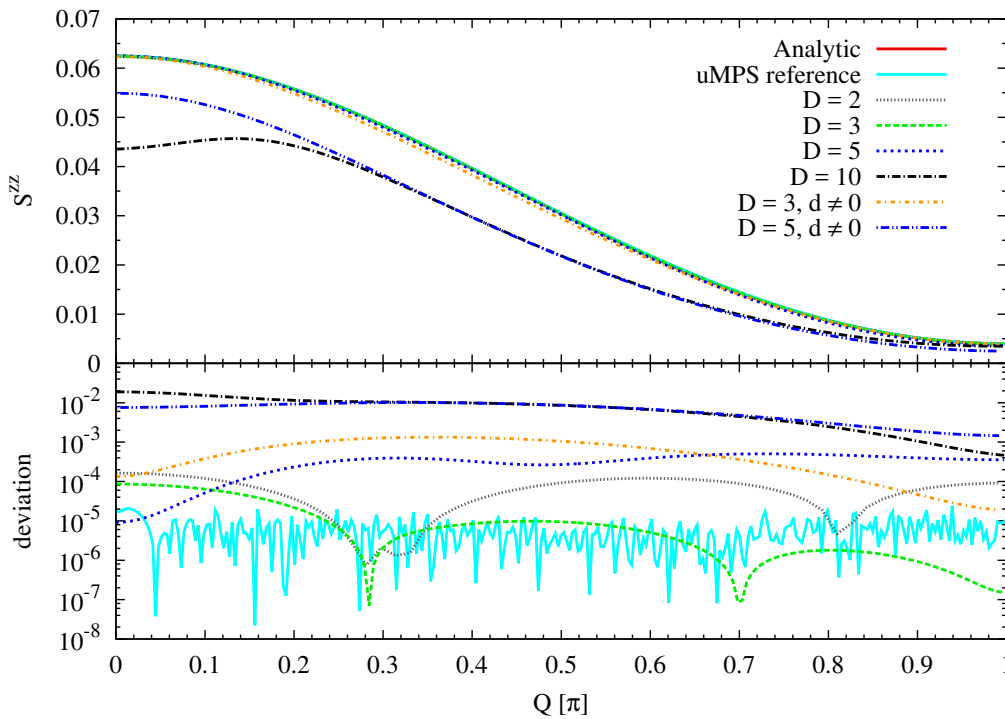


Figure 6.4: Two-particle spectral weight S_{2P}^{zz} for the TFIM at $\lambda = 0.5$ for various bond dimensions. In the upper panel, the spectral weight itself is plotted. The data sets labeled “ $d \neq 0$ ” were computed omitting the state with particle distance $d = 0$ from the orthonormalization. The lower panel shows the deviation of the uMPS reference from the analytical data (solid line), and the deviations of the 2QP iMPS results from the uMPS reference (dashed/dotted lines). The uMPS reference curve was computed using Eq. (6.32) with bond dimension $D = 10$. The analytical reference curve was obtained by numerically evaluating Eq. (7.4.44) of Ref. [57] and integrating over frequency.

Figure 6.4 shows the two-particle spectral weight in the zz -channel at $\lambda = 0.5$ for various bond dimensions D , in comparison with both the analytical result and the uMPS reference result from Eq. (6.32). In the upper panel, the spectral weight itself is plotted. The lower panel shows the deviation of the uMPS reference from the analytical data (solid line), and the deviations of the 2QP iMPS results from the uMPS reference (dashed/dotted lines). The analytical reference curve was obtained by integrating data [96] from numerically

evaluating Eq. (7.4.44) of Ref. [57] over frequency ω . It is apparent that the two reference results are in very good agreement. The jagged form of the deviation is a result of the finite resolution in frequency at which comparison data was computed. Due to this good agreement, the uMPS ground state result is trusted and used as a reference, to which the 2QP calculations are compared, since it can easily be computed.

First and foremost, the plot shows that our approach is capable of producing reasonable results and therefore the intended proof of concept can be considered successful. The results for both $D = 2$ and $D = 3$ show very good agreement with the reference, quantitatively comparable even to the 1QP result in Fig. 5.12. Note that for $D = 2$ there is no need for orthogonalization, as explained in the previous section.

For bond dimension $D \geq 3$, the data is subjected to the Gram-Schmidt orthogonalization scheme as described in App. A.8.

For bond dimensions $D = 3$ and $D = 5$, Fig. 6.4 shows the results both for including and omitting the state with $d = 0$ from the process. Although one could argue that any matrix elements of this state contradict a hard-core bosonic quasi-particle picture, the plot clearly shows that including this state leads to a better agreement with the analytic solution. It is apparent that for $D = 5$, the information carried by the $d = 0$ state is indeed substantial and should not be omitted, although the corresponding diagonal element of the metric tensor $N_{0,0}^Q$ is of the same order of magnitude as it is for $D = 3$.

This raises again the question of how to consistently handle the hard-core property. On the one hand, on the basis of the spectrum of the metric tensor one can clearly argue for a hard-core bosonic quasi-particle picture. On the other hand, these results for the spectral weight clearly indicate that the matrix elements of the state with $d = 0$ are indeed important.

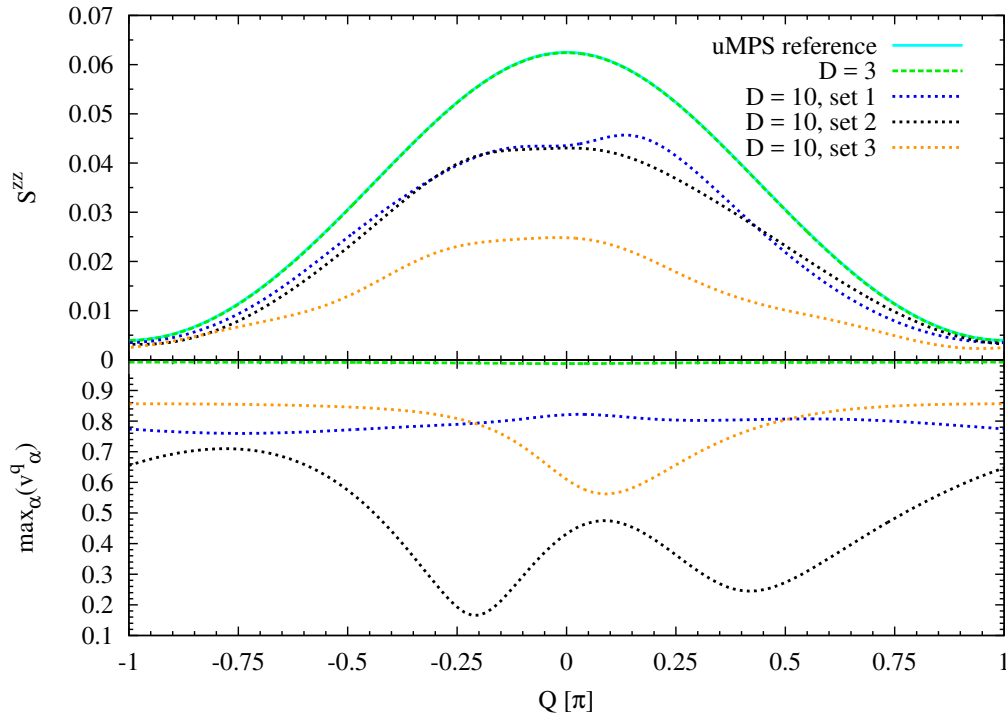


Figure 6.5: Two-particle spectral weight S_{2P}^{zz} for the TFIM at $\lambda = 0.5$ over the whole Brillouin zone. Several data sets from different program runs for the same bond dimension $D = 10$. In the upper panel, the spectral weight result is plotted. The lower panel shows the dominant component of the corresponding momentum eigenstate \vec{v}^q . For comparison the data with $D = 3$ from Fig. 6.4 is also included.

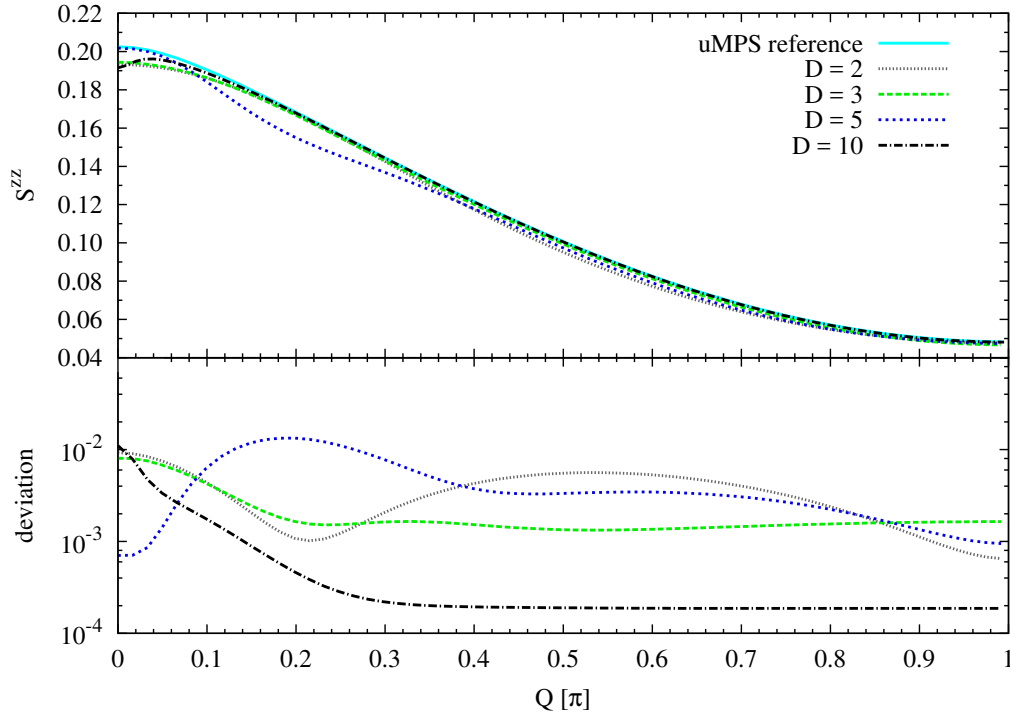


Figure 6.6: Two-particle spectral weight S_{2P}^{zz} for the TFIM at $\lambda = 0.9$ for various bond dimensions. In the upper panel, the spectral weight itself is plotted. The lower panel shows the deviations of the 2QP iMPS result from the uMPS reference. The uMPS reference curve was computed using Eq. (6.32) with bond dimension $D = 10$.

Also, the curve for $D = 5$ computed including the $d = 0$ state shows a larger deviation than those for smaller D . Thus, compared to the ground state and 1QP results, the increase in accuracy for increasing D is less systematic.

The result for $D = 10$ deviates from the reference to an extent which, unfortunately, must be considered unacceptable. The reason for this deviation reveals itself in Fig. 6.5, where the result for $D = 10$ is plotted over the whole Brillouin zone. There it is apparent that the curve does not show the expected even symmetry about $Q = 0$. Since this is clearly unphysical, the reason must be in the numerics. This becomes even clearer seeing that Fig. 6.5 contains the results from multiple different program runs, all with bond dimension $D = 10$. The data for $D = 3$ from Fig. 6.4 is also included for comparison. The curves should lie on top of each other within numerical tolerance, but clearly they do not. The lower panel shows the dominant component of the eigenstate \vec{v}^q for each data set.

While the dominant component of the $D = 3$ data set holds almost all the weight and shows the correct symmetry, neither is the case for the $D = 10$ data sets. Moreover, already the dominant \vec{v}^q components of the three $D = 10$ data sets differ significantly from each other, although they should describe the same system. Note that these different forms of \vec{v}^q are not just phases. The phase gauge introduced in Eq. (5.79) fixes the phase such that the dominant component is real and positive. The different forms and magnitudes of this component mean that the description of the elementary excitation is distributed differently over different \mathbf{B}_α tensors in each data set. Consequently, these tensors must vary significantly in the different data sets, even though they are solutions of the same EVP up to a norm conserving gauge transformation of the ground state tensor \mathbf{A} . The reason is most likely again numerical instability in the computation of the \mathbf{B}_α due to very small elements in the boundary matrix v . Considering that a contribution with $q'_1 = -q'_2$

should have two identical C_q tensors, it is not surprising that an asymmetric \vec{v}^q spoils the results.

Figure 6.6 shows the S_{2P}^{zz} for $\lambda = 0.9$ and various bond dimensions. Again, the results for $D = 2$ and $D = 3$ show qualitatively good agreement, although the peak height around $Q = 0$ deviates to some extent. Since $\lambda = 0.9$ is already relatively close to criticality, this is expected for low bond dimensions. At $D = 5$, the peak height is already captured more accurately, but there is considerable deviation around 0.2π . Still, this supports the expectation that the results should improve for increasing D . Unfortunately, at $D = 10$ the effects of the asymmetric \vec{v}^q become visible and spoil the result around the gap mode $Q = 0$. Note that the effect is far less pronounced than it is at $\lambda = 0.5$. This supports the hypothesis that the asymmetry in \vec{v}^q is indeed a result of excess parameters in the excitation parametrization X_α . Therefore, finding a more numerically stable algorithm to compute X_α should be a central step in future research.

6.4 Efficient computation of two-particle quantities

Equations (5.67) and (5.77) show that in real space, each particle is described by a set of $2\Theta + 1$ tensors C_ℓ . Therefore, for instance a two-particle overlap in real space

$$\langle j', j' + d' | j, d \rangle = \sum_{\ell', m'} \sum_{\ell, m} \langle C_{\ell'}, j' + \ell'; C_{m'}, j' + d' + m' | C_{\ell}, j + \ell; C_m, j + d + m \rangle \quad (6.33)$$

needs $(2\Theta + 1)^4$ TN evaluations. The same holds for 2QP matrix elements. This puts a severe limitation on real space computations. See Sec. 6.4.2 below for more details.

Once more, the key to an efficient computation is the switch to momentum space, and the observation that the ‘‘Fourier transform trick’’ from Eq. (5.86) also works for two-particle states

$$|Q, q_1\rangle = \frac{1}{L} \sum_{j=-\infty}^{\infty} \sum_{d=-\infty, d \neq 0}^{\infty} \sum_{\ell, m} e^{-iQj - iQd + iq_1 d} |C_{\ell}, j + \ell; C_m, j + d + m\rangle \quad (6.34a)$$

$$\stackrel{j \rightarrow j - \ell}{=} \frac{1}{L} \sum_{j, d} \sum_{\ell, m} e^{-iQ(j - \ell) - iQd + iq_1 d} |C_{\ell}, j; C_m, j - \ell + d + m\rangle \quad (6.34b)$$

$$\stackrel{d \rightarrow d + \ell - m}{=} \frac{1}{L} \sum_{j, d} \sum_{\ell, m} e^{-iQ(j - \ell) - iQ(d + \ell - m) + iq_1(d + \ell - m)} |C_{\ell}, j; C_m, j + d\rangle \quad (6.34c)$$

$$= \frac{1}{L} \sum_{j, d} e^{-iQj - iQd + iq_1 d} \sum_{\ell, m} e^{+i(Q - q_1)m + iq_1 \ell} |C_{\ell}, j; C_m, j + d\rangle \quad (6.34d)$$

$$= \frac{1}{L} \sum_{j, d} e^{-iQj - iQd + iq_1 d} |C_{q_1}, j; C_{q_2}, j + d\rangle, \quad (6.34e)$$

with C_ℓ in real space as defined in Eq. (5.67) and C_{q_i} in momentum space as defined in Eq. (5.87). As in the one-particle case, the sums over ℓ and m can be carried out on the C -tensor level now under two Fourier transformations. The result is a single tensor which can be interpreted as representing a particle with momentum q_i on a given site.

Note that it is essential that *both* Fourier transformations are carried out for this to work. It is therefore impossible to work efficiently in the hybrid basis directly. However, a Fourier transformation is also required from the real space basis to the hybrid basis, so this does

not mean a loss of performance.

In this formulation, the only instance of two \mathbf{C} tensors falling onto the same site is the case $d = 0$. As in the real space description, this contribution is omitted, which now has a strong resemblance with a hard-core constraint. However, this is *not* equivalent to omitting the entire contribution of real space states with $d = 0$. It still only means omitting all contributions with two \mathbf{C} -tensors on the same site, which can be seen by reversing the index shift in Eq. (6.34c)

$$d = 0 \quad d \xrightarrow{\Leftrightarrow} d - \ell + m \quad d + m = \ell. \quad (6.35)$$

For $D = 1$, both are actually the same, since the particle representation consists of a single $d \times 1 \times 1$ tensor \mathbf{C}_0 . But in general, as evident from the norm of the 2QP real space state in Fig. 6.1, there are two important differences. First, the same-site contributions hold most, but not all of the weight for $d = 0$, and second, they also have a significant share in states with small d .

6.4.1 2QP-ground state matrix element

Using the momentum space description of the 2QP state in Eq. (6.34), the matrix element from Eq. (6.28) can now be computed as

$$\langle Q, q'_1 | O_0 | GS \rangle = \frac{1}{L} \sum_{j', d'} e^{+iQ(j'+d') - iq'_1 d'} \langle \mathbf{C}_{q'_1, j'}; \mathbf{C}_{q'_2, j' + d'} | O_0 | GS \rangle \quad (6.36)$$

where $q'_2 = Q - q'_1$ and a general operator \hat{O} which acts on site 0 is considered. An implementation of the real space matrix element is straight forward, but leaves all the hard work to the CPU; the momentum space computation is a lot more challenging to implement. Due to the left-canonical gauge, any contribution with $\min(j', j' + d') < 0$ vanishes, because it contains the expression from Eq. (5.10). This leaves three topologically distinct classes of TNs which have to be evaluated. These will be discussed in some detail below, to illustrate the general procedure of momentum space computations.

In all following calculations, n is the number of sites which the operator \hat{O} acts on. For the spectral weight with $\hat{O} = S^z$, $n = 1$. The TNs are drawn for $n = 2$ for illustration, but the procedure works for any finite n .

Case i): The operator acts to the left of both \mathbf{C} -tensors

$$\langle \mathbf{C}_{q'_1, j'}; \mathbf{C}_{q'_2, j' + d'} | O_0 | GS \rangle = \left(\text{Diagram} \right) \quad (6.37)$$

where

$$\alpha' := \begin{cases} 1, & \text{if } d' > 0 \\ 2, & \text{if } d' < 0 \end{cases} \quad \text{and} \quad \bar{\alpha}' := \begin{cases} 2, & \text{if } \alpha' = 1 \\ 1, & \text{if } \alpha' = 2 \end{cases}. \quad (6.38)$$

The distances between the operator and the first \mathbf{C} -tensor, δ_0 , and between the two \mathbf{C} -tensors, δ_1 , must be summed from 0 to at least Ξ_T each to ensure convergence. The contributions converge to zero, since for large δ_0 and/or δ_1 , the TN factorizes and contains at least one overlap of an excited state with the ground state, which is zero by construction.

In terms of the distances $\delta_i \geq 0$, the particle positions read

$$j' = n + \delta_0, \quad d' = (\delta_1 + 1), \quad \text{if } \alpha' = 1 \ (d' > 0) \quad (6.39a)$$

$$j' = n + \delta_0 + 1 + \delta_1, \quad d' = -(\delta_1 + 1), \quad \text{if } \alpha' = 2 \ (d' < 0). \quad (6.39b)$$

Inserting this into the phase factor from Eq. (6.36) yields

$$\Phi_{\alpha'} := e^{+iQ(j'+d')-iq'_1 d'} = \begin{cases} e^{+iQ(n+\delta_0+\delta_1+1)-iq'_1(\delta_1+1)}, & \text{if } \alpha' = 1 \\ e^{+iQ(n+\delta_0+1+\delta_1-\delta_1-1)+iq'_1(\delta_1+1)}, & \text{if } \alpha' = 2 \end{cases} \quad (6.40a)$$

$$= \begin{cases} e^{iQ(n+\delta_0)+iq'_2(\delta_1+1)} \\ e^{iQ(n+\delta_0)+iq'_1(\delta_1+1)} \end{cases} \quad (6.40b)$$

$$= e^{iQ(n+\delta_0)+iq_{\bar{\alpha}'}(\delta_1+1)}. \quad (6.40c)$$

Rather than summing over positive and negative d' , it is easier to think of summing over the possible configurations of C_{q_1} and C_{q_2} , which are enumerated by α' . Then, the complete contribution from case i) is given by

$$\begin{aligned} & \langle Q, q'_1 | O_0 | GS \rangle \Big|_i \\ &= \sum_{\alpha'=1,2} \sum_{\delta_0, \delta_1=1}^{\Xi_T} e^{iQ(n+\delta_0)+iq_{\bar{\alpha}'}(\delta_1+1)} \\ & \quad \times \left((T^\dagger)^{\delta_0} [O^\dagger(A;A)[u]], \mathbf{1}^{(C_{q_{\alpha'}};A)} [T^{\delta_1} [\mathbf{1}^{(C_{q_{\bar{\alpha}'}};A)} [v]]] \right) \end{aligned} \quad (6.41a)$$

$$= \sum_{\alpha'} \left(\sum_{\delta_0} e^{-iQ(n+\delta_0)} (T^\dagger)^{\delta_0} [O^\dagger(A;A)[u]], \mathbf{1}^{(C_{q_{\alpha'}};A)} \left[\sum_{\delta_1} e^{+iq_{\bar{\alpha}'}(\delta_1+1)} T^{\delta_1} [\mathbf{1}^{(C_{q_{\bar{\alpha}'}};A)} [v]] \right] \right) \quad (6.41b)$$

due to the sesqui-linearity of the scalar product. Note that when pulled into the first argument, the phase factor needs to be complex conjugated. This allows the definition of two summed boundary matrices

$$v^{\bar{\alpha}'} := \sum_{\delta_1=1}^{\Xi_T} T^{\delta_1} [\mathbf{1}^{(C_{q_{\bar{\alpha}'}};A)} [v]] e^{+iq_{\bar{\alpha}'}(\delta_1+1)} \quad (6.42)$$

$$u_O^Q := \sum_{\delta_0=1}^{\Xi_T} (T^\dagger)^{\delta_0} [O^\dagger(A;A)[u]] e^{-iQ(n+\delta_0)} \quad (6.43)$$

in terms of which the contribution is given by just two scalar products

$$\langle Q, q'_1 | O_0 | GS \rangle \Big|_i = \sum_{\alpha'=1,2} \left(u_O^Q, \mathbf{1}^{(C_{q_{\alpha'}};A)} [v^{\bar{\alpha}'}] \right). \quad (6.44)$$

As in the case of the one-particle spectral weight in Sec. (5.7), the summed boundary matrices can be computed by successively applying the transfer operator.

Case ii): The operator acts on the site of one C-tensor

$$\langle C_{q'_1}, j'; C_{q'_2}, j' + d' | O_0 | GS \rangle = \begin{array}{c} \begin{array}{c} \bullet \\ \square \\ \bullet \end{array} \quad \begin{array}{c} \bullet \\ \square \\ \bullet \end{array} \quad \begin{array}{c} \bullet \\ \square \\ \bullet \end{array} \quad \begin{array}{c} \bullet \\ \square \\ \bullet \end{array} \\ \underbrace{\hspace{1.5cm}}_{\ell'} \quad \underbrace{\hspace{1.5cm}}_{\delta_1} \end{array} \quad (6.45)$$

In this case, there is one absolute particle position, ℓ' , and one relative distance, δ_1 , that need to be summed over. In terms of these, the particle positions read

$$j' = \ell', \quad d' = \delta_1 + n - \ell', \quad \text{if } \alpha' = 1 \quad (6.46a)$$

$$j' = n + \delta_1, \quad d' = -(\delta_1 + n - \ell'), \quad \text{if } \alpha' = 2. \quad (6.46b)$$

Inserting this into the phase factor again gives

$$\Phi_{\alpha'} := e^{+iQ(j'+d')-iq'_1 d'} = \begin{cases} e^{+iQ(\ell'+\delta_1+n-\ell')-iq'_1(\delta_1+n-\ell')}, & \text{if } \alpha' = 1 \\ e^{+iQ(n+\delta_1-(\delta_1+n-\ell'))+iq'_1(\delta_1+n-\ell')}, & \text{if } \alpha' = 2 \end{cases} \quad (6.47a)$$

$$= \begin{cases} e^{iq'_1 \ell' + iq'_2(n-1) + iq'_2(\delta_1+1)} \\ e^{iq'_2 \ell' + iq'_1(n-1) + iq'_1(\delta_1+1)} \end{cases} \quad (6.47b)$$

$$= e^{iq_{\alpha'} \ell' + iq_{\bar{\alpha}'}(n-1) + iq_{\bar{\alpha}'}(\delta_1+1)}. \quad (6.47c)$$

From this, the case ii) contribution follows as

$$\langle Q, q_1 | O_0 | GS \rangle \Big|_{\text{ii}} = \sum_{\alpha'=1,2} \sum_{\ell'=0}^{n-1} \sum_{\delta_1=0}^{\Xi_T} e^{iq_{\alpha'} \ell' + iq_{\bar{\alpha}'}(n-1) + iq_{\bar{\alpha}'}(\delta_1+1)} \left(u, O_{\ell'}^{(C_{q_{\alpha'}}; A)} [T^{\delta_1} [\mathbb{1}^{(C_{q_{\bar{\alpha}'}; A)} [v]]}] \right) \quad (6.48a)$$

$$= \sum_{\alpha'=1,2} \sum_{\ell'=0}^{n-1} e^{+iq_{\alpha'} \ell' + iq_{\bar{\alpha}'}(n-1)} \left(u, O_{\ell'}^{(C_{q_{\alpha'}}; A)} \left[\sum_{\delta_1=0}^{\Xi_T} T^{\delta_1} [\mathbb{1}^{(C_{q_{\bar{\alpha}'}; A)} [v]]} e^{+iq_{\bar{\alpha}'}(\delta_1+1)} \right] \right) \quad (6.48b)$$

$$= \sum_{\alpha'=1,2} \sum_{\ell'=0}^{n-1} e^{+iq_{\alpha'} \ell' + iq_{\bar{\alpha}'}(n-1)} \left(u, O_{\ell'}^{(C_{q_{\alpha'}}; A)} [v^{\bar{\alpha}'}] \right) \quad (6.48c)$$

where the summed right boundary matrix $v^{\bar{\alpha}'}$ defined in Eq. (6.42) was used.

Case iii): The operator acts on the sites of *both* C-tensors

$$\langle C_{q'_1}, j'; C_{q'_2}, j' + d' | O_0 | GS \rangle = \begin{array}{c} \begin{array}{c} C_{q_{\alpha'}} \quad C_{q_{\bar{\alpha}'}} \\ \downarrow \quad \downarrow \\ \square \quad \square \\ \uparrow \quad \uparrow \\ \bullet \quad \bullet \\ \ell' \quad m' \end{array} \\ \hat{O}_0 \end{array} \quad (6.49)$$

This case is conceptually the easiest. It consists of a finite number of $n^2 - n$ contributions since $\ell' = m'$ is excluded. Each contribution is unique and has to be computed in the same way, in which real space matrix elements of this type are computed (cf. Sec. 5.2.3). The particle positions are straight forwardly given by

$$j' = \ell', \quad d' = m' - \ell', \quad \text{if } \alpha' = 1 \quad (6.50a)$$

$$j' = m', \quad d' = -(m' - \ell'), \quad \text{if } \alpha' = 2, \quad (6.50b)$$

resulting in a phase factor of

$$\Phi_{\alpha'} := e^{+iQ(j'+d')-iq'_1 d'} = e^{+iq_{\alpha'} \ell' + iq_{\bar{\alpha}'} m'}. \quad (6.51)$$

The contribution to the matrix element from case iii) is thus

$$\langle Q, q_1 | O_0 | GS \rangle \Big|_{\text{iii}} = \sum_{\alpha'=1,2} \sum_{\ell'=0}^{n-2} \sum_{m'=\ell'+1}^{n-1} e^{+iq_{\alpha'} \ell' + iq_{\bar{\alpha}'} m'} \left(u, O_{\ell', m'}^{(C_{q_{\alpha'}}, C_{q_{\bar{\alpha}'}}; A)} [v] \right), \quad (6.52)$$

where the expression

$$O_{\ell',m'}^{(C_{q_{\alpha'}};C_{q_{\bar{\alpha}}};A)}[v] := O_0^{(A;A)}[\dots [O_{\ell'}^{(C_{q_{\alpha'}};A)}[\dots [O_{m'}^{(C_{q_{\bar{\alpha}}};A)}[\dots [O_n^{(A;A)}[v]]]]]]] \quad (6.53)$$

is defined as the application of the operator \hat{O} to the right boundary matrix v as seen in the TN in Eq. (6.49). For $n = 2$, there is actually only one such contribution

$$O_{0,1}^{(C_{q_{\alpha'}};C_{q_{\bar{\alpha}}};A)}[v] = O_0^{(C_{q_{\alpha'}};A)}[O_1^{(C_{q_{\bar{\alpha}}};A)}[v]] \quad (6.54)$$

and for $n = 1$, case iii) does not contribute at all.

Summary

Summing up the contributions from cases i) to iii), the complete matrix element is given by

$$\langle Q, q_1 | O_0 | GS \rangle = \sum_{\alpha'=1,2} \left(u_{\hat{O}}^Q, \mathbb{1}^{(C_{q_{\alpha'}};A)}[v^{\bar{\alpha}'}] \right) \quad (6.55a)$$

$$+ \sum_{\alpha'=1,2} \sum_{\ell'=0}^{n-1} e^{+iq_{\alpha'}\ell'} e^{+iq_{\bar{\alpha}}(n-1)} \left(u, O_{\ell'}^{(C_{q_{\alpha'}};A)}[v^{\bar{\alpha}'}] \right) \quad (6.55b)$$

$$+ \sum_{\alpha'=1,2} \sum_{\ell'=0}^{n-2} \sum_{m'=\ell'+1}^{n-1} e^{+iq_{\alpha'}\ell'} e^{+iq_{\bar{\alpha}}m'} \left(u, O_{\ell',m'}^{(C_{q_{\alpha'}};C_{q_{\bar{\alpha}}};A)}[v] \right). \quad (6.55c)$$

6.4.2 Complexity analysis

As mentioned at the beginning of this section, $\mathcal{O}(\Theta^4)$ TN evaluations are required to compute a single real space 2QP overlap. The computation time for each TN scales linearly with its width, which on average is also of the order Θ . Therefore, the complexity of each overlap scales as $\mathcal{O}(\Theta^5)$ with the particle representation cutoff Θ . In order to take the transform to the hybrid basis and exploit the orthogonality with respect to total momentum, an additional sum over $j' - j \in \{-\Theta, \dots, \Theta\}$ is required. Further, to span the non-trivial part of the two-particle space, overlaps for distances d and d' up to at least Θ each have to be computed, raising the overall complexity of the metric tensor to $\mathcal{O}(\Theta^8)$.

Each step in the evaluation of a TN is the application of an operator, either the transfer operator T or a non-trivial operator, to a boundary matrix u_{eff} or v_{eff} that currently represents the left or right part of the TN, respectively. Each operator application requires $2d^2$ products of $D \times D$ matrices, i.e. $\mathcal{O}(dD^3)$ complex multiplications (cf. Eq.(3.83)), where d is the dimension of the local unit cell Hilbert space.

For consistent results, Θ should be chosen equal to Ξ_T . But even if η is chosen to define the cutoff as in Eq. (5.77), Θ could easily be of the order 10^2 for a moderate bond dimension of $D = 10$. In case of the TFIM with local Hilbert space dimension $d = 2$, this results in a total of

$$2 \cdot 10^3 \cdot (10^2)^8 = 2 \cdot 10^{19} \quad (6.56)$$

operations to compute the metric tensor. Optimistically assuming $3 \cdot 10^9$ multiplications per second, one arrives at a staggering

$$\frac{2}{3} 10^{10} \text{ s} \approx 7.7 \cdot 10^4 \text{ d} \approx 211 \text{ a} \quad (6.57)$$

of computation time on a single CPU. Of course, the computation can easily be parallelized, but still the Θ which can be treated in reasonable time, and therefore the accessible effective correlation lengths, are dramatically limited.

By contrast, as seen in the previous section and App. B, the complexity of computing *any* 2QP overlap or matrix element in momentum space scales only *linearly* with Θ ! This has two reasons. First, four sums can be carried on the level of \mathbf{C} tensors, namely the transformations from \mathbf{C}_ℓ to \mathbf{C}_{q_α} . As shown in Eq. (5.88), this can be done directly from \vec{v}^q . The complexity is therefore in $\mathcal{O}(dD^4)$ independently of any cutoff Θ , and, moreover, \mathbf{C}_{q_α} still describes a system in the TDL up to the choice of L_q . Also, the \mathbf{C}_{q_α} tensors need to be computed only once for each overlap or matrix element. The second reason, as mentioned in Sec. 5.7, is that the \mathbf{C}_{q_α} tensors are the same for all sites, unlike their real space counterparts \mathbf{C}_ℓ . This allows the use of summed boundary matrices such as $v^{\bar{\alpha}'}$ and $u_{\bar{O}}^Q$. The computation of each of them scales as $\mathcal{O}(\Theta^1)$, as seen in Eqs. (6.42) and (6.43), respectively. But their scalar product corresponds to evaluating Θ^2 TNs as seen in Eq. (6.41). This enormous reduction makes it possible to sum any distances up to Ξ_T instead of settling for a potentially far too small cutoff Θ .

To properly describe a system with an effective correlation length Ξ_T , momentum resolution must be at least $L_q = 2\Xi_T$, as discussed above. This leads to a total of

$$\mathcal{O}(dD^3 \cdot \gamma \Xi_T \cdot \Xi_T^3) \quad (6.58)$$

complex multiplications to compute the metric tensor or an operator tensor in momentum space. Here γ is the number of sums over Ξ_T in boundary matrices such as $u_{\bar{O}}^Q$ and $v^{\bar{\alpha}'}$, which is needed to compute each overlap or matrix element, respectively. For the 2QP overlap, $\gamma = 3$ for $u_{\bar{\alpha}'}^{\alpha'}$, $v^{\bar{\alpha}'}$ and $v_{\bar{\alpha}}$ (cf. Sec. B.2.1). Assuming $\Xi_T = 2 \cdot 10^2$ and, again, bond dimension $D = 10$ and $3 \cdot 10^9$ multiplications per second, this results in a computation time of

$$\frac{2 \cdot 10^3 \cdot 3 \cdot (2 \cdot 2 \cdot 10^2)^4}{3 \text{ GHz}} \approx \frac{1.5 \cdot 10^{14}}{3 \text{ GHz}} \quad (6.59a)$$

$$\approx 5 \cdot 10^4 \text{ s} \quad (6.59b)$$

$$\approx 14 \text{ h} . \quad (6.59c)$$

Clearly, this is much more feasible, and since each Q sector can be handled independently, parallelization is very easy, even with distributed memory machines (MPI).

For matrix elements, γ is much larger, and there is some additional overhead. Still, these are constant factors and high resolution data can be produced in a matter of days.

6.5 Quasi-particle decay amplitude

The matrix elements $D_{q_3}^{q_1, q_2}$ and their complex conjugates from Eq. (1.1), which couple the 2QP sector to the 1QP sector, describe quasi-particle decay and fusion. The models from Chap. 2 are particle number conserving. Therefore, these elements must vanish in the orthogonalized basis, which is another opportunity to test the method.

Assuming total momentum conservation, the $D_{q_3}^{q_1, q_2}$ are given in the basis $\{|Q, q'_1\rangle\}$ by

$$D_{q_3}^{q_1, q_2} = D_{q'_1}^Q = \langle Q, q'_1 | D_{q'_1}^Q a_{q'_1}^\dagger a_{Q-q'_1}^\dagger a_Q | Q \rangle = \sqrt{L} \langle Q, q'_1 | H | Q \rangle . \quad (6.60)$$

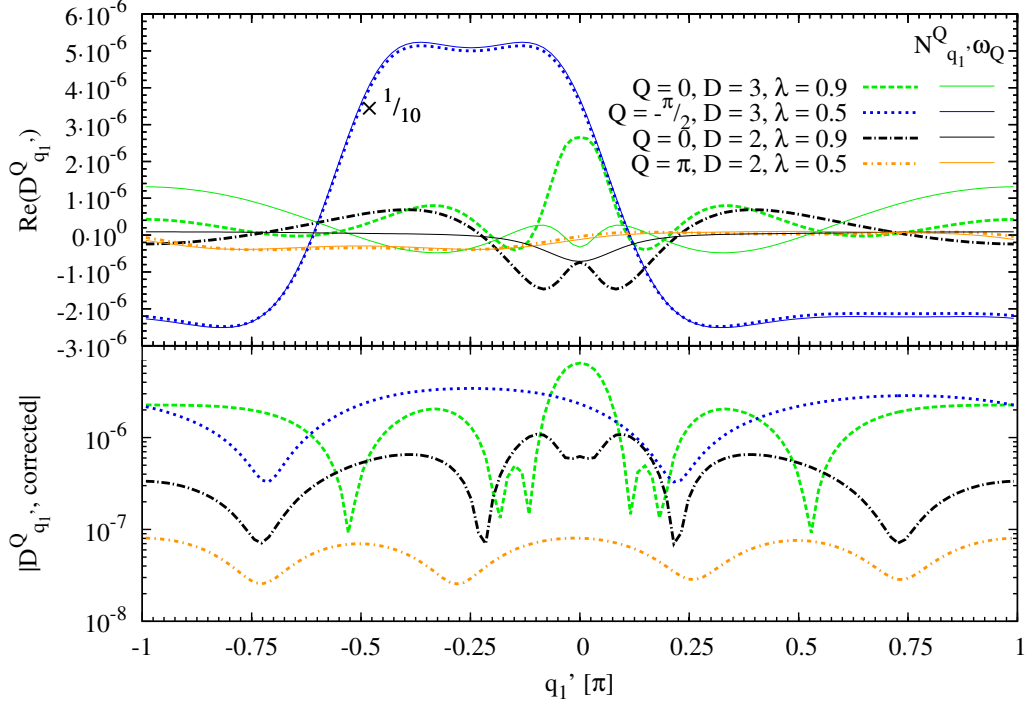


Figure 6.7: Quasi-particle decay amplitude $D_{q_1}^Q$ for various parameters λ , total momenta Q and low bond dimensions $D = 2$ and $D = 3$. The upper panel shows the matrix elements in the skew 2QP basis. For each set of D , λ and Q , the real part of the factorization $N_{q_1}^Q \omega_Q$ is plotted as thin solid lines in the same color. The curves for $Q = -\frac{\pi}{2}$, $D = 3$ and $\lambda = 0.5$ are scaled down by a factor of $\frac{1}{10}$ to fit the plot range. In the lower panel, the absolute value of the decay amplitude after the application of the orthogonalization algorithm is plotted on a logarithmic scale.

Making use of translation invariance, these matrix elements can be computed as

$$D_{q_1}^Q := \frac{1}{L} \sum_{j', d'} \sum_j e^{iQ(j'+d') - iq_1' d' - iQj} \left\langle j', j' + d' \left| \sum_i \tilde{h}_i \right| j \right\rangle \quad (6.61a)$$

$$= \sum_{j', d'} \sum_j e^{iQ(j'+d') - iq_1' d' - iQj} \langle j', j' + d' | \tilde{h}_0 | j \rangle \quad (6.61b)$$

$$= \sum_{j', d'} \sum_j e^{iQ(j'+d') - iq_1' d' - iQj} \langle C_{q_1', j'}; C_{q_2', j' + d'} | \tilde{h}_0 | C_Q, j \rangle, \quad (6.61c)$$

where in iMPS calculations the reduced Hamiltonian \tilde{H} has to be used.

To apply the orthogonalization as described in App. A.8, the Hamiltonian (or any general operator for that matter) has to be transformed into the hybrid basis and then brought into the same structure as the metric tensor in Eq. (6.19). As stated before, the Gram-Schmidt algorithm does not change the first vector \vec{w}_1 of the original basis. It also does not change subsequent vectors \vec{w}_i if they are already orthogonal to the previously orthogonalized ones. With the structure defined in Eq. (6.19), $\vec{w}_1 = |GS\rangle$ and $\vec{w}_2 = |Q\rangle$ holds. Both states are normalized and by construction orthogonal. Therefore, neither of them is changed, nor is the operator in the subspace they span. The expression for the 2QP-1QP matrix element

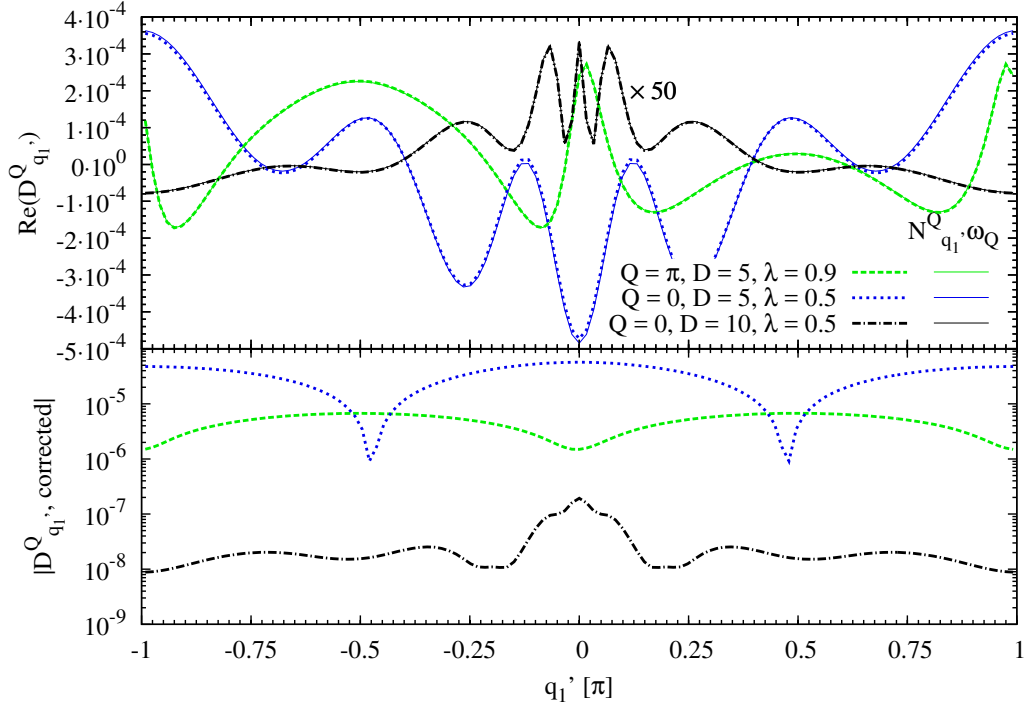


Figure 6.8: Quasi-particle decay amplitude $D_{q_1}^Q$ for various parameters λ , total momenta Q and medium bond dimensions $D = 5$ and $D = 10$. The upper panel shows the matrix elements in the skew 2QP basis. For each set of D , λ and Q , the real part of the factorization $N_{q_1}^Q \omega_Q$ is plotted as thin solid lines in the same color. In the lower panel, the absolute value of the decay amplitude after the application of the orthogonalization algorithm is plotted on a logarithmic scale.

derived from Eq. (A.8.12) therefore reads

$$\frac{\langle \widetilde{Q}, d' | \tilde{H} | Q \rangle}{\| |\widetilde{Q}, d' \rangle \|} = \frac{1}{\sqrt{\langle Q, d' | \widetilde{Q}, d' \rangle}} \left[\langle Q, d' | \tilde{H} | Q \rangle - \frac{\langle Q, d' | Q \rangle \langle Q | \tilde{H} | Q \rangle}{\langle Q | Q \rangle} \right. \\ \left. - \sum_{\ell' = d_{\max}, \ell' > d'} \frac{\langle Q, \ell' | Q \rangle}{\langle Q, \ell' | \widetilde{Q}, \ell' \rangle} \underbrace{\langle Q | \tilde{H} | \widetilde{Q}, \ell' \rangle}_{=0} \right] \quad (6.62a)$$

$$\Leftrightarrow \langle \widetilde{Q}, d' | \tilde{H} | Q \rangle = \langle Q, d' | \tilde{H} | Q \rangle - \langle Q, d' | Q \rangle \langle Q | \tilde{H} | Q \rangle. \quad (6.62b)$$

Thus, if the spurious decay elements are to be eliminated by the Gram-Schmidt algorithm, they necessarily have to be of the form

$$\langle Q, d' | \tilde{H} | Q \rangle \stackrel{!}{=} \langle Q, d' | Q \rangle \langle Q | \tilde{H} | Q \rangle. \quad (6.63)$$

Equation (6.62a) shows that if this is not the case for one d' , the error propagates into subsequent matrix elements, because the underbraced term does not vanish. This condition already applies to the skew momentum basis as

$$\langle Q, q_1' | \tilde{H} | Q \rangle \stackrel{!}{=} \langle Q, q_1' | Q \rangle \langle Q | \tilde{H} | Q \rangle = N_{q_1}^Q \omega_Q. \quad (6.64)$$

The matrix elements $D_{q_1}^Q$ do not have to be real, since the trilinear terms are not self-adjointed on their own.

In Fig. 6.7 the matrix element $D_{q_1}^Q$ is plotted for various parameters λ , total momenta Q and low bond dimensions $D = 2$ and $D = 3$. Since they are indeed complex, only the real parts are shown, but the imaginary parts behave very similarly. For each set of λ , D and Q , the real part of the factorization $N_{q_1}^Q \omega_Q$ is also plotted as thin solid lines in the same colors.

For three of the four plotted parameters sets, the orthogonalization algorithm does not improve the deviation visible in the upper panel. However, this is expected, since the deviation is already within acceptable error margins to begin with. In the upper panel, the curves for $Q = -\frac{\pi}{2}$, $D = 3$ and $\lambda = 0.5$ are scaled down by a factor of $\frac{1}{10}$ to fit the plot range. The matrix element in the orthogonalized basis for that set of parameters is *not* scaled, which shows that it is improved by an order of magnitude.

Figure 6.8 shows the real part of $D_{q_1}^Q$ for various parameters λ and total momenta Q , this time for medium bond dimensions $D = 5$ and $D = 10$. Note that in the upper panel the curve for $D = 10$ is scaled up by a factor of 50 for better visibility in the plot interval. All of these curves show rich features on a relatively large scale. Again, for each set of λ , D and Q , the factorization is plotted in thin solid lines of the same color. It is apparent that for these curves Eq. (6.64) is fulfilled to quite high precision, which leads to a reduction of the spurious decay amplitudes by at least one order of magnitude during the orthogonalization. It is emphasized that expression Eq. (6.61) is completely general and also holds true, if quasi-particle decay is possible. Therefore, this is by no means a trivial result, but should rather be considered as an indication that the method does indeed what it is supposed to do.

Like the other 2QP quantities, the decay amplitude can be computed much more efficiently in momentum space than in real space. The detailed calculation can be found in App. B.

6.6 Scattering matrix

The interaction matrix elements $V_{q_2, q_4}^{q_1, q_2}$ from Eq. (1.1) describe the amplitudes for one 2QP state being transformed into another under the action of the Hamiltonian. For the models considered in this thesis, this process happens under the constraints of conservation of energy and total momentum Q , and can therefore only change the relative momentum q . The interaction $V_{q_2, q_4}^{q_1, q_2}$ can therefore be interpreted as a potential term which facilitates scattering from an initial state $|\psi_i\rangle$ to a final state $\langle\psi_f|$. The matrix

$$S_{f,i} = \langle\psi_f|V|\psi_i\rangle \quad (6.65a)$$

$$:= V_{q_2, q_4}^{q_1, q_2} = V_{q_1, q_1}^Q \quad (6.65b)$$

$$= \langle Q, q_1' | V_{q_1', q_1}^Q q_{q_1'}^\dagger a_{Q-q_1'}^\dagger a_{q_1} a_{Q-q_1} | Q, q_1 \rangle \quad (6.65c)$$

is therefore also called scattering matrix or S -matrix [94].

Non-vanishing off-diagonal elements in S mean that the 2QP Fock basis is not an eigenbasis of the Hamiltonian, which is generically expected when constructing an effective Hamiltonian of an interacting system.

6.6.1 Matrix element computation

The 2QP interaction amplitude is defined as the irreducible matrix element of the Hamiltonian in the two-particle subspace [97], i.e., in real space as

$$V_{j,d}^{j',d'} := \langle j', j' + d' | H | j, j + d \rangle - \langle j', j' + d' | H_{1P} | j, j + d \rangle - \langle j', j' + d' | E_0 | j, j + d \rangle. \quad (6.66)$$

The real space matrix elements on a discrete lattice are also inherently discrete quantities which are somewhat inconvenient for comparing the numerical results to the exact solution. Therefore, a momentum space representation

$$\frac{1}{L} V_{q'_1, q_1}^Q := \langle Q, q'_1 | \tilde{H} | Q, q_1 \rangle - \langle Q, q'_1 | H_{1P} | Q, q_1 \rangle - C_{\eta, q'_1, q_1}^Q \quad (6.67)$$

is chosen. It provides continuous results within the boundaries of momentum discretization, and is much better suited to compare the results of the efficient computation algorithms to analytics. The full matrix element in momentum space is given by

$$\begin{aligned} & \langle Q, q'_1 | \tilde{H} | Q, q_1 \rangle \\ &= \frac{1}{L^2} \sum_{j', d'} \sum_{j, d} e^{+iQ(j'+d') - iq'_1 d'} e^{-iQ(j+d) + iq_1 d} \left\langle j', j' + d' \left| \sum_i \tilde{h}_i \right| j, j + d \right\rangle \end{aligned} \quad (6.68a)$$

$$= \frac{1}{L} \sum_{j', d'} \sum_{j, d} e^{+iQ(j'+d') - iq'_1 d'} e^{-iQ(j+d) + iq_1 d} \langle j', j' + d' | \tilde{h}_0 | j, j + d \rangle. \quad (6.68b)$$

Like the metric tensor and the decay amplitude, this matrix element can be computed much more efficiently in momentum space as

$$\begin{aligned} & \langle Q, q'_1 | \tilde{H} | Q, q_1 \rangle \\ &= \frac{1}{L} \sum_{j', d'} \sum_{j, d} e^{+iQ(j'+d') - iq'_1 d'} e^{-iQ(j+d) + iq_1 d} \\ & \quad \times \langle C_{q'_1, j'}; C_{q'_2, j' + d'} | \tilde{h}_0 | C_{q_1, j}; C_{q_2, j + d} \rangle. \end{aligned} \quad (6.69)$$

Note that in the iMPS computations the assumption must be made that the 2QP states do not contain significant admixtures of states with higher particle numbers.

The one-particle contribution consists of two parts

$$\langle Q, q'_1 | H_{1P} | Q, q_1 \rangle = (\delta_{q'_1, q_1} + \delta_{q'_1, q_2}) (\omega_{q'_1} + \omega_{q'_2}) - \frac{2}{L} (\omega_{q_1} + \omega_{q_2} + \omega_{q'_1} + \omega_{q'_2} - 2t_0). \quad (6.70)$$

The first is the diagonal bosonic part, which is just the sum of the one-particle energies. In spin systems, the hard-core property of the excitations also requires the correction to the diagonal part derived in App. A.10.2.

In the framework of iMPS, the ground state tensor \mathbf{A} is usually not an exact eigenstate of H , which leads to the error matrix element η defined in Eq. (4.1). This is what the additional correction term C_η in Eq. (6.67) compensates for.

The 1QP part in Eq. (6.70) appears in the same way, as the diagonal part of the 2QP metric tensor in Sec. B.2.1. This means it also requires either an a priori fixed summation range of $\frac{Lq}{2}$, or the thermodynamic limit to be well defined.

As with the metric tensor, a description in the TDL is chosen, up to the momentum discretization L_q . The 1QP part is therefore handled in the same way as the diagonal part of the metric tensor. Each TN in Eq. (6.69) contributes to the 1QP part, if it possesses one or more factorizations into a 1QP overlap and a 1QP matrix element. These factorizations are subtracted during computation. Note that the hard-core correction part in Eq. (6.70)

arises from excluding all contributions with $d' = 0$ and/or $d = 0$. Since this type of TN is not computed in the first place, no special treatment of the hard-core constraint is needed. The subtracted 1QP corrections already describe the hard-core property to the extent possible in the current iMPS representation.

The efficient momentum space computation algorithms for 2QP matrix elements constitute the central result of this thesis. However, their derivation is a fairly involved and lengthy calculation and a rather dry read. The inclined reader is referred to App. B, which contains all the details.

6.6.2 Results for the FMHC

Since the model can be described exactly by iMPS at bond dimension $D = 1$, there is only one \mathbf{C} tensor which is its own discrete Fourier transform, and describes the quasi-particles completely. Therefore, the 2QP states are already orthonormal in both real and momentum space. By excluding all contributions with two \mathbf{C} tensors on the same site, the hard-core property is implemented exactly, and no further orthogonalization is required.

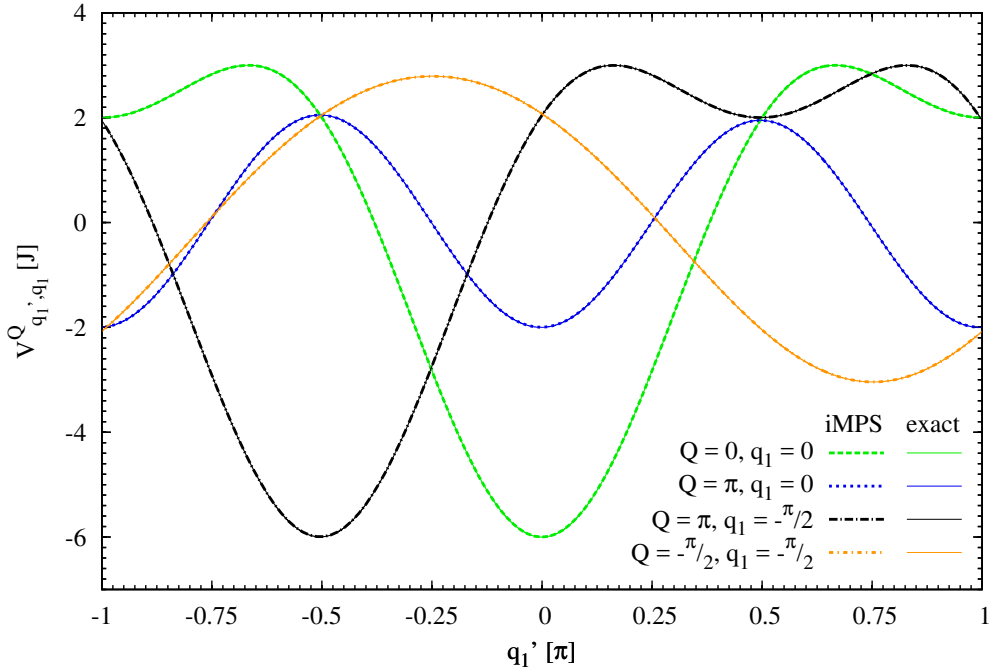


Figure 6.9: Element of the S -matrix for the FMHC at $\Gamma = 2.0$ and $J_2 = 0.5$, for various values of momenta Q and q_1 , compared to the exact solution from Eq. (2.19). Note that with odd L_q , neither π nor $\frac{\pi}{2}$ fall directly on the discretization grid. The corresponding curves are therefore taken from the nearest momentum sampling point.

Figure 6.9 shows the S -matrix element of the FMHC at $\Gamma = 2$ and $J_2 = 0.5$, as function of final momentum q_1' for various values of Q and q_1 , compared to the exact solution from Eq. (2.19). Note that for odd L_q , neither π nor $\frac{\pi}{2}$ fall directly on the discretization grid. The corresponding curves are therefore taken from the nearest momentum sampling point. No deviation is plotted for these results, because the ground state energy in Sec. 4.3.1 shows, that the description with bond dimension $D = 1$ is accurate to machine precision. This is also true for the 1QP dispersion and the 2QP interaction.

6.6.3 Results for the TFIM

Next, the results for the much more demanding TFIM are presented.

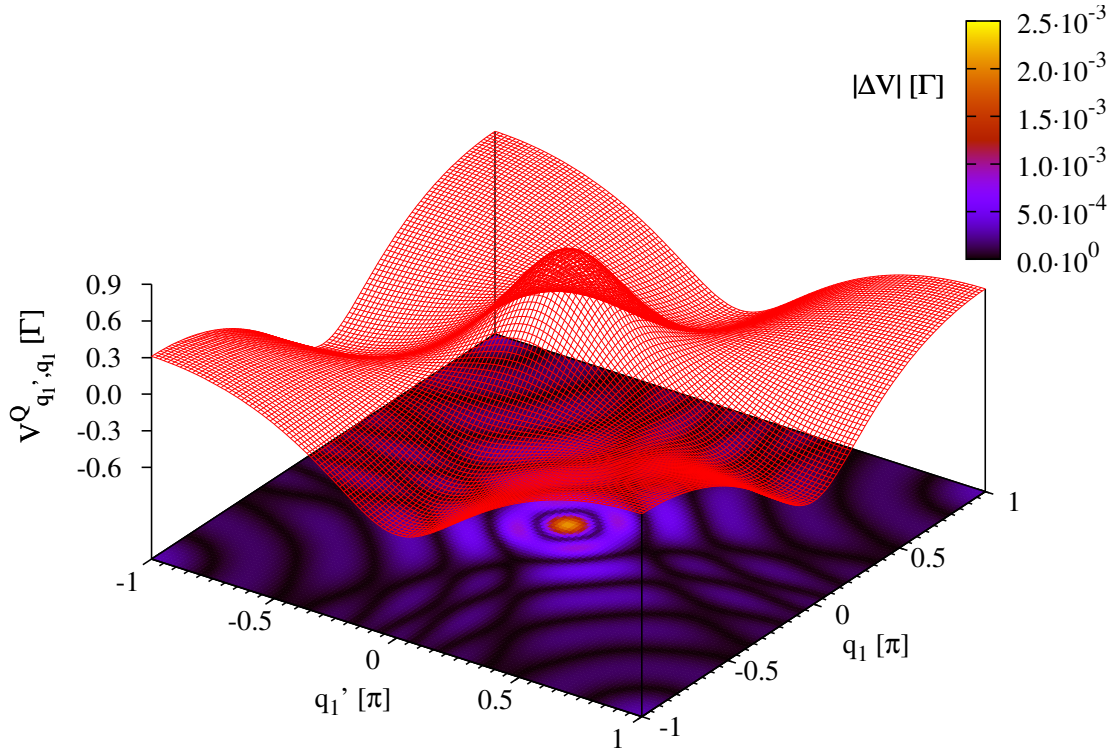


Figure 6.10: Elements of the S -matrix of the TFIM for total momentum $Q = 0$ at $\lambda = 0.5$ computed with bond dimension $D = 2$, as function of initial momentum q_1 and the final momentum q_1' . The coloring in the q_1' - q_1 -plane shows the absolute deviation from the exact result Eq. (2.42) as a heat map.

Figure 6.10 shows the entire S -matrix for total momentum $Q = 0$ at $\lambda = 0.5$ computed with bond dimension $D = 2$ as a surface plot. On the x -axis is the first particle momentum q_1' of the scattered state, and on the y -axis the first particle momentum q_1 of the initial state. The coloring of the q_1' - q_1 -plane indicates the absolute deviation of the iMPS result from the exact solution Eq. (2.42). This deviation shows a maximum around the gap mode at $q = 0$, but it stays under 1%. Clearly, the agreement with the exact solution is not as good as it is for the 1QP properties. However, given the small bond dimension, it is still remarkable. As for the two-particle spectral weight, the $D = 2$ data is already so close to exact hard-core bosons that no improvement can be reached by applying the orthonormalization scheme.

Figures 6.11 and 6.12 show the S -matrix element for several values of total momentum Q and initial state momentum q_1 , also at $\lambda = 0.5$. The lower panels show the absolute deviations on a logarithmic scale, which makes it easier to assess them quantitatively.

Figures 6.13 and 6.14 show the same curves as Figs. 6.11 and 6.12, but for the parameter value $\lambda = 0.9$. As expected, there are now more pronounced deviations, yet, considering that $D = 2$ is the lowest bond dimension which can produce *any* interaction in the TFIM, the agreement is still remarkably good.

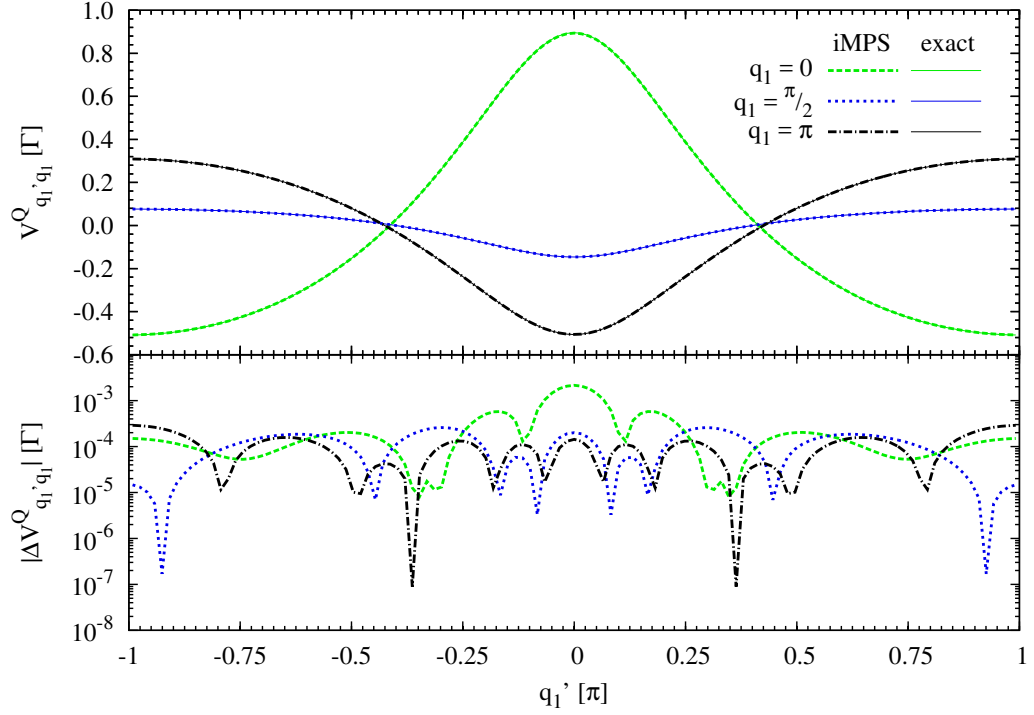


Figure 6.11: Elements of the S -matrix of the TFIM at $\lambda = 0.5$, for total momentum $Q = 0$ and various initial state momenta q_1 , computed with bond dimension $D = 2$. With odd L_q , neither $q = \pi$ nor $q = \frac{\pi}{2}$ are sampled exactly, and the corresponding curves are taken from the nearest available sampling point. The lower panel shows the absolute deviation from the exact result Eq. (2.42) on a logarithmic scale.

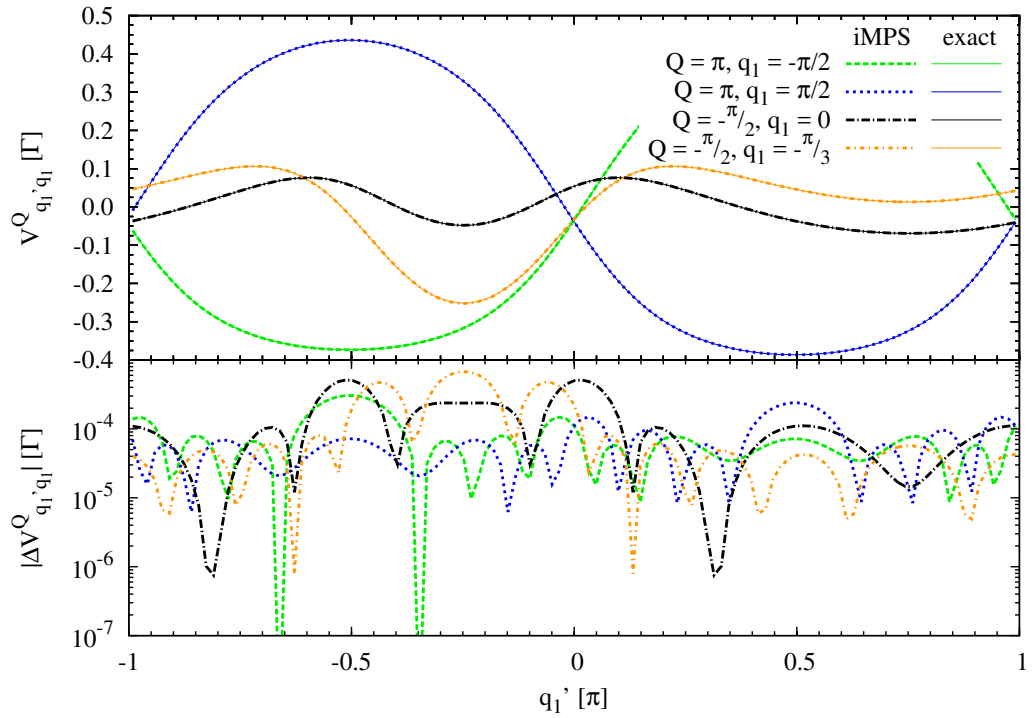


Figure 6.12: Same as Fig. 6.11 but for different Q and q_1 .

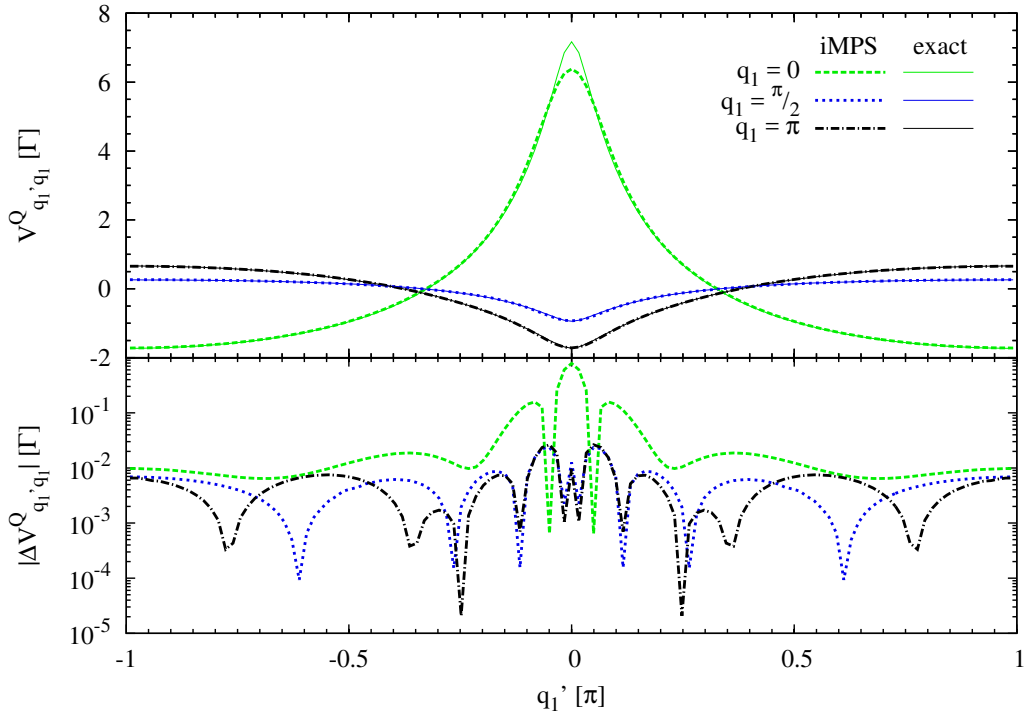


Figure 6.13: Elements of the S -matrix of the TFIM at $\lambda = 0.9$, for total momentum $Q = 0$ and various initial state momenta q_1 , computed with bond dimension $D = 2$. With odd L_q , neither $q = \pi$ nor $q = \frac{\pi}{2}$ are sampled exactly, and the corresponding curves are taken from the nearest available sampling point. The lower panel shows the absolute deviation from the exact result Eq. (2.42) on a logarithmic scale.

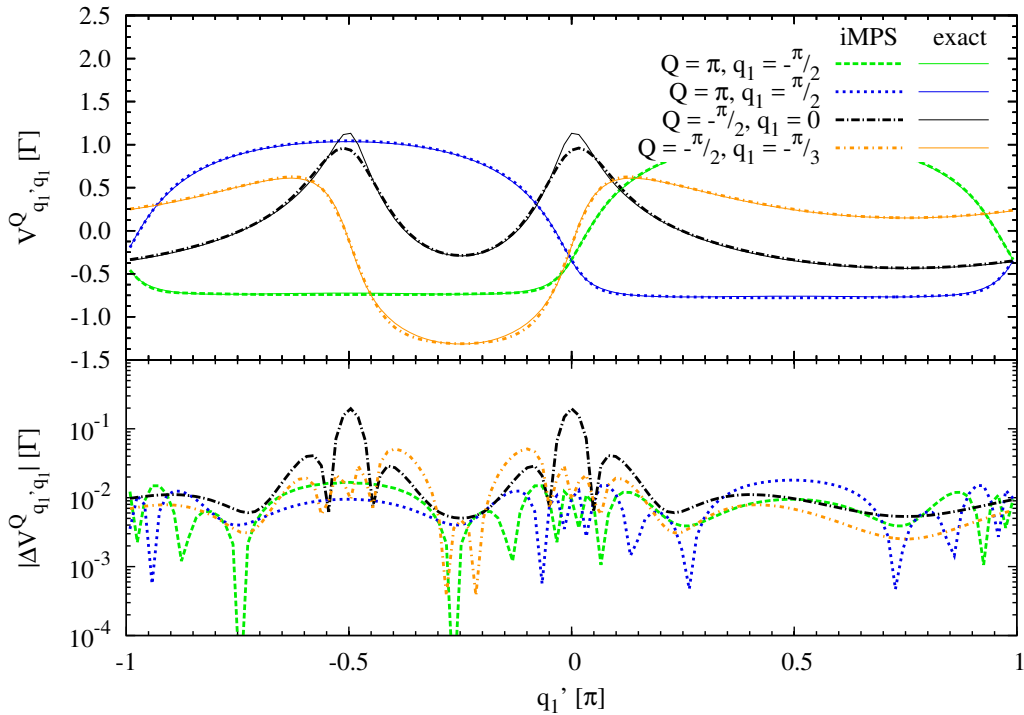


Figure 6.14: Same as Fig. 6.13 but for different Q and q_1 .

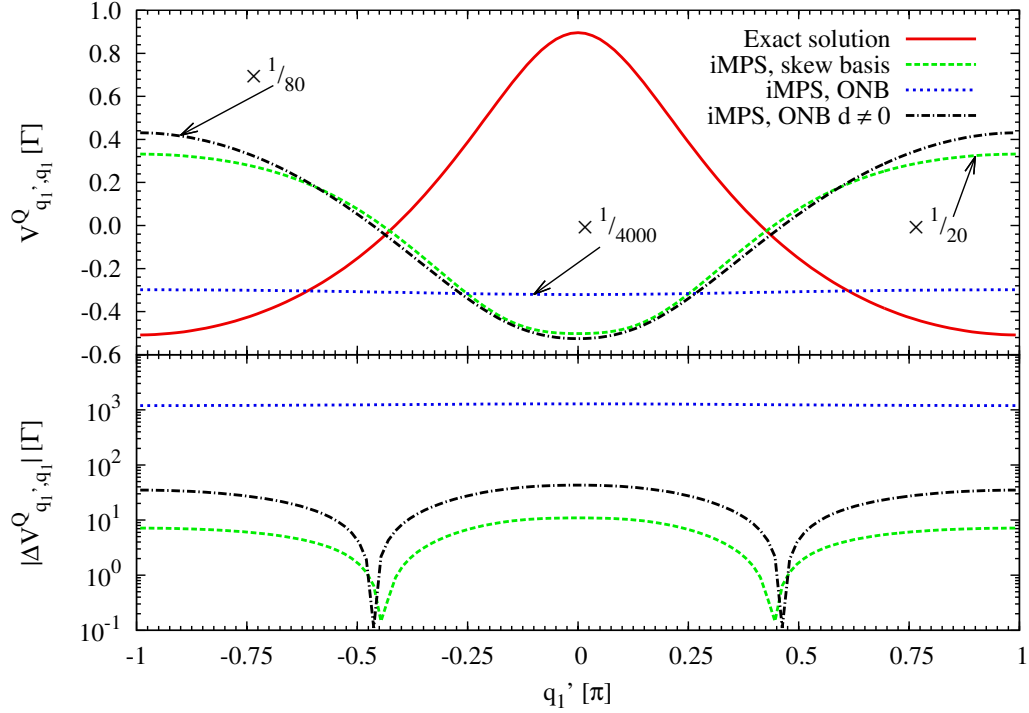


Figure 6.15: Element of the S -matrix of the TFIM at $\lambda = 0.5$, for total momentum $Q = 0$ and initial state momenta $q_1 = 0$, computed with bond dimension $D = 3$ and $L_q = 121$. In the upper panel, the exact solution from Eq. (2.42) is compared to the iMPS results in the skew basis, in the orthogonalized basis including and excluding the state with $d = 0$. The iMPS results in the upper panel are scaled to fit the plot range of the exact solution. The lower panel shows the absolute deviation on a logarithmic scale.

In Fig. 6.15 the matrix element at $\lambda = 0.5$ for total momentum $Q = 0$ and initial state momentum $q_1 = 0$, computed with $D = 3$, is compared to the exact solution from Eq. (2.42). The iMPS results in the upper panels are scaled to fit the plot range of the exact solution. The lower panel shows the absolute deviation on a logarithmic scale.

Three curves from the iMPS results are plotted. The first is the raw result in the skew basis. One can see that it is literally orders of magnitude worse than the $D = 2$ result, and it does not qualitatively agree with the exact solution, but rather seems inverted about the x -axis.

The second curve is the result of the orthogonalization *including* the state with particle distance $d = 0$. It is yet another two orders of magnitude further away from the exact solution than the result in original skew basis. The reasons for this are the very large matrix elements of the $d = 0$ state, caused by its normalization to unity in the Gram-Schmidt algorithm.

The third iMPS curve shows the result of the orthogonalization *excluding* the state with $d = 0$. This avoids the very large spurious matrix elements. The qualitative form still matches that of the result in the skew basis. However, the deviation is even increased by roughly a factor of four.

Unfortunately, even more advanced orthogonalization schemes, such as the ones proposed in Sec. 6.1.4.2, cannot be expected to correct the qualitative disagreement, since at $\lambda = 0.5$ a large portion of the 2QP subspace is already orthogonal.

Seeing that the results for the ground state, the 1QP properties, and even the 2QP spectral weight for this bond dimension at $\lambda = 0.5$ are consistently of very high quality, this behavior is really quite puzzling.

For other parameter values, the behavior stays qualitatively the same. The data in the skew basis shows a blatant disagreement with the exact solution which is not corrected by orthonormalization in any way. Higher bond dimensions unfortunately show the same problems as $D = 3$.

6.7 Chapter summary

In this chapter, the ansatz from the previous chapter was extended to describe states with two quasi-particles by applying the creation operator twice. It was found that in real space the resulting basis is orthonormal for sufficiently large particle distances d . For small particle distances, overlaps between the 2QP states and even with the 1QP sector were found for bond dimensions $D > 1$.

Examination of a momentum space basis showed that 2QP states are orthogonal with respect to total momentum Q , which allows us to treat each total momentum sector independently. However, the states are not orthogonal with respect to the second momentum quantum number.

Therefore, a hybrid basis of total momentum and particle distance was defined. Since these states are orthogonal for sufficiently large d , this basis provides a well motivated starting state for the Gram-Schmidt orthonormalization scheme.

Further, it was shown how the metric tensor in the skew basis is represented, which is required to obtain operator matrices in a Gram-Schmidt orthogonalized basis. It was pointed out why the application of the generic Gram-Schmidt algorithm can potentially produce unstable results and some alternatives were described.

The analysis of the metric tensor for the TFIM in the skew hybrid basis showed that for bond dimension $D = 2$, the iMPS representation is very close to exact hard-core bosons. Therefore, no additional orthogonalization is required. For bond dimension $D = 3$, considerable deviations from hard-core bosons were found.

As a first result of physical interest, the two-particle spectral weight for the TFIM in the zz -channel was computed. For low bond dimensions ($D \leq 5$), the results are in very good agreement with the analytic solution. For bond dimension $D = 10$, considerable deviations were found, which could be traced back to an asymmetry in the eigenstate \vec{v}^q . It was observed, that including the state with particle distance $d = 0$ into the Gram-Schmidt orthogonalization improved the result over omitting the state.

The Hamiltonian of the TFIM is particle number conserving; therefore, no matrix elements of the Hamiltonian should occur in the orthogonalized basis, which couple the 1QP sector and the 2QP sector. This was found to be case. For these matrix elements, the orthogonalization scheme works as intended. Quasi-particle decay amplitudes found in the skew basis are reduced by several orders of magnitude.

Finally, the 2QP interaction matrix was examined. For the FMHC, results were found to be in perfect agreement with the analytic solution, because the model can be described exactly by product states with bond dimension $D = 1$.

For the TFIM, results were mixed. The results for bond dimension $D = 2$ are encouraging and clearly show the potential of the presented method. However, some more research will be required to understand why the smallest possible increase of the bond dimension by only 1 results in the radical change for the worse that we observed.

Chapter 7

Conclusion and outlook

*To explain all nature is too difficult a task
for any one man or even for any one age.*
Isaac Newton

7.1 Summary of the method

In this thesis, a variational method to derive effective Hamiltonians in second quantization for one-dimensional spin systems was presented. The method is based on the framework of infinite system matrix product states (iMPSs) and works by iteratively constructing an approximate Fock space basis.

First, it was shown that the MPS language is well suited to describe the bulk properties of translation invariant lattice systems with uniform ground state. By using the transfer matrix, these systems can be handled very efficiently in the thermodynamic limit if the boundary conditions do not influence the bulk behavior. In this case, the ground state can be represented by a uniform MPS (uMPS), i.e., with the same matrices for every site, that reflects the underlying physics.

A DMRG inspired algorithm was presented to find a uMPS approximation of the ground state, by repeatedly varying the matrices on a single lattice site to reduce the ground state energy. After each step, the newly found matrices are used as new guess for the ground state in the next iteration. As function of the elements of the MPS matrices on a single site, the energy expectation value can be written as a bilinear form. Minimizing this form naturally leads to a generalized eigenvalue problem (EVP). When convergence is reached, the eigenvector to the lowest eigenvalue is used as approximation of the ground state uMPS. This provides the 0 quasi-particle (QP) sector of the effective model.

The eigenvectors belonging to higher eigenvalues of this EVP describe excitations. The MPSs that have the uniform ground state tensor on all lattice sites but one form a vector space which can be interpreted as the tangent space to the manifold of uMPS at the given ground state. They still describe an infinite system, but are no longer uniform and are therefore called infinite system matrix product states (iMPS) for distinction.

Although it is possible to use the eigenvectors of the converged ground state search EVP directly, it was shown that this description introduces spurious variational parameters. This leads to an overcomplete and therefore not orthogonal basis. A better description is given by the canonical gauge of excitation tensors which is found by restricting the search to the nullspace of the ground state tensor. This basis is then orthogonal with respect to the lattice site where the excitation tensor resides, and therefore greatly simplifies many

calculations. It also makes numerical computations more efficient.

It is found that in most cases one excitation tensor is not enough to describe the elementary excitation. Also, the excitations are generally not completely local. Therefore, the momentum superpositions of the real space iMPS, i.e., Wannier states are used. The linear combination of Wannier states with minimal energy above the ground state is determined in a second variational calculation. Minimization again leads to an EVP, the lowest eigenvalue of which is the variational approximation of the one-particle dispersion. The corresponding eigenvector describes an eigenstate of the effective Hamiltonian with one elementary excitation. This provides the basis of the 1QP space and a MPS description of the quasi-particle creation operator. The basis constructed in this way is normalized and orthogonal with respect to momentum. It can also be Fourier transformed into real space, where it is still normalized and orthogonal with respect to the lattice site at which the excitation is created. From this basis, further one-particle properties such as spectral weights can be determined.

It was shown that computing results in the one-particle basis is more efficient in momentum space than in real space for two reasons. The first reason is that the momentum space representation of the creation operator is more compact and allows computation of sums on the level of site tensors rather than on the level of whole matrix elements. The second reason is that partial results can easily be reused, so that redundant computations can largely be avoided. This reduces for the spectral weight from $\mathcal{O}(\Xi_T^3)$ to $\mathcal{O}(\Xi_T^2)$. The dispersion relation together with the 1QP basis constitute the 1QP sector of the effective model.

Seeing that a one-particle state can be described by a linear combination of iMPS with *one* excitation tensor each, it seems plausible to construct two-particle states by applying the creation operator twice. This results in a linear combination of iMPS with *two* excitation tensors each. For small particle distances, these excitation tensors can fall onto the same lattice site. Since the QPs in spin systems are hard-core bosons, these contributions are set to zero.

Unfortunately, the so constructed 2QP states are orthonormal only for bond dimension $D = 1$, where they describe product states. For higher bond dimensions, states where the two quasi-particles are close together are neither orthogonal nor normalized. Only for large distances, the states are orthonormal, because the quasi-particles behave like free particles. This is as expected for models with a finite interaction range. The non-orthogonality or skewness is found both in real space and in momentum space. It was shown, that for 2QP computations the benefits of working in momentum space are even much larger than for 1QP computations. Here, the computational cost reduces from $\mathcal{O}(\Xi_T^8)$ to $\mathcal{O}(\Xi_T^4)$. In fact, in many cases momentum space computation makes the difference between being able to obtain results on practical time scales or not.

The 2QP states must still be orthogonal with respect to total momentum, wherefore each total momentum sector can be handled independently. To overcome the problem of the remaining non-orthogonality in the second momentum, a hybrid basis of total momentum and relative particle distance is defined. It allows the application of the Gram-Schmidt orthogonalization scheme to obtain results in an orthonormal basis. This “detour” is necessary, because states with large particle distances are known to be orthogonal and therefore provide a good starting vector for the orthogonalization.

The metric tensor and operator matrices are computed in the original, non-orthogonal basis first. As a second step, they are then transformed into the hybrid basis, which is still not orthogonal with respect to the particle distance at first. After application of the orthogonalization scheme, the metric tensor is just the identity and the operator matrices

can be transformed back into real space or momentum space.

This way, results can be obtained for two-particle properties such as spectral weights, quasi-particle decay amplitude and the interaction matrix.

7.2 Summary of results

The success of the method was gauged by computing results for two different models. First, as a simple test case, the ferromagnetic, isotropic spin- $\frac{1}{2}$ Heisenberg chain in a transverse magnetic field (FMHC), both with and without ferromagnetic next-nearest neighbor interaction. The second model is the Ising model in a transverse magnetic field (TFIM), also on a one-dimensional chain.

7.2.1 Ground state results

The polarized ground state of the FMHC is a product state, and is therefore found to be described exactly by a uMPS of bond dimension $D = 1$. Consequently, the ground state energy of this model was obtained to machine precision for all parameters, and the correlation length and entanglement entropy are always zero.

By contrast, the TFIM does not have an exact uMPS ground state representation at finite bond dimension, except for the limits of vanishing magnetic field ($\lambda = \infty$) and vanishing Ising interaction ($\lambda = 0$). Close to the quantum critical point at $\lambda = 1$, the ground state energy per lattice site, the correlation length and the ground state magnetization in direction of the Ising coupling all show increasingly good agreement with the exact solution for increasing bond dimension. This is in accordance with the expectations, since the correlation length grows larger as λ approaches 1. This takes increasingly larger bond dimensions to encode the increasing entanglement. At the critical point, the correlation length diverges, which cannot be captured by any finite bond dimension. The maxima in the quantities or their deviations from the analytic solution, which indicate the phase transition, are consistently found at parameter values $\lambda \lesssim 1$ for low bond dimensions. For increasing D , the peaks all move towards the exact location of the critical point at $\lambda = 1$. Results were presented for bond dimensions from $D = 3$ up to $D = 30$, which are very accurate over the whole parameter range. Notably for larger bond dimensions and smaller λ , the results show wild oscillations and are considerably less accurate than those for small D . The reason for this is the excess number of variational parameters at high bond dimension which leads to numerical instabilities. Analyzing the right boundary matrix v , which in left-canonical gauge holds the squared Schmidt coefficients of a bipartition of the the chain, reveals that these become smaller than machine precision for high D and small λ . This corresponds to using a (numerically) overcomplete Schmidt basis and explains the decreased accuracy of the results.

The scaling of the effective correlation length ξ_T , defined by the transfer operator's second largest eigenvalue, with the inverse bond dimension was also examined. In the disordered phase linear least squares fits extrapolate quite precisely to the analytical values. However, the distribution of the data points does not allow us to conclusively deduct a linear relation $\Xi_T(D) \propto \frac{1}{D}$. In the Ising phase, the extrapolated value is approximately off by a factor of 2. The reason for this is presumably that the transfer operator of a single ground state does not properly capture the correlations of domain walls.

The entanglement entropy shows a very pronounced peak in the vicinity of the critical point. The position of this peak appears to converge to the exact value for increasing bond

dimension.

Finally, the order parameter, i.e., the magnetization in direction of the Ising coupling was examined. As with the other results, increasing agreement with the exact solution is observed around the phase transition with increasing bond dimension. An attempt was made to extrapolate the critical exponent β of the order parameter. The exact value is not contained in the error bracket of the value extrapolated from the available data. However, the agreement is still very good, with a relative error of only 2%.

7.2.2 One-particle results

For the FMHC, the one-particle dispersion can be obtained to machine precision at bond dimension $D = 1$ like the ground state energy. A very interesting result is the appearance of the two-particle bound state in the spectrum of the 1QP computation, if the bond dimension is increased beyond $D = 1$. Considering that it is not a 1QP state, its energy is captured with remarkable accuracy, at least in parts of the Brillouin zone, where it is well separated from the 2QP continuum. This is easy to understand, since the increased parameter space allows the variational algorithm to capture also localized multi-particle states.

The dispersion of the TFIM is also obtained to high precision, in both the disordered and the ordered phase. This shows that with the proper ansatz, domain walls can be described just as well as spin-flips. Away from criticality, a minimum in the deviation as function of bond dimension is observed. Beyond that, the error increases again, signaling that the numerical instability caused by very small Schmidt coefficients in v outweighs the gains from an increased number of variational parameters. At the critical point, the accuracy of the results increases more consistently with increased bond dimension. However, the very high precision of the $D = 3$ result over most of the Brillouin zone, except in the immediate vicinity of the gap, remains unexplained at this point.

The excitation gap, too, is found to be in very good agreement with the exact solution. The deviation shows behavior similar to that of the ground state energy, with wild oscillations for larger bond dimensions and small parameters λ .

Fourier transforming the eigenvector \vec{v}^q belonging to the dispersion yields a real space representation \vec{v}_ℓ of the quasi-particle. It can be interpreted as the dressing cloud of the elementary excitation, i.e., the degree of polarization at a distance ℓ from the central site of the particle. This dressing cloud is found to decay exponentially. The decay is governed by the effective correlation length ξ_T as expected.

To test the 1QP description, the one-particle spectral weight in the xx -channel is computed as well. At medium parameters, results are very accurate. As in the case of the dispersion, a minimum in the error as function of D is observed. Close to criticality, a high peak forms around $q = 0$ due to the gap being very small. This peak is consistently better captured by increasing bond dimensions.

Analysis of the effective Hamiltonian matrix in momentum space and its eigenvector \vec{v}^q reveals that the problem of excess parameters also carries over into the description of the quasi-particles. In a reflection symmetric system, even symmetry around the gap mode at $q = 0$ is expected. At low bond dimensions or close to criticality this is found to be true. However, for high bond dimension and small parameters, an asymmetry in both the Hamiltonian and \vec{v}^q is observed. The reason behind is probably a numerical instability in the computation of the excitation tensors due to very small Schmidt coefficients in v .

In the computation of the one-particle spectral weight, the asymmetry in \vec{v}^q appears to compensate for this fact.

7.2.3 Two-particle results

Since the FMHC is described exactly at $D = 1$, the two-particle basis is exact, too, in this case. Therefore, the 2QP interaction matrix could be computed to machine precision, without the need for orthogonalizing the basis. This would also allow for the computation of the exact energy of the 2QP bound state by diagonalizing the Hamiltonian in the 2QP subspace.

For the TFIM, the metric tensor was analyzed first. At bond dimension $D = 2$, it showed very little deviation from exact hard-core bosons, eliminating the need for further orthogonalization. At bond dimension $D = 3$, the deviations were found to be considerably larger.

Next, the two-particle spectral weight in the zz -channel was computed. At $\lambda = 0.5$, the results for low bond dimensions were found to be very accurate. The results for $D = 3$ and $D = 5$ show that including the state with particle distance $d = 0$ which should not contribute in a proper hard-core bosonic description, nonetheless improves the result visibly. This rises the question, if and how hard-core bosonic excitations can be described consistently. As of yet, this question cannot be answered conclusively. Unfortunately, the result with bond dimension $D = 10$ shows a very large deviation from the analytic result, which can be traced back to the problem of asymmetry in the eigenvector \vec{v}^q . This becomes even clearer seeing that \vec{v}^q results from different program runs look qualitatively completely different.

At the parameter value $\lambda = 0.9$, results are more consistent. They improve for increasing bond dimension until at $D = 10$, again, the problem of the asymmetric \vec{v}^q manifests itself.

Further, the quasi-particle decay amplitude was investigated. For a particle number conserving model such as the TFIM, it must vanish, at least in the orthogonalized basis. This is found to be the case within acceptable error margins. Surprisingly, the erroneous amplitude that results from the skewness of the initial 2QP basis, is reduced by four orders of magnitude for $D = 10$ at $\lambda = 0.5$. Despite the fact that the result for the two-particle spectral weight from this data set was so far off the exact solution.

The results on the scattering matrix for the TFIM are rather inconclusive. At bond dimension $D = 2$ and parameter $\lambda = 0.5$, agreement is remarkably good, and the results do not even require orthogonalization. At the same parameter value, the results for bond dimension $D = 3$ show very large deviations and do not even qualitatively match the form of the exact result. Seeing that all other results at this bond dimension and parameter were very accurate, this is quite surprising.

Closer to the critical point, at $\lambda = 0.9$, the picture stays qualitatively the same. The deviations for $D = 2$ are visibly larger, but that is expected for low bond dimension.

In summary, while the results for bond dimension $D = 2$ are very encouraging, the radical turn for the worse at $D = 3$ clearly calls for further research.

7.3 Outlook

As discussed in the last section, many interesting, convincing and encouraging results were obtained. Unfortunately, we encountered a number of problems on the way that are as of yet unsolved and require more research.

The DMRG like ground state search algorithm presented in Chap. 4, shows two problems: First, the generalized EVP becomes unstable if the bond dimension is much larger than is required to describe the system. This is due to very small Schmidt coefficients and subsequently small eigenvalues of the norm matrix. Here, an algorithm could be used that adaptively reduces the bond dimension, when Schmidt coefficients below a certain threshold are detected. The second problem is that for large bond dimensions, close to a fixed point, convergence can become very slow. Comparison to alternatives such as imaginary time evolution [84], or the recently proposed VUMPS algorithm [86] may help to identify better options.

As shown in Chap. 5, the canonical gauge form for excitation tensors has many attractive features. The resulting states are orthonormal in momentum space and the orthogonality in real space greatly reduces the computational effort, especially in 2QP calculations. However, their computation involves inverting the right boundary matrix v , which makes it sensitive to errors introduced by very small Schmidt coefficients. This manifests in the problem of the Hamiltonian not having the proper symmetry in momentum space, which carries over to its eigenvector belonging to the dispersion. Subsequently, 2QP results may prove unreliable. Using a Lanczos type algorithm that does not require an inversion of v , but rather uses it to define a scalar product, could help to improve stability.

Another challenge, which did not present itself as such in the context of this thesis, is the distinction between single-particle and multi-particle states. In the case of the FMHC it is clear that there is only one type of elementary excitation. Therefore, the two-particle bound state can be clearly identified as such. However, in more complicated models different types of elementary excitations can occur. If their energy is non-degenerate, it may no longer be clear which eigenvalues of the momentum space EVP describe single-particle states, and which describe multi-particle bound states.

For very low bond dimension $D = 2$, the hybrid 2QPs basis is found to describe hard-core bosons almost perfectly. In this case, no orthogonalization is required. For bond dimension $D = 3$, the hard-core property is found to be no longer described very accurately by only omitting contributions where the two excitation tensors fall onto the same site. The example of the two-particle spectral weight shows that in this case including the state with particle distance $d = 0$ is indeed necessary. The inconclusive results for the scattering matrix do not allow for a definitive statement if this is generally true at this point. As an alternative to the Gram-Schmidt algorithm, the metric tensor could be diagonalized, and the eigenspace to the lowest eigenvalue discarded. The spectrum of the metric tensor is invariant under the Fourier transformation, since it is unitary. Therefore, the diagonalization could be done directly in momentum space basis, without the detour through the hybrid basis.

The very accurate 2QP results which could be obtained nonetheless clearly show the potential of the method. However, the puzzling disagreement of the interaction matrix for bond dimension $D = 3$ also shows that there are still some unresolved problems. As shown in App. B, the momentum space algorithms for efficient computation of 2QP quantities are fairly involved. Errors in the calculations and the implementation cannot be excluded

completely at this point.

Once the problems have been resolved, the two particle approach can be extended to work with degenerate ground states. Then, the interaction of domain walls can be studied as well.

Alternatively, real space computation could also be improved. The enormously long computation times estimated in Sec. 6.4.2 are largely based on the naïve approach to compute overlaps and matrix elements one at a time. This results in a vast amount of redundant computations. If one could compute *all* overlaps and matrix elements simultaneously, summed boundary matrices could be reused similarly to the momentum space computation. However, such an algorithm would be even more involved than the momentum space calculations in App. B.

The example of the bound state in the FMHC shows that two QPs can behave very similar to a single particle when they are close to each other in real space. In Ref. [98] the one-particle approach from Ref. [90] was extended to 2QP states with an ansatz that takes this into account explicitly, and which in the notation of this thesis is given by

$$|q_1, q_2\rangle := \sum_{j=-\infty}^{\infty} e^{iQj} |\mathbb{F}_{q_1, q_2, j}\rangle + \sum_j e^{iQj} \sum_{d=1}^{\infty} \sum_{\alpha, \beta} c_{q_1, q_2}^{\alpha, \beta}(d) |\mathbb{B}_{\alpha, j}; \mathbb{B}_{\beta, j+d}\rangle, \quad (7.1a)$$

where $Q = q_1 + q_2$ is total momentum. The first term is a one-particle-like state that describes the two particles when they are close together. The second term describes the particles when they are further apart, including the free particle limit. In Eq. (7.1) the $|\mathbb{F}_{q_1, q_2, j}\rangle$ are states as in the one-particle ansatz Eq. (5.2), and the $|\mathbb{B}_{\alpha, j}; \mathbb{B}_{\beta, j+d}\rangle$ are states as defined in Eq. (6.2). However, in contrast to the ansatz in Chap. 6, the $|\mathbb{B}_{\alpha, j}; \mathbb{B}_{\beta, j+d}\rangle$ use the bare \mathbb{B}_{α} , which are the one-particle excitation tensors from Chap. 5, and new variational parameters $c_{q_1, q_2}^{\alpha, \beta}(d)$ are introduced instead of the already known v_{α}^q . The tensor \mathbb{F}_{q_1, q_2} is left with its entire $(d-1)D^2$ parameters for variation.

Variation with respect to the parameters $\{\mathbb{F}_{q_1, q_2}, c_{q_1, q_2}^{\alpha, \beta}(d)\}$ leads to another generalized EVP, which is half-infinite in d . However, the authors find the coefficients $c_{q_1, q_2}^{\alpha, \beta}(d)$ to show the asymptotic behavior

$$c_{q_1, q_2}^{\alpha, \beta}(d) \xrightarrow{d \rightarrow \infty} v_{\alpha}^{q_1} v_{\beta}^{q_2} e^{iq_2 d} - e^{-i\phi} v_{\alpha}^{q_2} v_{\beta}^{q_1} e^{iq_1 d} \quad (7.2)$$

where ϕ is the scattering phase. In numerical practice, this behavior is reached for $d \approx \Xi_T$, which is the length scale on which the particles become non-interacting. This is in accordance with our findings in Chap. 6.

This ansatz, although more sophisticated, produces reliable results for higher bond dimensions. It is therefore a viable alternative should the problems with our ansatz prove unsolvable.

Appendix A

Supplementary material

Never memorize something that you can look up.
Albert Einstein

A.1 The Kronecker identity

One relation that frequently requires special attention when dealing with iMPS in momentum space is

$$\frac{1}{L} \sum_{j=1}^L e^{i(q-q')j} = \delta_{q,q'} \quad (\text{A.1.1})$$

which is well known from solid state physics textbooks and will be referred to as Kronecker identity. It follows straight forwardly from

$$\frac{1}{L} \sum_{j=1}^L \exp\left(i \frac{2\pi}{L} (n-m)j\right) = \delta_{mn} \quad (\text{A.1.2})$$

by identifying $q = n \cdot \Delta q$ and $q' = m \cdot \Delta q$ with $\Delta q = \frac{2\pi}{L}$ which is the momentum resolution on a finite lattice.

Two important remarks are in order regarding Eq. (A.1.1). First, in the thermodynamic limit, the Kronecker- δ in Eq. (A.1.2) becomes a Dirac δ -distribution. However, in numerics one usually discretizes the Brillouin zone, allowing only a finite number of momenta in which case one is back at Eq. (A.1.1).

Second, on a finite lattice with discrete momenta Eq. (A.1.1) holds true, also in numerics. But only, if the summation is done over exactly L sites. This is because for $q \neq q'$ the exponentials in Eq. (A.1.1) are the L^{th} order roots of unity, which sum up to zero.

In the algorithms described in this thesis, cases occur where quantities are summed over as many lattice sites as it takes for them to converge to a limit value. In these cases, Eq. (A.1.1) is not really applicable, because this number of sites may not be the same as the number of discrete momenta chosen for the computation.

Instead, everything that is known to contribute to a Kronecker identity is subtracted in the computation and a contribution of $\delta_{q,q'}$ is added in the end. See the calculation on the 2QP overlap in Sec. B.2.1 for an example.

A.2 Hamiltonian of the FMHC in the 2QP sector

To obtain the energy of the bound state, the Hamiltonian is diagonalized in the two-particle subspace. Excitation energies are measured relative to the ground state, therefore the ground state energy is subtracted in this calculation. The matrix element with respect to the *bosonic* 2QP basis $|q_1, q_2\rangle$ is given by

$$\langle q'_1, q'_2 | (H - E_0) | q_1, q_2 \rangle = \langle q'_1, q'_2 | H_{1P} | q_1, q_2 \rangle + \langle q'_1, q'_2 | H_{\text{int}} | q_1, q_2 \rangle \quad (\text{A.2.1})$$

with

$$H_{1P} = \sum_k \omega_k a_k^\dagger a_k \quad \text{and} \quad H_{\text{int}} = \frac{1}{L} \sum_{k_1, k_2, k_3} V_{k_1 k_2 k_3} a_{k_1}^\dagger a_{k_2}^\dagger a_{k_3} a_{k_1+k_2-k_3} . \quad (\text{A.2.2})$$

The contribution of the one-particle part H_{1P} is

$$\langle q'_1, q'_2 | H_{1P} | q_1, q_2 \rangle = \langle q'_1, q'_2 | \sum_k \omega_k a_k^\dagger a_k | q_1, q_2 \rangle \quad (\text{A.2.3a})$$

$$= \omega_{q'_1} \delta_{q'_1, q_1} + \omega_{q'_1} \delta_{q'_1, q_2} + \omega_{q'_2} \delta_{q'_2, q_1} + \omega_{q'_2} \delta_{q'_2, q_2} \quad (\text{A.2.3b})$$

$$= \omega_{q'_1} (\delta_{q'_1, q_1} + \delta_{q'_1, q_2}) + \omega_{q'_2} (\delta_{q'_2, q_1} + \delta_{q'_2, q_2}) \quad (\text{A.2.3c})$$

$$= (\omega_{q'_1} + \omega_{q'_2}) (\delta_{q'_1, q_1} + \delta_{q'_1, q_2}) \quad (\text{A.2.3d})$$

where in the last step total momentum conservation

$$q'_1 + q'_2 = q_1 + q_2 = Q \quad (\text{A.2.4})$$

was used to identify

$$\delta_{q'_2, q_1} = \delta_{q_1+q_2-q'_1, q_1} = \delta_{q'_1, q_2} \quad \text{and} \quad \delta_{q'_2, q_2} = \delta_{q'_1, q_1} . \quad (\text{A.2.5})$$

Lastly, to account for the hard-core property of the excitations, the correction derived in App. A.10.2 needs to be subtracted, so that the complete contribution from the one-particle part H_{1P} reads

$$\langle q'_1, q'_2 | H_{1P} | q_1, q_2 \rangle = (\omega_{q'_1} + \omega_{q'_2}) (\delta_{q'_1, q_1} + \delta_{q'_1, q_2}) - \frac{2}{L} (\omega_{q_1} + \omega_{q_2} + \omega_{q'_1} + \omega_{q'_2} - 2t_0) . \quad (\text{A.2.6})$$

The contribution from the interaction part follows as

$$\begin{aligned} & \langle q'_1, q'_2 | H_{\text{int}} | q_1, q_2 \rangle \\ &= \langle q'_1, q'_2 | \left(\frac{1}{L} \sum_{k_1, k_2, k_3} V_{k_1 k_2 k_3} a_{k_1}^\dagger a_{k_2}^\dagger a_{k_3} a_{k_1+k_2-k_3} \right) | q_1, q_2 \rangle \end{aligned} \quad (\text{A.2.7a})$$

$$\begin{aligned} &= \frac{1}{L} \sum_{k_1, k_2, k_3} V_{k_1 k_2 k_3} (\delta_{q'_1, k_1} \delta_{q'_2, k_2} + \delta_{q'_1, k_2} \delta_{q'_2, k_1}) \\ & \quad \times (\delta_{q_1, k_3} \delta_{q_2, k_1+k_2-k_3} + \delta_{q_2, k_3} \delta_{q_1, k_1+k_2-k_3}) \end{aligned} \quad (\text{A.2.7b})$$

$$= \frac{1}{L} \left(V_{q'_1 q'_2 q_1} + V_{q'_1 q'_2 q_2} + V_{q'_2 q'_1 q_2} + V_{q'_2 q'_1 q_1} \right) \quad (\text{A.2.7c})$$

where in the last line total momentum conservation is implied. Inserting the expression

for the scattering amplitude Eq. (2.19) into Eq. (A.2.7) yields

$$\begin{aligned} & \langle q'_1, q'_2 | H_{\text{int}} | q_1, q_2 \rangle \\ &= -\frac{1}{L} \left\{ J [\cos(q'_1 - q_1) + \cos(q'_1 - q_2) + \cos(q'_2 - q_2) + \cos(q'_2 - q_1)] \right. \end{aligned} \quad (\text{A.2.8a})$$

$$\begin{aligned} & \left. + J_2 [\cos(2(q'_1 - q_1)) + \cos(2(q'_1 - q_2)) + \cos(2(q'_2 - q_2)) + \cos(2(q'_2 - q_1))] \right\} \\ & \stackrel{(\text{A.2.4})}{=} -\frac{2}{L} \left\{ J [\cos(q'_1 - q_1) + \cos(q'_1 - q_2)] + J_2 [\cos(2(q'_1 - q_1)) + \cos(2(q'_1 - q_2))] \right\} \end{aligned} \quad (\text{A.2.8b})$$

The energy of the bound state is only a function of total momentum Q , not of q_1 and q_2 individually. Since states with different total momentum are always orthogonal, the Hamiltonian matrix can be computed and diagonalized in each Q sector independently. In order to avoid the problem of an overcomplete basis, relative momentum q is chosen as second quantum number with the restriction $q \geq 0$. Total and relative momentum are herefore defined as

$$Q := q_1 + q_2 \quad q := q_1 - q_2 \quad (\text{A.2.9a})$$

$$\Leftrightarrow \quad q_1 = \frac{Q + q}{2} \quad q_2 = \frac{Q - q}{2}. \quad (\text{A.2.9b})$$

Using this to express all momenta using Q , q' and q yields the matrix element in the form of Eq. (2.24).

A.3 2QP interaction matrix of the TFIM

To compare the iMPS results for the 2QP interaction to the analytic solution from CUT [57], the interaction matrix element of the Hamiltonian $H_{2\text{P}}$ is calculated in the $|Q, q_1\rangle$ basis.

As shown in Sec. 2.2, the formulation of the Hamiltonian in string operators allows us to directly determine the 2QP interaction term as

$$H_{2\text{P}} = -2 \sum_j \sum_{n \geq 2} \sum_{m=1}^{n-1} t_n (a_j^\dagger a_{j+m}^\dagger a_{j+m} a_{j+n} + \text{h.c.}). \quad (\text{A.3.1})$$

Note that the summation ranges of n and m in Eq. (A.3.1) exclude the creation and annihilation of two quasi-particles on the same site. Therefore, no special treatment of the hard-core constraint is required.

In order to derive the expression Eq. (2.42), the real space matrix element of $H_{2\text{P}}$ is calculated first

$$\begin{aligned} & \langle j', j' + d' | H_{2\text{P}} | j, j + d \rangle \\ &= -2 \sum_{\ell} \sum_{n=2}^{\infty} \sum_{m=1}^{n-1} t_n \langle j', j' + d' | (a_{\ell}^\dagger a_m^\dagger a_m a_{\ell+n} + a_{\ell+n}^\dagger a_m^\dagger a_m a_{\ell}) | j, j + d \rangle \end{aligned} \quad (\text{A.3.2a})$$

$$\begin{aligned} &= -2 \sum_{\ell} \sum_{n=2}^{\infty} \sum_{m=1}^{n-1} t_n \left[(\delta_{j', \ell} \delta_{j'+d', m} + \delta_{j', m} \delta_{j'+d', \ell}) (\delta_{j, \ell+n} \delta_{j+d, m} + \delta_{j, m} \delta_{j+d, \ell+n}) \right. \\ & \quad \left. + (\delta_{j', \ell+n} \delta_{j'+d', m} + \delta_{j', m} \delta_{j'+d', \ell+n}) (\delta_{j, \ell} \delta_{j+d, m} + \delta_{j, m} \delta_{j+d, \ell}) \right]. \end{aligned} \quad (\text{A.3.2b})$$

The expression Eq. (A.3.2) can now be inserted into the momentum space matrix element

$$\langle Q, q'_1 | H_{2P} | Q, q_1 \rangle = L \langle Q, q'_1 | h_0 |_{2P} | Q, q_1 \rangle \quad (\text{A.3.3a})$$

$$= \frac{1}{L^2} \sum_{j', j} \sum_{d', d} e^{+iQ(j'+d')-iq'_1 d'} e^{-iQ(j+d)+iq_1 d} \langle j', j' + d' | H_{2P} | j, j + d \rangle \quad (\text{A.3.3b})$$

$$= \frac{1}{L} \sum_{j', j} \sum_{d', d} e^{+iQ(j'+d')-iq'_1 d'} e^{-iQ(j+d)+iq_1 d} \langle j', j' + d' | H_{2P} |_{\ell=0} | j, j + d \rangle \quad (\text{A.3.3c})$$

$$= \frac{1}{L} \sum_{j', j} \sum_{d', d} e^{+iQ(j'+d')-iq'_1 d'} e^{-iQ(j+d)+iq_1 d} \left[-2 \sum_{n=2}^{\infty} \sum_{m=1}^{n-1} t_n \right. \\ \left. \times \left(\delta_{j', 0} \delta_{j'+d', m} \delta_{j, n} \delta_{j+d, m} + \delta_{j', 0} \delta_{j'+d', m} \delta_{j, m} \delta_{j+d, n} \right. \right. \\ \left. \left. + \delta_{j', m} \delta_{j'+d', 0} \delta_{j, n} \delta_{j+d, m} + \delta_{j', m} \delta_{j'+d', 0} \delta_{j, m} \delta_{j+d, n} \right. \right. \\ \left. \left. + \delta_{j', n} \delta_{j'+d', m} \delta_{j, 0} \delta_{j+d, m} + \delta_{j', n} \delta_{j'+d', m} \delta_{j, m} \delta_{j+d, 0} \right. \right. \\ \left. \left. + \delta_{j', m} \delta_{j'+d', n} \delta_{j, 0} \delta_{j+d, m} + \delta_{j', m} \delta_{j'+d', n} \delta_{j, m} \delta_{j+d, 0} \right) \right] \quad (\text{A.3.3d})$$

where TI has been used to set $\ell = 0$ everywhere and to gain a factor of L which cancels out one power of L^{-1} in the normalization. Carrying out the sums over j' , j , d' and d yields

$$\langle Q, q'_1 | H_{2P} | Q, q_1 \rangle = -\frac{2}{L} \sum_{n=2}^{\infty} \sum_{m=1}^{n-1} t_n \left[\left(e^{+iQm-iq'_1 m-iQm+iq_1(m-n)} + e^{+iQm-iq'_1 m-iQn+iq_1(n-m)} \right. \right. \\ \left. \left. + e^{-iq'_1(-m)-iQm+iq_1(m-n)} + e^{-iq'_1(-m)-iQn+iq_1(n-m)} \right. \right. \\ \left. \left. + e^{+iQm-iq'_1(m-n)-iQm+iq_1 m} + e^{+iQm-iq'_1(m-n)+iq_1(-m)} \right. \right. \\ \left. \left. + e^{+iQn-iq'_1(n-m)-iQm+iq_1 m} + e^{+iQn-iq'_1(n-m)+iq_1(-m)} \right) \right]. \quad (\text{A.3.4})$$

For each summand, the values of m run from 1 to $n-1$. Therefore, under the sum m can be exchanged with $n-m$, which then takes the same values $n-1$ to 1 only in reverse order. With this, the exponentials can be written as cosine functions

$$\langle Q, q'_1 | H_{2P} | Q, q_1 \rangle = -\frac{4}{L} \sum_{n=2}^{\infty} \sum_{m=1}^{n-1} t_n \left[\cos(q'_2(n-m) + q_1 m) + \cos(q'_1(n-m) + q_2 m) \right. \\ \left. + \cos(q'_1(n-m) + q_1 m) + \cos(q'_2(n-m) + q_2 m) \right]. \quad (\text{A.3.5})$$

Lastly, in the TDL the following index mapping can be made

$$\{n, m\} \rightarrow \{d', d\} \quad \text{with} \quad n = d' + d, \quad m = d, \quad d', d > 0. \quad (\text{A.3.6})$$

Inserting this into Eq. (A.3.5) finally yields the matrix element as given in Eq. (2.41).

A.4 Properties of transfer operator T

This section provides a more detailed discussion of the properties of the spectrum of the transfer matrix T and the eigenmatrices associated with the largest modulus EV Λ_0 . These are the arguments used to motivate the iMPS formalism as implemented for the purposes of this thesis. For a more in-depth analysis see for instance Refs. [21, 22].

A.4.1 Largest eigenvalue

We define T^S by

$$T = \sum_s T^s := \sum_s A^{s*} \otimes A^s, \quad (\text{A.4.1})$$

with $A^s \in \mathbb{C}^{D \times D}$. Some statements can be made about the spectrum of each summand T^s . For the EVs c_{ij} of a Kronecker product of two matrices A and B with EVs a_i and b_j , respectively, the relation

$$c_{ij} = a_i b_j \quad (\text{A.4.2})$$

holds, i.e., the EVs of the Kronecker product are the products of the EVs of the individual matrices A and B . For T^s , $B = A^*$ holds, and the EVs of A^* are the complex conjugates of the EVs of A .

Therefore, T^s has at least D real and positive eigenvalues that are the squared absolute values of the EVs of A^s . Moreover, if the largest modulus EV is unique, it is the square of the absolute value of the largest magnitude EV of A^s and therefore real and positive. If the largest magnitude EV of A^s is n -fold degenerate, then T^s has n^2 EVs with the same modulus. At least one of them is real and positive. All complex EVs come in conjugate pairs, as can be seen from Eq. (A.4.2). Note that if the largest magnitude EV of A^s is zero, then all EVs are zero and A^s is nilpotent and therefore describes the null-vector in the uMPS class of $D \times D$ matrices, since $A^n = 0$ with $n \leq D \ll L$.

Unfortunately, there are only few rigorous statements that can be made about the spectrum of the sum of matrices. In practice, we find, that this structure of the spectrum of T^s carries over to the spectrum of the sum $T = \sum_s T^s$. However, there is no proof that this must be so.

Therefore, at this point the statement

$$\Lambda_0 \in \mathbb{R}^+, \quad \Lambda_i \neq \Lambda_0 \quad \forall i \neq 0 \quad (\text{A.4.3})$$

must be taken as an axiom or, alternatively, as a necessary condition for the ansatz to work.

If Λ_0 is truly degenerate, i.e.,

$$\Lambda_i = \Lambda_0, \quad i = 1, \dots, n, \quad (\text{A.4.4})$$

in the thermodynamic limit the norm takes the form

$$\langle \psi | \psi \rangle = \text{Tr} \left(\tilde{Q} \left(\Lambda_0^L \sum_{i=0}^n \vec{v}_i \vec{u}_i^\dagger \right) \right) = \Lambda_0^L \sum_i \vec{u}_i^\dagger \tilde{Q} \vec{v}_i. \quad (\text{A.4.5})$$

This can in theory still be normalizeable through Q , if $\vec{u}_i^\dagger \tilde{Q} \vec{v}_i \in \mathbb{R}$ for all i and the sum is positive. However, since $\vec{u}_i^\dagger \tilde{Q} \vec{v}_i = \vec{u}_j^\dagger \tilde{Q} \vec{v}_j$ cannot be assumed for $i \neq j$, this would require extended bookkeeping on the normalization for all norms and matrix elements.

If Λ_0 is degenerate in the absolute value, i.e.,

$$|\Lambda_i| = \Lambda_0, \quad i = 1, \dots, n, \quad (\text{A.4.6})$$

one faces another problem the thermodynamic limit. This is because the limit

$$\lim_{L \rightarrow \infty} \left(\frac{\Lambda_j}{\Lambda_0} \right)^L = \lim_{L \rightarrow \infty} (e^{i\theta_j})^L \quad (\text{A.4.7})$$

does not take a defined value for $\theta_j \neq 0$. For a more detailed discussion see Ref. [99].

In general, a degenerate largest magnitude EV is a strong indicator that some of the premises of the iMPS formalism are violated. For instance, in 1D the ground state of the Majumdar-Ghosh Hamiltonian [100, 101, 102]

$$H = J \sum_j \vec{S}_j \vec{S}_{j+1} + \frac{J}{2} \sum_j \vec{S}_j \vec{S}_{j+2} \quad (\text{A.4.8})$$

is two-fold degenerate, as it consists of singlets forming either on the odd or on the even bonds. Therefore, the system will favor one or the other ground state, depending on the boundary conditions. There is, however, a uMPS representation that accounts for *both* realizations simultaneously, using matrices of dimension 3×3

$$A^\uparrow := \begin{pmatrix} 0 & \frac{1}{\sqrt{2}} & 0 \\ 0 & 0 & 0 \\ 1 & 0 & 0 \end{pmatrix}, \quad A^\downarrow := \begin{pmatrix} 0 & 0 & -\frac{1}{\sqrt{2}} \\ 1 & 0 & 0 \\ 0 & 0 & 0 \end{pmatrix}. \quad (\text{A.4.9})$$

The resulting transfer matrix T

$$T = \begin{pmatrix} 0 & 0 & 0 & 0 & \frac{1}{2} & 0 & 0 & 0 & 0 \\ 0 & 0 & 0 & 0 & 0 & 0 & -\frac{1}{\sqrt{2}} & 0 & 0 \\ 0 & 0 & 0 & \frac{1}{\sqrt{2}} & 0 & 0 & 0 & 0 & 0 \\ 0 & 0 & -\frac{1}{\sqrt{2}} & 0 & 0 & 0 & 0 & 0 & 0 \\ 1 & 0 & 0 & 0 & 0 & 0 & 0 & 0 & 0 \\ 0 & 0 & 0 & 0 & 0 & 0 & 0 & 0 & 0 \\ 0 & \frac{1}{\sqrt{2}} & 0 & 0 & 0 & 0 & 0 & 0 & 0 \\ 0 & 0 & 0 & 0 & 0 & 0 & 0 & 0 & 0 \\ 1 & 0 & 0 & 0 & 0 & 0 & 0 & 0 & 0 \end{pmatrix} \quad (\text{A.4.10})$$

has modulus degenerate EVs $\{\Lambda_0 = +1, \Lambda_1 = -1\}$. As a result, this ground state uMPS cannot reliably be determined by the algorithms described in this thesis.

A.4.2 Properties of eigenmatrices

If we assume (A.4.3), we can prove that the corresponding left and right eigenmatrices u and v must be Hermitian and can be chosen positive semi-definite as shown next.

First note that the relation

$$(T[v])^\dagger = \left(\sum_s A^s v A^{s\dagger} \right)^\dagger \quad (\text{A.4.11a})$$

$$= \sum_s A^s v^\dagger A^{s\dagger} \quad (\text{A.4.11b})$$

$$= T[v^\dagger] \quad (\text{A.4.11c})$$

holds. It follows that if v is an eigenmatrix of T to EV Λ , then v^\dagger is an eigenmatrix to EV Λ^*

$$T[v] = \Lambda v \quad (\text{A.4.12a})$$

$$\Rightarrow (T[v])^\dagger = \Lambda^* v^\dagger = T[v^\dagger] \quad (\text{A.4.12b})$$

$$\Rightarrow v^\dagger = v \quad \text{if } \Lambda \in \mathbb{R} \text{ and unique.} \quad (\text{A.4.12c})$$

The same argument holds for the left eigenmatrix u .

A matrix v is called positive (negative) definite, if the form $f(\vec{w}) = \vec{w}^\dagger v \vec{w}$ is greater (less) than zero for all possible arguments $\vec{w} \neq \vec{0}$. If $f(\vec{w}) = 0$ can occur, the matrix is called positive or negative *semi* definite, respectively. For Hermitian matrices, this is equivalent to all EVs being greater (less) than or equal to zero.

To prove that u and v can be chosen positive semi-definite, we note that T is an endomorphism of the positive or negative (semi) definite matrices. Let v_α be the EVs of v and $\vec{\alpha}$ the corresponding eigenvectors. Then

$$\vec{w}^\dagger T[v] \vec{w} = \vec{w}^\dagger \left(\sum_s A^s \left(\sum_\alpha v_\alpha \vec{\alpha} \vec{\alpha}^\dagger \right) A^{s\dagger} \right) \vec{w} \quad (\text{A.4.13a})$$

$$= \sum_s \sum_\alpha v_\alpha |\vec{w}^\dagger A^s \vec{\alpha}|^2 \quad (\text{A.4.13b})$$

$$\begin{cases} \geq 0 \quad \forall \vec{w} & \text{if } v_\alpha \geq 0 \quad \forall \alpha \\ \leq 0 \quad \forall \vec{w} & \text{if } v_\alpha \leq 0 \quad \forall \alpha \end{cases} \quad (\text{A.4.13c})$$

Next, let v be a positive semi-definite eigenmatrix of T to EV Λ . Then, on the one hand it follows from Eq. (A.4.13) that Λ must be positive

$$\vec{w}^\dagger v \vec{w} \geq 0 \quad (\text{A.4.14a})$$

$$\Rightarrow \vec{w}^\dagger T[v] \vec{w} \geq 0 \quad (\text{A.4.14b})$$

$$\Rightarrow \Lambda \vec{w}^\dagger v \vec{w} \geq 0 \quad (\text{A.4.14c})$$

$$\Rightarrow \Lambda \geq 0. \quad (\text{A.4.14d})$$

On the other hand, a unique EV determines its corresponding eigenmatrix up to multiplication by a scalar. We have shown in Eq. (A.4.12) that eigenmatrices corresponding to unique, real EVs must be Hermitian. If we assume v to be normalized, then it is uniquely determined by Λ up to multiplication by -1 . Therefore, the eigenmatrices corresponding to unique, positive EVs of T must be either positive or negative semi-definite, and can thus be chosen to be positive semi-definite.

Lastly, it remains to be shown that $v \geq 0$ implies $u \geq 0$. Since they are left and right eigenvectors to the same EV, their scalar product is one. Let u_β be the EVs and $\{\vec{\beta}\}$ the eigenvectors of u . Then

$$(u, v) = \text{Tr}(u^\dagger v) = \text{Tr}(uv) \quad (\text{A.4.15a})$$

$$= \text{Tr} \left(\sum_\beta u_\beta \vec{\beta} \vec{\beta}^\dagger v \right) \quad (\text{A.4.15b})$$

$$= \sum_\beta u_\beta \underbrace{\vec{\beta}^\dagger v \vec{\beta}}_{\geq 0} \quad (\text{A.4.15c})$$

$$= 1 \quad (\text{A.4.15d})$$

$$\Rightarrow u_\beta \geq 0. \quad (\text{A.4.15e})$$

If, in addition to (A.4.3)

$$|\Lambda_i| < 1 \quad \forall i > 0 \quad (\text{A.4.16})$$

is assumed, the thermodynamic limit is always well defined and the boundary matrices can be linked to the singular values of the uMPS. This allows us to conclude, that v and u are positive definite, i.e. cannot have zero EVs.

Let $\{\tilde{\Gamma}^s, \tilde{\lambda}\}$ be the composite form of a uMPS as defined in Sec. 3.6.4. Then, as shown in Sec. A.4.3, the norm TN takes one of the following forms

where u and v are the left and right eigenmatrices of

$$\tilde{T}_L = \sum_s (\lambda \Gamma^{s*}) \otimes (\lambda \Gamma^s) \quad \text{and} \quad \tilde{T}_R = \sum_s (\Gamma^{s*} \lambda) \otimes (\Gamma^s \lambda), \quad (\text{A.4.18})$$

respectively. The symbol $//$ denotes that an arbitrary number of rungs is left out. The matrix λ is the diagonal $D \times D$ matrix of Schmidt coefficients of the Schmidt decomposition of the uMPS across *any* bond. As singular values the elements λ_i of λ are real and non-negative. Additionally, we can assume them to be Strictly positive $\lambda_i > 0 \quad \forall i$. Because if \mathbf{A} had n singular values equal to zero, then the state could be represented by matrices of dimension $(D - n) \times (D - n)$, which then would have again only positive singular values. In the norm in Eq. (A.4.17) one of the matrix products

$$\lambda^* u^\dagger \lambda \quad \text{or} \quad \lambda v \lambda^* \quad (\text{A.4.19})$$

occurs. Since the rank of the product of matrices cannot exceed the minimum rank of the factors, u and v must have full rank. Otherwise, there would be one Schmidt decomposition with an effective Schmidt rank $K < D$, which would again mean that *every* Schmidt decomposition had rank $K < D$.

Therefore, the boundary matrices u and v are Hermitian, have full rank and can be chosen positive definite. This proves, that the scalar product Eq. (3.69) is well defined, given the conditions (A.4.3) and (A.4.16) are met. It also means, that u and v are invertible, which is a requirement for computing the canonical form of a uMPS.

A.4.3 TN boundaries in the thermodynamic limit

This section describes the special form of TNs that occur for overlaps and matrix elements in the thermodynamic limit. As can be seen from Eq. (3.42), the TN for a norm of a state with PBC is

$$\langle \psi | \psi \rangle = \sum_{s_1, \dots, s_L} c_{s_1, \dots, s_L}^* c_{s_1, \dots, s_L} \quad (\text{A.4.20a})$$

$$= \sum_{s_1, \dots, s_L} \text{Tr}(A^{s_L \dagger} \dots A^{s_1 \dagger}) \text{Tr}(A^{s_1} \dots A^{s_L}) \quad (\text{A.4.20b})$$

$$= \begin{array}{c} \text{---} A^{s_1^*} \text{---} \bullet \text{---} \bullet \text{---} // \text{---} \bullet \text{---} \bullet \text{---} A^{s_L^*} \text{---} \\ | \quad | \quad | \quad | \quad | \\ \text{---} A^{s_1} \text{---} \bullet \text{---} \bullet \text{---} // \text{---} \bullet \text{---} \bullet \text{---} A^{s_L} \text{---} \end{array} \quad (\text{A.4.20c})$$

i.e. it represents a sum of *products of traces*. In contrast, the TN

$$\begin{array}{c} A^{s_1^*} \quad \quad \quad A^{s_L^*} \\ \bullet \quad \bullet \quad \bullet // \quad \bullet \quad \bullet \quad \bullet \\ | \quad | \quad | \quad | \quad | \\ \bullet \quad \bullet \quad \bullet // \quad \bullet \quad \bullet \quad \bullet \\ A^{s_1} \quad \quad \quad A^{s_L} \end{array} u^\dagger \quad v = \sum_{s_1, \dots, s_L} \text{Tr}(u^\dagger A^{s_L \dagger} \dots A^{s_1 \dagger} v A^{s_1} \dots A^{s_L}) \quad (\text{A.4.21})$$

represents a sum of *traces of matrix products*. In general, these are not the same

$$\text{Tr}(A)\text{Tr}(B) \neq \text{Tr}(AB) . \quad (\text{A.4.22})$$

However, in the thermodynamic limit and *only* in the thermodynamic limit, given $\{A^{s_i}\}$ represent a properly normalized state, both expressions take the same value, namely 1, and can thus be identified

$$\langle \psi | \psi \rangle = \sum_{s_1, \dots, s_L} \text{Tr}(A^{s_1^*} \dots A^{s_L^*}) \text{Tr}(A^{s_1} \dots A^{s_L}) \quad (\text{A.4.23a})$$

$$= \text{Tr}(T^L) \quad (\text{A.4.23b})$$

$$= \text{Tr}(\Lambda_0^L \vec{v}_0 \vec{u}_0^\dagger) \quad (\text{A.4.23c})$$

$$= \Lambda_0^L \text{Tr}(\vec{u}_0^\dagger \vec{v}_0) \quad (\text{A.4.23d})$$

$$= \Lambda_0^L \vec{u}_0^\dagger \vec{v}_0 \quad (\text{A.4.23e})$$

$$= 1 . \quad (\text{A.4.23f})$$

The critical step is (A.4.23c), where the TDL is used to reduce T^L to a dyadic product using the spectral representation

$$\lim_{L \rightarrow \infty} T^L = \lim_{L \rightarrow \infty} \sum_{i=0}^{D^2-1} \Lambda_i^L \vec{v}_i \vec{u}_i^\dagger = \Lambda_0^L \vec{v}_0 \vec{u}_0^\dagger \quad (\text{A.4.24})$$

since $|\Lambda_i| < 1$ for $i > 0$ and therefore $\lim_{L \rightarrow \infty} \Lambda_{i>0}^L = 0$. This makes the argument of the trace operation already a scalar, and for scalars the product of traces is indeed equal to the trace of the product, since the trace operation is trivial.

Since u and v are eigenvectors of T to EV $\Lambda_0 = 1$, the following relations hold

$$\begin{array}{c} \bullet \\ \text{---} \\ \bullet \end{array} \begin{array}{c} \text{---} \\ \text{---} \\ \text{---} \end{array} \begin{array}{c} \text{---} \\ \text{---} \\ \text{---} \end{array} \blacklozenge v = T[v] = v = \blacklozenge v \quad (\text{A.4.25a})$$

$$u^\dagger \blacklozenge \begin{array}{c} \bullet \\ \text{---} \\ \bullet \end{array} = T^\dagger[u^\dagger] = u^\dagger = u^\dagger \blacklozenge \quad (\text{A.4.25b})$$

and it is easy to see that the entire TN in Eq. (A.4.21) therefore collapses to

$$u^\dagger \blacklozenge \text{---} \blacklozenge v = \text{Tr}(u^\dagger v) . \quad (\text{A.4.26})$$

This means, in general the TN in Eq. (A.4.20) corresponds to the matrix interpretation Eq. (3.54) of T , while the TN in Eq. (A.4.21) corresponds to the superoperator interpretation Eq. (3.67). Since the latter is numerically advantageous, it is chosen for this thesis, along with the TN type in Eq. (A.4.21).

As shown in Sec. 3.6.4, for a left-canonical uMPS, the left boundary matrix is the $D \times D$ identity matrix $u = \mathbb{1}$. This translates in TN notation to

$$\text{Tr}(u^\dagger v) = \text{Tr}(\mathbb{1}v) = \text{Tr}(v) = \text{---} \blacklozenge v \Rightarrow \left[\text{---} \right] = \mathbb{1} . \quad (\text{A.4.27})$$

Since the left-canonical gauge is the used, the TNs appearing for iMPSs are generically of the form

$$\langle \psi' | \hat{O} | \psi \rangle = \text{---} \begin{array}{c} \bullet \\ \text{---} \\ \bullet \end{array} \begin{array}{c} \bullet \\ \text{---} \\ \bullet \end{array} \begin{array}{c} \bullet \\ \text{---} \\ \bullet \end{array} \begin{array}{c} \bullet \\ \text{---} \\ \bullet \end{array} \begin{array}{c} \bullet \\ \text{---} \\ \bullet \end{array} \begin{array}{c} \bullet \\ \text{---} \\ \bullet \end{array} \blacklozenge . \quad (\text{A.4.28})$$

In the arguments leading up to the TN form in Eq. (A.4.28), the boundary operator Q was not discussed. The reason is that in the limit $L \rightarrow \infty$ Eq. (A.4.24) also holds for $T^{\frac{L}{2}}$. Therefore, in the TDL any relevant matrix element or overlap takes the following form

$$\lim_{L \rightarrow \infty} \text{Tr}(\tilde{Q} T^L O T^L) = \lim_{L \rightarrow \infty} \text{Tr}(T^{\frac{L}{2}} \tilde{Q} T^L O T^{\frac{L}{2}}) \quad (\text{A.4.29a})$$

$$= \text{Tr}(\underbrace{\vec{v}_0 \vec{u}_0^\dagger \tilde{Q} \vec{v}_0 \vec{u}_0^\dagger}_=1 O \vec{v}_0 \vec{u}_0^\dagger) \quad (\text{A.4.29b})$$

$$= \underbrace{\vec{u}_0^\dagger \vec{v}_0 \vec{u}_0^\dagger}_=1 O \vec{v}_0 \quad (\text{A.4.29c})$$

$$= \vec{u}_0^\dagger O \vec{v}_0 \quad (\text{A.4.29d})$$

where O is a $D^2 \times D^2$ matrix or a rank-4 tensor that holds all information on the finite number of lattice sites that are different from the ground state. The first equality is due to the cyclic property of the trace, the second due to Eq. (A.4.24) and the rest follows from normalization. Therefore, if the uMPS described by \mathbf{A} is normalizable, the boundary operator is irrelevant and can be omitted from the notation entirely.

A.4.4 uMPS and iMPS

Although uniform matrix product states (uMPSs) and infinite system matrix product states (iMPSs) both describe infinite systems in the context of this thesis, there are differences. This is why two different acronyms are used.

The class of uMPS discussed in Sec. 3.6.2, that is assumed to describe the ground state, does not form a vector space, but rather a manifold [92]. This means if two states $|\psi\rangle$ and $|\phi\rangle$ can be described as uMPSs, this is not necessarily true for their sum. Especially if

$$\mathbf{A} \mapsto |\psi\rangle, \tilde{\mathbf{A}} \mapsto |\phi\rangle, \mathbf{C} \mapsto |\chi\rangle = |\psi\rangle + |\phi\rangle \not\Rightarrow \mathbf{C} = \mathbf{A} + \tilde{\mathbf{A}}. \quad (\text{A.4.30})$$

Although manifolds are locally isomorphic to vector spaces, not knowing the isomorphism (and its inverse) makes it very hard to define a scalar product for uMPSs.

Looking at the analysis of the uMPS norm in Sec. 3.6.2, one could think of defining a transfer operator

$$\bar{T} := \sum_s \tilde{A}^{s*} \otimes A^s \quad (\text{A.4.31})$$

in terms of which the overlap then reads

$$\langle \phi | \psi \rangle = \lim_{L \rightarrow \infty} \text{Tr}(\bar{T}^L). \quad (\text{A.4.32})$$

Assuming both $|\psi\rangle$ and $|\phi\rangle$ are normalized, generically the largest magnitude EV of \bar{T} is smaller than 1, and therefore, the overlap vanishes in the TDL. This means, that with respect to this scalar product, *all* uMPSs are orthogonal. Alternatively, one could define the largest magnitude EV of \bar{T} as the value of the scalar product. However, this is not a good definition, either. For instance, the two degenerate ground states in the ordered phase of the TFIM are orthogonal. Yet, the largest magnitude EV of \bar{T} formed from two uMPSs describing both ground states is non-zero. Arguably, the uMPSs do not describe the true ground states, and therefore orthogonality can only be expected in the limit $D \rightarrow \infty$. In this case $\bar{\Lambda}_0$ should at least decrease for increasing bond dimension and extrapolate to a value near zero. However, at least in the case of the TFIM, this is not what we observe. This problem makes working with degenerate ground states in the TDL challenging.

In contrast, the iMPSs formed by replacing a finite number n of consecutive tensors in a uMPS *do* form a vector space. It is of dimension $(dD^2)^n$ and can be interpreted as the tangent space to the manifold of uMPS at the given point. Therefore, provided they are based on the same uMPS, i.e., are elements of the same tangent space, the sum of two iMPSs is again a iMPS. Also, the scalar product of two iMPSs is well-defined. Since this type of iMPS is used describe excited states, their overlaps and matrix elements are well-defined, too.

A.5 Ground state degeneracy

As mentioned in Sec. 3.6.1, ground state degeneracy can be handled to some extent in the framework of iMPS. This section describes the algorithmic changes necessary to work with a model that has a degenerate ground state. Some caveats and limitations are discussed. Also, some considerations explicitly for the TFIM are made.

A.5.1 Working with degenerate ground states

For instance, the TFIM Hamiltonian Eq. (2.25) has a \mathbb{Z}_2 symmetry for $S^x \rightarrow -S^x$ which is spontaneously broken in the Ising phase $\lambda > 1$. This symmetry breaking is reflected in the ground state uMPS as found by the algorithm in Sec. 4.1, since the result describes either one or the other ground state realization, not a superposition of both. This is due to the manifold structure of the set of uMPS, meaning that a superposition of the two ground states is not contained in that manifold, although it has the same energy per lattice site. In the case of the TFIM, as discussed in Sec. 4.5, the order parameter M_x can be used to determine which ground state the algorithm converged to. This can be generalized to other models, if ground state degeneracy is expected. Usually, there is an order parameter by which the different possible realizations can be told apart. Therefore, the algorithm can be run multiple times with different random initial guesses to find the different uMPSs of the ground states.

A.5.2 Transformation for ground state uMPS in the TFIM

For the TFIM running the ground state search multiple times is not required. Although the transverse field introduces quantum fluctuations, the ground state of the Ising phase can still be understood as all spins aligning in either positive or negative x -direction. There is a simple transformation that converts one into the other, namely $-\sigma^z$ which can be interpreted as a spin-flip operator in the σ^x eigenbasis.

By expressing the Hamiltonian in spin- $\frac{1}{2}$ operators,

$$S^\alpha = \frac{1}{2}\sigma^\alpha \quad \text{with } \alpha \in \{x,y,z\} \quad (\text{A.5.1})$$

with the Pauli matrices σ^α

$$\sigma^x = \begin{pmatrix} 0 & 1 \\ 1 & 0 \end{pmatrix}, \quad \sigma^y = \begin{pmatrix} 0 & -i \\ i & 0 \end{pmatrix}, \quad \sigma^z = \begin{pmatrix} 1 & 0 \\ 0 & -1 \end{pmatrix}, \quad (\text{A.5.2})$$

the eigenbasis of σ^z was chosen as basis for the local Hilbert space of each spin. The eigenstates of σ^z are

$$|\uparrow\rangle = \begin{pmatrix} 1 \\ 0 \end{pmatrix}, \quad \sigma^z |\uparrow\rangle = +1 |\uparrow\rangle \quad \text{and} \quad |\downarrow\rangle = \begin{pmatrix} 0 \\ 1 \end{pmatrix}, \quad \sigma^z |\downarrow\rangle = -1 |\downarrow\rangle \quad (\text{A.5.3})$$

and those of σ^x are

$$|\psi_{x,+}\rangle = \frac{1}{\sqrt{2}}(|\downarrow\rangle + |\uparrow\rangle) = \frac{1}{\sqrt{2}} \begin{pmatrix} 1 \\ 1 \end{pmatrix}, \quad \sigma^x |\psi_{x,+}\rangle = +1 |\psi_{x,+}\rangle \quad \text{and} \quad (\text{A.5.4a})$$

$$|\psi_{x,-}\rangle = \frac{1}{\sqrt{2}}(|\downarrow\rangle - |\uparrow\rangle) = \frac{1}{\sqrt{2}} \begin{pmatrix} -1 \\ 1 \end{pmatrix}, \quad \sigma^x |\psi_{x,-}\rangle = -1 |\psi_{x,-}\rangle. \quad (\text{A.5.4b})$$

It is thus easy to see that a multiplication by $-\sigma^z$ turns $|\psi_{x,+}\rangle$ into $|\psi_{x,-}\rangle$ and vice versa

$$-\sigma^z |\psi_{x,+}\rangle = \begin{pmatrix} -1 & 0 \\ 0 & 1 \end{pmatrix} \frac{1}{\sqrt{2}} \begin{pmatrix} 1 \\ 1 \end{pmatrix} = \frac{1}{\sqrt{2}} \begin{pmatrix} -1 \\ 1 \end{pmatrix} = |\psi_{x,-}\rangle \quad (\text{A.5.5a})$$

$$-\sigma^z |\psi_{x,-}\rangle = \begin{pmatrix} -1 & 0 \\ 0 & 1 \end{pmatrix} \frac{1}{\sqrt{2}} \begin{pmatrix} -1 \\ 1 \end{pmatrix} = \frac{1}{\sqrt{2}} \begin{pmatrix} 1 \\ 1 \end{pmatrix} = |\psi_{x,+}\rangle. \quad (\text{A.5.5b})$$

Therefore,

$$|GS^+\rangle = \left(\bigotimes_{j=-\infty}^{\infty} -\sigma_j^z \right) |GS^-\rangle \quad (\text{A.5.6})$$

where $|GS^+\rangle$ is the ground state with spin orientation in positive x -direction, and $|GS^-\rangle$ the one with magnetization in negative x -direction. In contrast to the local operators dealt with so far, this is actually a *global* operation that acts on *all* the spins in the same way. It is one of the rare cases where an MPO can be applied to a uMPS

$$\left(\bigotimes_{j=-\infty}^{\infty} -\sigma_j^z \right) |GS^-\rangle = \text{Tr} \left[\left(\sum_{s'_1} (-\sigma^{z'})_{s_1 s'_1} A^{s'_1} \right) \cdots \left(\sum_{s'_L} (-\sigma^{z'})_{s_L s'_L} A^{s'_L} \right) \right] |\{s_i\}\rangle. \quad (\text{A.5.7})$$

Applying this operator to the ground state uMPS yields

$$\sum_{s'} (e^{-i\pi S^y})_{s,s'} A^{s'} = \begin{cases} -A^1, & \text{if } s = 1 \\ A^2, & \text{if } s = 2 \end{cases}, \quad (\text{A.5.8})$$

i.e, ultimately only a relative sign between the two A^s matrices

$$|GS^-\rangle : \{A^1, A^2\} \rightarrow |GS^+\rangle : \{-A^1, A^2\}. \quad (\text{A.5.9})$$

Note that this operation transforms both ground states into each other.

A.5.3 Dispersion for degenerate ground states

If a one-dimensional system has a degenerate ground state, this is of fundamental importance, because it greatly changes the type of the elementary excitations. With a degenerate ground state, very often the least amount of energy that can be put into the system is no longer a local perturbation such as a spin flip or a triplet excitation, but a domain wall between sections with different ground states. Therefore, a single excitation cannot be created by a local operation, but rather involves an infinite number of lattices sites being changed from one ground state to another.

In this case, assuming the same ground state on both ends of the system then implies that elementary excitations can only be created in pairs. This is easy to see for the example of the TFIM in the Ising phase, where flipping a single spin means creating *two* domain walls, which in the limit $\Gamma = 0$ can move apart at no additional energy cost, cf. Fig. 2.1.

This type of domain wall excitation can indeed be described within the iMPS framework using the ansatz in Eq. (5.2)

$$|B_{\alpha,j}\rangle := \sum_{s_1, \dots, s_L} \text{Tr}(A^{s_1} \cdots A^{s_{j-1}} B_{\alpha}^{s_j} \tilde{A}^{s_{j+1}} \cdots \tilde{A}^{s_L}) |s_1, \dots, s_L\rangle \quad (\text{A.5.10})$$

where A describes one ground state and \tilde{A} the other. Finding the B_{α} tensors with degenerate ground state works the same way as described for a unique ground state in Sec. 5.1.2.3. The only difference is that when computing the matrix M , the left eigenmatrix u of T and the right eigenmatrix \tilde{v} of \tilde{T} are used, where \tilde{T} is constructed from \tilde{A} according to Eq. (3.54).

The same is true for the matrix elements

$$\langle B_{\alpha,j'} | \tilde{h}_0 | B_{\beta,j} \rangle = \text{Diagram} \quad (\text{A.5.11})$$

where the open circles denote the $\tilde{\mathbf{A}}$ tensor, the open diamond shape denotes \tilde{v} , and the solid circles denote \mathbf{A} . For the example TN, $j' < 0$ and $j > 0$ was assumed. Intermediate transfer operators on the sites $j' < k < 0$ and $n < k < j$ are replaced by

$$T = \mathbb{1}^{(\mathbf{A};\mathbf{A})} = \begin{array}{c} \bullet \\ | \\ \bullet \end{array} \rightarrow \bar{T} = \mathbb{1}^{(\tilde{\mathbf{A}};\mathbf{A})} = \begin{array}{c} \circ \\ | \\ \bullet \end{array} \quad \text{or} \quad \bar{T} = \mathbb{1}^{(\mathbf{A};\tilde{\mathbf{A}})} = \begin{array}{c} \bullet \\ | \\ \circ \end{array} . \quad (\text{A.5.12})$$

Since the application of the transfer operator is implemented as an identity operation anyway, this requires only minor adjustments for 1QP computations.

Note that the orthogonality of the states in Eq. (5.2) with respect to α and j is in no way influenced by the ground state being degenerate.

The above sketched ansatz captures the dispersion relation of domain wall excitations perfectly, as evidenced by the results for the TFIM in the Ising regime in Sec. 5.4.2. However, it requires that the presence of ground state degeneracy is known, and that uMPS descriptions for the different ground states on both sides of the domain wall are available. As mentioned above, if a system with ground state degeneracy is treated as having a unique ground state, the resulting \mathbf{B}_α tensors describe two elementary excitations close together. This results in an overestimation of the energy gap by a factor of two, which can be seen in Fig. 5.6.

As a side note, applying the transformation Eq. (A.5.9) to a ground state uMPS of the TFIM in the strong field phase and treating the system as having a degenerate ground state, does not change the results for the dispersion or the creation operator. This can easily be understood, since the spins are polarized in z direction and the flip in x direction does not change the nature of the ground state.

In summary, the iMPS formalism is capable of producing very accurate results for domain wall type excitations. However, it is not capable of determining the nature of the excitations automatically. For a degenerate ground state, the domain wall character of the excitations has to be explicitly incorporated into the ansatz for excited states.

A.6 Orthogonality of Wannier states

The following text book argument proves the orthogonality of the one-particle momentum states. Note that an infinite system with OBC or translational invariance for PBC are necessary prerequisites, but are assumed throughout this thesis anyway. Let T_a be the translation operator, that shifts the whole lattice by one lattice constant a , i.e. by one site. It is generated by the momentum operator \hat{q}

$$T_a = e^{i\hat{q}a} \quad \Rightarrow \quad T_a^\dagger = e^{-i\hat{q}^\dagger a} = e^{-i\hat{q}a} = T_{-a} . \quad (\text{A.6.1})$$

Let now $|j\rangle$ be a one-particle real space state with the particle located at site j . And let

$$|q\rangle := \sum_j e^{-iqj} |j\rangle \quad (\text{A.6.2})$$

be the equal weight momentum superposition of all states $|j\rangle$. It is easily seen, that $|q\rangle$ is an eigenstate of the translation

$$T_a |q\rangle = T_a \sum_j e^{-iqj} |j\rangle = \sum_j e^{-iqj} T_a |j\rangle \quad (\text{A.6.3a})$$

$$= \sum_j e^{-iqj} |j+1\rangle = \sum_j e^{-iq(j-1)} |j\rangle \quad (\text{A.6.3b})$$

$$= e^{iq} \sum_j e^{-iqj} |j\rangle \quad (\text{A.6.3c})$$

$$= e^{iq} |q\rangle \quad (\text{A.6.3d})$$

where the index shift $j \rightarrow j-1$ is possible due to TI and the infinite system size. On the bra state $\langle q|$ the operator T_a acts in the same way, but yields the complex conjugate eigenvalue

$$T_a \langle q| = e^{-iq} \langle q| \quad (\text{A.6.4a})$$

$$\Rightarrow T_a^\dagger \langle q| = T_{-a} \langle q| = e^{iq} \langle q| . \quad (\text{A.6.4b})$$

Now consider the matrix element

$$\langle q'|T_a |q\rangle = \left(\langle q'|T_a^\dagger \right) |q\rangle = \langle q'| \left(T_a |q\rangle \right) \quad (\text{A.6.5a})$$

$$= \langle q'|e^{iq'} |q\rangle = \langle q'|e^{iq} |q\rangle \quad (\text{A.6.5b})$$

$$\Rightarrow e^{iq'} \langle q'|q\rangle = e^{iq} \langle q'|q\rangle \quad (\text{A.6.5c})$$

$$\Rightarrow q = q' \quad \text{or} \quad \langle q'|q\rangle = 0 \quad (\text{A.6.5d})$$

given q is a good quantum number which is ensured under the aforementioned assumptions.

A.7 Occupation-number and Hilbert space dimensions

In numerical computations, momentum in the Brillouin zone needs to be discretized into L_q sampling points, even if the system is considered to be in the TDL. However, this effectively means working on a finite system with $L = L_q$ lattice sites in real space, that has periodic boundary conditions due to the properties of the discrete Fourier transformation.

Choosing L_q odd is much more convenient than having L_q even, although this may seem counter-intuitive. This is so because with odd L_q each sector with total momentum Q contains the same well-defined number of states, and therefore all Q sectors can be handled in the same way.

Consider a bosonic system with a finite number L of lattice sites and PBC. Let $|j,\ell\rangle$ be an orthonormal basis of the two-particle Fock space \mathcal{F}_2 represented in real space. For distinguishable particles, the dimension of \mathcal{F}_2 is L^2 since for each particle there are L lattice sites to put it on. The states with doubly occupied sites

$$|j,j\rangle = a_j^\dagger a_j^\dagger |0\rangle , \quad (\text{A.7.1})$$

where $|0\rangle$ is the vacuum state, are uniquely determined. However, for bosons every other state in occupation number space can be created in two ways

$$|j,\ell\rangle = a_j^\dagger a_\ell^\dagger |0\rangle = a_\ell^\dagger a_j^\dagger |0\rangle = |\ell,j\rangle . \quad (\text{A.7.2})$$

Thus the actual Hilbert space dimension is only

$$\dim(\mathcal{H}_2) = L + \frac{L^2 - L}{2} = L + \frac{L(L-1)}{2} . \quad (\text{A.7.3})$$

Note that due to Eq. (A.7.2) for bosons the dimension of \mathcal{F}_2 is also given by Eq. (A.7.3), and the distinction between Fock space and Hilbert space is artificial. But allowing both $|j,\ell\rangle$ and $|\ell,j\rangle$ is much more convenient for Fourier transformation.

The overlap is given by

$$\langle j',\ell' | j,\ell \rangle = \delta_{j'j} \delta_{\ell'\ell} + \delta_{j'\ell} \delta_{\ell'j} . \quad (\text{A.7.4})$$

When expressing the two-particle Fock basis in real space, one can also choose the basis of one absolute and one relative coordinate

$$|j,j+d\rangle = |j,\ell\rangle \quad (\text{A.7.5})$$

with $d := \ell - j$ where for now $d \geq 0$ is assumed. One can now split the Fock space into sectors \mathcal{F}_2^j labeled by the first particle position j . Each sector holds one unique state $|j,j\rangle$ and $L-1$ states, that can be created in two different ways and therefore also appear in another sector since

$$\mathcal{F}_2^j \ni |j,j+d\rangle = |j+d,j\rangle \in \mathcal{F}_2^{j+d} . \quad (\text{A.7.6})$$

Therefore, if each state is attributed with one half to each sector, there are

$$\dim(\mathcal{H}_2^j) = 1 + \frac{(L-1)}{2} \quad (\text{A.7.7})$$

unique states in each sector. However, this is only an average number.

The important fact to note about this is that if L is even, this number is not an integer. It is therefore impossible to assign the same well-defined number of unique states to each j -sector, which is inconvenient for systematic handling of subspaces. For odd L , this problem does not occur.

As will be shown next, this problem carries over to momentum space and to the hybrid basis. Let $|q_1, q_2\rangle$ be a state with two particles of individual momenta q_1 and q_2

$$|q_1, q_2\rangle := \frac{1}{L} \sum_{j,\ell} e^{-iq_1 j - iq_2 \ell} |j,\ell\rangle . \quad (\text{A.7.8})$$

Total momentum Q and relative momentum q of the two particles are defined as in Eq. (A.2.9) and the center-of-mass coordinate r_{CM} and relative coordinate d as

$$r_{\text{CM}} := \frac{j+\ell}{2} \quad \text{and} \quad d := \frac{\ell-j}{2} , \quad (\text{A.7.9})$$

respectively. With this, the state $|q_1, q_2\rangle$ can also be written as Fourier transform of the center-of-mass and relative coordinates associated with total and relative momentum

$$|q_1, q_2\rangle = \frac{1}{L} \sum_{j,\ell} e^{-iq_1 j - iq_2 \ell} |j,\ell\rangle \quad (\text{A.7.10a})$$

$$= \frac{1}{L} \sum_{j,\ell} e^{-i\frac{Q-q}{2} j - i\frac{Q+q}{2} \ell} |j,\ell\rangle \quad (\text{A.7.10b})$$

$$= \frac{1}{L} \sum_{j,\ell} e^{-i(\frac{Q}{2} j + \frac{Q}{2} \ell) - i(\frac{q}{2} \ell - \frac{q}{2} j)} |j,\ell\rangle \quad (\text{A.7.10c})$$

$$= \frac{1}{L} \sum_{j,\ell} e^{-iQ\frac{j+\ell}{2} - iq\frac{\ell-j}{2}} |j,\ell\rangle \quad (\text{A.7.10d})$$

$$= \frac{1}{L} \sum_{j,d} e^{-iQr_{\text{CM}} - iq\frac{d}{2}} |j,j+d\rangle \quad (\text{A.7.10e})$$

$$= \frac{1}{L} \sum_{j,d} e^{-iQ\frac{2j+d}{2} - iq\frac{d}{2}} |j,j+d\rangle \quad (\text{A.7.10f})$$

$$= \frac{1}{L} \sum_{j,d} e^{-iQj - iQ\frac{d}{2} - iq\frac{d}{2}} |j,j+d\rangle. \quad (\text{A.7.10g})$$

Now, the hybrid basis defined in Eq. (6.14) is simply obtained by dropping the Fourier transformation in d .

Using TI and the real space overlap in Eq. (A.7.4), the overlap of two hybrid states is given by

$$\langle Q,d'|Q,d\rangle = e^{-iQ\frac{d-d'}{2}} \sum_{j'} e^{+iQj'} \langle j',j'+d'|0,d\rangle \quad (\text{A.7.11a})$$

$$= e^{-iQ\frac{d-d'}{2}} \sum_{j'} e^{+iQj'} (\delta_{j',0}\delta_{d',d} + \delta_{j',d}\delta_{d',-d}) \quad (\text{A.7.11b})$$

$$= e^{-iQ\frac{d-d'}{2}} (e^{+iQ0}\delta_{d',d} + e^{+iQd}\delta_{d',-d}) \quad (\text{A.7.11c})$$

$$= e^{-iQ\frac{d-d'}{2}} \delta_{d',d} + e^{+iQ\frac{d+d'}{2}} \delta_{d',-d}. \quad (\text{A.7.11d})$$

Equation (A.7.11d) shows that the states with $+d$ and $-d$ are the same, since they have an overlap of 1. Two states require special attention. Using this overlap definition, the $d=0$ state has norm $\sqrt{2}$ because for $d'=d=0$ both Kronecker deltas contribute. This is usually fixed by normalizing the bosonic creation operator a^\dagger

$$|n_i + 1\rangle = \frac{a_i^\dagger}{\sqrt{n_i + 1}} |n_i\rangle \quad (\text{A.7.12})$$

where n_i is the number of particles already present on site i . For hard-core bosons this is not required since $(a_i^\dagger)^2 = 0$. See Sec. A.10 on how the hard-core constraint is handled for the purposes of this thesis.

The second state with special properties is the one with $d = \frac{L}{2}$ which can only occur for even L . Then, with PBC, $d = \frac{L}{2} \Leftrightarrow d = -\frac{L}{2}$. This means that as for $d=0$ both Kronecker deltas are 1. However, the phases are non-trivial. Note that the discretized momentum can be written as

$$Q = n_Q \Delta Q = n_Q \frac{2\pi}{L}, \quad n_Q \in \{0, \dots, L-1\} \quad (\text{A.7.13})$$

where the set of n_Q was chosen for convenience. The norm of the state $|Q, \frac{L}{2}\rangle$ is

$$\left\langle Q, \frac{L}{2} \left| Q, \frac{L}{2} \right. \right\rangle = e^{-iQ\frac{1}{2}(\frac{L}{2} - \frac{L}{2})} + e^{+iQ\frac{1}{2}(\frac{L}{2} + \frac{L}{2})} \quad (\text{A.7.14a})$$

$$= 1 + e^{iQ\frac{L}{2}} \quad (\text{A.7.14b})$$

$$= 1 + e^{in_Q \frac{2\pi}{L} \frac{L}{2}} \quad (\text{A.7.14c})$$

$$= 1 + e^{in_Q \pi} \quad (\text{A.7.14d})$$

$$= \begin{cases} 2, & \text{if } n_Q \text{ even} \\ 0, & \text{if } n_Q \text{ odd} \end{cases}. \quad (\text{A.7.14e})$$

Therefore, there are $\frac{L}{2}$ states in even n_Q sectors and $\frac{L}{2} - 1$ states in odd n_Q sectors. This is consistent with the average half-integer number of unique states in each j sector found in Eq. (A.7.7). With $\frac{L}{2}$ odd and $\frac{L}{2}$ even values for n_Q , the overall number of unique states is still

$$\underbrace{\frac{L}{2} \left(1 + \frac{L}{2}\right)}_{n_Q \text{ even}} + \underbrace{\frac{L}{2} \left(1 + \frac{L}{2} - 1\right)}_{n_Q \text{ odd}} = L + \frac{L(L-1)}{2}. \quad (\text{A.7.15})$$

However, the alternating number of unique states makes an even L_q an inconvenient choice, since it requires different handling for even and odd Q sectors. This is the reason, why for this thesis L_q is always chosen odd. This choice also avoids the problem, that the $d = \frac{L}{2}$ state has norm $\sqrt{2}$ where it exists, which would require additional normalization.

Obviously, there are $L = L_q$ possible values for the total momentum in the first Brillouin zone. In each Q sector, there is one unique state with $d = 0$. Since the states for $+d$ and $-d$ are equivalent as expected for bosons, there are then $\frac{L-1}{2}$ more unique states in each Q sector for odd L_q . This amounts once more to

$$L \left(1 + \frac{L-1}{2}\right) = L + \frac{L(L-1)}{2} \quad (\text{A.7.16})$$

unique states total, in accordance with Eq. (A.7.3).

A.8 Gram-Schmidt orthonormalization without vectors

The Gram-Schmidt orthogonalization algorithm is a well known tool to orthogonalize a skew set of vectors. Given a set $\{w_i\}$ of skew vectors, an orthogonal set $\{v_i\}$ can be constructed from it iteratively by the following scheme

$$|v_1\rangle = |w_1\rangle \quad (\text{A.8.1a})$$

$$|v_n\rangle = |w_n\rangle - \sum_{j=1}^{n-1} \frac{\langle v_j | w_n \rangle}{\langle v_j | v_j \rangle} |v_j\rangle. \quad (\text{A.8.1b})$$

This means, each next orthogonal vector $|v_n\rangle$ is constructed by taking the vector $|w_n\rangle$ and subtracting contributions that are parallel to the orthogonal set $\{v_{j < n}\}$. Each orthogonal vector can be normalized easily in the end.

The 2QP states defined in Sec. 6.1 are orthonormal for large particle distances. As seen in Eq. (A.8.1a), the first vector in the Gram-Schmidt sequence is not changed. Therefore, the natural idea is to start with an orthonormal 2QP state for sufficiently large d and build an orthonormal basis of the 2QP sector by successively adding states with smaller d . Operators can then be evaluated in this new orthonormal 2QP basis.

However, unfortunately there is no vector space representation of the 2QP states in memory, and therefore the algorithm as it is stated in Eq. (A.8.1) cannot be used directly. Overlaps and matrix elements in the skew basis can be computed though. Therefore, a version of the algorithm that works with the metric tensor \tilde{G}

$$\tilde{G}_{ij} := \langle w_i | w_j \rangle \quad (\text{A.8.2})$$

and the operator matrix \tilde{O}

$$\tilde{O}_{ij} := \langle w_i | O | w_j \rangle \quad (\text{A.8.3})$$

in the skew basis must be formulated.

In order to keep the following calculations a bit tidier, an auxiliary matrix V is defined

$$V_{ij} := \begin{cases} \langle v_i | v_i \rangle, & \text{if } i = j \\ \langle v_i | w_j \rangle, & \text{if } i < j \\ 0, & \text{otherwise} \end{cases} \quad (\text{A.8.4})$$

i.e., the diagonal elements are the squared norms of the orthogonalized basis. The elements for $i < j$ (upper triangular part) are the expansion coefficients of the old basis $\{w_i\}$ in the new $\{v_i\}$. It will become evident below that the lower triangular part ($i > j$) must be zero. In terms of the elements of V , Eq. (A.8.1b) reads

$$|v_n\rangle = |w_n\rangle - \sum_{j < n} \frac{V_{jn}}{V_{jj}} |v_j\rangle. \quad (\text{A.8.5})$$

To find the required algorithm, the normalization of the orthogonalized basis of Eq. (A.8.1) is examined first

$$\langle v_n | v_n \rangle = \left\langle w_n - \sum_{j < n} \frac{V_{jn}^*}{V_{jj}} v_j \left| w_n - \sum_{j' < n} \frac{V_{j'n}}{V_{j'j'}} v_{j'} \right. \right\rangle \quad (\text{A.8.6a})$$

$$= \langle w_n | w_n \rangle - \left\langle w_n \left| \sum_{j' < n} \frac{V_{j'n}}{V_{j'j'}} v_{j'} \right. \right\rangle - \left\langle \sum_{j < n} \frac{V_{jn}^*}{V_{jj}} v_j \left| w_n \right. \right\rangle + \left\langle \sum_{j < n} \frac{V_{jn}^*}{V_{jj}} v_j \left| \sum_{j' < n} \frac{V_{j'n}}{V_{j'j'}} v_{j'} \right. \right\rangle \quad (\text{A.8.6b})$$

$$= \langle w_n | w_n \rangle - \sum_{j' < n} \frac{V_{j'n}}{V_{j'j'}} \langle w_n | v_{j'} \rangle - \sum_{j < n} \frac{V_{jn}^*}{V_{jj}} \langle v_j | w_n \rangle + \sum_{j < n} \sum_{j' < n} \frac{V_{jn}^*}{V_{jj}} \frac{V_{j'n}}{V_{j'j'}} \langle v_j | v_{j'} \rangle \quad (\text{A.8.6c})$$

$$= \tilde{G}_{nn} - \sum_{j' < n} \frac{V_{j'n} V_{j'n}^*}{V_{j'j'}} - \sum_{j < n} \frac{V_{jn}^* V_{jn}}{V_{jj}} + \sum_{j < n} \frac{V_{jn}^* V_{jn}}{V_{jj}^2} V_{jj} + \sum_{j < n} \sum_{j' < n, j' \neq j} \frac{V_{jn}^*}{V_{jj}} \frac{V_{j'n}}{V_{j'j'}} \underbrace{\langle v_j | v_{j'} \rangle}_{=0} \quad (\text{A.8.6d})$$

$$= \tilde{G}_{nn} - \sum_{j < n} \frac{|V_{jn}|^2}{V_{jj}} \quad (\text{A.8.6e})$$

where in line (A.8.6d) the terms of the double sum with $j' = j$ were separated from those with $j' \neq j$. Now one can see that separating the $i = j$ case in Eq. (A.8.4) is somewhat artificial, since actually

$$\langle v_j | w_j \rangle = \left\langle w_j - \sum_{k < j} \frac{V_{kj}^*}{V_{kk}} v_k \left| w_j \right. \right\rangle \quad (\text{A.8.7a})$$

$$= \langle w_j | w_j \rangle - \sum_{k < j} \frac{V_{kj}^*}{V_{kk}} \langle v_k | w_j \rangle \quad (\text{A.8.7b})$$

$$= \tilde{G}_{jj} - \sum_{k < j} \frac{|V_{kj}|^2}{V_{kk}} \quad (\text{A.8.7c})$$

$$= \langle v_j | v_j \rangle. \quad (\text{A.8.7d})$$

From this and Eq. (A.8.5) follows that the vector $|w_n\rangle$ from the skew basis can be expressed as an expansion in the new basis $\{|v_i\rangle\}$ as

$$|w_n\rangle = |v_n\rangle + \sum_{j<n} \frac{V_{jn}}{V_{jj}} |v_j\rangle = \sum_{j\leq n} \frac{V_{jn}}{V_{jj}} |v_j\rangle \quad (\text{A.8.8a})$$

$$= \sum_j \frac{V_{jn}}{V_{jj}} |v_j\rangle. \quad (\text{A.8.8b})$$

The last equality holds since by construction the subsets $\{|w_1\rangle, \dots, |w_n\rangle\}$ and $\{|v_1\rangle, \dots, |v_n\rangle\}$ span the same vector space. From this follows that all expansion coefficients V_{ij} with $i > j$ must be zero (cf Eq. (A.8.4)).

It thus remains to be shown what the coefficients V_{ij} for $i < j$ look like. Since Eq. (A.8.1) is an iterative scheme, only a recursive definition can be given

$$V_{ij} = \langle v_i | w_j \rangle = \langle w_i | w_j \rangle - \sum_{k<i} \frac{V_{ki}^*}{V_{kk}} \langle v_k | w_j \rangle \quad (\text{A.8.9a})$$

$$= \langle w_i | w_j \rangle - \sum_{k<i} \frac{V_{ki}^* V_{kj}}{V_{kk}} \quad (\text{A.8.9b})$$

$$\text{with } \langle v_1 | w_1 \rangle = \langle v_1 | v_1 \rangle = \langle w_1 | w_1 \rangle. \quad (\text{A.8.9c})$$

This means that V can be computed iteratively column-wise, from left to right and from the top down to the diagonal element.

Then, the matrix elements of the operator in the orthonormal basis are given by

$$\frac{\langle v_i | \hat{O} | v_j \rangle}{\| |v_i\rangle \| \| |v_j\rangle \|} = \frac{1}{\sqrt{V_{ii} V_{jj}}} \left\langle w_i - \sum_{k<i} \frac{V_{ki}^*}{V_{kk}} v_k \left| \hat{O} \right| w_j - \sum_{k'<j} \frac{V_{k'j}}{V_{k'k'}} v_{k'} \right\rangle \quad (\text{A.8.10a})$$

$$= \frac{1}{\sqrt{V_{ii} V_{jj}}} \left[\tilde{O}_{ij} - \sum_{k<i} \frac{V_{ki}^*}{V_{kk}} \langle v_k | \hat{O} | w_j \rangle - \sum_{k'<j} \frac{V_{k'j}}{V_{k'k'}} \langle w_i | \hat{O} | v_{k'} \rangle + \sum_{k<i} \sum_{k'<j} \frac{V_{ki}^* V_{k'j}}{V_{kk} V_{k'k'}} \langle v_k | \hat{O} | v_{k'} \rangle \right]. \quad (\text{A.8.10b})$$

With a second auxiliary matrix W defined as

$$W_{ij} = \langle w_i | \hat{O} | v_j \rangle \quad (\text{A.8.11})$$

and $O_{ij} = \langle v_i | \hat{O} | v_j \rangle$ being the elements of the operator in the orthogonalized basis this becomes

$$\frac{O_{ij}}{\| |v_i\rangle \| \| |v_j\rangle \|} = \frac{1}{\sqrt{V_{ii} V_{jj}}} \left[\tilde{O}_{ij} - \sum_{k<i} \frac{V_{ki}^*}{V_{kk}} W_{jk} - \sum_{k'<j} \frac{V_{k'j}}{V_{k'k'}} W_{ik'} + \sum_{k<i} \sum_{k'<j} \frac{V_{ki}^* V_{k'j}}{V_{kk} V_{k'k'}} O_{kk'} \right]. \quad (\text{A.8.12})$$

The elements W_{ij} are given by

$$W_{ij} = \left\langle w_i \left| \hat{O} \right| w_j - \sum_{k<j} \frac{V_{kj}}{V_{kk}} v_k \right\rangle \quad (\text{A.8.13a})$$

$$= \langle w_i | \hat{O} | w_j \rangle - \sum_{k<j} \frac{V_{kj}}{V_{kk}} \langle w_i | \hat{O} | v_k \rangle \quad (\text{A.8.13b})$$

$$= \tilde{O}_{ij} - \sum_{k<j} \frac{V_{kj}}{V_{kk}} W_{ik}, \quad (\text{A.8.13c})$$

i.e., they can be computed row-wise, recursively. For $i = 1$ the computation simplifies considerably, yielding

$$\frac{O_{1j}}{\| |v_1\rangle \| \| |v_j\rangle \|} = \frac{1}{\sqrt{V_{11}V_{jj}}} \left[\tilde{O}_{1j} - \sum_{k < j} \frac{V_{kj}}{V_{kk}} O_{1k} \right]. \quad (\text{A.8.14})$$

As stated in the beginning of this section, in iMPS computations no direct vector space representation of the states is available, that would allow the application of the orthogonalization scheme as defined in Eq. (A.8.1). But, by first computing the auxiliary matrices V and W , the Gram-Schmidt orthogonalization can be applied using only overlaps and matrix elements computed in the skew basis. These can be computed in the iMPS formalism.

A.9 2QP basis transformations

This section provides a reference summary of the different bases used to describe 2QP states, as well as the transformations for overlaps and matrix elements between them. Note that in all Fourier transformations L is the number of lattice sites. Since all numerical momentum space computations require a discretization of momentum, a finite system with PBC is implied for which

$$L = L_q \quad (\text{A.9.1})$$

holds, where L_q is the number of momentum intervals in the first Brillouin zone (cf. Sec. 5.3).

The *real space* basis is obtained by “applying the creation operator twice”. It can be expressed using two independent coordinates j and k

$$|j, k\rangle := a_j^\dagger a_k^\dagger |GS\rangle \quad (\text{A.9.2})$$

or equivalently with one absolute coordinate j and the particle distance $d = k - j$

$$|j, j + d\rangle := a_j^\dagger a_{j+d}^\dagger |GS\rangle. \quad (\text{A.9.3})$$

Taking the Fourier transform in both coordinates yields the momentum space basis of *individual particle momenta*

$$|q_1, q_2\rangle := \frac{1}{L} \sum_{j, k} e^{-iq_1 j} e^{-iq_2 k} |j, k\rangle \quad (\text{A.9.4a})$$

$$= \frac{1}{L} \sum_{j, d} e^{-iq_1 j} e^{-iq_2(j+d)} |j, j + d\rangle \quad (\text{A.9.4b})$$

$$= \frac{1}{L} \sum_{j, d} e^{-i(q_1+q_2)j} e^{-iq_2 d} |j, j + d\rangle. \quad (\text{A.9.4c})$$

The last equality naturally leads to the definition of total momentum

$$Q = q_1 + q_2 \quad (\text{A.9.5})$$

and the basis of *total momentum and one particle momentum*

$$|Q, q_1\rangle := \frac{1}{L} \sum_{j,d} e^{-iQj} e^{-i(Q-q_1)d} |j, j+d\rangle \quad (\text{A.9.6a})$$

$$= \frac{1}{L} \sum_{j,d} e^{-iQj} e^{-iQd} e^{+iq_1d} |j, j+d\rangle . \quad (\text{A.9.6b})$$

Introducing also relative momentum

$$q = q_2 - q_1 \quad (\text{A.9.7})$$

and inserting the resulting expression for q_2

$$q_2 = \frac{Q+q}{2} . \quad (\text{A.9.8})$$

into Eq. (A.9.4c) yields the basis of *total and relative momentum*

$$|Q, q\rangle := \frac{1}{L} \sum_{j,d} e^{-iQj} e^{-i\frac{Q+q}{2}d} |j, j+d\rangle \quad (\text{A.9.9a})$$

$$= \frac{1}{L} \sum_{j,d} e^{-iQj} e^{-iQ\frac{d}{2}} e^{-iq\frac{d}{2}} |j, j+d\rangle . \quad (\text{A.9.9b})$$

Note, that relative momentum q is associated with $\frac{d}{2}$ rather than d . Finally, dropping the Fourier transformation in relative distance d defines the *hybrid basis*

$$|Q, d\rangle := \frac{1}{\sqrt{L}} e^{-iQ\frac{d}{2}} \sum_j e^{-iQj} |j, j+d\rangle . \quad (\text{A.9.10})$$

The inverse transformations from momentum space and the hybrid basis to real space read

$$|j, j+d\rangle = \frac{1}{L} \sum_{Q, q_1} e^{+iQ(j+d)} e^{-iq_1d} |Q, q_1\rangle \quad (\text{A.9.11a})$$

$$= \frac{1}{\sqrt{L}} \sum_Q e^{+iQ\frac{d}{2}} e^{+iQj} |Q, d\rangle . \quad (\text{A.9.11b})$$

Inserting Eq. (A.9.11a) into Eq. (A.9.10) yields the transformation from momentum space to the hybrid basis

$$|Q, d\rangle = \frac{1}{L\sqrt{L}} e^{-iQ\frac{d}{2}} \sum_j e^{-iQj} \left(\sum_{Q', q_1} e^{+iQ'(j+d)} e^{-iq_1d} |Q', q_1\rangle \right) \quad (\text{A.9.12a})$$

$$= \frac{1}{\sqrt{L}} e^{-iQ\frac{d}{2}} \sum_{Q', q_1} \underbrace{\left(\frac{1}{L} \sum_j e^{i(Q'-Q)j} \right)}_{=\delta_{Q, Q'}} e^{i(Q'-q_1)d} |Q', q_1\rangle \quad (\text{A.9.12b})$$

$$= \frac{1}{\sqrt{L}} e^{+iQ\frac{d}{2}} \sum_{q_1} e^{-iq_1d} |Q, q_1\rangle , \quad (\text{A.9.12c})$$

which is easily inverted to

$$|Q, q_1\rangle = \frac{1}{\sqrt{L}} \sum_d e^{-iQ\frac{d}{2}} e^{+iq_1d} |Q, d\rangle . \quad (\text{A.9.13})$$

For the purposes of this thesis, the metric tensor N and operator tensors O are computed either in the real space basis

$$N_{j,d}^{j',d'} := \langle j', j' + d' | 0, d \rangle \quad (\text{A.9.14a})$$

$$O_{j,d}^{j',d'} := \langle j', j' + d' | O_0 | j, j + d \rangle, \quad (\text{A.9.14b})$$

or in the (Q, q_1) -basis

$$N_{q'_1, q_1}^Q := \langle Q, q'_1 | Q, q_1 \rangle \quad (\text{A.9.15a})$$

$$O_{q'_1, q_1}^Q := \langle Q, q'_1 | O_0 | Q, q_1 \rangle. \quad (\text{A.9.15b})$$

A note on the number of indices is in order at this point. Due to TI, the real space overlap actually only depends on *three* relative distances, not four coordinates, which allows to fix one of the absolute indices j' or j . In Eq. (A.9.14a) j was fixed to 0. In contrast, the real space matrix element potentially depends on the relative distances of all *four* particles from the operator position. Now consider the transformation of a matrix element from real space to the (Q, q_1) basis

$$O_{q'_1, q_1}^Q = \frac{1}{L^2} \sum_{j', d'} \sum_{j, d} e^{+iQj' + iQd' - iq'_1 d'} e^{-iQj - iQd + iq_1 d} \langle j', j' + d' | O_0 | j, j + d \rangle \quad (\text{A.9.16a})$$

$$= \frac{1}{L^2} \sum_{j', d'} \sum_{j, d} e^{iQ(j' - j + d' - d)} e^{-iq'_1 d' + iq_1 d} O_{j, d}^{j', d'}. \quad (\text{A.9.16b})$$

Apparently, one index was “lost” in the transformation. Actually, it went into the assumption, that the operator is total momentum conserving, and therefore Q must be the same in both states. This is, what allows to use the orthogonality argument to treat each Q -sector independently, and it is the reason why total momentum is chosen as the primary quantum number. This means, that the matrix element Eq. (A.9.14b) can in fact not really depend on all the distances independently for momentum conserving operators O . However, the relation is not apparent from the definition. And especially in the case of a non-orthogonal basis, the transformation Eq. (A.9.16) is not generally invertible.

But, this is not a requirement for the matrix elements of the Hamiltonians under consideration here. Since they are translation invariant themselves, their matrix elements only depend on *three* distances, like the overlap

$$H_{j,d}^{j',d'} = \langle j', j' + d' | \tilde{H} | j, j + d \rangle = \langle j', j' + d' | \tilde{H} | 0, d \rangle = H_{d', d}^{j'}. \quad (\text{A.9.17})$$

In order to apply the Gram-Schmidt algorithm in a well defined manner, these results need to be transformed into the hybrid basis using

$$N_{d', d}^Q = \frac{1}{L} e^{iQ \frac{d-d'}{2}} \sum_{q'_1, q_1} e^{iq'_1 d'} e^{-iq_1 d} N_{q'_1, q_1}^Q \quad (\text{A.9.18a})$$

$$O_{d', d}^Q = \frac{1}{L} e^{iQ \frac{d-d'}{2}} \sum_{q'_1, q_1} e^{iq'_1 d'} e^{-iq_1 d} O_{q'_1, q_1}^Q \quad (\text{A.9.18b})$$

and

$$N_{d',d}^Q = \frac{1}{L} e^{iQ\frac{d-d'}{2}} \sum_{j',j} e^{iQ(j'-j)} \langle j', j' + d' | j, j + d \rangle \quad (\text{A.9.19a})$$

$$= e^{iQ\frac{d-d'}{2}} \sum_{j'} e^{iQj'} \langle j', j' + d' | 0, d \rangle \quad (\text{A.9.19b})$$

$$= e^{iQ\frac{d-d'}{2}} \sum_{j'} e^{iQj'} N_{d',d}^{j'} \quad (\text{A.9.19c})$$

$$O_{d',d}^Q = \frac{1}{L} e^{iQ\frac{d-d'}{2}} \sum_{j',j} e^{iQ(j'-j)} O_{j,d}^{j',d'} \quad (\text{A.9.19d})$$

respectively, where in Eq. (A.9.19) again TI was used to fix $j = 0$.

Following the application of the Gram-Schmidt orthonormalization, the operator tensor can be transformed back to real or momentum space as needed by

$$O_{q'_1, q_1}^Q = \frac{1}{L} \sum_{d',d} e^{iQ\frac{d'-d}{2}} e^{-iq'_1 d'} e^{+iq_1 d} O_{d',d}^Q \quad (\text{A.9.20})$$

and

$$O_{d',d}^{j'} = \frac{1}{L} \sum_Q e^{iQ\frac{d'-d}{2}} e^{iQj'} O_{d',d}^Q \quad (\text{A.9.21})$$

Matrix elements coupling the 2QP subspace to the 1QP subspace, and also the spurious overlaps between these subspaces

$$O_j^{j',d'} := \langle j', j' + d' | O_0 | j \rangle \quad (\text{A.9.22a})$$

$$N^{j',d'} := \langle j', j' + d' | 0 \rangle \quad (\text{A.9.22b})$$

$$O_{q'_1}^Q := \langle Q, q'_1 | O_0 | Q \rangle \quad (\text{A.9.22c})$$

$$N_{q_1}^Q := \langle Q, q_1 | Q \rangle \quad (\text{A.9.22d})$$

need to be transformed in the same way. With the one-particle momentum eigenstate

$$|Q\rangle := \frac{1}{\sqrt{L}} \sum_j e^{-iQj} |j\rangle \quad (\text{A.9.23})$$

the transformations from momentum space to the hybrid basis and vice versa are

$$N_{d'}^Q = \frac{1}{\sqrt{L}} \sum_{q'_1} e^{-iQ\frac{d'}{2}} e^{iq'_1 d'} N_{q'_1}^Q \quad (\text{A.9.24a})$$

$$O_{d'}^Q = \frac{1}{\sqrt{L}} \sum_{q'_1} e^{-iQ\frac{d'}{2}} e^{iq'_1 d'} O_{q'_1}^Q \quad (\text{A.9.24b})$$

$$O_{q'_1}^Q = \frac{1}{\sqrt{L}} \sum_{d'} e^{+iQ\frac{d'}{2}} e^{-iq'_1 d'} O_{d'}^Q \quad (\text{A.9.24c})$$

and from real space to the hybrid basis and back

$$N_{d'}^Q = \frac{1}{L} e^{+iQ\frac{d'}{2}} \sum_{j',j} e^{+iQ(j'-j)} \langle j', j' + d' | j \rangle \quad (\text{A.9.25a})$$

$$= e^{+iQ\frac{d'}{2}} \sum_{j'} e^{+iQj'} N^{j',d'} \quad (\text{A.9.25b})$$

$$O_{d'}^Q = \frac{1}{L} e^{+iQ\frac{d'}{2}} \sum_{j',j} e^{+iQ(j'-j)} O_j^{j',d'} \quad (\text{A.9.25c})$$

$$O^{j',d'} = \frac{1}{\sqrt{L}} \sum_Q e^{-iQ\frac{d'}{2}} e^{-iQj'} O_{d'}^Q. \quad (\text{A.9.25d})$$

Note that there is no need to transform the metric tensor back from the orthogonalized hybrid basis, since in this basis it is simply the identity.

A.10 Hard-core bosons in momentum space

In real space, the hard-core constraint

$$(a_i^\dagger)^2 |0\rangle = 0 \quad (\text{A.10.1})$$

is completely local and easy to interpret. However, in momentum space it is not as transparent.

A.10.1 Hard-core bosonic metric tensor in momentum space

A momentum space representation of the hard-core constraint can be found by noting the following. Instead of directly applying the constraint Eq. (A.10.1), one can carry out calculations with ordinary, unnormalized bosons, and subtract all contributions from states with doubly occupied sites “by hand”. For instance, the overlap of two 2QP states with hard-core bosons is then given by

$$\langle j', \ell' | j, \ell \rangle = \delta_{j',j} \delta_{\ell',\ell} + \delta_{j',\ell} \delta_{\ell',j} - 2\delta_{j',j} \delta_{j',\ell'} \delta_{j,\ell} \quad (\text{A.10.2})$$

or in the formulation with particle distance d as

$$\langle j', j' + d' | j, j + d \rangle = \delta_{j',j} \delta_{d',d} + \delta_{j',j+d} \delta_{d',-d} - 2\delta_{j',j} \delta_{d,0} \delta_{d',0}. \quad (\text{A.10.3})$$

Now, one can again take the Fourier transform in both coordinates yielding

$$\langle q'_1, q'_2 | q_1, q_2 \rangle = \frac{1}{L^2} \sum_{j',\ell'} \sum_{j,\ell} e^{+iq'_1 j' + iq'_2 \ell'} e^{-iq_1 j - iq_2 \ell} (\delta_{j',j} \delta_{\ell',\ell} + \delta_{j',\ell} \delta_{\ell',j} - 2\delta_{j',j} \delta_{j',\ell'} \delta_{j,\ell}) \quad (\text{A.10.4a})$$

$$= \frac{1}{L^2} \sum_{j,\ell} \left[e^{+iq'_1 j + iq'_2 \ell} e^{-iq_1 j - iq_2 \ell} + e^{+iq'_1 \ell + iq'_2 j} e^{-iq_1 j - iq_2 \ell} - 2e^{iq'_1 j + iq'_2 j} e^{-iq_1 j - iq_2 \ell} \delta_{j,\ell} \right] \quad (\text{A.10.4b})$$

$$= \frac{1}{L^2} \sum_{j,\ell} \left[e^{i(q'_1 - q_1)j} e^{i(q'_2 - q_2)\ell} + e^{i(q'_1 - q_2)j} e^{i(q'_2 - q_1)\ell} \right] - \frac{2}{L^2} \sum_j e^{i(q'_1 + q'_2 - q_1 - q_2)j} \quad (\text{A.10.4c})$$

$$= \delta_{q'_1, q_1} \delta_{q'_2, q_2} + \delta_{q'_1, q_2} \delta_{q'_2, q_1} - \frac{2}{L} \delta_{q'_1 + q'_2, q_1 + q_2}. \quad (\text{A.10.4d})$$

In each of the contributions the Kronecker deltas ensure the conservation of total momentum, i.e.,

$$q'_1 + q'_2 = q_1 + q_2 = Q. \quad (\text{A.10.5})$$

If this condition is considered to be implied in all overlaps, Eq. (A.10.4) can be simplified to

$$\langle q'_1, q'_2 | q_1, q_2 \rangle = \delta_{q'_1, q_1} + \delta_{q'_1, q_2} - \frac{2}{L}. \quad (\text{A.10.6})$$

One can now identify the correction term $-\frac{2}{L}$ as the momentum space formulation of the hard-core constraint.

The basis $|q_1, q_2\rangle$ can be made unique by the condition $q_2 \geq q_1$. The metric tensor of this basis including the hard-core constraint has one eigenvalue (EV) equal to zero, which accounts for the reduced dimensionality of the Hilbert space of hard-core bosons. But, the state corresponding to this zero EV does not have a simple or intuitive form.

A.10.2 Hard-core corrections for bilinear Hamiltonians

In order to determine the 2QP interaction matrix elements from evaluating the Hamiltonian in the 2QP subspace, the contribution from the 1QP part of the Hamiltonian must be subtracted (cf. Eq. (6.66)). See also Ref. [97] for a detailed discussion. While in the 1QP subspace the particles behave like normal bosons, in the 2QP subspace the hard-core constraint becomes important. Again, calculations can be carried out with normal bosons, if all the contributions from states with double occupancies are subtracted.

In this section, these hard-core corrections for a generic bilinear Hamiltonian are derived, because in any particle-number conserving model this is what the 1QP part of the effective Hamiltonian is. Let the one-particle Hamiltonian be

$$H_{1P} = \sum_i \sum_\delta \frac{1}{2} \left(t_\delta a_i^\dagger a_{i+\delta} + t_\delta^* a_{i+\delta}^\dagger a_i \right) \quad (\text{A.10.7})$$

where a^\dagger (a) creates (annihilates) an effective particle and t_δ is the hopping amplitude for distance δ , i.e. t_0 is the local on-site energy, $t_{\pm 1}$ is the nearest neighbor hopping element etc. The hopping amplitudes are the Fourier transform of the dispersion and vice versa

$$t_\delta = \frac{1}{L} \sum_q e^{+iq\delta} \omega_q \quad (\text{A.10.8a})$$

$$\omega_q = \sum_\delta e^{-iq\delta} t_\delta = t_0 + 2 \sum_{\delta>0} \Re(t_\delta) \cos(q\delta) + \Im(t_\delta) \sin(q\delta). \quad (\text{A.10.8b})$$

In equilibrium, the relation

$$t_{-\delta} = t_\delta^* \quad (\text{A.10.9})$$

must hold, since otherwise the system would favor hopping in one direction. Reflection symmetry even yields $t_{-\delta} = t_\delta$, which simplifies Eq. (A.10.8b).

To determine the momentum space hard-core correction, all matrix elements from states with double occupancies in real space must be found first. In a translation invariant system, the sum over all lattice sites (index i in Eq. (A.10.7)) only yields a factor of L , therefore it suffices to do the calculations for $i = 0$.

In an orthonormal 2QP basis $|j, j+d\rangle$ the first term yields

$$\begin{aligned} \langle j', j' + d' | \sum_{\delta} \frac{1}{2} t_{\delta} a_0^{\dagger} a_{\delta} | j, j + d \rangle \\ = \sum_{\delta} \frac{1}{2} t_{\delta} [(\langle j' + d' | \delta_{0, j'} + \langle j' | \delta_{0, j' + d'})(\delta_{\delta, j} | j + d \rangle + \delta_{\delta, j + d} | j \rangle)] \end{aligned} \quad (\text{A.10.10a})$$

$$\begin{aligned} = \sum_{\delta} \frac{1}{2} t_{\delta} [\delta_{0, j'} \delta_{\delta, j} \delta_{j' + d', j + d} + \delta_{0, j'} \delta_{\delta, j + d} \delta_{j' + d', j} \\ + \delta_{0, j' + d'} \delta_{\delta, j} \delta_{j', j + d} + \delta_{0, j' + d'} \delta_{\delta, j + d} \delta_{j', j}] . \end{aligned} \quad (\text{A.10.10b})$$

Evaluating the second term analogously yields the full matrix element as

$$\begin{aligned} \langle j', j' + d' | H_{1P} | j, j + d \rangle |_{i=0} \\ = \frac{1}{2} \sum_{\delta} \left[t_{\delta} (\delta_{0, j'} (\delta_{\delta, j} \delta_{j' + d', j + d} + \delta_{\delta, j + d} \delta_{j' + d', j}) \right. \\ \quad + \delta_{0, j' + d'} (\delta_{\delta, j} \delta_{j', j + d} + \delta_{\delta, j + d} \delta_{j', j}) \\ \quad + t_{\delta}^* (\delta_{j', \delta} (\delta_{j, 0} \delta_{j' + d', j + d} + \delta_{j + d, 0} \delta_{j' + d', j}) \\ \quad \left. + \delta_{j' + d', \delta} (\delta_{j, 0} \delta_{j', j + d} + \delta_{j + d, 0} \delta_{j', j})) \right] . \end{aligned} \quad (\text{A.10.11})$$

The matrix elements relevant for the hard-core correction are those with $d = 0$ or $d' = 0$. For $d' = 0$ the expression in Eq. (A.10.11) becomes

$$\begin{aligned} \langle j', j' + d' | H_{1P} | j, j + d \rangle |_{i=0, d'=0} = \frac{1}{2} \sum_{\delta} \left[t_{\delta} 2\delta_{0, j'} (\delta_{j, \delta} \delta_{j', j + d} + \delta_{j + d, \delta} \delta_{j', j}) \right. \\ \quad \left. + t_{\delta}^* 2\delta_{j', d} (\delta_{0, j} \delta_{j', j + d} + \delta_{0, j + d} \delta_{j', j}) \right] \end{aligned} \quad (\text{A.10.12})$$

and for $d = 0$

$$\begin{aligned} \langle j', j' + d' | H_{1P} | j, j + d \rangle |_{i=0, d=0} = \frac{1}{2} \sum_{\delta} \left[t_{\delta} 2\delta_{j, \delta} (\delta_{0, j'} \delta_{j' + d', j} + \delta_{0, j' + d'} \delta_{j', j}) \right. \\ \quad \left. + t_{\delta}^* 2\delta_{0, j} (\delta_{j', \delta} \delta_{j' + d', j} + \delta_{j' + d', \delta} \delta_{j', j}) \right] . \end{aligned} \quad (\text{A.10.13})$$

However, summing both contributions overcounts the matrix elements with $d' = d = 0$, since they appear in both cases. Therefore, they must be calculated and subtracted once

$$\begin{aligned} -\langle j', j' + d' | H_{1P} | j, j + d \rangle |_{i=0, d'=d=0} \\ = -\frac{1}{2} \sum_{\delta} \left[t_{\delta} (\delta_{0, j'} (\delta_{j, \delta} \delta_{j', j} + \delta_{j, \delta} \delta_{j', j}) + \delta_{j, \delta} (\delta_{0, j'} \delta_{j', j} + \delta_{0, j'} \delta_{j', j})) \right. \\ \quad \left. + t_{\delta}^* (\delta_{j', \delta} (\delta_{0, j'} \delta_{j', j} + \delta_{0, j} \delta_{j', j}) + \delta_{0, j} (\delta_{j', \delta} \delta_{j', j} + \delta_{j', \delta} \delta_{j', j})) \right] \end{aligned} \quad (\text{A.10.14a})$$

$$= -\frac{1}{2} \sum_{\delta} [(t_{\delta} + t_{\delta}^*) 4\delta_{0, j'} \delta_{j, \delta} \delta_{j', j}] \quad (\text{A.10.14b})$$

$$= -4t_0 \delta_{0, j'} \delta_{j, \delta} \delta_{j', j} \quad (\text{A.10.14c})$$

where the last equality holds since the on-site energy t_0 must be real. Taking the Fourier

transform of Eqs. (A.10.12), (A.10.13) and (A.10.14) yields

$$\begin{aligned}
& \langle q'_1, q'_2 | H_{1P} | q_1, q_2 \rangle \Big|_{d'=0, d=0} \\
&= \frac{1}{L} \sum_{j', j} \sum_{d', d} \left\{ \sum_{\delta} e^{+iq'_1 j' + iq'_2 (j' + d')} e^{-iq_1 j - iq_2 (j + d)} \right. \\
&\quad \times \left[t_{\delta} (\delta_{0, j'} \delta_{d', 0} (\delta_{j, \delta} \delta_{d, -\delta} + \delta_{0, j} \delta_{d, \delta}) + \delta_{j, \delta} \delta_{d, 0} (\delta_{0, j'} \delta_{d', \delta} + \delta_{j', \delta} \delta_{d', -\delta})) \right. \\
&\quad \left. + t_{\delta}^* (\delta_{j', \delta} \delta_{d', 0} (\delta_{0, j} \delta_{d, \delta} + \delta_{j, \delta} \delta_{d, -\delta}) + \delta_{0, j} \delta_{d, 0} (\delta_{j', \delta} \delta_{d', -\delta} + \delta_{0, j'} \delta_{d', \delta})) \right] \\
&\quad \left. - 4t_0 \delta_{0, j'} \delta_{0, j} \delta_{d', 0} \delta_{d, 0} \right\} \tag{A.10.15a}
\end{aligned}$$

$$\begin{aligned}
&= \frac{1}{L} \left\{ \sum_{\delta} \left[t_{\delta} \left(e^{-iq_1 \delta} + e^{-iq_2 \delta} + e^{+iq'_2 \delta - i(q_1 + q_2) \delta} + e^{+iq'_1 \delta - i(q_1 + q_2) \delta} \right) \right. \right. \\
&\quad \left. \left. + t_{\delta}^* \left(e^{+i(q'_1 + q'_2) \delta - iq_2 \delta} + e^{+i(q'_1 + q'_2) \delta - iq_1 \delta} + e^{+iq'_1 \delta} + e^{+iq'_2 \delta} \right) \right] - 4t_0 \right\} \\
&\tag{A.10.15b}
\end{aligned}$$

$$\stackrel{(A.10.9)}{=} \frac{2}{L} \left\{ \sum_{\delta} t_{\delta} \left(e^{-iq_1 \delta} + e^{-iq_2 \delta} + e^{-iq'_2 \delta} + e^{-iq'_1 \delta} \right) - 2t_0 \right\} \tag{A.10.15c}$$

$$= \frac{2}{L} \left(\omega_{q_1} + \omega_{q_2} + \omega_{q'_1} + \omega_{q'_2} - 2t_0 \right) . \tag{A.10.15d}$$

In the step from (A.10.15b) to (A.10.15c) conservation of total momentum, i.e., relations of the type

$$q_1 + q_2 - q'_2 = Q - q'_2 = q'_1 \tag{A.10.16}$$

were used in addition to Eq. (A.10.9) to bring all exponentials to the form $e^{-iq\delta}$, so that the expressions can be identified as dispersion relations by means of Eq. (A.10.8b).

Appendix B

Efficient computation of 2QP quantities

Die Mühsal ist eine Erhaltungsgröße.
traditional, cited after Joachim Stolze

This appendix shows in detail how to compute the 2QP metric tensor and the matrix elements of the reduced Hamiltonian \tilde{H} efficiently in momentum space. Although this is the main result of this thesis, it is a lengthy calculation and a rather dry read, wherefore it is not contained in the main text.

The basic techniques are the same described in Chap. 6 to compute the 2QP-ground state matrix element. The reader is therefore encouraged to read sections 5.2 and 6.4 first, to familiarize with the concepts and notations. Sections B.2.1 and B.2.2 show in some detail how to compute the metric tensor. The matrix element is much more involved than the overlap, due to the additional relative distance, and because the operator thwarts the benefits of the left-canonical gauge when it acts to the left of all involved particles.

Section B.4 of this appendix also shows how to compute the 2QP-1QP matrix element. Albeit this matrix element vanishes for the particle-number conserving Hamiltonians under investigation, confirming this is a good way to assess how well the method is working.

Note that although the Hamiltonian is considered here explicitly, this scheme can of course be applied to any operator that has a matrix element of the same form.

B.1 General approach

In order to efficiently compute matrix elements in momentum space, one first needs to identify all types of topologically distinct TNs that can occur. Because there can be quite many of them, similar TN types are grouped together in so-called cases. For the 2QP matrix element, these cases are defined in Sec. B.3.3, and for the 2QP-1QP matrix element in Sec. B.4.2.

Each topologically distinct TN type from every case then needs to be analyzed, using the techniques from Sec. 6.4.1.

As always, primed letters j' , d' , $q_{\alpha'}$ etc. refer to the bra-state, i.e., the upper “rail” of the TN ladder. Plain letters like j , d , $q_{\bar{\alpha}}$ etc. refer to the ket-state, i.e., the lower rail.

In the Fourier transformations the relative particle distances d' and d are summed over both positive and negative values. This results in the same TN appearing four times, with

different configurations of the four C_q tensors. For instance

$$(B.1.1a)$$

$$(B.1.1b)$$

All four TNs can be addressed by the sum

$$\sum_{\alpha'=1,2} \sum_{\alpha=1,2} (B.1.2)$$

where

$$\bar{\alpha} := \begin{cases} 2, & \text{if } \alpha = 1 \\ 1, & \text{if } \alpha = 2 \end{cases} \quad \text{and} \quad \bar{\alpha}' := \begin{cases} 2, & \text{if } \alpha' = 1 \\ 1, & \text{if } \alpha' = 2 \end{cases}. \quad (B.1.3)$$

This allows the distances δ_i (see for instance TNs in Sec. B.3.3) between the operator and any particles or between any two particles to be defined strictly non-negative. They can therefore be described by powers of the transfer operator

$$T = \mathbb{1}^{(A;A)} \quad (B.1.4)$$

where T^0 is defined as not applying T at all, i.e.

$$T^0[m] := m \quad (B.1.5)$$

for any $D \times D$ matrix m .

For the 2QP overlap and the 2QP matrix element, the algorithm to determine the contribution of most TN types is therefore as follows.

1. Determine the particle positions j' , $j'+d'$, j and $j+d$ as functions of the non-negative distances δ_i for the momentum configuration $\alpha' = \alpha = 1$.
2. Insert the particle positions into the phase factor from the Fourier transformation, to express it in terms of the δ_i .

In order to write the contributions as sums over α' and α as in (B.1.2), the phase factor $\Phi_{\alpha'\alpha}$ must be known as function of α' and α . In Sec. B.2.1, it is calculated explicitly for all four momentum configurations for one type of TN. Equation (B.2.9) shows that the form of the phase factor is the same for all momentum configurations. Therefore, the general form $\Phi_{\alpha'\alpha}$ can be determined from the configuration $\alpha' = \alpha = 1$, simply by replacing q'_1 with $q_{\alpha'}$, q'_2 with $q_{\bar{\alpha}'}$ etc. in Φ_{11} .

3. Write the TN evaluation as a scalar product of an effective u , that describes the left part, and an effective v , that describes the right part.

4. Pull the summations over distances δ_i into the scalar product, so as to minimize the number of operator applications needed to compute the TN value.
5. Identify parts of the TN that were already calculated before.

Many effective u and v matrices appear in several different TN types. They can then be computed once and used whenever needed, which greatly increases the overall efficiency of the computation.

The TN types that require a slightly different approach are those, where there are one or more \mathbf{C} tensors on sites that the operator acts on. Note that the operator (in a product of local operators the first one) always acts on site $i = 0$, and, as always, n is the number of sites the operator acts on. For \mathbf{C} tensors on these sites, absolute site indices $\ell^{(l)}$ and $m^{(l)}$ are used, that each can take values from 0 to $n - 1$. They have to be included when determining the correct phase factor.

For the 2QP-1QP overlap and the 2QP-1QP matrix element, the procedure is in principle exactly the same. The only differences are that there are only three particle positions j' , $j' + d'$ and j instead of four, and only two momentum configurations enumerated by α' for each TN.

B.2 Metric tensor

The metric tensor in the skew momentum space basis consists of the 2QP overlaps $\langle Q, q'_1 | Q, q_1 \rangle$ and the spurious overlaps with the 1QP sector $\langle Q, q'_1 | Q \rangle$. For proper orthonormalization of operator matrices, the ground state must be included as well, but this is trivial since it is orthogonal to both 1QP and 2QP states in left-canonical gauge.

B.2.1 2QP overlap

The overlap of two two-particle states is given by

$$\langle Q, q'_1 | Q, q_1 \rangle = \frac{1}{L^2} \sum_{j', d'} \sum_{j, d} e^{+iQ(j'+d') - iq'_1 d'} e^{-iQ(j+d) + iq_1 d} \langle j', j' + d' | j, j + d \rangle \quad (\text{B.2.1a})$$

$$= \frac{1}{L^2} \sum_{j', d'} \sum_{j, d} e^{+iQ(j'+d') - iq'_1 d'} e^{-iQ(j+d) + iq_1 d} \times \langle \mathbf{C}_{q'_1, j'}; \mathbf{C}_{q'_2, j' + d'} | \mathbf{C}_{q_1, j}; \mathbf{C}_{q_2, j + d} \rangle \quad (\text{B.2.1b})$$

$$= \frac{1}{L} \sum_{j', d'} \sum_d e^{+iQ(j'+d') - iq'_1 d'} e^{-iQd + iq_1 d} \langle \mathbf{C}_{q'_1, j'}; \mathbf{C}_{q'_2, j' + d'} | \mathbf{C}_{q_1, 0}; \mathbf{C}_{q_2, d} \rangle . \quad (\text{B.2.1c})$$

For this overlap, the use of left-canonical gauge implies that the left \mathbf{C} tensors must be on the same site

$$\min(j', j' + d') = \min(j, j + d) , \quad (\text{B.2.2})$$

otherwise there is no contribution due to Eq. (5.10). This leaves three topologically distinct types of TNs, distinguished by the sign of

$$\delta := \max(j', j' + d') - \max(j, j + d) . \quad (\text{B.2.3})$$

Case i): $\delta > 0$

This case has the following characteristic TN

$$\langle C_{q'_1}, j'; C_{q'_2}, j' + d' | C_{q_1}, j; C_{q_2}, j + d \rangle = \text{Diagram} , \quad (\text{B.2.4})$$

which would not contribute in an orthogonal basis. For large δ_1 and/or δ_2 , the value of this TN converges to zero, since it then factorizes in one of the following ways

$$\langle C_{q'_1}, j'; C_{q'_2}, j' + d' | C_{q_1}, j; C_{q_2}, j + d \rangle \xrightarrow{\delta_1 \geq \bar{\epsilon}_T} \langle C_{q_{\alpha'}}, 0 | C_{q_{\alpha}}, 0 \rangle \underbrace{\langle C_{q_{\bar{\alpha}'}, \delta_2 + 1 | C_{q_{\alpha}}, 0 \rangle}_{=0} \quad (\text{B.2.5a})$$

$$\xrightarrow{\delta_2 \geq \bar{\epsilon}_T} \langle C_{q_{\alpha'}}, j' | C_{q_{\alpha}}, j; C_{q_{\bar{\alpha}}}, j + d \rangle \underbrace{\langle C_{q_{\bar{\alpha}'}, 0 | GS \rangle}_{=0} \quad (\text{B.2.5b})$$

$$\xrightarrow{\delta_1, \delta_2 \geq \bar{\epsilon}_T} \langle C_{q_{\alpha'}}, 0 | C_{q_{\alpha}}, 0 \rangle \underbrace{\langle GS | C_{q_{\bar{\alpha}}}, 0 \rangle}_{=0} \underbrace{\langle C_{q_{\bar{\alpha}'}, 0 | GS \rangle}_{=0} . \quad (\text{B.2.5c})$$

Since now both states are two-particle states, in contrast to Sec. 6.4.1, there are four C_q tensors with in general different momenta involved. Again the distances δ_1 and δ_2 are defined to be non-negative. With α and $\bar{\alpha}$ defined analogously to α' and $\bar{\alpha}'$ (cf. Eq. (6.38)) as

$$\alpha := \begin{cases} 1, & \text{if } d > 0 \\ 2, & \text{if } d < 0 \end{cases} \quad \text{and} \quad \bar{\alpha} := \begin{cases} 2, & \text{if } \alpha = 1 \\ 1, & \text{if } \alpha = 2 \end{cases} , \quad (\text{B.2.6})$$

there are $2 \cdot 2 = 4$ possible momentum configurations

$$\alpha' = 1, \alpha = 1, \quad d' > 0, d > 0 \quad (\text{B.2.7a})$$

$$\alpha' = 1, \alpha = 2, \quad d' > 0, d < 0 \quad (\text{B.2.7b})$$

$$\alpha' = 2, \alpha = 1, \quad d' < 0, d > 0 \quad (\text{B.2.7c})$$

$$\alpha' = 2, \alpha = 2, \quad d' < 0, d < 0 \quad (\text{B.2.7d})$$

to sum over. Similar to the matrix element in Sec. 6.4.1, to carry out the summations over δ_1 and δ_2 , the particle positions must be expressed in terms of these distances, and the result inserted into the phase factor from Eq. (B.2.1). Using translation invariance, the position of $C_{q_{\alpha}}$ can be fixed to 0. The positions follow as

$$j' = \begin{cases} 0, & \text{if } \alpha' = 1 \\ \delta_1 + 1 + \delta_2 + 1, & \text{if } \alpha' = 2 \end{cases}, \quad d' = \begin{cases} \delta_1 + 1 + \delta_2 + 1, & \text{if } \alpha' = 1 \\ -(\delta_1 + 1 + \delta_2 + 1), & \text{if } \alpha' = 2 \end{cases} \quad (\text{B.2.8a})$$

$$j = \begin{cases} 0, & \text{if } \alpha = 1 \\ \delta_1 + 1, & \text{if } \alpha = 2 \end{cases}, \quad d = \begin{cases} \delta_1 + 1, & \text{if } \alpha = 1 \\ -(\delta_1 + 1), & \text{if } \alpha = 2 \end{cases}, \quad (\text{B.2.8b})$$

and the resulting phase factors are

$$\begin{aligned}\Phi_{11} &= e^{+iQ(0+\delta_1+1+\delta_2+1)-iq'_1(\delta_1+1+\delta_2+1)} e^{-iQ(0+\delta_1+1)+iq_1(\delta_1+1)} \\ &= e^{+iQ(\delta_1+1)-iQ(\delta_1+1)+i(Q-q'_1)(\delta_2+1)-iq'_1(\delta_1+1)+iq_1(\delta_1+1)} \\ &= e^{+i(q_1-q'_1)(\delta_1+1)+iq'_2(\delta_2+1)}\end{aligned}\quad (\text{B.2.9a})$$

$$\begin{aligned}\Phi_{12} &= e^{+iQ(0+\delta_1+1+\delta_2+1)-iq'_1(\delta_1+1+\delta_2+1)} e^{-iQ0-iq_1(\delta_1+1)} \\ &= e^{+i(q_2-q'_1)(\delta_1+1)+iq'_2(\delta_2+1)}\end{aligned}\quad (\text{B.2.9b})$$

$$\begin{aligned}\Phi_{21} &= e^{+iQ0+iq'_1(\delta_1+1+\delta_2+1)} e^{-iQ(0+\delta_1+1)+iq_1(\delta_1+1)} \\ &= e^{+i(q_1-q'_2)(\delta_1+1)+iq'_1(\delta_2+1)}\end{aligned}\quad (\text{B.2.9c})$$

$$\begin{aligned}\Phi_{22} &= e^{+iQ0+iq'_1(\delta_1+1+\delta_2+1)} e^{-iQ0-iq_1(\delta_1+1)} \\ &= e^{-iQ(\delta_1+1)+iQ(\delta_1+1)+iq'_1(\delta_1+1)-iq_1(\delta_1+1)+iq'_1(\delta_2+1)} \\ &= e^{+i(q_2-q'_2)(\delta_1+1)+iq'_1(\delta_2+1)}\end{aligned}\quad (\text{B.2.9d})$$

$$\Rightarrow \Phi_{\alpha'\alpha} = e^{i(q_\alpha-q_{\alpha'}) (\delta_1+1) + iq_{\bar{\alpha}'} (\delta_2+1)} . \quad (\text{B.2.9e})$$

With this, the contribution from the case $\delta > 0$ can now be denoted as

$$\begin{aligned}\Delta N_{q'_1, q_1}^Q \Big|_{ij} &= \sum_{\alpha', \alpha=1,2} \sum_{\delta_1, \delta_2=0}^{\Xi_T} e^{i(q_\alpha-q_{\alpha'}) (\delta_1+1) + iq_{\bar{\alpha}'} (\delta_2+1)} \\ &\quad \times \left((T^\dagger)^{\delta_1} [\mathbb{1}^\dagger(C_{q_{\alpha'}}, C_{q_\alpha})[u]], \mathbb{1}^{(A; C_{q_{\bar{\alpha}}})} [T^{\delta_2} [\mathbb{1}^{(C_{q_{\bar{\alpha}'}}; A)} [v]]] \right)\end{aligned}\quad (\text{B.2.10a})$$

$$\begin{aligned}&= \sum_{\alpha', \alpha=1,2} \left(\sum_{\delta_1=0}^{\Xi_T} (T^\dagger)^{\delta_1} [\mathbb{1}^\dagger(C_{q_{\alpha'}}, C_{q_\alpha})[u]] e^{-i(q_\alpha-q_{\alpha'}) (\delta_1+1)}, \right. \\ &\quad \left. \mathbb{1}^{(A; C_{q_{\bar{\alpha}}})} \left[\sum_{\delta_2=0}^{\Xi_T} T^{\delta_2} [\mathbb{1}^{(C_{q_{\bar{\alpha}'}}; A)} [v]] e^{+iq_{\bar{\alpha}'} (\delta_2+1)} \right] \right)\end{aligned}\quad (\text{B.2.10b})$$

$$= \sum_{\alpha', \alpha=1,2} \left(u_{\alpha'}^{\alpha'}, \mathbb{1}^{(A; C_{q_{\bar{\alpha}}})} [v^{\bar{\alpha}'}] \right)\quad (\text{B.2.10c})$$

with $v^{\bar{\alpha}'}$ as defined in Eq. (6.42), and

$$u_{\alpha'}^{\alpha'} := \sum_{\delta_1=0}^{\Xi_T} (T^\dagger)^{\delta_1} [\mathbb{1}^\dagger(C_{q_{\alpha'}}, C_{q_\alpha})[u]] e^{-i(q_\alpha-q_{\alpha'}) (\delta_1+1)} . \quad (\text{B.2.11})$$

Again, the phase factor $e^{i(q_\alpha-q_{\alpha'}) (\delta_1+1)}$ is complex conjugated when pulled into the first argument of the scalar product.

Case ii): $\delta < 0$

The TN class for this case has the form

$$\langle C_{q'_1, j'}; C_{q'_2, j' + d'} | C_{q_1, j}; C_{q_2, j + d} \rangle = \begin{array}{c} \begin{array}{c} \text{C}_{q_{\alpha'}} \\ \downarrow \\ \text{C}_{q_{\alpha'}} \\ \downarrow \\ \text{C}_{q_{\alpha'}} \\ \downarrow \\ \text{C}_{q_{\alpha'}} \\ \downarrow \\ \text{C}_{q_{\alpha'}} \end{array} \\ \begin{array}{c} \text{C}_{q_{\alpha}} \quad \underbrace{\hspace{2cm}}_{\delta_1} \quad \underbrace{\hspace{2cm}}_{\delta_2} \quad \text{C}_{q_{\bar{\alpha}}} \\ \delta < 0 \end{array} \end{array} \quad (\text{B.2.12})$$

which, like the one from case i), only contributes in a skew basis and converges to zero for large δ_i . From the TN it is immediately clear, that for this case the positions (j', d') and (j, d) in Eq. (B.2.8) are simply interchanged. The phase factors are calculated analogously to Eq. (B.2.9) and result in

$$\Phi_{\alpha'\alpha} = e^{+i(q_\alpha - q_{\alpha'}) (\delta_1 + 1) - i q_{\bar{\alpha}} (\delta_2 + 1)} . \quad (\text{B.2.13})$$

The complete contribution from case ii) is thus

$$\begin{aligned} \Delta N_{q'_1, q_1}^Q \Big|_{\text{ii)}} &= \sum_{\alpha', \alpha=1,2} \sum_{\delta_1, \delta_2=0}^{\Xi_T} e^{+i(q_\alpha - q_{\alpha'}) (\delta_1 + 1) - i q_{\bar{\alpha}} (\delta_2 + 1)} \\ &\quad \times \left((T^\dagger)^{\delta_1} [\mathbb{1}^\dagger(C_{q_{\alpha'}}; C_{q_\alpha}) [u]], \mathbb{1}^{(C_{q_{\bar{\alpha}}}; A)} [T^{\delta_2} [\mathbb{1}^{(A; C_{q_{\bar{\alpha}}})} [v]]] \right) \end{aligned} \quad (\text{B.2.14a})$$

$$= \sum_{\alpha', \alpha=1,2} \left(u_{\alpha'}^{\alpha'}, \mathbb{1}^{(C_{q_{\bar{\alpha}}}; A)} \left[\sum_{\delta_2=0}^{\Xi_T} T^{\delta_2} [\mathbb{1}^{(A; C_{q_{\bar{\alpha}}})} [v]] e^{-i q_{\bar{\alpha}} (\delta_2 + 1)} \right] \right) \quad (\text{B.2.14b})$$

$$= \sum_{\alpha', \alpha=1,2} \left(u_{\alpha'}^{\alpha'}, \mathbb{1}^{(C_{q_{\bar{\alpha}}}; A)} [v_{\bar{\alpha}}] \right) \quad (\text{B.2.14c})$$

where the summed left boundary matrix $v_{\bar{\alpha}}$ is defined by

$$v_{\bar{\alpha}} := \sum_{\delta_2=0}^{\Xi_T} T^{\delta_2} [\mathbb{1}^{(A; C_{q_{\bar{\alpha}}})} [v]] e^{-i q_{\bar{\alpha}} (\delta_2 + 1)} . \quad (\text{B.2.15})$$

Case iii): $\delta = 0$

The TN for this case takes the simple and symmetric form

$$\langle C_{q'_1, j'}; C_{q'_2, j' + d'} | C_{q_1, j}; C_{q_2, j + d} \rangle = \text{Diagram} , \quad (\text{B.2.16})$$

and this is the only kind that contributes in an orthogonal basis.

Note that in both of the above cases the phase containing δ_2 relates to the rightmost C tensor. From the TNs it is clear that in the (excluded) limit $\delta_2 = -1$ both cases transition into case iii). Therefore, the phase factor follows from that of either case by inserting $\delta_2 = -1$ as

$$\Phi_{\alpha'\alpha} = e^{+i(q_\alpha - q_{\alpha'}) (\delta_1 + 1)} . \quad (\text{B.2.17})$$

However, despite the simple form, this case requires special attention. In contrast to the other two cases, the value of the TN does not converge to zero for large δ_1 . It rather factorizes into two 1QP overlaps like this

$$\langle C_{q'_1, j'}; C_{q'_2, j' + d'} | C_{q_1, j}; C_{q_2, j + d} \rangle \xrightarrow{\delta_1 \gg \Xi_T} \langle C_{q_{\alpha'}}, 0 | C_{q_\alpha}, 0 \rangle \langle C_{q_{\bar{\alpha}'}} , 0 | C_{q_{\bar{\alpha}}}, 0 \rangle . \quad (\text{B.2.18})$$

For convenience, a shorthand for the one-particle overlap is defined as

$$f_{\alpha'\alpha} := \langle C_{q_{\alpha'}}, 0 | C_{q_\alpha}, 0 \rangle = \left(u, \mathbb{1}^{(C_{q_{\alpha'}}; C_{q_\alpha})} [v] \right) . \quad (\text{B.2.19})$$

It shows the following behavior

$$f_{\alpha'\alpha} = \begin{cases} 1, & \text{if } q_{\alpha'} = q_{\alpha} \\ z \in \mathbb{C}, \text{ with } |z| < 1, & \text{if } q_{\alpha'} \neq q_{\alpha} \end{cases}. \quad (\text{B.2.20})$$

In the thermodynamic limit, the expression

$$\lim_{L \rightarrow \infty} \frac{1}{L} \sum_{d=-\frac{L}{2}}^{\frac{L}{2}} e^{i(q_{\alpha}-q_{\alpha'})d} f_{\alpha'\alpha} = \lim_{L \rightarrow \infty} \frac{1}{L} \sum_{d=0}^L (f_{\alpha'\alpha} e^{i(q_{\alpha}-q_{\alpha'})})^d \quad (\text{B.2.21a})$$

$$= \begin{cases} \lim_{L \rightarrow \infty} \frac{1}{L} \sum_{d=0}^L 1 = 1, & \text{if } q_{\alpha} = q_{\alpha'} \\ \lim_{L \rightarrow \infty} \frac{1}{L} \frac{1}{1 - f_{\alpha'\alpha} e^{i(q_{\alpha}-q_{\alpha'})}} = 0, & \text{if } q_{\alpha} \neq q_{\alpha'} \end{cases} \quad (\text{B.2.21b})$$

$$= \delta_{q_{\alpha'}, q_{\alpha}} \quad (\text{B.2.21c})$$

represents a Kronecker delta. However, for finite L , it is zero for $q_{\alpha'} \neq q_{\alpha}$ only, if $L = L_q$ (cf App. A.1). In numerical practice, this is hard to ascertain, as δ_1 is summed up to Ξ_T , which may not be equal to $\frac{L_q}{2}$. The solution to this problem is, to subtract the limit value Eq. (B.2.18) from each TN. With this, also the contributions from the diagonal TNs converge to zero for large δ_1 .

In summary, since the 2QP states are orthogonal for large particle distance, the metric tensor does contain a diagonal, bosonic part

$$N_{\text{bos } q'_1, q_1}^Q = \delta_{q'_1, q_1} + \delta_{q'_1, q_2} \quad (\text{B.2.22})$$

in the thermodynamic limit. By subtracting everything that is known to contribute to this part during the computation, the result is only the deviation from ΔN from orthogonal bosons. However, in the computation one diagonal TN is left out, namely that with $d' = d = 0$. But in order for the limit in Eq. (B.2.21) to hold, the subtracted part needs to include the $d = 0$ contribution, which is given by the sum of all factorizations of the theoretical 4C TN with $d' = d = 0$, i.e.

$$\Delta N_{\text{hcb } q'_1, q_1}^Q := f_{11} f_{22} + f_{12} f_{21}. \quad (\text{B.2.23})$$

In general, this contribution is a function of the momenta Q , q'_1 and q_1 , as apparent from the definition of $f_{\alpha'\alpha}$ in Eq. (B.2.19). In the limit, that in the iMPS representation the elementary excitation is described fully by a single tensor \mathbf{B}_0 , for instance for product states at $D = 1$,

$$\mathbf{C}_q = \mathbf{C}_{\ell=0} = \mathbf{B}_0 \quad \forall q \quad (\text{B.2.24})$$

follows. In this case, $f_{\alpha'\alpha} = 1 \forall q_{\alpha'}, q_{\alpha}$, and Eq. (B.2.23) therefore exactly implements the hard-core constraint, hence the denotation as ΔN_{hcb} .

For $D > 1$, it can be interpreted as describing the hard-core constraint to the extend implied by omitting contributions with two tensors on the same site.

The corrected contribution from the case iii) TNs is thus

$$\begin{aligned} \Delta N_{q'_1, q_1}^Q \Big|_{\text{iii)}} &= \sum_{\alpha', \alpha=1,2} \sum_{\delta_1=0}^{\Xi_T} e^{+i(q_\alpha - q_{\alpha'}) (\delta_1 + 1)} \\ &\quad \times \left((T^\dagger)^{\delta_1} [\mathbb{1}^\dagger(C_{q_{\alpha'}; C_{q_\alpha}})[u]], \mathbb{1}^{(C_{q_{\alpha'}; C_{q_\alpha}})}[v] \right) \end{aligned} \quad (\text{B.2.25a})$$

$$- \sum_{\alpha', \alpha=1,2} \sum_{\delta_1=0}^{\Xi_T} e^{+i(q_\alpha - q_{\alpha'}) (\delta_1 + 1)} f_{\alpha' \alpha} f_{\bar{\alpha}' \bar{\alpha}} - (f_{11} f_{22} + f_{12} f_{21}) \quad (\text{B.2.25b})$$

$$= \sum_{\alpha', \alpha=1,2} \left(u_{\alpha'}^{\alpha'}, \mathbb{1}^{(C_{q_{\bar{\alpha}'}; C_{q_{\bar{\alpha}}})}}[v] \right) \quad (\text{B.2.25c})$$

$$- \sum_{\alpha', \alpha=1,2} \left(\sum_{\delta_1=0}^{\Xi_T} e^{-i(q_\alpha - q_{\alpha'}) (\delta_1 + 1)} (T^\dagger)^{\delta_1} [\mathbb{1}^\dagger(C_{q_{\alpha'}; C_{q_\alpha}})[u]], v \right) f_{\bar{\alpha}' \bar{\alpha}} \quad (\text{B.2.25d})$$

$$- (f_{11} f_{22} + f_{12} f_{21}) \quad (\text{B.2.25e})$$

$$= \sum_{\alpha', \alpha=1,2} \left(u_{\alpha'}^{\alpha'}, \mathbb{1}^{(C_{q_{\bar{\alpha}'}; C_{q_{\bar{\alpha}}})}}[v] - v f_{\bar{\alpha}' \bar{\alpha}} \right) - (f_{11} f_{22} + f_{12} f_{21}) \quad (\text{B.2.25f})$$

where the properties of the scalar product and the fact, that v is an eigenmatrix of T , i.e.

$$f_{\alpha' \alpha} = \left(u, \mathbb{1}^{(C_{q_{\alpha'}; C_{q_\alpha}})}[v] \right) \quad (\text{B.2.26a})$$

$$= \left(\mathbb{1}^\dagger(C_{q_{\alpha'}; C_{q_\alpha}})[u], v \right) \quad (\text{B.2.26b})$$

$$= \left(\mathbb{1}^\dagger(C_{q_{\alpha'}; C_{q_\alpha}})[u], T^{\delta_1}[v] \right) \quad (\text{B.2.26c})$$

$$= \left((T^\dagger)^{\delta_1} [\mathbb{1}^\dagger(C_{q_{\alpha'}; C_{q_\alpha}})[u]], v \right) \quad \forall \delta_1 \geq 0 \quad (\text{B.2.26d})$$

were used to pull most of the corrections into the scalar product, instead of computing the sum of scalars in Eq. (B.2.25b) explicitly.

Summary

At this point, the summed contributions from all three cases are the same, up to the effective v matrix that represents the right half of the TN. Therefore, the complete overlap can be written down very compactly as

$$\begin{aligned} \Delta N_{q'_1, q_1}^Q &= \sum_{\alpha', \alpha=1,2} \left(u_{\alpha'}^{\alpha'}, \mathbb{1}^{(C_{q_{\bar{\alpha}'}; C_{q_{\bar{\alpha}}})}}[v] + \mathbb{1}^{(C_{q_{\bar{\alpha}'}; A})}[v_{\bar{\alpha}}] + \mathbb{1}^{(A; C_{q_{\bar{\alpha}}})}[v^{\bar{\alpha}'}] - v f_{\bar{\alpha}' \bar{\alpha}} \right) \\ &\quad - (f_{11} f_{22} + f_{12} f_{21}) . \end{aligned} \quad (\text{B.2.27})$$

With this, the metric tensor in the 2QP subspace is given by

$$N_{q'_1, q_1}^Q = \frac{1}{L_q} \Delta N_{q'_1, q_1}^Q + \delta_{q'_1, q_1} + \delta_{q'_1, q_2} \quad (\text{B.2.28})$$

where the hard-core property is now included in $\Delta N_{q'_1, q_1}^Q$ to the extent that it is captured by the *iMPS* description. One could also think of dropping the correction in Eq. (B.2.23) from the computation of ΔN , and instead use the exact hard-core bosonic expression Eq. (6.16) rather than Eq. (B.2.22) as analytic part of the metric tensor. However, this can lead to an imaginary and therefore unphysical norm of the state $|Q, d=0\rangle$ when transformed into

the hybrid basis. Therefore, implementing $\Delta N_{\text{hcb } q'_1, q_1}^Q$ from Eq. (B.2.23) presents itself as the better choice. It is also less biased, since it does not impose additional assumptions on the statistical properties of the quasi-particles. Furthermore, it is also compatible with any approach to handling TNs with $d' = d = 0$ other than leaving them out.

Note that by choosing Ξ_T as summation cutoff in the computation, ΔN still describes a system in the thermodynamic limit. The transition to a finite, periodic system happens only through the choice of the number L_q of momentum sampling points. Therefore, $\frac{1}{L_q}$ is indeed the correct normalization.

B.2.2 2QP-1QP overlap

As stated above, in an ONB there is no overlap between the one- and two-particle subspaces. However, Fig. 6.1 shows that in the iMPS description overlaps exist for small particle distances. Therefore, the one-particle state must be included in the orthogonalization process, to ensure that the corrected two-particle basis is orthogonal to it, too. In momentum space, the overlap is given by

$$N_{q'_1}^Q := \langle Q, q'_1 | Q \rangle \quad (\text{B.2.29a})$$

$$= \frac{1}{\sqrt{L}^3} \sum_{j', d'} \sum_j e^{+iQ(j'+d') - iq'_1 d' - iQj} \langle j', j' + d' | j \rangle \quad (\text{B.2.29b})$$

$$= \frac{1}{\sqrt{L}^3} \sum_{j', d'} \sum_j e^{+iQ(j'-j) + iQd' - iq'_1 d'} \langle j' - j, j' - j + d' | 0 \rangle \quad (\text{B.2.29c})$$

$$= \frac{1}{\sqrt{L}} \sum_{j', d'} e^{+iQ(j'+d') - iq'_1 d'} \langle C_{q'_1, j'}; C_{q'_2, j' + d'} | C_{Q, 0} \rangle. \quad (\text{B.2.29d})$$

Again, due to left-canonical gauge, $\min(j', j' + d') = 0$ must hold. The TNs are therefore all of the form

$$\langle C_{q'_1, j'}; C_{q'_2, j' + d'} | C_{Q, 0} \rangle = \text{Diagram} \quad (\text{B.2.30})$$

Following the methods used to calculate the two-particle overlap, it is straight forward to show, that the overlap is given by

$$N_{q'_1}^Q = \frac{1}{\sqrt{L_q}} \sum_{\alpha'=1,2} \left(\mathbb{1}^{\dagger(C_{q_{\alpha'}}, C_Q)}[u], v^{\bar{\alpha}'} \right), \quad (\text{B.2.31})$$

with $v^{\bar{\alpha}'}$ as defined in Eq. (6.42).

B.3 2QP matrix element

As already stated in Sec. 6.6.1, the term “2QP matrix element” refers to the operator matrix element in the 2QP subspace, corrected by any contributions from the 0QP and 1QP parts of the operator. Specifically for the Hamiltonian this means

$$V_{q'_1, q_1}^Q := \langle Q, q'_1 | H | Q, q_1 \rangle - \langle Q, q'_1 | H_{1P} | Q, q_1 \rangle - \langle Q, q'_1 | E_0 | Q, q_1 \rangle - C_{\eta q'_1, q_1}^Q. \quad (\text{B.3.1})$$

The 0QP part, i.e., the ground state energy, is taken care of by using the reduced Hamiltonian \tilde{H} .

The matrix element $\langle Q, q'_1 | \tilde{H} | Q, q_1 \rangle$ then still contains contributions from the 1QP part and is therefore referred to as the raw or reducible 2QP matrix element. Using the representation Eq. (6.34), it is given by

$$\begin{aligned} & \langle Q, q'_1 | \tilde{H} | Q, q_1 \rangle \\ &= \frac{1}{L} \sum_{j', d'} \sum_{j, d} e^{+iQ(j'+d') - iq'_1 d'} e^{-iQ(j+d) + iq_1 d} \langle j', j' + d' | \tilde{h}_0 | j, j + d \rangle \end{aligned} \quad (\text{B.3.2a})$$

$$\begin{aligned} &= \frac{1}{L} \sum_{j', d'} \sum_{j, d} e^{+iQ(j'+d') - iq'_1 d'} e^{-iQ(j+d) + iq_1 d} \\ & \quad \times \langle C_{q'_1, j'}; C_{q'_2, j' + d'} | \tilde{h}_0 | C_{q_1, j}; C_{q_2, j + d} \rangle. \end{aligned} \quad (\text{B.3.2b})$$

As explained in Chap. 6, in the computation of this matrix element any contributions with $d' = 0$ or $d = 0$ are excluded. Each sub-matrix element $\langle C_{q'_1, j'}; C_{q'_2, j' + d'} | \tilde{h}_0 | C_{q_1, j}; C_{q_2, j + d} \rangle$ is therefore represented by a TN with four C tensors on distinct sites, which is thus called the 4C contribution.

To obtain the irreducible interaction matrix element $V_{q'_1, q_1}^Q$, the raw matrix element needs to be corrected by the 1QP contribution $\langle Q, q'_1 | H_{1P} | Q, q_1 \rangle$, and the correction term $C_{\eta q'_1, q_1}^Q$, that compensates for the fact, that in iMPS computations \mathbf{A} is not usually an exact eigenstate of H . Both of these corrections are described in detail in the following two sections.

B.3.1 1QP contributions

The contribution of the 1QP part of H to the 2QP matrix element is given by summing up all possibilities to factorize the 2QP matrix element into a 1QP matrix element and a 1QP overlap

$$\begin{aligned} & \langle Q, q'_1 | H_{1P} | Q, q_1 \rangle \\ &= \frac{1}{L^2} \sum_{j', d'} \sum_{j, d} e^{+iQ(j'+d') - iq'_1 d'} e^{-iQ(j+d) + iq_1 d} \\ & \quad \times \langle j', j' + d' | \sum_i \tilde{h}_i |_{1P} | j, j + d \rangle \end{aligned} \quad (\text{B.3.3a})$$

$$\begin{aligned} &= \frac{1}{L} \sum_{j', d'} \sum_{j, d} e^{+iQ(j'+d') - iq'_1 d'} e^{-iQ(j+d) + iq_1 d} \\ & \quad \times \langle j', j' + d' | \tilde{h}_i |_{1P} | j, j + d \rangle \end{aligned} \quad (\text{B.3.3b})$$

$$\begin{aligned} &= \frac{1}{L} \sum_{j', d'} \sum_{j, d} e^{+iQ(j'+d') - iq'_1 d'} e^{-iQ(j+d) + iq_1 d} \\ & \quad \times \left(\langle j' | j \rangle \langle j' + d' | \tilde{h}_0 | j + d \rangle + \langle j' + d' | j + d \rangle \langle j' | \tilde{h}_0 | j \rangle \right. \\ & \quad \left. + \langle j' | j + d \rangle \langle j' + d' | \tilde{h}_0 | j \rangle + \langle j' + d' | j \rangle \langle j' | \tilde{h}_0 | j + d \rangle \right) \end{aligned} \quad (\text{B.3.3c})$$

where in the last form the restriction to one particle can be dropped, since by definition only the 1QP part of the operator contributes to the matrix elements.

For regular bosons, assuming a bilinear one-particle Hamiltonian

$$H_{1P} := \sum_i \sum_{\delta} t_{\delta} a_i^{\dagger} a_{i+\delta} \quad (\text{B.3.4})$$

with real hopping amplitudes t_δ , it can straight forwardly be calculated as

$$\begin{aligned} & \langle Q, q'_1 | H_{1P} | Q, q_1 \rangle \\ &= \frac{1}{L} \sum_{j', d'} \sum_{j, d} \sum_{\delta} t_\delta e^{+iQ(j'+d') - iq'_1 d'} e^{-iQ(j+d) + iq_1 d} \\ & \quad \left(\langle j' | j \rangle \langle j' + d' | a_0^\dagger a_\delta | j + d \rangle + \langle j' + d' | j + d \rangle \langle j' | a_0^\dagger a_\delta | j \rangle \right. \\ & \quad \left. + \langle j' | j + d \rangle \langle j' + d' | a_0^\dagger a_\delta | j \rangle + \langle j' + d' | j \rangle \langle j' | a_0^\dagger a_\delta | j + d \rangle \right) \end{aligned} \quad (\text{B.3.5a})$$

$$\begin{aligned} &= \frac{1}{L} \sum_{j', d'} \sum_{j, d} \sum_{\delta} t_\delta e^{+iQ(j'+d') - iq'_1 d'} e^{-iQ(j+d) + iq_1 d} \\ & \quad \times \left(\delta_{j', j} \delta_{j'+d', 0} \delta_{j+d, \delta} + \delta_{j'+d', j+d} \delta_{j', 0} \delta_{j, \delta} \right. \\ & \quad \left. + \delta_{j', j+d} \delta_{j'+d', 0} \delta_{j, \delta} + \delta_{j'+d', j} \delta_{j', 0} \delta_{j+d, \delta} \right) \end{aligned} \quad (\text{B.3.5b})$$

$$\begin{aligned} &= \frac{1}{L} \sum_{\delta} t_\delta \left\{ \sum_j e^{+iQ0 - iq'_1(-j)} e^{-iQ\delta + iq_1(\delta-j)} + \sum_d e^{+iQ(\delta+d) - iq'_1(\delta+d)} e^{-iQ(\delta+d) + iq_1 d} \right. \\ & \quad \left. + \sum_{j'} e^{+iQ0 - iq'_1(-j')} e^{-iQj' + iq_1(j'-\delta)} + \sum_{d'} e^{+iQd' - iq'_1 d'} e^{-iQ\delta + iq_1(\delta-d')} \right\} \end{aligned} \quad (\text{B.3.5c})$$

$$\begin{aligned} &= \sum_{\delta} t_\delta \left\{ \left(\frac{1}{L} \sum_j e^{i(q'_1 - q_1)j} \right) e^{-iq_2 \delta} + \left(\frac{1}{L} \sum_d e^{i(q'_2 - q_2)d} \right) e^{-iq'_1 \delta} \right. \\ & \quad \left. + \left(\frac{1}{L} \sum_{j'} e^{i(q'_1 - q_2)j'} \right) e^{-iq_1 \delta} + \left(\frac{1}{L} \sum_{d'} e^{i(q'_2 - q_1)d'} \right) e^{-iq_2 \delta} \right\} \end{aligned} \quad (\text{B.3.5d})$$

$$= \sum_{\delta} t_\delta \left\{ \delta_{q'_1, q_1} e^{-iq_2 \delta} + \delta_{q'_2, q_2} e^{-iq'_1 \delta} + \delta_{q'_1, q_2} e^{-iq_1 \delta} + \delta_{q'_2, q_1} e^{-iq_2 \delta} \right\} \quad (\text{B.3.5e})$$

$$= \sum_{\delta} t_\delta \left(\delta_{q'_1, q_1} (e^{-iq_2} + e^{-iq_1}) + \delta_{q'_1, q_2} (e^{-iq_1} + e^{-iq_2}) \right) \quad (\text{B.3.5f})$$

$$= (\delta_{q'_1, q_1} + \delta_{q'_1, q_2}) (\omega_{q_1} + \omega_{q_2}) . \quad (\text{B.3.5g})$$

Since the one-particle Hamiltonian derived in Chap. 5 is of the form Eq. (B.3.4), this analytical result can be used to determine the full 1QP contribution if needed.

Note that the result in Eq. (B.3.5) requires to drop the restriction $d', d \neq 0$. If this hard-core constraint is kept, the result is Eq. (B.3.5g) minus the hard-core correction derived in App. A.10.2, i.e.,

$$\langle Q, q'_1 | H_{1P} | Q, q_1 \rangle = (\delta_{q'_1, q_1} + \delta_{q'_1, q_2}) (\omega_{q_1} + \omega_{q_2}) - \frac{2}{L} \left(\omega_{q_1} + \omega_{q_2} + \omega_{q'_1} + \omega_{q'_2} - 2t_0 \right) . \quad (\text{B.3.6})$$

In terms of C_{q_α} tensors Eq. (B.3.3) becomes

$$\begin{aligned} & \langle Q, q'_1 | \sum_i \tilde{h}_i \Big|_{1P} | Q, q_1 \rangle \\ &= \frac{1}{L} \sum_{j', d'} \sum_{j, d} e^{+iQ(j'+d') - iq'_1 d'} e^{-iQ(j+d) + iq_1 d} \\ & \quad \times \left(\langle C_{q'_1}, j' | C_{q_1}, j \rangle \langle C_{q'_2}, j' + d' | \tilde{h}_0 | C_{q_2}, j + d \rangle \right. \\ & \quad + \langle C_{q'_2}, j' + d' | C_{q_2}, j + d \rangle \langle C_{q'_1}, j' | \tilde{h}_0 | C_{q_1}, j \rangle \\ & \quad + \langle C_{q'_1}, j' | C_{q_2}, j + d \rangle \langle C_{q'_2}, j' + d' | \tilde{h}_0 | C_{q_1}, j \rangle \\ & \quad \left. + \langle C_{q'_2}, j' + d' | C_{q_1}, j \rangle \langle C_{q'_1}, j' | \tilde{h}_0 | C_{q_2}, j + d \rangle \right) . \end{aligned} \quad (\text{B.3.7a})$$

In left-canonical gauge this simplifies to

$$\begin{aligned}
& \langle Q, q_1 | \sum_i \tilde{h}_i |_{1P} | Q, q_1 \rangle \\
&= \frac{1}{L} \sum_{j', d'} \sum_{j, d} e^{+iQ(j'+d') - iq_1 d'} e^{-iQ(j+d) + iq_1 d} \\
&\quad \times \left(f_{1,1} \delta_{j', j} \langle C_{q_2', j' + d'} | \tilde{h}_0 | C_{q_2, j + d} \rangle \right. \\
&\quad + f_{2,2} \delta_{j'+d', j+d} \langle C_{q_1', j'} | \tilde{h}_0 | C_{q_1, j} \rangle \\
&\quad + f_{1,2} \delta_{j', j+d} \langle C_{q_2', j' + d'} | \tilde{h}_0 | C_{q_1, j} \rangle \\
&\quad \left. + f_{2,1} \delta_{j'+d', j} \langle C_{q_1', j'} | \tilde{h}_0 | C_{q_2, j + d} \rangle \right). \tag{B.3.8a}
\end{aligned}$$

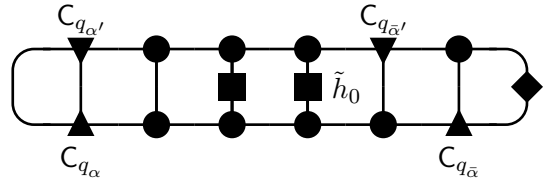
with $f_{\alpha'\alpha}$ as defined in Eq. (B.2.19).

Note, however, that as in the case of the diagonal part of the metric tensor in Sec. B.2.1, the analytical result in Eq. (B.3.6) relies on the Kronecker identity to produce the $\delta_{q_{\alpha'}, q_{\alpha}}$ expressions. Therefore, again, the factorized value from Eq. (B.3.8) has to be subtracted directly from any 4C TN that contributes to the diagonal part. Since all 4C TNs where two C tensors fall onto the same site are omitted, there are also no contributions to the 1QP part with d' or $d = 0$ that need to be subtracted.

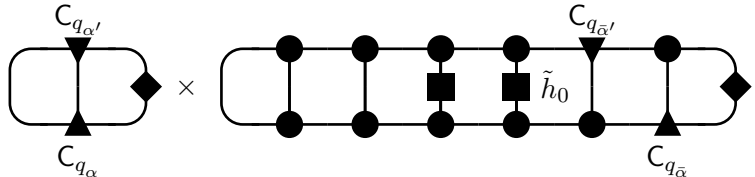
Due to the orthogonality of the 1QP basis, which is reflected in the Kronecker deltas in Eq. (B.3.8), as a general rule a TN contributes to the 1QP part if the following two conditions are fulfilled.

1. It contains at least one ‘‘rung’’ with C tensors on both ends, and
2. the remaining part with the C rung replaced by the transfer operator T is non zero in left-canonical gauge.

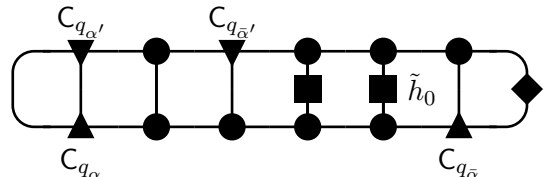
For instance, the TN


(B.3.9)

contains a rung with C tensors on both ends and factorizes into a 1QP overlap and a 1QP matrix element like this


(B.3.10)

It contributes to the 1QP part, since the TN remaining after factoring out the C rung can have non-zero values in left-canonical gauge. In contrast, the TN


(B.3.11)

does *not* contribute, since in its factorization

$$\text{Diagram 1} \times \text{Diagram 2} \quad (\text{B.3.12})$$

the remaining part is always zero in left-canonical gauge.

Although Eqs. (B.3.3) and (B.3.8) are straight forward about them, a note is in order on contributions that fulfill two of the δ -conditions in Eq. (B.3.8). These contributions make up the local on-site energy t_0 in Eq. (B.3.5), and the corresponding TNs are of the form

$$\text{Diagram} \quad (\text{B.3.13})$$

This allows for two non-vanishing factorizations

$$\text{Diagram 1} \times \text{Diagram 2} = \text{Diagram 3} \times \text{Diagram 4} \quad (\text{B.3.14})$$

and

$$\text{Diagram 1} \times \text{Diagram 2} = \text{Diagram 3} \times \text{Diagram 4} \quad (\text{B.3.15})$$

While in a completely local basis clearly only the first one would contribute, in the iMPS description *both* must be taken into account, since the operator can “see” the \mathbb{C} tensors over a range of Ξ_T sites away. This argument even holds, if the operator does not act directly act on any sites with a \mathbb{C} tensor.

B.3.2 Ground state-1QP matrix element corrections

As mentioned in Chap. 4, generally the ground state uMPS \mathbf{A} is only an approximation, and therefore not an exact eigenstate of the Hamiltonian. As a result, the Hamiltonian couples the approximate ground state to excited states, starting with the one-particle sector as

$$\eta := \langle j | \tilde{H} | GS \rangle = \langle GS | a_j \tilde{H} | GS \rangle \neq 0. \quad (\text{B.3.16})$$

Of course, this property carries over to momentum space under the Fourier transformation

$$\eta_q := \langle q | \tilde{H} | GS \rangle \neq 0 . \quad (\text{B.3.17})$$

And it also poses a problem for the computation of 2QP matrix elements, due to the non-orthogonality of the basis. Consider for instance the matrix element

$$H_{0,d}^{0,d'} = \langle 0, d' | \tilde{H} | 0, d \rangle . \quad (\text{B.3.18})$$

For small d and large d' it factorizes into a 2QP-1QP overlap and a 1QP-GS matrix element

$$H_{0,d}^{0,d'} \xrightarrow{d' > 2\Xi_T} \underbrace{\langle 0 | 0, d \rangle}_{\neq 0} \underbrace{\langle d' | \tilde{H} | GS \rangle}_{\eta} . \quad (\text{B.3.19})$$

These contributions should vanish, but do not. And since in the Fourier transformation many of them are summed up, this can lead to significant errors.

In the efficient momentum space algorithms of Sec. 6.4, all relative distances are summed up to Ξ_T , because beyond that, C tensors and operators cannot “see” each other. Therefore, any TN is then equivalent to its factorization. However, this computation scheme relies on the assumption, that one of the factors is zero to machine precision. In the case of the diagonal overlap TN Eq. (B.2.16), this was achieved by subtracting the factorized limit value for $\delta_1 \geq \Xi_T$ from each contribution.

Now consider the following TN, that contributes to the 2QP matrix element

$$\langle C_{q'_1, j'; C_{q'_2, j' + d'} | \tilde{h}_0 | C_{q_1, j; C_{q_2, j + d} \rangle$$

$$= \text{Diagram} . \quad (\text{B.3.20})$$

Assuming left-canonical gauge, the value converges to zero for both large δ_1 and large δ_3 , independently of the other distances. But, if both δ_1 and δ_3 are small, for large δ_2 the TN factorizes like this

$$\langle C_{q'_1, j'; C_{q'_2, j' + d'} | \tilde{h}_0 | C_{q_1, j; C_{q_2, j + d} \rangle$$

$$\rightarrow \text{Diagram} \times \text{Diagram} \quad (\text{B.3.21})$$

where, however, neither factor is zero. Therefore, the total error from this type of TN is roughly

$$\eta_{\text{TN}} \approx \langle C_{q_{\alpha'}, j' | C_{q_{\alpha}, j; C_{q_{\alpha}, j + d} \rangle \langle C_{q_{\alpha'}, j' + d' | \tilde{h}_0 | GS \rangle \Xi_T , \quad (\text{B.3.22})$$

where the factor Ξ_T results from the sum over δ_2 . The problem is not only the absolute error, but also the fact, that it does not converge as function of Ξ_T .

To prevent this type of error from spoiling the matrix element result, the 4C contribution must be corrected by this factorization as well. Not all 4C TNs have a non-vanishing factorization of this type in left-canonical gauge.

In a strict analysis, C_η takes a form analogous to the 1QP part. This means, it is given by the sum over all possibilities to factorize the 2QP matrix element into a 2QP-1QP overlap and a 1QP-ground state matrix element

$$\begin{aligned}
C_{\eta q'_1, q_1}^Q &= \frac{1}{L} \sum_{j', d'} \sum_{j, d} e^{+iQ(j'+d')-iq'_1 d'} e^{-iQ(j+d)+iq_1 d} \\
&\quad \times \left(\langle j', j'+d' | j \rangle \langle GS | \tilde{h}_0 | j+d \rangle + \langle j', j'+d' | j+d \rangle \langle GS | \tilde{h}_0 | j \rangle \right. \\
&\quad \left. + \langle j' | j, j+d \rangle \langle j'+d' | \tilde{h}_0 | GS \rangle + \langle j'+d' | j, j+d \rangle \langle j' | \tilde{h}_0 | GS \rangle \right) \quad (\text{B.3.23a})
\end{aligned}$$

$$\begin{aligned}
&= \frac{1}{L} \sum_{j', d'} \sum_{j, d} e^{+iQ(j'+d')-iq'_1 d'} e^{-iQ(j+d)+iq_1 d} \\
&\quad \times \left(\langle C_{q'_1, j'}; C_{q'_2, j'+d'} | C_{q_1, j} \rangle \langle GS | \tilde{h}_0 | C_{q_2, j+d} \rangle \right. \\
&\quad + \langle C_{q'_1, j'}; C_{q'_2, j'+d'} | C_{q_2, j+d} \rangle \langle GS | \tilde{h}_0 | C_{q_1, j} \rangle \\
&\quad + \langle C_{q'_1, j'} | C_{q_1, j}; C_{q_2, j+d} \rangle \langle C_{q'_2, j'+d'} | \tilde{h}_0 | GS \rangle \\
&\quad \left. + \langle C_{q'_2, j'+d'} | C_{q_1, j}; C_{q_2, j+d} \rangle \langle C_{q'_1, j'} | \tilde{h}_0 | GS \rangle \right). \quad (\text{B.3.23b})
\end{aligned}$$

In this formulation, *many* TN types actually contain contributions to C_η , even if they converge as function of all δ_i or if the non-convergence is remedied by the 1QP corrections. However, these contributions do not grow with Ξ_T . For a fully consistent computation they would need to be included. However, the expected change in the results is of the order of η , i.e., very small, so that they are considered negligible for now.

B.3.3 Different TN types

Depending on the location of the operator in relation to the C tensors representing the particles, five basic types of TNs can be distinguished. Most of these TN types can then further be split into sub-types, depending on, e.g., how many C tensors the operator acts on, and the positions of the C tensors relative to each other. First, the main types are introduced, showing exemplary TNs for each case.

i) The operator acts right of all C tensors

$$\begin{aligned}
&\langle C_{q'_1, j'}; C_{q'_2, j'+d'} | \tilde{h}_0 | C_{q_1, j}; C_{q_2, j+d} \rangle \\
&= \text{Diagram (B.3.24)} \quad (\text{B.3.24})
\end{aligned}$$

ii) The operator acts in between the C tensors

$$\begin{aligned}
&\langle C_{q'_1, j'}; C_{q'_2, j'+d'} | \tilde{h}_0 | C_{q_1, j}; C_{q_2, j+d} \rangle \\
&= \text{Diagram (B.3.25)} \quad (\text{B.3.25})
\end{aligned}$$

iii) Transitions between the cases i) and ii)

$$\langle C_{q'_1, j'}; C_{q'_2, j' + d'} | \tilde{h}_0 | C_{q_1, j}; C_{q_2, j + d} \rangle$$
(B.3.26)

iv) The operator acts left of all C tensors

$$\langle C_{q'_1, j'}; C_{q'_2, j' + d'} | \tilde{h}_0 | C_{q_1, j}; C_{q_2, j + d} \rangle$$
(B.3.27)

v) Transitions between case iv) and the other cases

$$\langle C_{q'_1, j'}; C_{q'_2, j' + d'} | \tilde{h}_0 | C_{q_1, j}; C_{q_2, j + d} \rangle$$
(B.3.28)

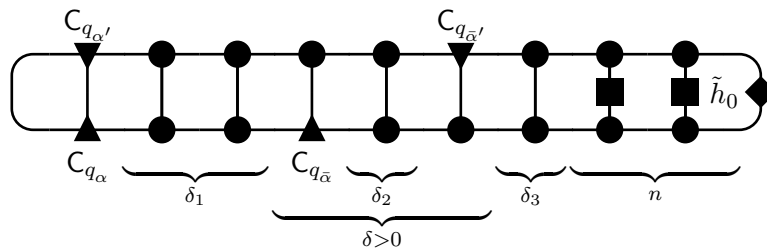
Beginning with Sec. B.3.4, each case is examined in detail and its contribution to the irreducible 2QP matrix element is calculated. Section B.1 describes the general approach to evaluating each case.

A summary of all the contributions can be found in App. C.

B.3.4 Case i)

B.3.4.1 4C TN contributions

Looking at the example TN for this case



suggests that the calculation should be very similar to that of the 2QP overlap in Sec. B.2.1. In fact, a short calculation shows, that the result is exactly the same up to switching out the bare right boundary matrix v with a summed effective boundary matrix

$$v \rightarrow v_{\tilde{h}} := \sum_{\delta_3=0}^{\Xi_T} T^{\delta_3} [\tilde{h}^{(A;A)}[v]] . \tag{B.3.29}$$

To see this, consider the case $\alpha' = \alpha = 1$. For the TN shown above, the particle positions are defined analogous to Eq. (B.2.8)

$$j' = -(\delta_1 + 1 + \delta_2 + 1 + \delta_3 + 1), \quad d' = \delta_1 + 1 + \delta_2 + 1 \quad (\text{B.3.30})$$

$$j = -(\delta_1 + 1 + \delta_2 + 1 + \delta_3 + 1) = j', \quad d = \delta_1 + 1 \quad (\text{B.3.31})$$

which, inserted into the phase factor, yield

$$\Phi_{11} = e^{+iQ(-\delta_3-1)-iq'_1(\delta_1+1+\delta_2+1)} e^{-iQ(-\delta_2-1-\delta_3-1)+iq_1(\delta_1+1)} \quad (\text{B.3.32a})$$

$$= e^{-iq'_1(\delta_1+1+\delta_2+1)+iQ(\delta_2+1)+iq_1(\delta_1+1)} \quad (\text{B.3.32b})$$

$$= e^{-iq'_1(\delta_1+1)+iq'_2(\delta_2+1)+iq_1(\delta_1+1)} \quad (\text{B.3.32c})$$

$$= e^{i(q_1-q'_1)(\delta_1+1)+iq'_2(\delta_2+1)}, \quad (\text{B.3.32d})$$

i.e., exactly the same as the phase factor Φ_{11} from the overlap computation (cf. Eq. (B.2.9)). Therefore, the contribution from this case is clearly given by the result in Eq. (B.2.10), with the substitution $v \rightarrow v_{\tilde{h}}$ from Eq. (B.3.29) above. The other momentum configurations can be calculated analogously and yield corresponding results.

The cases $\delta < 0$ and $\delta = 0$ follow exactly as shown in the overlap calculation, too. The combined 4C contribution from case i) is thus

$$H_{4C}^Q \left. \vphantom{H_{4C}^Q} \right|_{q'_1, q_1} \Big|_i = \sum_{\alpha', \alpha=1,2} \left(u_{\alpha'}^{\alpha'}, v_{\tilde{h}\bar{\alpha}}^{\alpha'} \right) \quad (\text{B.3.33})$$

where

$$v_{\tilde{h}\bar{\alpha}}^{\alpha'} := \mathbb{1}^{(C_{q_{\bar{\alpha}}}; C_{q_{\alpha}})} [v_{\tilde{h}}] + \mathbb{1}^{(C_{q_{\bar{\alpha}}}; A)} [v_{\tilde{h}\bar{\alpha}}] + \mathbb{1}^{(A; C_{q_{\bar{\alpha}}})} [v_{\tilde{h}}^{\alpha'}] \quad (\text{B.3.34a})$$

$$\text{with } v_{\tilde{h}}^{\alpha'} := \sum_{\delta_2=0}^{\Xi_T} T^{\delta_2} [\mathbb{1}^{(C_{q_{\bar{\alpha}}}; A)} [v_{\tilde{h}}]] e^{+iq_{\bar{\alpha}}'(\delta_2+1)} \quad (\text{B.3.34b})$$

$$\text{and } v_{\tilde{h}\bar{\alpha}} := \sum_{\delta_2=0}^{\Xi_T} T^{\delta_2} [\mathbb{1}^{(A; C_{q_{\bar{\alpha}}})} [v_{\tilde{h}}]] e^{-iq_{\bar{\alpha}}(\delta_2+1)}. \quad (\text{B.3.34c})$$

B.3.4.2 1QP corrections

Although in case i) the operator does not directly act on any sites where a C tensor is located, it can still “see” them several sites away. Therefore, this case does nonetheless contribute to the one-particle content of the matrix element, which must be subtracted. In left-canonical gauge, the only non-vanishing factorizations are those with $\delta = 0$, where both the types from Eqs. (B.3.14) and (B.3.15) occur.

From the first TN factorization in Eq. (B.3.14) one can see, that the contributions follow from the 4C TN results by replacing

$$\mathbb{1}^{\dagger(C_{q_{\alpha'}}; C_{q_{\alpha}})} [u] \quad \rightarrow \quad u f_{\alpha'\alpha}^* . \quad (\text{B.3.35})$$

For the second, shown in (B.3.15), the correction follows from the 4C calculation by replacing

$$\mathbb{1}^{(C_{q_{\bar{\alpha}}}; C_{q_{\bar{\alpha}}})} \quad \rightarrow \quad T \cdot f_{\bar{\alpha}\bar{\alpha}} . \quad (\text{B.3.36})$$

Since the phase factors are the same for the 4C TN and the 1QP factorizations, the con-

tribution from case i) amounts to

$$H_{\text{IP } q'_1, q_1}^Q \Big|_i := \sum_{\alpha', \alpha=1,2} \left(\sum_{\delta_1=0}^{\Xi_T} u f_{\alpha'\alpha}^* e^{-i(q_\alpha - q_{\alpha'}) (\delta_1 + 1)}, v_{\tilde{h} \bar{\alpha}}^{\alpha'} \right) + \sum_{\alpha', \alpha=1,2} \left(u_\alpha^{\alpha'}, T[v_{\tilde{h}}] \right) f_{\bar{\alpha}' \bar{\alpha}} \quad (\text{B.3.37a})$$

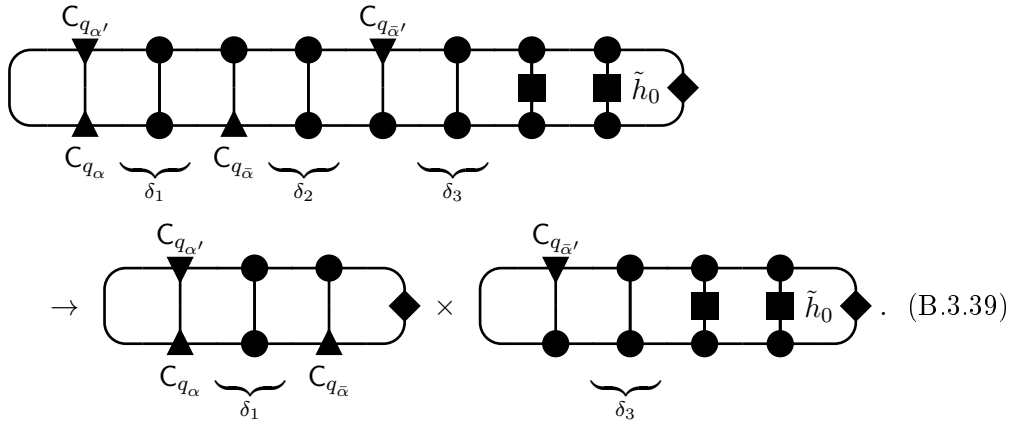
$$:= \sum_{\alpha', \alpha=1,2} \left(u f_{\alpha'\alpha}^* \varphi_{\alpha'\alpha}^*, v_{\tilde{h} \bar{\alpha}}^{\alpha'} \right) + \sum_{\alpha', \alpha=1,2} \left(u_\alpha^{\alpha'}, T[v_{\tilde{h}}] \right) f_{\bar{\alpha}' \bar{\alpha}}, \quad (\text{B.3.37b})$$

where $\varphi_{\alpha'\alpha}$ is defined as

$$\varphi_{\alpha'\alpha} := \sum_{\delta_1=0}^{\Xi_T} e^{+i(q_\alpha - q_{\alpha'}) (\delta_1 + 1)}. \quad (\text{B.3.38})$$

B.3.4.3 Ground state-1QP matrix element corrections

Case i) does not require contributions to the C_η correction term, if left-canonical gauge is used. Any TN factorization that includes the operator and a single C tensor vanishes. For example, the $\delta > 0$ TN factorizes like this for large δ_2



Although the left factor can be finite for small δ_1 , the right factor is always zero in left-canonical gauge. Therefore, this type of TN is convergent for all δ_i , and does not contribute to the error matrix elements η . The same is true for the TN in the $\delta < 0$ case. The $\delta = 0$ TN does not contribute by definition. It does not converge as function of δ_2 , but this is already taken care of by subtracting the 1QP corrections.

B.3.4.4 Summary

Taking together all the results from this section, the final, 1QP corrected contribution of case i) to the 2QP matrix elements reads

$$V_{q'_1, q_1}^Q \Big|_i = \sum_{\alpha', \alpha=1,2} \left(u_\alpha^{\alpha'}, v_{\tilde{h} \bar{\alpha}}^{\alpha'} \right) - \sum_{\alpha', \alpha=1,2} \left(u f_{\alpha'\alpha}^* \varphi_{\alpha'\alpha}^*, v_{\tilde{h} \bar{\alpha}}^{\alpha'} \right) - \sum_{\alpha', \alpha=1,2} \left(u_\alpha^{\alpha'}, T[v_{\tilde{h}}] \right) f_{\bar{\alpha}' \bar{\alpha}} \quad (\text{B.3.40a})$$

$$= \sum_{\alpha', \alpha=1,2} \left(u_{\alpha, \text{1Pc}}^{\alpha'}, v_{\tilde{h} \bar{\alpha}}^{\alpha'} \right) - \left(u_\alpha^{\alpha'}, T[v_{\tilde{h}}] \right) f_{\bar{\alpha}' \bar{\alpha}} \quad (\text{B.3.40b})$$

with the 1QP corrected summed left boundary matrix

$$u_{\alpha, \text{1Pc}}^{\alpha'} := u_\alpha^{\alpha'} - u \cdot f_{\alpha'\alpha}^* \varphi_{\alpha'\alpha}^*. \quad (\text{B.3.41})$$

B.3.5 Case ii)

This case consists of three subcases, depending on the operator position.

B.3.5.1 Subcase iia)

The first one, with two C tensors left, and the other two right of the operator has TNs of the following type

which, depending on δ , can actually be seen as three subcases. However, the example of the $\delta > 0$ case will show, that all three can be handled in a way very similar to case i) above.

With $\alpha = \alpha' = 1$, the particle positions for the TN (B.3.42) are given by

$$j' = -(\delta_1 + 1), \quad d' = \delta_1 + n + \delta_2 + 1 + \delta_3 + 1 \quad (\text{B.3.43})$$

$$j = -(\delta_1 + 1) = j', \quad d = \delta_1 + n + \delta_2 + 1. \quad (\text{B.3.44})$$

Inserting this into the phase factor from Eq. (B.3.2) yields

$$\Phi_{11} = e^{+iQ(n+\delta_2+\delta_3+1)-iq'_1(\delta_1+n+\delta_2+1+\delta_3+1)} e^{-iQ(n+\delta_2)+iq_1(\delta_1+n+\delta_2+1)} \quad (\text{B.3.45a})$$

$$= e^{+iQ(\delta_3+1)-iq'_1(\delta_1+n+\delta_2+1+\delta_3+1)} e^{+iq_1(\delta_1+n+\delta_2+1)} \quad (\text{B.3.45b})$$

$$= e^{+iq'_2(\delta_3+1)-iq'_1(\delta_1+n+\delta_2+1)} e^{+iq_1(\delta_1+n+\delta_2+1)} \quad (\text{B.3.45c})$$

$$= e^{+i(q_1-q'_1)(\delta_1+1)+i(q_1-q'_1)n+i(q_1-q'_1)\delta_2+iq'_2(\delta_3+1)} \quad (\text{B.3.45d})$$

$$= e^{+i(q_1-q'_1)(\delta_1+1)+i(q_1-q'_1)(n-1)+i(q_1-q'_1)(\delta_2+1)+iq'_2(\delta_3+1)} \quad (\text{B.3.45e})$$

The phase factors for the other momentum configurations follow analogously, wherefore

$$\Phi_{\alpha'\alpha} = e^{+i(q_\alpha-q_{\alpha'})(\delta_1+1)+i(q_\alpha-q_{\alpha'})(n-1)+i(q_\alpha-q_{\alpha'})(\delta_2+1)+iq_{\alpha'}(\delta_3+1)}. \quad (\text{B.3.46})$$

Again, for the $\delta < 0$ case, the positions (j', d') and (j, d) from Eq. (B.3.43) are simply interchanged. The general phase factor follows analogously as

$$\Phi_{\alpha'\alpha} = e^{+i(q_\alpha-q_{\alpha'})(\delta_1+1)+i(q_\alpha-q_{\alpha'})(n-1)+i(q_\alpha-q_{\alpha'})(\delta_2+1)-iq_{\alpha'}(\delta_3+1)}. \quad (\text{B.3.47})$$

The $\delta = 0$ case is again the so far excluded limit $\delta_3 = -1$ of either of the other two cases. From this, the 4C contribution can be determined as follows

$$\begin{aligned} & H_{4C}^Q \Big|_{q'_1, q_1} \Big|_{\text{iia)}} \\ &= \sum_{\alpha', \alpha=1,2} \sum_{\delta_1=0}^{\Xi_T} \sum_{\delta_2=0}^{\Xi_T} \sum_{\delta_3=0}^{\Xi_T} e^{+i(q_\alpha-q_{\alpha'})(\delta_1+1)+i(q_\alpha-q_{\alpha'})(n-1)+i(q_\alpha-q_{\alpha'})(\delta_2+1)} e^{+iq_{\alpha'}(\delta_3+1)} \\ & \quad \times \left((T^\dagger)^{\delta_1} [\mathbb{1}^\dagger (C_{q_{\alpha'}}; C_{q_\alpha}) [u]], \tilde{h}^{(A;A)} [T^{\delta_2} [\mathbb{1}^{(A;C_{q_{\alpha'}})} [T^{\delta_3} [\mathbb{1}^{(C_{q_{\alpha'}}; A)} [v]]]]]] \right) \\ &+ \sum_{\alpha', \alpha=1,2} \sum_{\delta_1=0}^{\Xi_T} \sum_{\delta_2=0}^{\Xi_T} \sum_{\delta_3=0}^{\Xi_T} e^{+i(q_\alpha-q_{\alpha'})(\delta_1+1)+i(q_\alpha-q_{\alpha'})(n-1)+i(q_\alpha-q_{\alpha'})(\delta_2+1)} e^{-iq_{\alpha'}(\delta_3+1)} \end{aligned}$$

$$\begin{aligned}
& \times \left((T^\dagger)^{\delta_1} [\mathbb{1}^\dagger(C_{q_{\alpha'}}; C_{q_\alpha})[u]], \tilde{h}^{(A;A)} [T^{\delta_2} [\mathbb{1}^{(C_{q_{\bar{\alpha}'}}; A)} [T^{\delta_3} [\mathbb{1}^{(A; C_{q_{\bar{\alpha}}})} [v]]]]]] \right) \\
& + \sum_{\alpha', \alpha=1,2} \sum_{\delta_1=0}^{\Xi_T} \sum_{\delta_2=0}^{\Xi_T} e^{+i(q_\alpha - q_{\alpha'}) (\delta_1 + 1) + i(q_\alpha - q_{\alpha'}) (n-1) + i(q_\alpha - q_{\alpha'}) (\delta_2 + 1)} \\
& \quad \times \left((T^\dagger)^{\delta_1} [\mathbb{1}^\dagger(C_{q_{\alpha'}}; C_{q_\alpha})[u]], \tilde{h}^{(A;A)} [T^{\delta_2} [\mathbb{1}^{(C_{q_{\bar{\alpha}'}}; C_{q_{\bar{\alpha}}})} [v]]]] \right) \tag{B.3.48a} \\
= & \sum_{\alpha', \alpha=1,2} e^{+i(q_\alpha - q_{\alpha'}) (n-1)} \\
& \times \left\{ \left(\sum_{\delta_1=0}^{\Xi_T} (T^\dagger)^{\delta_1} [\mathbb{1}^\dagger(C_{q_{\alpha'}}; C_{q_\alpha})[u]] e^{-i(q_\alpha - q_{\alpha'}) (\delta_1 + 1)}, \right. \right. \\
& \quad \left. \tilde{h}^{(A;A)} \left[\sum_{\delta_2=0}^{\Xi_T} T^{\delta_2} [\mathbb{1}^{(A; C_{q_{\bar{\alpha}}})} \left[\sum_{\delta_3=0}^{\Xi_T} T^{\delta_3} [\mathbb{1}^{(C_{q_{\bar{\alpha}'}}; A)} [v]] e^{+iq_{\bar{\alpha}'} (\delta_3 + 1)} \right]] e^{+i(q_\alpha - q_{\alpha'}) (\delta_2 + 1)} \right] \right) \\
& + \left(\sum_{\delta_1=0}^{\Xi_T} (T^\dagger)^{\delta_1} [\mathbb{1}^\dagger(C_{q_{\alpha'}}; C_{q_\alpha})[u]] e^{-i(q_\alpha - q_{\alpha'}) (\delta_1 + 1)}, \right. \\
& \quad \left. \tilde{h}^{(A;A)} \left[\sum_{\delta_2=0}^{\Xi_T} T^{\delta_2} [\mathbb{1}^{(A; C_{q_{\bar{\alpha}}})} \left[\sum_{\delta_3=0}^{\Xi_T} T^{\delta_3} [\mathbb{1}^{(A; C_{q_{\bar{\alpha}}})} [v]] e^{-iq_{\bar{\alpha}} (\delta_3 + 1)} \right]] e^{+i(q_\alpha - q_{\alpha'}) (\delta_2 + 1)} \right] \right) \\
& + \left. \left(\sum_{\delta_1=0}^{\Xi_T} (T^\dagger)^{\delta_1} [\mathbb{1}^\dagger(C_{q_{\alpha'}}; C_{q_\alpha})[u]] e^{-i(q_\alpha - q_{\alpha'}) (\delta_1 + 1)}, \right. \right. \\
& \quad \left. \left. \tilde{h}^{(A;A)} \left[\sum_{\delta_2=0}^{\Xi_T} T^{\delta_2} [\mathbb{1}^{(A; C_{q_{\bar{\alpha}}})} [\mathbb{1}^{(C_{q_{\bar{\alpha}'}}; C_{q_{\bar{\alpha}}})} [v]]] e^{+i(q_\alpha - q_{\alpha'}) (\delta_2 + 1)} \right] \right) \right\} \tag{B.3.48b}
\end{aligned}$$

$$\begin{aligned}
= & \sum_{\alpha', \alpha=1,2} e^{+i(q_\alpha - q_{\alpha'}) (n-1)} \left\{ \left(u_{\alpha'}^{\alpha'}, \tilde{h}^{(A;A)} \left[\sum_{\delta_2=0}^{\Xi_T} T^{\delta_2} [\mathbb{1}^{(A; C_{q_{\bar{\alpha}}})} [v^{\bar{\alpha}'}] e^{+i(q_\alpha - q_{\alpha'}) (\delta_2 + 1)} \right] \right) \right. \\
& + \left(u_{\alpha'}^{\alpha'}, \tilde{h}^{(A;A)} \left[\sum_{\delta_2=0}^{\Xi_T} T^{\delta_2} [\mathbb{1}^{(C_{q_{\bar{\alpha}'}}; A)} [v_{\bar{\alpha}}] e^{+i(q_\alpha - q_{\alpha'}) (\delta_2 + 1)} \right] \right) \\
& + \left. \left(u_{\alpha'}^{\alpha'}, \tilde{h}^{(A;A)} \left[\sum_{\delta_2=0}^{\Xi_T} T^{\delta_2} [\mathbb{1}^{(C_{q_{\bar{\alpha}'}}; C_{q_{\bar{\alpha}}})} [v] e^{+i(q_\alpha - q_{\alpha'}) (\delta_2 + 1)} \right] \right) \right\} \tag{B.3.48c}
\end{aligned}$$

$$= \sum_{\alpha', \alpha=1,2} e^{+i(q_\alpha - q_{\alpha'}) (n-1)} \left(u_{\alpha'}^{\alpha'}, \tilde{h}^{(A;A)} [v_{\bar{\alpha}}^{\alpha'}] \right) \tag{B.3.48d}$$

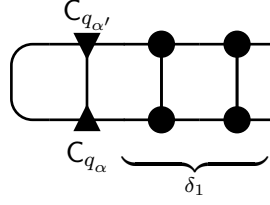
with $v_{\bar{\alpha}}^{\alpha'}$ defined as

$$v_{\bar{\alpha}}^{\alpha'} = \sum_{\delta_2=0}^{\Xi_T} T^{\delta_2} [\mathbb{1}^{(C_{q_{\bar{\alpha}'}}; A)} [v_{\bar{\alpha}}] + \mathbb{1}^{(A; C_{q_{\bar{\alpha}}})} [v^{\bar{\alpha}'}] + \mathbb{1}^{(C_{q_{\bar{\alpha}'}}; C_{q_{\bar{\alpha}}})} [v]] e^{+i(q_\alpha - q_{\alpha'}) (\delta_2 + 1)}. \tag{B.3.49}$$

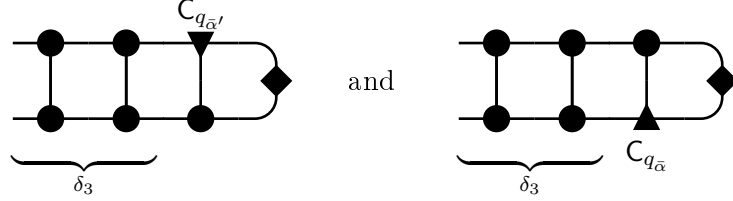
In Eq. (B.3.48), three previously defined summed boundary matrices are used to express the TN evaluations: $u_{\alpha'}^{\alpha'}$, $v^{\bar{\alpha}'}$ and $v_{\bar{\alpha}}$.

The unsurprising yet important to note fact about this is, that parts of a TN that look the same also evaluate to the same expressions, including even the phase factors. For instance,

the left end of a TN in left-canonical gauge



always produces the summed boundary matrix $u_{\alpha'}^{\alpha}$, and the right TN boundaries of the type



yield the summed boundary matrices $v_{\alpha'}^{\alpha}$ and $v_{\bar{\alpha}}$ respectively.

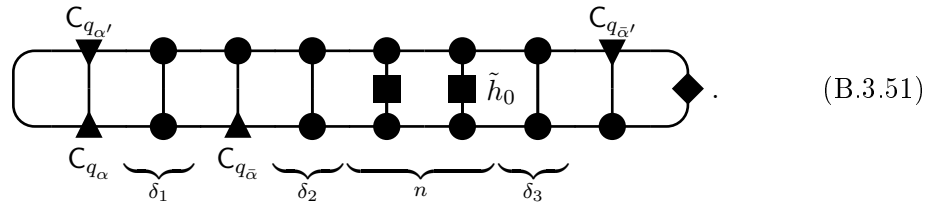
The TN (B.3.42) also contributes to the 1QP corrections. Again, there are two types of non-vanishing factorizations. First, the one analogous to Eq. (B.3.14). This type can be handled in the same way as in case i) by the substitution $u_{\alpha'}^{\alpha} \rightarrow u \cdot f_{\alpha'\alpha}$. The second type results from the factorization Eq. (B.3.15), which only appears in the $\delta = 0$ TNs. As in case i), it can be computed by the substitution $\mathbb{1}^{(C_{q_{\alpha'}}, C_{q_{\alpha}})} \rightarrow T \cdot f_{\bar{\alpha}'\bar{\alpha}}$, thus yielding a total 1QP correction of

$$\begin{aligned}
 H_{\text{IP } q'_1, q_1}^Q \Big|_{\text{ii a)}} & := \sum_{\alpha', \alpha=1,2} e^{+i(q_{\alpha}-q_{\alpha'})(n-1)} \left(u \cdot f_{\alpha'\alpha}^* \varphi_{\alpha'\alpha}^*, \tilde{h}^{(A;A)} [v_{\bar{\alpha}}^{\alpha'}] \right) \\
 & + \sum_{\alpha', \alpha=1,2} e^{+i(q_{\alpha}-q_{\alpha'})(n-1)} \left(u_{\alpha'}^{\alpha}, \tilde{h}^{(A;A)} [T[v]] \cdot f_{\bar{\alpha}'\bar{\alpha}} \varphi_{\alpha'\alpha} \right). \quad (\text{B.3.50a})
 \end{aligned}$$

When taking into account the one-particle corrections, this type of TN converges to zero as function of all δ_i independently, and therefore the contributions to C_{η} are neglected.

B.3.5.2 Subcase iib)

This case is defined by the following TN type



The particle positions and phase factor for $\alpha' = \alpha = 1$ are given by

$$j' = -(\delta_1 + 1 + \delta_2 + 1), \quad d' = \delta_1 + 1 + \delta_2 + n + \delta_3 + 1 \quad (\text{B.3.52})$$

$$j = -(\delta_1 + 1 + \delta_2 + 1) = j', \quad d = \delta_1 + 1, \quad (\text{B.3.53})$$

and

$$\Phi_{11} = e^{+iQ(n+\delta_3)-iq'_1(\delta_1+1+\delta_2+n+\delta_3+1)} e^{-iQ(-\delta_2-1)+iq_1(\delta_1+1)} \quad (\text{B.3.54a})$$

$$= e^{+i(q_1-q'_1)(\delta_1+1)+iq'_2(n+\delta_2)+iq'_2(\delta_3+1)} \quad (\text{B.3.54b})$$

$$= e^{+i(q_1-q'_1)(\delta_1+1)+iq'_2(\delta_2+1)+iq'_2(n-1)+iq'_2(\delta_3+1)}, \quad (\text{B.3.54c})$$

from which the general phase factor can be read off to be

$$\Phi_{\alpha'\alpha} = e^{i(q_\alpha-q_{\alpha'}) (\delta_1+1) + iq_{\alpha'} (\delta_2+1) + iq_{\alpha'} (n-1) + iq_{\alpha'} (\delta_3+1)}. \quad (\text{B.3.55})$$

The 4C contribution follows as

$$\begin{aligned} H_{4C}^Q \Big|_{q'_1, q_1} \Big|_{\text{iib}} &= \sum_{\alpha', \alpha=1,2} \sum_{\delta_2=0}^{\Xi_T} e^{+iq_{\alpha'}(n-1)} \left((T^\dagger)^{\delta_2} \mathbb{1}^{\dagger(A; C_{q_{\alpha'}})} [u_{\alpha'}^{\alpha'}] e^{-iq_{\alpha'}(\delta_2+1)}, \tilde{h}^{(A;A)} [v^{\alpha'}] \right) \\ &=: \sum_{\alpha', \alpha=1,2} e^{+iq_{\alpha'}(n-1)} \left(u_{\alpha\alpha'}^{\alpha'}, \tilde{h}^{(A;A)} [v^{\alpha'}] \right), \end{aligned} \quad (\text{B.3.56a})$$

with $u_{\alpha\alpha'}^{\alpha'}$ defined as

$$u_{\alpha\alpha'}^{\alpha'} := \sum_{\delta_2=0}^{\Xi_T} (T^\dagger)^{\delta_2} \mathbb{1}^{\dagger(A; C_{q_{\alpha'}})} [u_{\alpha'}^{\alpha'}] e^{-iq_{\alpha'}(\delta_2+1)}. \quad (\text{B.3.57})$$

In left-canonical gauge, there are no non-vanishing factorizations of the TN (B.3.51). Therefore, there are no 1QP corrections for this case.

However, there are contributions to the C_η correction, since this case is exactly the example from Sec. B.3.4.3. The relevant TN factorization is therefore the one in Eq. (B.3.21). Its value must be subtracted once for each possible δ_2 , weighted with the corresponding phase factor. The correction is thus

$$\begin{aligned} C_{\eta}^Q \Big|_{q'_1, q_1} \Big|_{\text{iib}} &:= \sum_{\alpha', \alpha=1,2} \sum_{\delta_2=0}^{\Xi_T} e^{+iq_{\alpha'}(n-1)+iq_{\alpha'}(\delta_2+1)} \left(u_{\alpha'}^{\alpha'}, \mathbb{1}^{(A; C_{q_{\alpha'}})} [v] \right) \cdot \left(u, \tilde{h}^{(A;A)} [v^{\alpha'}] \right) \end{aligned} \quad (\text{B.3.58a})$$

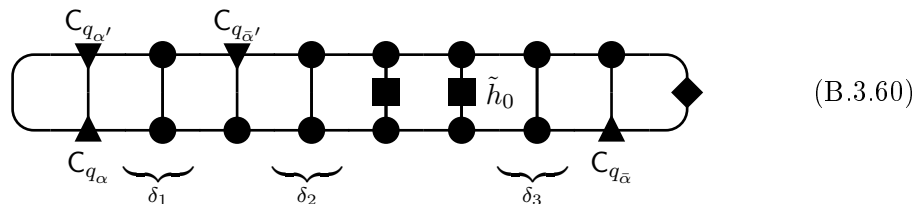
$$= \sum_{\alpha', \alpha=1,2} e^{+iq_{\alpha'}(n-1)} \left(u_{\alpha'}^{\alpha'}, \mathbb{1}^{(A; C_{q_{\alpha'}})} [v] \right) \cdot \left(u, \tilde{h}^{(A;A)} [v^{\alpha'}] \right) \varphi_{\alpha'} \quad (\text{B.3.58b})$$

where $\varphi_{\alpha'}$ is defined as

$$\varphi_{\alpha'} := \sum_{\delta_2=0}^{\Xi_T} e^{+iq_{\alpha'}(\delta_2+1)}. \quad (\text{B.3.59})$$

B.3.5.3 Subcase iic)

The TN type for this case is



which is symmetrical to subcase iib). The 4C contributions are then given by

$$H_{4C}^Q \Big|_{q_1, q_1}^{\text{iic}} := \sum_{\alpha', \alpha=1,2} e^{-iq_{\bar{\alpha}}(n-1)} \left(u_{\alpha}^{\alpha' \bar{\alpha}'}, \tilde{h}^{(A;A)}[v_{\bar{\alpha}}] \right) \quad (\text{B.3.61})$$

and the contribution to the C_{η} correction by

$$C_{\eta}^Q \Big|_{q_1, q_1}^{\text{iic}} := \sum_{\alpha', \alpha=1,2} e^{-iq_{\bar{\alpha}}(n-1)} \left(u_{\alpha}^{\alpha'}, \mathbf{1}^{(C_{q_{\alpha'}}; A)}[v] \right) \cdot \left(u, \tilde{h}^{(A;A)}[v_{\bar{\alpha}}] \right) \varphi_{\bar{\alpha}}^*. \quad (\text{B.3.62})$$

The boundary matrix $u_{\alpha}^{\alpha' \bar{\alpha}'}$ is defined analogously to $u_{\alpha \bar{\alpha}}^{\alpha'}$ as

$$u_{\alpha}^{\alpha' \bar{\alpha}'} := \sum_{\delta_2=0}^{\Xi_T} (T^{\dagger})^{\delta_2} \mathbf{1}^{(C_{q_{\alpha'}}; A)}[u_{\alpha}^{\alpha'}] e^{+iq_{\bar{\alpha}}(\delta_2+1)}. \quad (\text{B.3.63})$$

B.3.5.4 Summary

The combined contribution to the irreducible 2QP matrix element from case ii) is thus

$$\begin{aligned} & V_{q_1, q_1}^Q \Big|_{\text{ii}} \\ &= \sum_{\alpha', \alpha=1,2} e^{+i(q_{\alpha} - q_{\alpha'})(n-1)} \left\{ \left(u_{\alpha, 1Pc}^{\alpha'}, \tilde{h}^{(A;A)}[v_{\bar{\alpha}'}] \right) - \left(u_{\alpha}^{\alpha'}, \tilde{h}^{(A;A)}[v] \right) f_{\bar{\alpha}' \bar{\alpha}} \varphi_{\alpha' \alpha} \right\} \end{aligned} \quad (\text{B.3.64a})$$

$$\begin{aligned} & + \sum_{\alpha', \alpha=1,2} e^{+iq_{\bar{\alpha}'}(n-1)} \left\{ \left(u_{\alpha \bar{\alpha}}^{\alpha'}, \tilde{h}^{(A;A)}[v_{\bar{\alpha}'}] \right) \right. \\ & \quad \left. - \left(u_{\alpha}^{\alpha'}, \mathbf{1}^{(A; C_{q_{\bar{\alpha}'}})}[v] \right) \cdot \left(u, \tilde{h}^{(A;A)}[v_{\bar{\alpha}'}] \right) \varphi_{\bar{\alpha}'} \right\} \end{aligned} \quad (\text{B.3.64b})$$

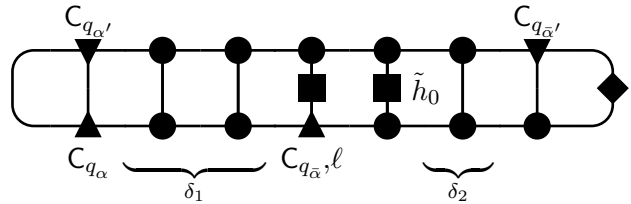
$$\begin{aligned} & + \sum_{\alpha', \alpha=1,2} e^{-iq_{\bar{\alpha}}(n-1)} \left\{ \left(u_{\alpha}^{\alpha' \bar{\alpha}'}, \tilde{h}^{(A;A)}[v_{\bar{\alpha}}] \right) \right. \\ & \quad \left. - \left(u_{\alpha}^{\alpha'}, \mathbf{1}^{(C_{q_{\bar{\alpha}'}}; A)}[v] \right) \cdot \left(u, \tilde{h}^{(A;A)}[v_{\bar{\alpha}}] \right) \varphi_{\bar{\alpha}}^* \right\}. \end{aligned} \quad (\text{B.3.64c})$$

B.3.6 Case iii)

This case describes the transitions between cases i) and ii) and consists itself of five subcases, each with a distinct TN form.

B.3.6.1 Subcase iiiia)

This is the case of the operator acting only on the right, ket-side particle $C_{q_{\bar{\alpha}'}}$, and the right bra-side particle is located to the right of the operator. The corresponding TN is



$$(\text{B.3.65})$$

The absolute position of the $C_{q_{\bar{\alpha}'}}$ is defined as ℓ . For $\alpha' = \alpha = 1$, the particle positions are

$$j' = -(\delta_1 + 1), \quad d' = \delta_1 + n + \delta_2 + 1 \quad (\text{B.3.66})$$

$$j = -(\delta_1 + 1) = j', \quad d = \delta_1 + 1 + \ell. \quad (\text{B.3.67})$$

which yield a phase factor of

$$\begin{aligned} \Phi_{11} &= e^{+iQ(-\delta_1-1+\delta_1+n+\delta_2+1)-iq'_1(\delta_1+n+\delta_2+1)} \\ &\quad \times e^{-iQ(-\delta_1-1+\delta_1+1+\ell)+iq_1(\delta_1+1+\ell)} \end{aligned} \tag{B.3.68a}$$

$$= e^{-iq'_1(\delta_1+1)-iq'_1(n-1)+iq'_2(\delta_2+1)} e^{+iq_1(\delta_1+1)-iq_2\ell} \tag{B.3.68b}$$

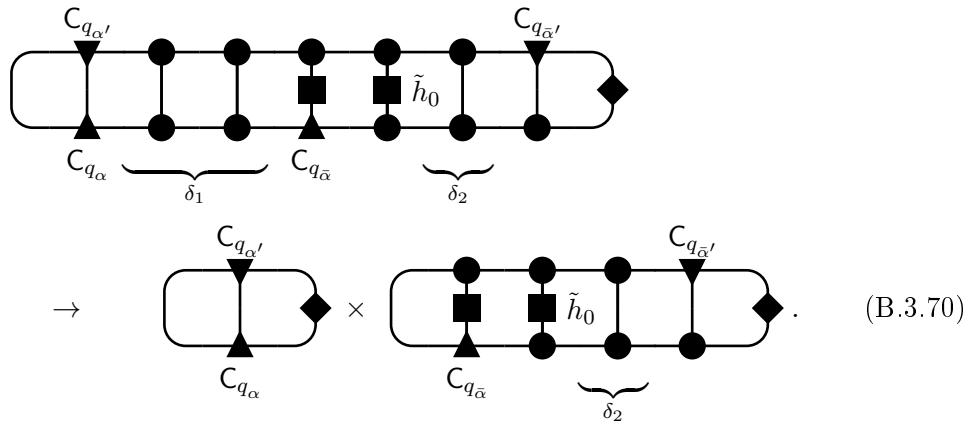
$$= e^{+i(q_1-q'_1)(\delta_1+1)+iq'_2(n-1)-iq_2\ell+iq'_2(\delta_2+1)} \tag{B.3.68c}$$

$$\Rightarrow \Phi_{\alpha'\alpha} = e^{+i(q_\alpha-q_{\alpha'}) (\delta_1+1)+iq_{\alpha'}(n-1)-iq_{\alpha}\ell+iq_{\alpha'}(\delta_2+1)}. \tag{B.3.68d}$$

Now the 4C contribution can be calculated as

$$H_{4C}^Q_{q'_1, q_1} \Big|_{\text{iiia}} := \sum_{\alpha', \alpha=1,2} \sum_{\ell=0}^{n-1} e^{+iq_{\alpha'}(n-1)-iq_{\alpha}\ell} \left(u_{\alpha}^{\alpha'}, \tilde{h}_{\ell}^{(A; C_{q_{\alpha'}})} [v_{\alpha'}] \right). \tag{B.3.69}$$

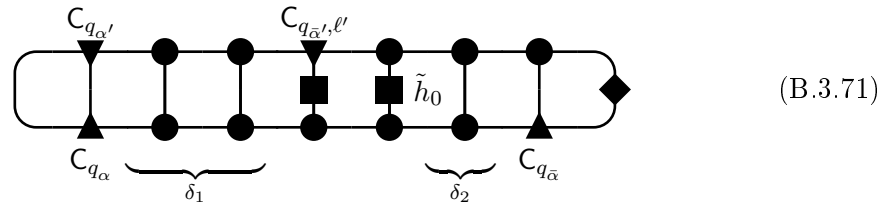
This case does require 1QP corrections, namely from the factorization of the type



These can easily be accounted for by using the left boundary matrix $u_{\alpha, 1Pc}^{\alpha'}$ defined in Eq. (B.3.41). The TN value is then convergent, and the contributions to C_{η} are neglected.

B.3.6.2 Subcase iiib)

This case is defined by the TN type



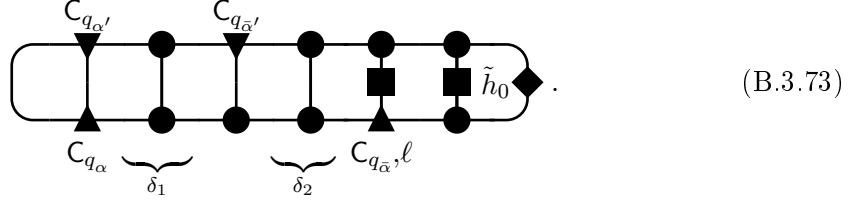
which is symmetrical to subcase iia) and therefore produces contributions symmetrical to Eq. (B.3.69)

$$H_{4C}^Q_{q'_1, q_1} \Big|_{\text{iiib}} := \sum_{\alpha', \alpha=1,2} \sum_{\ell'=0}^{n-1} e^{-iq_{\alpha}(n-1)+iq_{\alpha'}\ell'} \left(u_{\alpha}^{\alpha'}, \tilde{h}_{\ell'}^{(C_{q_{\alpha'}; A})} [v_{\alpha'}] \right). \tag{B.3.72}$$

The 1QP corrections follow the same scheme as in the subcase iia), and are therefore covered by using $u_{\alpha, 1Pc}^{\alpha'}$.

B.3.6.3 Subcase iiic)

This subcase is similar to iia), but with $\max(j', j' + d') < 0$, i.e., the TN type



For $\alpha' = \alpha = 1$, the particle positions are

$$j' = -(\delta_1 + 1 + \delta_2 + 1), \quad d' = \delta_1 + 1 \quad (\text{B.3.74})$$

$$j = -(\delta_1 + 1 + \delta_2 + 1) = j', \quad d = \delta_1 + 1 + \delta_2 + 1 + \ell, \quad (\text{B.3.75})$$

which result in the phase factor

$$\Phi_{11} = e^{+iQ(-\delta_2-1)-iq_1'(\delta_1+1)} e^{-iQ(\ell)+iq_1(\delta_1+1+\delta_2+1+\ell)} \quad (\text{B.3.76a})$$

$$= e^{-iq_1'(\delta_1+1)} e^{-iq_2(\delta_2+1)+iq_1(\delta_1+1)-iq_2\ell} \quad (\text{B.3.76b})$$

$$= e^{+i(q_1-q_1')(\delta_1+1)-iq_2(\delta_2+1)-iq_2\ell} \quad (\text{B.3.76c})$$

$$\Rightarrow \Phi_{\alpha'\alpha} = e^{+i(q_\alpha-q_{\alpha'}) (\delta_1+1) - iq_\alpha (\delta_2+1) - iq_\alpha \ell}. \quad (\text{B.3.76d})$$

Using the already defined left boundary matrix $u_\alpha^{\alpha'\bar{\alpha}'}$, the 4C contribution can be written as

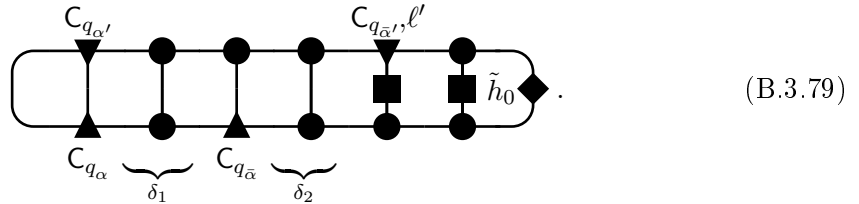
$$H_{4C}^Q |_{q_1', q_1} |_{\text{iiic)}} := \sum_{\alpha', \alpha=1,2} \sum_{\ell=0}^{n-1} e^{-iq_{\bar{\alpha}}\ell} \left(u_\alpha^{\alpha'\bar{\alpha}'}, \tilde{h}_\ell^{(A; C_{q_{\bar{\alpha}}})} [v] \right). \quad (\text{B.3.77})$$

In left-canonical gauge, there are no non-vanishing factorizations of TN (B.3.73) that would contribute to the 1QP part. But, contributions to the C_η correction are needed, since the TN value does not converge to zero for large δ_2 , if δ_1 is small. The corrections follow the scheme of case iic) and are thus given by

$$C_{\eta}^Q |_{q_1', q_1} |_{\text{iiic)}} := \sum_{\alpha', \alpha=1,2} \sum_{\ell=0}^{n-1} e^{-iq_{\bar{\alpha}}\ell} \left(u_\alpha^{\alpha'}, \mathbf{1}^{(C_{q_{\bar{\alpha}}}; A)} [v] \right) \left(u, \tilde{h}_\ell^{(A; C_{q_{\bar{\alpha}}})} [v] \right) \varphi_\alpha^*. \quad (\text{B.3.78})$$

B.3.6.4 Subcase iiid)

This subcase is again the counterpart of subcase iic) with the operator acting on a bra-side C tensor. Its TNs have the form



With the absolute position of the tensor $C_{q_{\bar{\alpha}'}}$ defined as ℓ' , the positions are again simply given by interchanging (j', d') and (j, d) from case iic). This results in the following 4C contribution

$$H_{4C}^Q |_{q_1', q_1} |_{\text{iiid)}} := \sum_{\alpha', \alpha=1,2} \sum_{\ell'=0}^{n-1} e^{+iq_{\bar{\alpha}}\ell'} \left(u_{\alpha\bar{\alpha}}^{\alpha'}, \tilde{h}_{\ell'}^{(C_{q_{\bar{\alpha}'}}; A)} [v] \right) \quad (\text{B.3.80})$$

and the C_η correction

$$C_{\eta}^Q |_{q_1', q_1} |_{\text{iiid)}} := \sum_{\alpha', \alpha=1,2} \sum_{\ell'=0}^{n-1} e^{+iq_{\bar{\alpha}}\ell'} \left(u_\alpha^{\alpha'}, \mathbf{1}^{(A; C_{q_{\bar{\alpha}}})} [v] \right) \left(u, \tilde{h}_{\ell'}^{(C_{q_{\bar{\alpha}'}}; A)} [v] \right) \varphi_{\bar{\alpha}'}. \quad (\text{B.3.81})$$

B.3.6.5 Subcase iiiie)

The final subcase is that of the operator acting on both the right C tensors, i.e., TNs of the type

$$(B.3.82)$$

Looking at the resulting phase factors from the last two subcases, the 4C contribution can directly be read off as

$$H_{4C, q'_1, q_1}^Q \Big|_{\text{iiiie)} := \sum_{\alpha', \alpha=1,2} \sum_{\ell', \ell=0}^{n-1} e^{+iq_{\bar{\alpha}'}\ell' - iq_{\bar{\alpha}}\ell} \left(u_{\alpha'}^{\alpha'}, \tilde{h}_{\ell'; \ell}^{(C_{q_{\bar{\alpha}'}, \ell'}, C_{q_{\bar{\alpha}}, \ell})} [v] \right). \quad (B.3.83)$$

This subcase also contributes to the 1QP part. The factorization of type Eq. (B.3.14) are, as in the other cases, taken care of by using $u_{\alpha, 1Pc}^{\alpha'}$. The factorization of type Eq. (B.3.15) is non-zero only, if $\ell' = \ell$. The resulting correction is then

$$H_{1P, q'_1, q_1}^Q \Big|_{\text{iiiie)} := \sum_{\alpha', \alpha=1,2} \sum_{\ell'=0}^{n-1} e^{+i(q_{\bar{\alpha}'} - q_{\bar{\alpha}})\ell'} \left(u_{\alpha'}^{\alpha'}, \tilde{h}^{(A; C_{q_{\bar{\alpha}}})} [v] \right) f_{\bar{\alpha}\bar{\alpha}}. \quad (B.3.84)$$

With these 1QP corrections the TN values are convergent, wherefore contributions to C_n are neglected.

B.3.6.6 Summary

With all the subcases analyzed individually, the complete, corrected contribution of case iii) to the irreducible 2QP matrix element is given by

$$V_{q'_1, q_1}^Q \Big|_{\text{iii)} := \sum_{\alpha', \alpha=1,2} \sum_{\ell=0}^{n-1} e^{+iq_{\bar{\alpha}'}(n-1) - iq_{\bar{\alpha}}\ell} \left(u_{\alpha, 1Pc}^{\alpha'}, \tilde{h}_{\ell}^{(A; C_{q_{\bar{\alpha}}})} [v_{\bar{\alpha}'}] \right) \quad (B.3.85a)$$

$$+ \sum_{\alpha', \alpha=1,2} \sum_{\ell'=0}^{n-1} e^{-iq_{\bar{\alpha}}(n-1) + iq_{\bar{\alpha}'}\ell'} \left(u_{\alpha, 1Pc}^{\alpha'}, \tilde{h}_{\ell'}^{(C_{q_{\bar{\alpha}'}, A})} [v_{\bar{\alpha}}] \right) \quad (B.3.85b)$$

$$+ \sum_{\alpha', \alpha=1,2} \sum_{\ell=0}^{n-1} e^{-iq_{\bar{\alpha}}\ell} \left(u_{\alpha}^{\alpha'\bar{\alpha}'}, \tilde{h}_{\ell}^{(A; C_{q_{\bar{\alpha}}})} [v] \right) - \sum_{\alpha', \alpha=1,2} \sum_{\ell=0}^{n-1} e^{-iq_{\bar{\alpha}}\ell} \left(u_{\alpha}^{\alpha'}, \mathbb{1}^{(C_{q_{\bar{\alpha}'}, A})} [v] \right) \left(u, \tilde{h}_{\ell}^{(A; C_{q_{\bar{\alpha}}})} [v] \right) \varphi_{\bar{\alpha}}^* \quad (B.3.85c)$$

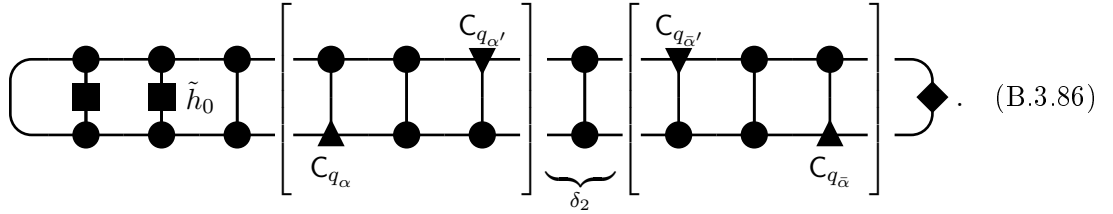
$$+ \sum_{\alpha', \alpha=1,2} \sum_{\ell'=0}^{n-1} e^{+iq_{\bar{\alpha}}\ell'} \left(u_{\alpha\bar{\alpha}}^{\alpha'}, \tilde{h}_{\ell'}^{(C_{q_{\bar{\alpha}'}, A})} [v] \right) - \sum_{\alpha', \alpha=1,2} \sum_{\ell=0}^{n-1} e^{+iq_{\bar{\alpha}}\ell} \left(u_{\alpha}^{\alpha'}, \mathbb{1}^{(A; C_{q_{\bar{\alpha}}})} [v] \right) \left(u, \tilde{h}_{\ell}^{(C_{q_{\bar{\alpha}'}, A})} [v] \right) \varphi_{\bar{\alpha}'} \quad (B.3.85d)$$

$$\begin{aligned}
 & + \sum_{\alpha', \alpha=1,2} \sum_{\ell', \ell=0}^{n-1} e^{+iq_{\bar{\alpha}}\ell' - iq_{\bar{\alpha}}\ell} \left(u_{\alpha', 1\text{Pc}}^{\alpha'}, \tilde{h}_{\ell'; \ell}^{(C_{q_{\bar{\alpha}}'}, C_{q_{\bar{\alpha}}})} [v] \right) \\
 & - \sum_{\alpha', \alpha=1,2} \sum_{\ell'=0}^{n-1} e^{+i(q_{\bar{\alpha}}' - q_{\bar{\alpha}})\ell'} \left(u_{\alpha'}^{\alpha'}, \tilde{h}^{(A;A)} [v] \right) f_{\bar{\alpha}'\bar{\alpha}}. \tag{B.3.85e}
 \end{aligned}$$

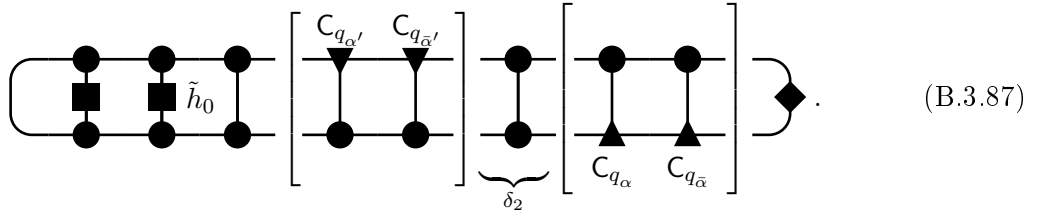
B.3.7 Case iv)

This case is quite difficult to deal with, since the operator acting to the left of all the C tensors thwarts the benefits of the left-canonical gauge as Eq. (5.10) is not applicable. Due to this lack of gauge induced simplifications, this case consists of a total of 13 subcases. They can be divided into three categories, distinguished by how two particles can be grouped together. Because the TNs resemble a ladder, these categories are called “rung grouping”, “rail grouping” and “transition cases”.

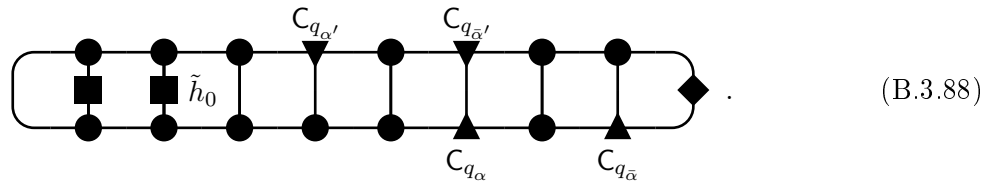
The TNs of the rung grouping category look like the example TN in Eq. (B.3.27) and allow the group each pair of two C tensors in a rung type structure



Accordingly, the rail grouping category holds TNs where each pair can be grouped on one rail like this



And lastly the transition cases, that allow neither the first nor the second grouping, have TNs of the type



B.3.7.1 Left TN boundary matrix

Before all the different subcases are analyzed, a closer look at the left boundary of the TNs is in order. For case iv), independently of the actual particle positions, the left boundary of the TN always has the form



Note that the operator width n and the distance δ_0 between the operator and the first C tensor only enter into the reference particle positions j' and j , not into the particle distances d' and d . Let

$$j' = n + \delta_0 + x' \quad \text{and} \quad j = n + \delta_0 + x, \quad (\text{B.3.90})$$

which is always possible regardless of the signs of d' and d . The phase factor from Eq. (B.3.2) can then be written as

$$\Phi = e^{+iQ(j'+d')-iq_1'd'} e^{-iQ(j+d)+iq_1d} \quad (\text{B.3.91a})$$

$$= e^{+iQj'+i(Q-q_1')d'-iQj-i(Q-q_1)d} \quad (\text{B.3.91b})$$

$$= e^{+iQ(n+\delta_0+x')+iq_2'd'-iQ(n+\delta_0+x)-iq_2d} \quad (\text{B.3.91c})$$

$$= e^{+iQx'+iq_2'd'-iQx-iq_2d}. \quad (\text{B.3.91d})$$

This means, the phases related to n and δ_0 *always* cancel out. Therefore, n and δ_0 do not need to be taken into account explicitly when determining the particle positions.

This also allows to define a summed left boundary matrix

$$u_{\tilde{h}} := \sum_{\delta_0=0}^{\Xi_T} (T^\dagger)^{\delta_0} [\tilde{h}^\dagger \text{(A:A)}[u]] \quad (\text{B.3.92})$$

that is the same for all groupings and subcases.

B.3.7.2 Subcase iva): Rung grouping category

This category is by far the largest. Each block in square brackets in (B.3.86) has three topologically distinct states

$$(\text{B.3.93})$$

depending on whether the bra-side C tensor is located left, right or on the same site as the ket-side C tensor. This results in a total of nine subcases in this category.

However, recall that parts of TNs that look the same, also evaluate to the same expressions. Therefore, the right block in (B.3.86), including both the boundary matrix v and the block marked δ_2 , is described in all its three states by the summed boundary matrix $v_{\tilde{\alpha}}^{\alpha'}$ defined in Eq. (B.3.49). This will be demonstrated on the example TN

$$(\text{B.3.94})$$

Noting that n and δ_0 can be neglected, the relevant particle positions for $\alpha' = \alpha = 1$ are given by

$$j' = \delta_1 + 1, \quad d' = \delta_2 + 1 \quad (\text{B.3.95})$$

$$j = 0, \quad d = \delta_1 + 1 + \delta_2 + 1 + \delta_3 + 1. \quad (\text{B.3.96})$$

They yield the phase factor

$$\begin{aligned} \Phi_{11} &= e^{+iQ(\delta_1+1+\delta_2+1)-iq'_1(\delta_2+1)} \\ &\quad \times e^{-iQ(\delta_1+1+\delta_2+1+\delta_3+1)+iq_1(\delta_1+1+\delta_2+1+\delta_3+1)} \end{aligned} \quad (\text{B.3.97a})$$

$$= e^{+iq_1(\delta_1+1)+i(q'_2-q_2)(\delta_2+1)-iq_2(\delta_3+1)} \quad (\text{B.3.97b})$$

$$= e^{+iq_1(\delta_1+1)+i(q_1-q'_1)(\delta_2+1)-iq_2(\delta_3+1)} \quad (\text{B.3.97c})$$

$$\Rightarrow \Phi_{\alpha'\alpha} = e^{+iq_\alpha(\delta_1+1)+i(q_\alpha-q_{\alpha'}) (\delta_2+1)-iq_{\bar{\alpha}}(\delta_3+1)} . \quad (\text{B.3.97d})$$

As always, the phase factor can be split into separate factors related to each individual distance δ_i .

The summed 4C contribution from this TN is thus

$$\begin{aligned} &H_{4C}^Q \Big|_{q'_1, q_1} \Big|_{\text{iv}a1} \\ &:= \sum_{\alpha', \alpha=1,2} \sum_{\delta_1=0}^{\Xi_T} \sum_{\delta_2=0}^{\Xi_T} \sum_{\delta_3=0}^{\Xi_T} e^{+iq_\alpha(\delta_1+1)+i(q_\alpha-q_{\alpha'}) (\delta_2+1)-iq_{\bar{\alpha}}(\delta_3+1)} \\ &\quad \times \left((T^\dagger)^{\delta_1} [\mathbb{1}^\dagger(\text{A}; \text{C}_{q_\alpha}) [u_{\bar{h}}]], \mathbb{1}(\text{C}_{q_{\alpha'}}; \text{A}) [T^{\delta_2} [\mathbb{1}(\text{C}_{q_{\bar{\alpha}}}; \text{A}) [T^{\delta_3} [\mathbb{1}(\text{A}; \text{C}_{\bar{\alpha}}) [v]]]]]] \right) \end{aligned} \quad (\text{B.3.98a})$$

$$\begin{aligned} &= \sum_{\alpha', \alpha=1,2} \left(\sum_{\delta_1=0}^{\Xi_T} (T^\dagger)^{\delta_1} [\mathbb{1}^\dagger(\text{A}; \text{C}_{q_\alpha}) [u_{\bar{h}}]] e^{-iq_\alpha(\delta_1+1)} , \right. \\ &\quad \left. \mathbb{1}(\text{C}_{q_{\alpha'}}; \text{A}) \left[\sum_{\delta_2=0}^{\Xi_T} T^{\delta_2} [\mathbb{1}(\text{C}_{q_{\bar{\alpha}}}; \text{A}) \left[\sum_{\delta_3=0}^{\Xi_T} T^{\delta_3} [\mathbb{1}(\text{A}; \text{C}_{\bar{\alpha}}) [v]] e^{-iq_{\bar{\alpha}}(\delta_3+1)} \right]] e^{+i(q_\alpha-q_{\alpha'}) (\delta_2+1)} \right] \right) \end{aligned} \quad (\text{B.3.98b})$$

$$=: \sum_{\alpha', \alpha=1,2} \left(u_{\bar{h}\alpha}, \mathbb{1}(\text{C}_{q_{\alpha'}}; \text{A}) \left[\sum_{\delta_2=0}^{\Xi_T} T^{\delta_2} [\mathbb{1}(\text{C}_{q_{\bar{\alpha}}}; \text{A}) [v_{\bar{\alpha}}]] e^{+i(q_\alpha-q_{\alpha'}) (\delta_2+1)} \right] \right) \quad (\text{B.3.98c})$$

where $u_{\bar{h}\alpha}$ is defined as

$$u_{\bar{h}\alpha} := \sum_{\delta_1=0}^{\Xi_T} (T^\dagger)^{\delta_1} [\mathbb{1}^\dagger(\text{A}; \text{C}_{q_\alpha}) [u_{\bar{h}}]] e^{-iq_\alpha(\delta_1+1)} . \quad (\text{B.3.99})$$

Note that the rightmost part of the TN can directly be identified as $v_{\bar{\alpha}}$; and the expression

$$\sum_{\delta_2=0}^{\Xi_T} T^{\delta_2} [\mathbb{1}(\text{C}_{q_{\bar{\alpha}}}; \text{A}) [v_{\bar{\alpha}}]] e^{+i(q_\alpha-q_{\alpha'}) (\delta_2+1)} \quad (\text{B.3.100})$$

is the contribution of the $\delta < 0$ case to $v_{\bar{\alpha}}^{\alpha'}$ as defined in Eq. (B.3.49). It is left to the inclined reader as an exercise, to convince themselves that the results for the other configurations of the right rung block are consistent with the use of $v_{\bar{\alpha}}^{\alpha'}$.

The example TN in (B.3.94) shows the $\delta > 0$ case of the left particle group (cf. (B.3.93)). As seen in Eqs. (B.3.98) and (B.3.99), the left particle in the group and the distance δ_1 can be absorbed into a new summed boundary matrix $u_{\bar{h}\alpha}$. The $\delta < 0$ case of the left rung group results in another summed boundary matrix

$$u_{\bar{h}}^{\alpha'} := \sum_{\delta_1=0}^{\Xi_T} (T^\dagger)^{\delta_1} [\mathbb{1}^\dagger(\text{C}_{q_{\alpha'}}; \text{A}) [u_{\bar{h}}]] e^{+iq_{\alpha'}(\delta_1+1)} , \quad (\text{B.3.101})$$

and in the case $\delta = 0$ there is no summation over δ_1 , which yields the left boundary matrix

$$\mathbb{1}^\dagger(\text{C}_{q_{\alpha'}}; \text{C}_{q_\alpha}) [u_{\bar{h}}] . \quad (\text{B.3.102})$$

Taking all three cases together, allows us to define the left side analog of $v_{\tilde{h}\bar{\alpha}}^{\alpha'}$ from Eq. (B.3.34), namely

$$u_{\tilde{h}\alpha}^{\alpha'} := \mathbb{1}^{\dagger(C_{q_{\alpha'}}; C_{q_{\alpha}})}[u_{\tilde{h}}] + \mathbb{1}^{\dagger(C_{q_{\alpha'}}; A)}[u_{\tilde{h}\alpha}] + \mathbb{1}^{\dagger(A; C_{q_{\alpha}})}[u_{\tilde{h}}^{\alpha'}]. \quad (\text{B.3.103})$$

Now, the entire 4C contribution from the rung grouping category can be written very compactly as

$$H_{4C, q'_1, q_1}^Q \Big|_{\text{iva}} := \sum_{\alpha', \alpha=1,2} \left(u_{\tilde{h}\alpha}^{\alpha'}, v_{\tilde{\alpha}}^{\alpha'} \right). \quad (\text{B.3.104})$$

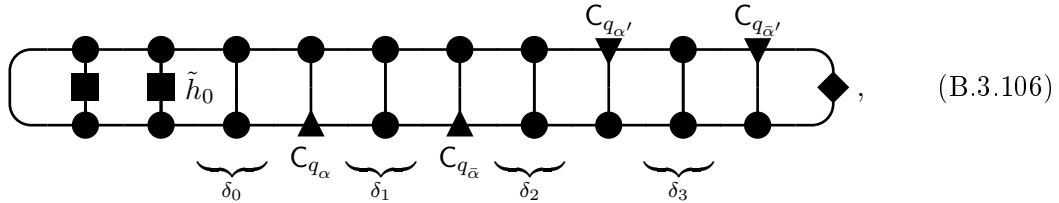
This subcase also contributes to the 1QP part of the matrix element, namely for either of the rung groups having $\delta = 0$. The contributions to the 1QP part where the right rung is factored out is easily obtained from the 4C result by replacing $v_{\tilde{\alpha}}^{\alpha'}$ with $v \cdot f_{\tilde{\alpha}\bar{\alpha}} \varphi_{\alpha'\alpha}$ (cf. Eq. (B.3.120) below). The contribution where the left rung is factored out is also simply retrieved from the 4C result by substituting the rung group with $T \cdot f_{\alpha'\alpha}$. The complete 1QP correction is then given by

$$H_{1P, q'_1, q_1}^Q \Big|_{\text{iva}} := \sum_{\alpha', \alpha=1,2} \left(u_{\tilde{h}\alpha}^{\alpha'}, v \cdot f_{\tilde{\alpha}\bar{\alpha}} \varphi_{\alpha'\alpha} \right) + \left(u_{\tilde{h}}, T[v_{\tilde{\alpha}}^{\alpha'}] \right) f_{\alpha'\alpha} \quad (\text{B.3.105})$$

Including these 1QP corrections, all TN types from this subcase are convergent, thus the contributions to C_{η} are neglected.

B.3.7.3 Subcase ivb): Rail grouping

This category contains only two types of TNs. The one shown as an example in (B.3.87), and its horizontally mirrored counterpart. Only the latter is discussed in some detail, since it is then immediately clear, how to derive the contribution from the TN (B.3.87). The mirrored TN is thus



from which the relevant particle positions for $\alpha' = \alpha = 1$ follow as

$$j' = \delta_1 + 1 + \delta_2 + 1, \quad d' = \delta_3 + 1 \quad (\text{B.3.107})$$

$$j = 0, \quad d = \delta_1 + 1. \quad (\text{B.3.108})$$

The resulting phase factor is

$$\Phi_{11} = e^{+iQ(\delta_1+1+\delta_2+1+\delta_3+1)-iq'_1(\delta_3+1)} e^{-iQ(\delta_1+1)+iq_1(\delta_1+1)} \quad (\text{B.3.109a})$$

$$= e^{+iq_1(\delta_1+1)+iQ(\delta_2+1)+iq'_2(\delta_3+1)} \quad (\text{B.3.109b})$$

$$\Rightarrow \Phi_{\alpha'\alpha} = e^{+iq_{\alpha}(\delta_1+1)+iQ(\delta_2+1)+iq_{\alpha'}(\delta_3+1)}. \quad (\text{B.3.109c})$$

The 4C contribution is then

$$\begin{aligned}
 & H_{4C q'_1, q_1}^Q \Big|_{\text{ivb}}, (\text{B.3.106}) \\
 & := \sum_{\alpha', \alpha=1,2} \sum_{\delta_1=0}^{\Xi_T} \sum_{\delta_2=0}^{\Xi_T} \sum_{\delta_3=0}^{\Xi_T} e^{+iq_\alpha(\delta_1+1)+iQ(\delta_2+1)+iq_{\alpha'}(\delta_3+1)} \\
 & \quad \times \left(\mathbb{1}^\dagger(\text{A}; C_{q_{\bar{\alpha}}}) [(T^\dagger)^{\delta_1} \mathbb{1}^\dagger(\text{A}; C_{q_\alpha}) [u_{\tilde{h}}]], T^{\delta_2} [\mathbb{1}^{(C_{q_{\alpha'}}; \text{A})}] [T^{\delta_3} [\mathbb{1}^{(C_{q_{\bar{\alpha}'}}; \text{A})}] [v]]] \right) \quad (\text{B.3.110a})
 \end{aligned}$$

$$\begin{aligned}
 & = \sum_{\alpha', \alpha=1,2} \left(\mathbb{1}^\dagger(\text{A}; C_{q_{\bar{\alpha}}}) \left[\sum_{\delta_1=0}^{\Xi_T} (T^\dagger)^{\delta_1} \mathbb{1}^\dagger(\text{A}; C_{q_\alpha}) [u_{\tilde{h}}] e^{-iq_\alpha(\delta_1+1)} \right], \right. \\
 & \quad \left. \sum_{\delta_2=0}^{\Xi_T} T^{\delta_2} \left[\mathbb{1}^{(C_{q_{\alpha'}}; \text{A})} \left[\sum_{\delta_3=0}^{\Xi_T} [\mathbb{1}^{(C_{q_{\bar{\alpha}'}}; \text{A})}] [v]] e^{+iq_{\alpha'}(\delta_3+1)} \right] \right] e^{+iQ(\delta_2+1)} \right) \quad (\text{B.3.110b})
 \end{aligned}$$

$$= \sum_{\alpha', \alpha=1,2} \left(\mathbb{1}^\dagger(\text{A}; C_{q_{\bar{\alpha}}}) [u_{\tilde{h} \alpha}], v^{\alpha' \bar{\alpha}'} \right) \quad (\text{B.3.110c})$$

with $v^{\alpha' \bar{\alpha}'}$ defined as

$$v^{\alpha' \bar{\alpha}'} := \sum_{\delta_2=0}^{\Xi_T} T^{\delta_2} [\mathbb{1}^{(C_{q_{\alpha'}}; \text{A})}] [v^{\bar{\alpha}'}] e^{+iQ(\delta_2+1)}. \quad (\text{B.3.111})$$

The contribution from the TN (B.3.87) follows analogously as

$$H_{4C q'_1, q_1}^Q \Big|_{\text{ivb}}, (\text{B.3.87}) := \sum_{\alpha', \alpha=1,2} \left(\mathbb{1}^\dagger(C_{q_{\bar{\alpha}'}}; \text{A}) [u_{\tilde{h}}^{\alpha'}], v_{\alpha \bar{\alpha}} \right) \quad (\text{B.3.112})$$

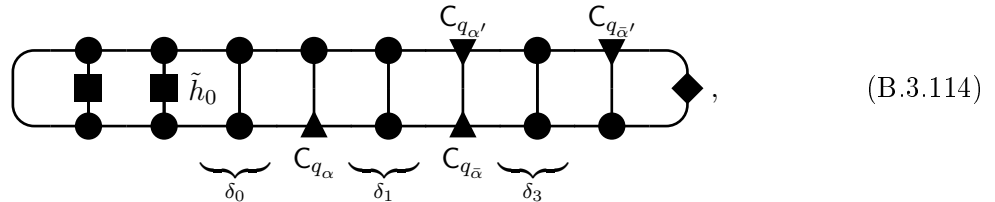
with

$$v_{\alpha \bar{\alpha}} := \sum_{\delta_2=0}^{\Xi_T} T^{\delta_2} [\mathbb{1}^{(\text{A}; C_\alpha)} [v_{\bar{\alpha}}]] e^{-iQ(\delta_2+1)}. \quad (\text{B.3.113})$$

The TNs for this subcase do not have any non-vanishing factorizations, and therefore contribute neither to the 1QP part nor to the C_η correction.

B.3.7.4 Subcase ivc): Transitions between iva) and ivb)

This subcase, too, holds two types of TNs. The one shown in (B.3.88), which can be seen as the $\delta_2 = -1$ limit case of the rail grouped TN (B.3.87). And the counterpart with the positions of the ungrouped particles interchanged



which in turn can be interpreted as the $\delta_2 = -1$ limit case of (B.3.106). The interpretation as $\delta_2 = -1$ limits allows us to read off the 4C contributions immediately as

$$\begin{aligned}
 H_{4C q'_1, q_1}^Q \Big|_{\text{ivc}} & = H_{4C q'_1, q_1}^Q \Big|_{\text{ivc}}, (\text{B.3.88}) + H_{4C q'_1, q_1}^Q \Big|_{\text{ivc}}, (\text{B.3.114}) \\
 & := \sum_{\alpha', \alpha=1,2} \left(u_{\tilde{h}}^{\alpha'}, \mathbb{1}^{(C_{q_{\bar{\alpha}'}}; C_{q_\alpha})} [v_{\bar{\alpha}}] \right) + \sum_{\alpha', \alpha=1,2} \left(u_{\tilde{h} \alpha'}, \mathbb{1}^{(C_{q_{\alpha'}}; C_{q_{\bar{\alpha}'}})} [v^{\bar{\alpha}'}] \right). \quad (\text{B.3.115})
 \end{aligned}$$

This subcase also contributes to the 1QP part of the matrix element with TN factorizations of the type

$$(B.3.116)$$

From this factorization it is evident, that the contributions to the 1QP part are once more given by simply replacing $\mathbb{1}^{(C_{q_{\alpha'}}; C_{q_{\bar{\alpha}}})}$ with $T \cdot f_{\alpha' \bar{\alpha}}$ in the 4C result

$$H_{1P, q_1', q_1}^Q \Big|_{\text{ivc}} := \sum_{\alpha', \alpha=1,2} \left\{ \left(u_{\tilde{h}}^{\alpha'}, T[v_{\bar{\alpha}}] \right) f_{\bar{\alpha}' \alpha} + \left(u_{\tilde{h}, \alpha}, T[v_{\bar{\alpha}'}] \right) f_{\alpha' \bar{\alpha}} \right\}. \quad (B.3.117)$$

Lastly, the TNs of this case also allow for decompositions of the type

$$(B.3.118)$$

which stay finite for large δ_1 if both δ_0 and δ_3 are small, and therefore require contributions to the C_η correction. The contributions are given by the TN product times the summed phases for δ_1 as defined in Eq. (B.3.59), i.e.,

$$\begin{aligned} C_{\eta, q_1', q_1}^Q \Big|_{\text{ivc}} &:= \sum_{\alpha', \alpha=1,2} \left(u_{\tilde{h}}, \mathbb{1}^{(C_{q_{\alpha'}}; A)}[v] \right) \cdot \left(u, \mathbb{1}^{(C_{q_{\bar{\alpha}'}}; C_{q_{\alpha}})}[v_{\bar{\alpha}}] \right) \varphi_{\alpha'}^* \\ &+ \sum_{\alpha', \alpha=1,2} \left(u_{\tilde{h}}, \mathbb{1}^{(A; C_{q_{\alpha}})}[v] \right) \cdot \left(u, \mathbb{1}^{(C_{q_{\alpha'}}; C_{q_{\bar{\alpha}}})}[v_{\bar{\alpha}'}] \right) \varphi_{\alpha}. \end{aligned} \quad (B.3.119)$$

B.3.7.5 Summary

Defining a 1QP corrected right boundary matrix $v_{\bar{\alpha}, 1Pc}^{\alpha'}$ analogous to $u_{\alpha, 1Pc}^{\alpha'}$ as

$$v_{\bar{\alpha}, 1Pc}^{\alpha'} := v_{\bar{\alpha}}^{\alpha'} - v \cdot f_{\bar{\alpha}' \bar{\alpha}} \phi_{\alpha' \alpha}, \quad (B.3.120)$$

the complete contribution to the irreducible 2QP matrix element from case iv) is

$$V_{q_1, q_1}^Q \Big|_{\text{iv)}} := \sum_{\alpha', \alpha=1,2} \left\{ \left(u_{\tilde{h}\alpha'}^{\alpha'}, v_{\tilde{\alpha}, \text{IPc}}^{\alpha'} \right) - \left(u_{\tilde{h}}, T[v_{\tilde{\alpha}}^{\alpha'}] \right) f_{\alpha'\alpha} \right\} \quad (\text{B.3.121a})$$

$$+ \sum_{\alpha', \alpha=1,2} \left\{ \left(\mathbb{1}^{\dagger(\text{A}; \text{C}_{q_{\tilde{\alpha}}})} [u_{\tilde{h}\alpha'}], v_{\alpha'\tilde{\alpha}'} \right) + \left(\mathbb{1}^{\dagger(\text{C}_{q_{\tilde{\alpha}'}; \text{A})} [u_{\tilde{h}}^{\alpha'}], v_{\alpha\tilde{\alpha}} \right) \right\} \quad (\text{B.3.121b})$$

$$+ \sum_{\alpha', \alpha=1,2} \left\{ \left(u_{\tilde{h}}^{\alpha'}, \mathbb{1}^{(\text{C}_{q_{\tilde{\alpha}'}; \text{C}_{q_{\alpha}}})} [v_{\tilde{\alpha}}] \right) - \left(u_{\tilde{h}}, T[v_{\tilde{\alpha}}] \right) f_{\tilde{\alpha}'\alpha} \right\}$$

$$+ \sum_{\alpha', \alpha=1,2} \left\{ \left(u_{\tilde{h}\alpha'}, \mathbb{1}^{(\text{C}_{q_{\alpha'}; \text{C}_{q_{\tilde{\alpha}}})} [v_{\tilde{\alpha}'}] \right) - \left(u_{\tilde{h}\alpha'}, T[v_{\tilde{\alpha}'}] \right) f_{\alpha'\tilde{\alpha}} \right\}$$

$$- \sum_{\alpha', \alpha=1,2} \left(u_{\tilde{h}}, \mathbb{1}^{(\text{C}_{q_{\alpha'}; \text{A})} [v] \right) \cdot \left(u, \mathbb{1}^{(\text{C}_{q_{\tilde{\alpha}'}; \text{C}_{q_{\alpha}}})} [v_{\tilde{\alpha}}] \right) \varphi_{\alpha'}^*$$

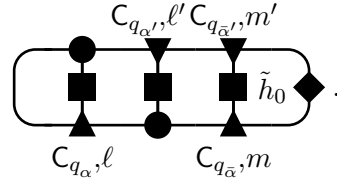
$$- \sum_{\alpha', \alpha=1,2} \left(u_{\tilde{h}}, \mathbb{1}^{(\text{A}; \text{C}_{q_{\alpha}}}) [v] \right) \cdot \left(u, \mathbb{1}^{(\text{C}_{q_{\alpha'}; \text{C}_{\tilde{\alpha}}})} [v_{\tilde{\alpha}'}] \right) \varphi_{\alpha}. \quad (\text{B.3.121c})$$

B.3.8 Case v)

This case covers the transitions from case iv) to the other three cases. Depending on how many and which C tensors the operator acts on, this case falls into six subcases and is quite involved, too.

B.3.8.1 Subcase va)

The first subcase considered is that of the operator acting on all four C tensors. The corresponding TNs are of the form



$$\quad (\text{B.3.122})$$

In this case, the concept of a reference site j and relative particle distance d is of no particular help. Instead, the restrictions $\ell < m$ and $\ell' < m'$ are made. The phase factor is then straight forward to determine as

$$\Phi_{\alpha'\alpha} = e^{+iq_{\alpha}\ell' + iq_{\tilde{\alpha}}m' - iq_{\alpha}\ell - iq_{\tilde{\alpha}}m} \quad (\text{B.3.123})$$

and the 4C contribution follows as

$$H_{4\text{C}}^Q \Big|_{\text{va)}} := \sum_{\alpha', \alpha=1,2} \sum_{\ell'=0}^{n-2} \sum_{\ell=0}^{n-2} \sum_{m'=\ell'+1}^{n-1} \sum_{m=\ell+1}^{n-1} e^{+iq_{\alpha}\ell' + iq_{\tilde{\alpha}}m' - iq_{\alpha}\ell - iq_{\tilde{\alpha}}m} \times \left(u, \tilde{h}_{\ell', m'; \ell, m}^{(\text{C}_{q_{\alpha'}; \text{C}_{q_{\tilde{\alpha}}}; \text{C}_{q_{\alpha}}; \text{C}_{q_{\tilde{\alpha}}})} [v] \right). \quad (\text{B.3.124})$$

This subcase also contributes to the 1QP part, namely if any one, or two compatible, of the following conditions are met

$$\ell' = \ell, \quad m' = m, \quad \ell' = m, \quad \ell = m', \quad (\text{B.3.125})$$

in other words, whenever there is at least one “rung” in the TN ladder, that has C tensors on both ends. Due to the lack of gauge induced simplifications, TNs of the type (B.3.122) allow a lot of different factorizations, for instance

$$\rightarrow \text{[Diagram]} \times \text{[Diagram]} \quad (\text{B.3.126a})$$

$$\rightarrow \text{[Diagram]} \times \text{[Diagram]} \quad (\text{B.3.126b})$$

which all occurred before, but never all in the same subcase. This makes the 1QP contributions of this subcase the most complex ones of all. Here it is helpful, to abandon the rule, that the C tensors with barred momenta $C_{q_{\bar{\alpha}'}}$ and $C_{q_{\bar{\alpha}}}$ are always right of the non-barred ones. Instead, the momenta $q_{\alpha'}$ and q_{α} are fixed to the C rung that is factored out, and which is given the site index j . The remaining particles are designated by absolute site indices ℓ' and ℓ which are summed over values both larger *and* smaller than j , and $\ell' \neq j$ and $\ell \neq j$ is implied. The phase factor can then be determined as

$$\Phi_{\alpha'\alpha} = e^{+iq_{\alpha'}j+iq_{\bar{\alpha}'}\ell'} e^{-iq_{\alpha}j-iq_{\bar{\alpha}}\ell} \quad (\text{B.3.127a})$$

$$= e^{+i(q_{\alpha'}-q_{\alpha})j+iq_{\bar{\alpha}'}\ell'-iq_{\bar{\alpha}}\ell} \quad (\text{B.3.127b})$$

$$= e^{+i(Q-\bar{\alpha}'-Q+\bar{\alpha})j+iq_{\bar{\alpha}'}\ell'-iq_{\bar{\alpha}}\ell} \quad (\text{B.3.127c})$$

$$= e^{+iq_{\bar{\alpha}}(j-\ell)-iq_{\bar{\alpha}'}(j-\ell')} . \quad (\text{B.3.127d})$$

Note that in this description each set $\{j, \ell', \ell\}$ forms a unique TN, and therefore the sums over α' and α are still required to count all necessary contributions.

The contributions the 1QP pare are then

$$H_{1P}^Q \Big|_{q_1', q_1} \Big|_{\text{va}} := \sum_{\alpha', \alpha=1,2} \sum_{j=0}^{n-1} \sum_{\ell'=0, \ell' \neq j}^{n-1} \sum_{\ell=0, \ell \neq j}^{n-1} e^{+iq_{\bar{\alpha}}(j-\ell)-iq_{\bar{\alpha}'}(j-\ell')} \times \left(u, \tilde{h}_{\ell'; \ell}^{(C_{q_{\alpha'}}, C_{q_{\bar{\alpha}}})} [v] \right) f_{\alpha'\alpha} . \quad (\text{B.3.128})$$

Although non-vanishing factorizations of some TNs of this type into a 2QP-1QP overlap and a 1QP-ground state matrix element are possible, these contributions to the C_{η} correction are neglected, since their number is very small compared to the other cases.

B.3.8.2 Subcase vb)

The second subcase is that of the operator acting on two C tensors, described by TNs of the type

$$\text{[Diagram]} \quad (\text{B.3.129})$$

Again, the positions of the C tensors that the operator acts on are labeled ℓ' and ℓ , and the right part of the TN, including the δ_1 block, is actually described by the compound boundary matrix $v_{\bar{\alpha}}^{\alpha'}$. The particle positions for $\alpha' = \alpha = 1$ are

$$j' = \ell', \quad d' = n - 1 - \ell' + \delta_1 + 1 \quad (\text{B.3.130a})$$

$$j = \ell, \quad d = n - 1 - \ell + \delta_1 + 1 + \delta_2 + 1 . \quad (\text{B.3.130b})$$

The resulting phase factor is

$$\begin{aligned} \Phi_{11} &= e^{+iQ(\ell'+n-1-\ell'+\delta_1+1)-iq'_1(n-1-\ell'+\delta_1+1)} \\ &\quad \times e^{-iQ(\ell+n-1-\ell+\delta_1+1+\delta_2+1)+iq_1(n-1-\ell+\delta_1+1+\delta_2+1)} \end{aligned} \quad (\text{B.3.131a})$$

$$= e^{+iq'_1\ell'+iq'_2(n-1)+iq'_2(\delta_1+1)} e^{-iq_1\ell-iq_2(n-1)-iq_2(\delta_1+1+\delta_2+1)} \quad (\text{B.3.131b})$$

$$= e^{+iq'_1\ell'-iq_1\ell+i(q'_2-q_2)(n-1)} e^{+i(q'_2-q_2)(\delta_1+1)-iq_2(\delta_2+1)} \quad (\text{B.3.131c})$$

$$= e^{+iq'_1\ell'-iq_1\ell+i(q_1-q'_1)(n-1)} e^{+i(q_1-q'_1)(\delta_1+1)-iq_2(\delta_2+1)} \quad (\text{B.3.131d})$$

$$\Rightarrow \Phi_{\alpha'\alpha} = e^{+iq_{\alpha'}\ell'-iq_{\alpha}\ell+i(q_{\alpha}-q_{\alpha'})(n-1)} e^{+i(q_{\alpha}-q_{\alpha'})(\delta_1+1)-iq_{\bar{\alpha}}(\delta_2+1)} \quad (\text{B.3.131e})$$

and can be split into a first factor that relates only to the operator part of the TN, and a second factor that relates only to the right part. The second factor is indeed again consistent with $v_{\bar{\alpha}}^{\alpha'}$. Now the 4C contribution can be determined easily as

$$H_{4C}^Q \left. q'_1, q_1 \right|_{\text{vb}} := \sum_{\alpha', \alpha=1,2} \sum_{\ell'=0}^{n-1} \sum_{\ell=0}^{n-1} e^{+iq_{\alpha'}\ell'-iq_{\alpha}\ell+i(q_{\alpha}-q_{\alpha'})(n-1)} \left(u, \tilde{h}_{\ell';\ell}^{(C_{q_{\alpha'}}, C_{q_{\alpha}})} [v_{\bar{\alpha}}^{\alpha'}] \right). \quad (\text{B.3.132})$$

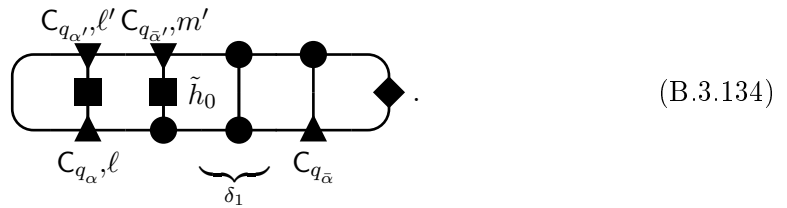
The TN of this case, (B.3.129), is the mirror complement of case iiie), and therefore also contributes to the 1QP part with both the factorization types from Eqs. (B.3.14) and (B.3.14). The contribution where the right C rung is factored out is taken care of by using $v_{\bar{\alpha},1Pc}^{\alpha'}$. The contribution where left pair of C tensors is factored out is non-vanishing if $\ell' = \ell$ and reads

$$H_{1P}^Q \left. q'_1, q_1 \right|_{\text{vb}), (\text{B.3.15})} := \sum_{\alpha', \alpha=1,2} \sum_{\ell'=0}^{n-1} e^{i(q_{\alpha}-q_{\alpha'})(n-1-\ell')} \left(u, \tilde{h}^{(A;A)} [v_{\bar{\alpha}}^{\alpha'}] \right) f_{\alpha'\alpha}. \quad (\text{B.3.133})$$

Taking into account the 1QP corrections, the TN values of this subcase all converge to zero, and the contributions to C_{η} are neglected.

B.3.8.3 Subcase vc)

This is the first of two subcases where the operator acts on three C tensors, described by TNs of the type



Obviously, this is just a mixture of the previous two subcases, where the right part of the TN is now described by $v_{\bar{\alpha}}$. This allows us to write down the 4C contributions immediately by using the corresponding phase factors from subcases va) and vb)

$$H_{4C}^Q \left. q'_1, q_1 \right|_{\text{vc})} := \sum_{\alpha', \alpha=1,2} \sum_{\ell'=0}^{n-2} \sum_{m'=\ell'+1}^{n-1} \sum_{\ell=0}^{n-1} e^{+iq_{\alpha'}\ell'+iq_{\bar{\alpha}'}m'-iq_{\alpha}\ell-iq_{\bar{\alpha}}(n-1)} \left(u, \tilde{h}_{\ell', m'; \ell}^{(C_{q_{\alpha'}}, C_{q_{\bar{\alpha}'}, C_{q_{\alpha}})} [v_{\bar{\alpha}}] \right). \quad (\text{B.3.135})$$

Like in the previous subcases, there are also contributions to the 1QP part. Non-vanishing factorizations exist for $\ell' = \ell$ or $m' = \ell$.

The proper technique is therefore the same as for subcase va), where the momenta $q_{\alpha'}$ and q_{α} are fixed to the position of the factored out C rung, which is named j . The position ℓ'

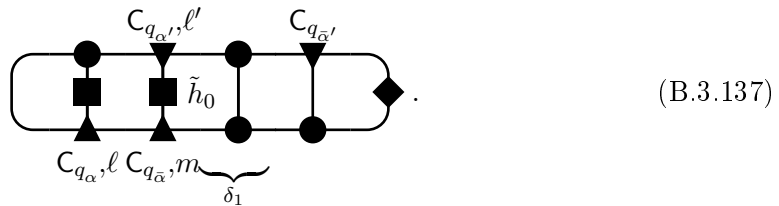
of the remaining particle that the operator acts on is then summed over values both larger and smaller than j . This results in a 1QP contribution of

$$H_{1P}^Q \Big|_{q'_1, q_1} \Big|_{\text{vc}} := \sum_{\alpha', \alpha=1,2} \sum_{j=0}^{n-1} \sum_{\ell'=0, \ell' \neq j}^{n-1} e^{+i(q_{\alpha'} - q_{\alpha})j - iq_{\bar{\alpha}}(n-1) + iq_{\bar{\alpha}}\ell'} \left(u, \tilde{h}_{\ell'}^{(C_{q_{\alpha'}}; A)} [v_{\bar{\alpha}}] \right) f_{\alpha'\alpha} . \tag{B.3.136}$$

As with subcase va), factorizations into 2QP-1QP overlaps and 1QP-ground state matrix elements are possible, but are neglected, since none of them are finite for large δ_1 .

B.3.8.4 Subcase vd)

This is the second subcase where the operator acts on three C tensors and is the vertically flipped counterpart of subcase vc)



Both the 4C and the 1QP contribution therefore follow analogously as

$$H_{4C}^Q \Big|_{q'_1, q_1} \Big|_{\text{vd}} := \sum_{\alpha', \alpha=1,2} \sum_{\ell'=0}^{n-1} \sum_{\ell=0}^{n-2} \sum_{m=\ell+1}^{n-1} e^{+iq_{\alpha'}\ell' + iq_{\bar{\alpha}'}(n-1) - iq_{\alpha}\ell - iq_{\bar{\alpha}}m} \left(u, \tilde{h}_{\ell', \ell, m}^{(C_{q_{\alpha'}}, C_{q_{\alpha}}, C_{q_{\bar{\alpha}}})} [v_{\bar{\alpha}'}] \right) \tag{B.3.138}$$

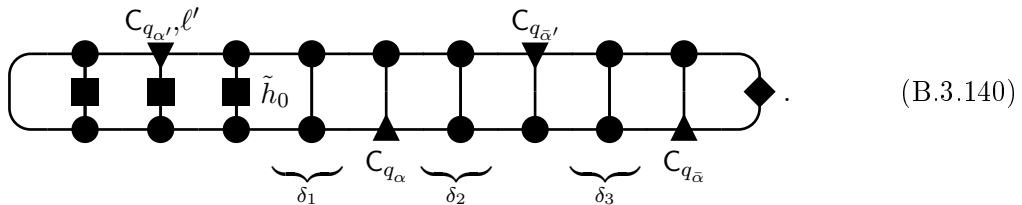
and

$$H_{1P}^Q \Big|_{q'_1, q_1} \Big|_{\text{vd}} := \sum_{\alpha', \alpha=1,2} \sum_{j=0}^{n-1} \sum_{\ell=0, \ell \neq j}^{n-1} e^{+i(q_{\alpha'} - iq_{\alpha})j - iq_{\bar{\alpha}}\ell + iq_{\bar{\alpha}'}(n-1)} \left(u, \tilde{h}_{\ell}^{(A; C_{q_{\bar{\alpha}}})} [v_{\bar{\alpha}'}] \right) f_{\alpha'\alpha} . \tag{B.3.139}$$

In this case, too, the contributions to C_{η} are neglected.

B.3.8.5 Subcase ve)

This is the first of two subcases where the operator acts on a single C tensor and the other three are located to the right of the operator



Actually, this subcase further splits into three sub-subcases, depending on the relative positions of the three C tensors that the operator does not act on. The first is shown in (B.3.140). Once more, the left end of the TN will prove to be describable by $v_{\bar{\alpha}}^{\alpha'}$. The particle positions for $\alpha' = \alpha = 1$ are

$$j' = \ell', \tag{B.3.141a}$$

$$d' = n - 1 - \ell' + \delta_1 + 1 + \delta_2 + 1 \tag{B.3.141a}$$

$$j = n - 1 + \delta_1 + 1, \tag{B.3.141b}$$

$$d = \delta_2 + 1 + \delta_3 + 1 . \tag{B.3.141b}$$

Inserting them into the phase factor yields

$$\begin{aligned} \Phi_{11} &= e^{+iQ(\ell'+n-1-\ell'+\delta_1+1+\delta_2+1)-iq'_1(n-1-\ell'+\delta_1+1+\delta_2+1)} \\ &\quad \times e^{-iQ(n-1+\delta_1+1+\delta_2+1+\delta_3+1)+iq_1(\delta_2+1+\delta_3+1)} \end{aligned} \quad (\text{B.3.142a})$$

$$= e^{-iq'_1(n-1-\ell'+\delta_1+1)+iq'_2(\delta_2+1)-iq_2(\delta_2+1+\delta_3+1)} \quad (\text{B.3.142b})$$

$$= e^{-iq'_1(n-1-\ell'+\delta_1+1)+i(q_1-q'_1)(\delta_2+1)-iq_2(\delta_3+1)} \quad (\text{B.3.142c})$$

$$\Rightarrow \Phi_{\alpha'\alpha} = e^{-iq_{\alpha'}(n-1-\ell')-iq_{\alpha'}(\delta_1+1)} e^{+i(q_\alpha-q_{\alpha'})(\delta_2+1)-iq_\alpha(\delta_3+1)}, \quad (\text{B.3.142d})$$

where the second factor is consistent with the $\delta < 0$ part of $v_{\bar{\alpha}}^{\alpha'}$, as expected. The 4C contribution from this TN type then follows as

$$\begin{aligned} H_{4C, q'_1, q_1}^Q \Big|_{\text{ve}, (\text{B.3.140})} &:= \sum_{\alpha', \alpha=1,2} \sum_{\ell'=0}^{n-1} \sum_{\delta_1=0}^{\Xi_T} e^{-iq_{\alpha'}(n-1-\ell')-iq_{\alpha'}(\delta_1+1)} \left((T^\dagger)^{\delta_1} [\tilde{h}_{\ell'}^\dagger(\text{C}_{q_{\alpha'}; \text{A}})[u]], \mathbf{1}^{(\text{A}; \text{C}_{q_\alpha})}[v_{\bar{\alpha}}^{\alpha'}] \right) \\ &= \sum_{\alpha', \alpha=1,2} \left(u_{\tilde{h}_{\ell'}}^{\alpha'}, \mathbf{1}^{(\text{A}; \text{C}_{q_\alpha})}[v_{\bar{\alpha}}^{\alpha'}] \right), \end{aligned} \quad (\text{B.3.143a})$$

$$= \sum_{\alpha', \alpha=1,2} \left(u_{\tilde{h}_{\ell'}}^{\alpha'}, \mathbf{1}^{(\text{A}; \text{C}_{q_\alpha})}[v_{\bar{\alpha}}^{\alpha'}] \right), \quad (\text{B.3.143b})$$

where $u_{\tilde{h}_{\ell'}}^{\alpha'}$ is defined as

$$u_{\tilde{h}_{\ell'}}^{\alpha'} := \sum_{\delta_1=0}^{\Xi_T} (T^\dagger)^{\delta_1} \left[\sum_{\ell'=0}^{n-1} \tilde{h}_{\ell'}^\dagger(\text{C}_{q_{\alpha'}; \text{A}})[u] e^{+iq_{\alpha'}(n-1-\ell')} \right] e^{+iq_{\alpha'}(\delta_1+1)}. \quad (\text{B.3.144})$$

This type of TN requires 1QP corrections, which arise from the $\delta_3 = -1$ boundary case contained in $v_{\bar{\alpha}}^{\alpha'}$. They can therefore be taken care of by using $v_{\bar{\alpha}, 1\text{Pc}}^{\alpha'}$. There are no non-vanishing C_η type factorizations, hence no corrections are needed.

The second type of TN in this subcase is the $\delta_2 = -1$ limit case of (B.3.140), where $\text{C}_{q_{\bar{\alpha}'}}$ and C_{q_α} form a C rung. The correct phase factor is obtained by inserting $\delta_2 = -1$ into Eq. (B.3.142), and the rightmost part of the TN is still described by $v_{\bar{\alpha}}$. This results in a 4C contribution of

$$H_{4C, q'_1, q_1}^Q \Big|_{\text{ve}, \delta_2=-1} := \sum_{\alpha', \alpha=1,2} \left(u_{\tilde{h}_{\ell'}}^{\alpha'}, \mathbf{1}^{(\text{C}_{q_{\bar{\alpha}'}; \text{C}_{q_\alpha})}[v_{\bar{\alpha}}] \right).$$

This TN type requires both 1QP corrections and contributions to C_η . The 1QP corrections are obtained by replacing $\mathbf{1}^{(\text{C}_{\bar{\alpha}'}; \text{C}_{q_\alpha})}$ with $T \cdot f_{\bar{\alpha}'\alpha}$ in the 4C result.

The contribution to C_η arises from the TN value not converging to zero for large δ_1 if δ_3 is small. The corrections are therefore given by replacing the δ_1 block with $\varphi_{\alpha'}^*$ as

$$\begin{aligned} C_{\eta, q'_1, q_1}^Q \Big|_{\text{ve}, \delta_2=-1} &:= \sum_{\alpha', \alpha=1,2} \sum_{\ell'=0}^{n-1} e^{-iq_{\alpha'}(n-1-\ell')} \left(\tilde{h}_{\ell'}^\dagger(\text{C}_{q_{\alpha'}; \text{A}})[u], v \right) \cdot \left(u, \mathbf{1}^{(\text{C}_{q_{\bar{\alpha}'}; \text{C}_{q_\alpha})}[v_{\bar{\alpha}}] \right) \varphi_{\alpha'}^*. \end{aligned} \quad (\text{B.3.145})$$

Complex conjugation is required due to the definition of $\varphi_{\alpha'}$ with positive sign.

The last type of TN in this subcase results from (B.3.140) by swapping the positions of C_{q_α} and $C_{q_{\bar{\alpha}'}}$

i.e. there is now “rail grouping” of the particles on the ket-side. For $\alpha' = \alpha = 1$, the particle positions are

$$j' = \ell', \quad d' = n - 1 - \ell' + \delta_1 + 1 \quad (\text{B.3.147a})$$

$$j = n - 1 + \delta_1 + 1 + \delta_2 + 1, \quad d = \delta_3 + 1, \quad (\text{B.3.147b})$$

from which the phase factor follows as

$$\begin{aligned} \Phi_{11} &= e^{+iQ(\ell'+n-1-\ell'+\delta_1+1)-iq'_1(n-1-\ell'+\delta_1+1)} \\ &\quad \times e^{-iQ(n-1+\delta_1+1+\delta_2+1+\delta_3+1)+iq_1(\delta_3+1)} \end{aligned} \quad (\text{B.3.148a})$$

$$= e^{-iq'_1(n-1-\ell'+\delta_1+1)-iQ(\delta_2+1)-iq_2(\delta_3+1)} \quad (\text{B.3.148b})$$

$$\Rightarrow \Phi_{\alpha'\alpha} = e^{-iq_{\alpha'}(n-1-\ell')-iq_{\alpha'}(\delta_1+1)} e^{-iQ(\delta_2+1)-iq_{\bar{\alpha}}(\delta_3+1)}. \quad (\text{B.3.148c})$$

As expected, the second factor is consistent with the summed boundary matrix $v_{\alpha\bar{\alpha}}$ defined in Eq. (B.3.113), which describes the right part of the TN. The 4C contribution follows as

$$H_{4C}^Q \Big|_{(ve), (B.3.146)} := \sum_{\alpha', \alpha=1,2} \left(u_{\tilde{h}_{\ell'}}^{\alpha'}, \mathbb{1}^{(C_{q_{\bar{\alpha}'}}; A)} [v_{\alpha\bar{\alpha}}] \right). \quad (\text{B.3.149})$$

Thankfully, this TN type does neither contribute to the 1QP part nor require C_η corrections.

B.3.8.6 Subcase vf)

This is the vertically flipped counterpart to subcase ve), i.e. the operator acts on one ket-side C tensor

The calculations are completely analogous to case ve) and yield three 4C contributions, two 1QP corrections and one contribution to C_η . With $u_{\tilde{h}_\ell \alpha}$ defined analogous to Eq. (B.3.144) as

$$u_{\tilde{h}_\ell \alpha} := \sum_{\delta_1=0}^{\Xi_T} (T^\dagger)^{\delta_1} \left[\sum_{\ell=0}^{n-1} \tilde{h}_\ell^{\dagger(A; C_{q_\alpha})} [u] e^{-iq_\alpha(n-1-\ell)} \right] e^{-iq_\alpha(\delta_1+1)}, \quad (\text{B.3.151})$$

the complete contribution of this subcase can be written down very compactly as

$$\begin{aligned} &V_{q_1, q_1}^Q \Big|_{(vf)} \\ &:= \sum_{\alpha', \alpha=1,2} \left(u_{\tilde{h}_\ell \alpha}, \mathbb{1}^{(C_{q_{\alpha'}}; A)} [v_{\bar{\alpha}, 1PC}^{\bar{\alpha}'}] + \mathbb{1}^{(C_{q_{\alpha'}}; C_{\bar{\alpha}})} [v^{\bar{\alpha}'}] - T[v^{\bar{\alpha}'}] f_{\alpha' \bar{\alpha}} + \mathbb{1}^{(A; C_{q_{\bar{\alpha}}})} [v^{\bar{\alpha}' \bar{\alpha}}] \right) \\ &\quad - \sum_{\alpha', \alpha=1,2} \sum_{\ell=0}^{n-1} e^{+iq_\alpha(n-1-\ell)} \left(\tilde{h}_\ell^{\dagger(A; C_{q_\alpha})} [u], v \right) \cdot \left(u, \mathbb{1}^{(C_{q_{\alpha'}}; C_{\bar{\alpha}})} [v^{\bar{\alpha}'}] \right) \varphi_\alpha. \end{aligned} \quad (\text{B.3.152a})$$

B.3.8.7 Subcase vg)

The last type of subcase can be seen as a transition from subcase vc) to ve) and from vd) to vf) respectively. It is described by TNs with the operator acting on two C tensors of the same state, i.e.,

The diagram shows a tensor network with two horizontal strands. The top strand has a sequence of tensors: a square tensor labeled $C_{q_{\alpha'}, \ell'}$, a circle tensor, a square tensor labeled $C_{q_{\bar{\alpha}'}, m'}$, a circle tensor, a circle tensor labeled \tilde{h}_0 , a circle tensor, a circle tensor, and a circle tensor. The bottom strand has a sequence of tensors: a circle tensor, a circle tensor, a circle tensor, a circle tensor, a circle tensor, a circle tensor, and a circle tensor. Vertical lines connect the top and bottom strands. Brackets below the bottom strand indicate segments of length δ_2 and δ_3 . The right boundary is a diamond tensor.

The particle positions for $\alpha' = \alpha = 1$ are

$$j' = \ell', \quad d' = m' - \ell' \quad (\text{B.3.154a})$$

$$j = n - 1 + \delta_2 + 1 \quad d = \delta_3 + 1, \quad (\text{B.3.154b})$$

which yield the following phase factor

$$\Phi_{11} = e^{+iQ(\ell'+m'-\ell')-iq_1'(m'-\ell')} e^{-iQ(n-1+\delta_2+1+\delta_3+1)+iq_1(\delta_3+1)} \quad (\text{B.3.155a})$$

$$= e^{+iq_1'\ell'+iq_2'm'} e^{-iQ(n-1+\delta_2+1)-iq_2(\delta_3+1)} \quad (\text{B.3.155b})$$

$$\Rightarrow \Phi_{\alpha'\alpha} = e^{+iq_{\alpha'}\ell'+iq_{\bar{\alpha}'}m'-iQ(n-1)} e^{-iQ(\delta_2+1)-q_{\bar{\alpha}}(\delta_3+1)}. \quad (\text{B.3.155c})$$

The second factor is clearly consistent with the use of the summed boundary matrix $v_{\alpha\bar{\alpha}}$ for the right part of the TN. The 4C contribution thus follows as

$$H_{4C}^Q \Big|_{q_1, q_1} \Big|_{\text{vg}} := \sum_{\alpha', \alpha=1, 2} \sum_{\ell'=0}^{n-2} \sum_{m'=\ell'+1}^{n-1} e^{+iq_{\alpha'}\ell'+iq_{\bar{\alpha}'}m'-iQ(n-1)} \left(\tilde{h}_{\ell', m'}^{\dagger(C_{q_{\alpha'}}, C_{q_{\bar{\alpha}'}; A})} [u], v_{\alpha\bar{\alpha}} \right). \quad (\text{B.3.156})$$

Like the related TN (B.3.146), this case does not require neither 1QP corrections nor a contribution to C_{η} .

B.3.8.8 Subcase vh)

The last subcase is again the vertically flipped counterpart of the previous one. Its TN is

The diagram shows a tensor network with two horizontal strands. The top strand has a sequence of tensors: a circle tensor, a circle tensor, a circle tensor, a circle tensor, a circle tensor labeled $C_{q_{\alpha'}, \ell}$, a circle tensor, and a circle tensor labeled $C_{q_{\bar{\alpha}'}, m}$. The bottom strand has a sequence of tensors: a square tensor labeled $C_{q_{\alpha}, \ell}$, a square tensor, a square tensor labeled $C_{q_{\bar{\alpha}}, m}$, a circle tensor, a circle tensor, a circle tensor, and a circle tensor. Vertical lines connect the top and bottom strands. Brackets below the bottom strand indicate segments of length δ_2 and δ_3 . The right boundary is a diamond tensor.

and the 4C contribution is given analogously to subcase vg) as

$$H_{4C}^Q \Big|_{q_1, q_1} \Big|_{\text{vh}} := \sum_{\alpha', \alpha=1, 2} \sum_{\ell=0}^{n-2} \sum_{m=\ell+1}^{n-1} e^{-iq_{\alpha}\ell-iq_{\bar{\alpha}}m+iQ(n-1)} \left(\tilde{h}_{\ell, m}^{\dagger(A; C_{q_{\alpha}}, C_{q_{\bar{\alpha}}})} [u], v^{\alpha'\bar{\alpha}'} \right). \quad (\text{B.3.158})$$

B.3.8.9 Summary

Due to the vast amount of subcases and contributions, no intermediate case summary is given at this point, but the reader is referred directly to the summary in appendix C.

B.4 2QP-1QP matrix element

As matrix element of the Hamiltonian, the quantity

$$D_{q'_1}^Q := \langle Q, q'_1 | H | Q \rangle = \langle q'_1, q'_2 | H | Q \rangle \quad (\text{B.4.1})$$

and its complex conjugate describe the amplitudes for quasi-particle decay and fusion processes, that can occur if particle number is not a conserved quantity.

For particle number conserving models, such as those described in Chap. 2, these matrix elements should vanish in the orthonormalized basis.

With the momentum space description Eq. (6.34) for the 2QP state, and the 1QP state

$$|Q\rangle := \frac{1}{\sqrt{L}} \sum_j e^{-iQj} |C_Q, j\rangle \quad (\text{B.4.2})$$

the matrix element is given by

$$D_{q'_1}^Q = \frac{1}{\sqrt{L}} \sum_{j', d'} \sum_j e^{iQ(j'+d') - iq'_1 d' - iQj} \langle C_{q'_1}, j'; C_{q'_2}, j' + d' | \tilde{h}_0 | C_Q, j \rangle - C_{\eta q'_1}^Q. \quad (\text{B.4.3})$$

In contrast to the 2QP matrix element, the 1QP part of the Hamiltonian does not contribute anything here. Therefore, no 1QP corrections are required. However, a correction $C_{\eta q'_1}^Q$ for A not being an eigenstate of H is needed.

B.4.1 1QP-ground state matrix element correction

In analogy to Eq. (B.3.23), the correction term $C_{\eta q'_1}^Q$ is given by factorizing $D_{q'_1}^Q$ into a 1QP overlap and a 1QP-ground state matrix element

$$C_{\eta q'_1}^Q := \frac{1}{\sqrt{L}} \sum_{j', d'} \sum_j e^{iQ(j'+d') - iq'_1 d' - iQj} \times \left(\langle C_{q'_1}, j' | C_Q, j \rangle \langle C_{q'_2}, j' + d' | \tilde{h}_0 | GS \rangle + \langle C_{q'_2}, j' + d' | C_Q, j \rangle \langle C_{q'_1}, j' | \tilde{h}_0 | GS \rangle \right) \quad (\text{B.4.4a})$$

$$\frac{1}{\sqrt{L}} \sum_{j', d'} \sum_j e^{iQ(j'+d') - iq'_1 d' - iQj} \times \left(f_{1Q} \delta_{j', j} \langle C_{q'_2}, j' + d' | \tilde{h}_0 | GS \rangle + f_{2Q} \delta_{j'+d', j} \langle C_{q'_1}, j' | \tilde{h}_0 | GS \rangle \right) \quad (\text{B.4.4b})$$

with $f_{\alpha'Q}$ defined as the overlap

$$f_{\alpha'Q} := \langle C_{q_{\alpha'}}, 0 | C_Q, 0 \rangle = \left(u, \mathbb{1}^{(C_{q_{\alpha'}}; C_Q)} [v] \right). \quad (\text{B.4.5})$$

Again, this includes TN types that do either converge as function of Ξ_T , or add only a fixed number of contributions.

In case of this matrix element it was found, that including *all* of these contributions to $C_{\eta q'_1}^Q$ considerably reduces the magnitude of the residual decay amplitudes after orthonormalization.

B.4.2 Different TN types

Like for the 2QP matrix element, first the different types of TNs that occur in the calculations are introduced. In the following sections, the cases are then analyzed in detail one by one.

i) The operator acts to the right of all C tensors

$$\langle C_{q'_1}, j'; C_{q'_2}, j' + d' | \tilde{h}_0 | C_Q, j \rangle$$

$$= \text{Diagram (B.4.6)}$$

(B.4.6)

ii) The operator acts in between the C tensors

$$\langle C_{q'_1}, j'; C_{q'_2}, j' + d' | \tilde{h}_0 | C_Q, j \rangle$$

$$= \text{Diagram (B.4.7)}$$

(B.4.7)

iii) Transition between cases i) and ii)

$$\langle C_{q'_1}, j'; C_{q'_2}, j' + d' | \tilde{h}_0 | C_Q, j \rangle$$

$$= \text{Diagram (B.4.8)}$$

(B.4.8)

iv) The operator acts to the left of all C tensors

$$\langle C_{q'_1}, j'; C_{q'_2}, j' + d' | \tilde{h}_0 | C_Q, j \rangle$$

$$= \text{Diagram (B.4.9)}$$

(B.4.9)

v) Transitions between case iv) and the other cases

$$\langle C_{q'_1}, j'; C_{q'_2}, j' + d' | \tilde{h}_0 | C_Q, j \rangle = \text{Diagram (B.4.10)}$$

(B.4.10)

Although there are five different types of TNs for this case, too, compared to the 2QP matrix element, calculating the 2QP-1QP matrix element is a cake-walk.

B.4.3 Case i)

As can be seen from the TN

$$(B.4.11)$$

this case is simply the overlap calculation with $v_{\tilde{h}}$ from Eq. (B.3.29) as right boundary matrix instead of v , just as for the 2QP matrix element. However, it is beneficial, to chose a different way of computing it. The particle positions for $\alpha' = 1$ are given by

$$j' = -(\delta_1 + 1 + \delta_2 + 1), \quad d' = \delta_1 + 1 \quad (B.4.12a)$$

$$j = -(\delta_1 + 1 + \delta_2 + 1) = j' \quad (B.4.12b)$$

from which the phase factors follows as

$$\Phi_1 = e^{+iQ(-\delta_1-1-\delta_2-1+\delta_1+1)-iq'_1(\delta_1+1)} e^{-iQ(-\delta_1-1-\delta_2-1)} \quad (B.4.13a)$$

$$= e^{+iq'_2(\delta_1+1)} \quad (B.4.13b)$$

$$\Rightarrow \Phi_{\alpha'} = e^{+iq_{\alpha'}(\delta_1+1)} \quad (B.4.13c)$$

$$= e^{+iq_{\alpha'}d'} . \quad (B.4.13d)$$

The last form of the phase factor $\Phi_{\alpha'}$ is actually universal for any 3C TN with the left boundary seen in (B.4.11), and is therefore also valid for cases ii) and iii).

The 3C contribution is then given by

$$\begin{aligned} & H_{3C}^Q \Big|_{q'_1} \Big|_i \\ & := \sum_{\alpha'=1,2} \sum_{\delta_1=0}^{\Xi_T} \sum_{\delta_2=0}^{\Xi_T} e^{+iq_{\alpha'}(\delta_1+1)} \left((T^\dagger)^{\delta_1} [\mathbb{1}^{\dagger(C_{q_{\alpha'};C_Q})}[u]], \mathbb{1}^{(C_{q_{\alpha'};A})} [T^{\delta_2} [\tilde{h}^{(A;A)}[v]]] \right) \end{aligned} \quad (B.4.14a)$$

$$= \sum_{\alpha'=1,2} \left(\sum_{\delta_1=0}^{\Xi_T} (T^\dagger)^{\delta_1} [\mathbb{1}^{\dagger(C_{q_{\alpha'};C_Q})}[u]] e^{-iq_{\alpha'}(\delta_1+1)} , \mathbb{1}^{(C_{q_{\alpha'};A})} \left[\sum_{\delta_2=0}^{\Xi_T} T^{\delta_2} [\tilde{h}^{(A;A)}[v]] \right] \right) \quad (B.4.14b)$$

$$= \sum_{\alpha'=1,2} \left(u_Q^{\alpha'} , \mathbb{1}^{(C_{q_{\alpha'};A})} [v_{\tilde{h}}] \right) \quad (B.4.14c)$$

with $v_{\tilde{h}}$ as defined in Eq. (B.3.29), and $u_Q^{\alpha'}$ defined analogously to $u_{\alpha'}^{\alpha'}$ as

$$u_Q^{\alpha'} := \sum_{\delta_1=0}^{\Xi_T} (T^\dagger)^{\delta_1} [\mathbb{1}^{\dagger(C_{q_{\alpha'};C_Q})}[u]] e^{-iq_{\alpha'}(\delta_1+1)} . \quad (B.4.15)$$

The advantage of using this newly defined summed boundary matrix instead of $v_O^{\alpha'}$ from Eq. (B.3.34b) is that $u_Q^{\alpha'}$ also appears in the following cases ii) and iii).

No non-vanishing factorizations of the TN (B.4.11) exist, hence there are no contributions to C_η .

B.4.4 Case ii)

For the 2QP-1QP matrix element, case ii) consists of a single TN type

(B.4.16)

Inserting

$$|d'| = \delta_1 + 1 + n - 1 + \delta_2 + 1 \quad (\text{B.4.17})$$

into the phase factor Eq. (B.4.13d), allows to write down the 3C contribution directly as

$$H_{3C}^Q \Big|_{\text{ii)}} := \sum_{\alpha'=1,2} \sum_{\delta_1=0}^{\Xi_T} \sum_{\delta_2=0}^{\Xi_T} e^{+iq_{\alpha'}(\delta_1+1+n-1+\delta_2+1)} \times \left((T^\dagger)^{\delta_1} [\mathbf{1}^{\dagger(C_{q_{\alpha'}; C_Q})}[u]], \tilde{h}^{(A;A)} [T^{\delta_2} [\mathbf{1}^{(C_{q_{\bar{\alpha}'}; A)}[v]]]] \right) \quad (\text{B.4.18a})$$

$$= \sum_{\alpha'=1,2} e^{+iq_{\bar{\alpha}'}(n-1)} \left(u_Q^{\alpha'}, \tilde{h}^{(A;A)} [v^{\bar{\alpha}'}] \right) \quad (\text{B.4.18b})$$

with $v^{\bar{\alpha}'}$ as defined in Eq. (6.42). This type of TN does not require contributions to C_η , since it may stay finite for large δ_1 , if δ_2 is small. The contributions are readily derived from the 3C result by replacing the TN with the factorization

(B.4.19)

and the δ_1 block with $\varphi_{\bar{\alpha}'}$ as defined in Eq. (B.3.59). It then reads

$$C_{\eta}^Q \Big|_{\text{ii)}} := \sum_{\alpha'=1,2} e^{+iq_{\bar{\alpha}'}(n-1)} \left(u, \tilde{h}^{(A;A)} [v^{\bar{\alpha}'}] \right) f_{\alpha'Q} \varphi_{\bar{\alpha}'}. \quad (\text{B.4.20})$$

B.4.5 Case iii)

This case, too, consists of only one TN type, namely

(B.4.21)

With

$$|d'| = \delta_1 + 1 + \ell' \quad (\text{B.4.22})$$

inserted into Eq. (B.4.13d), the 3C contribution follows as

$$H_{3C q'_1}^Q \Big|_{\text{iii}} := \sum_{\alpha'=1,2} \sum_{\ell'=0}^{n-1} e^{+iq_{\bar{\alpha}'}\ell'} \left(u_Q^{\alpha'}, \tilde{h}_{\ell'}^{(C_{q_{\bar{\alpha}'};A})} [v] \right). \quad (\text{B.4.23})$$

Like the previous case, it requires contributions to C_η , which follow in the same way and are therefore given by

$$C_{\eta q'_1}^Q \Big|_{\text{iii}} := \sum_{\alpha'=1,2} \sum_{\ell'=0}^{n-1} e^{+iq_{\bar{\alpha}'}\ell'} \left(u, \tilde{h}_{\ell'}^{(C_{q_{\bar{\alpha}'};A})} [v] \right) f_{\alpha'Q} \varphi_{\alpha'}. \quad (\text{B.4.24})$$

B.4.6 Case iv)

This is again the case, where the operator acts to left of all the C tensors, and therefore no simplifications arise from left-canonical gauge. There are three subcases, that can be identified by the positions of the C tensors relative to each other as “rung grouping”, “rail grouping” and “transition case” (cf. Sec. B.3.7).

B.4.6.1 Subcase iva): Rung grouping

The rung grouping case is the one shown in the example TN for case iv)

$$, \quad (\text{B.4.25})$$

where the two rightmost C tensors can be grouped in a rung type structure. The particle positions for $\alpha' = 1$ are

$$j' = n + \delta_0, \quad d' = \delta_1 + 1 + \delta_2 + 1 \quad (\text{B.4.26a})$$

$$j = n + \delta_0 + \delta_1 + 1 \quad (\text{B.4.26b})$$

which result in a phase factor of

$$\Phi_1 = e^{+iQ(n+\delta_0+\delta_1+1+\delta_2+1)-iq'_1(\delta_1+1+\delta_2+1)} e^{-iQ(n+\delta_0+\delta_1+1)} \quad (\text{B.4.27a})$$

$$= e^{-iq'_1(\delta_1+1)+iq'_2(\delta_2+1)} \quad (\text{B.4.27b})$$

$$= e^{+i(q'_2-Q)(\delta_1+1)+iq'_2(\delta_2+1)} \quad (\text{B.4.27c})$$

$$\Rightarrow \Phi_{\alpha'} = e^{+i(q_{\bar{\alpha}'}-Q)(\delta_1+1)+iq_{\bar{\alpha}'}(\delta_2+1)}. \quad (\text{B.4.27d})$$

Unsurprisingly, the phases related to n and δ_0 cancel out completely, which allows the use of $u_{\tilde{h}}$ as defined in Eq. (B.3.92) to describe the left part of the TN up to $C_{q_{\bar{\alpha}'}}$. The 3C contribution is then

$$H_{3C q'_1}^Q \Big|_{\text{iva}} := \sum_{\alpha'=1,2} \left(u_{\tilde{h}}, \mathbf{1}^{(C_{q_{\bar{\alpha}'};A})} [v_Q^{\bar{\alpha}'}] \right) \quad (\text{B.4.28})$$

where $v_Q^{\bar{\alpha}'}$ is defined as

$$v_Q^{\bar{\alpha}'} := \sum_{\delta_1=0}^{\Xi_T} T^{\delta_1} [\mathbf{1}^{(C_{q_{\bar{\alpha}'};C_Q})} [v] + \mathbf{1}^{(C_{q_{\bar{\alpha}'};A})} [v_Q] + \mathbf{1}^{(A;C_Q)} [v^{\bar{\alpha}'}]] e^{+i(q_{\bar{\alpha}'}-Q)(\delta_1+1)} \quad (\text{B.4.29a})$$

$$\text{with } v_Q := \sum_{\delta_2=0}^{\Xi_T} T^{\delta_2} [\mathbf{1}^{(A;C_Q)} [v]] e^{-iQ(\delta_2+1)} \quad (\text{B.4.29b})$$

which is nothing but $v_{\bar{\alpha}}^{\alpha'}$ with $q_{\bar{\alpha}} = Q$. As apparent from the definition in Eq. (B.4.29), $v_{\bar{Q}}^{\alpha'}$ contains the $\delta_2 = -1$ limit case of the TN (B.4.25). That type of TN can have a finite value for large δ_1 , if δ_0 is small, wherefore it requires contributions to C_{η} . Inserting $\delta_2 = -1$ into the phase factor yields them as

$$C_{\eta q'_1}^Q \Big|_{\text{iva}} := \sum_{\alpha'=1,2} \sum_{\delta_1=0}^{\Xi_T} e^{+i(q_{\bar{\alpha}'}-Q)(\delta_1+1)} \left(u_{\tilde{h}}, \mathbb{1}^{(C_{q_{\alpha'};A})}[v] \right) f_{\bar{\alpha}'Q} \quad (\text{B.4.30a})$$

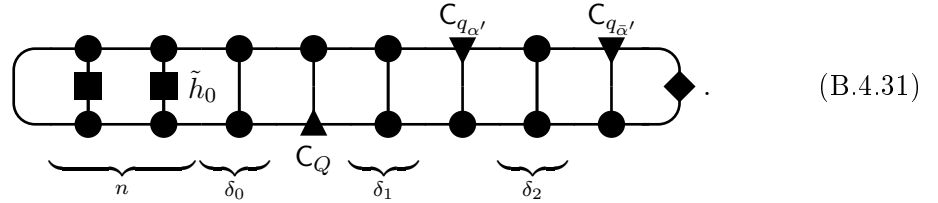
$$= \sum_{\alpha'=1,2} \sum_{\delta_1=0}^{\Xi_T} e^{-iq_{\alpha'}(\delta_1+1)} \left(u_{\tilde{h}}, \mathbb{1}^{(C_{q_{\alpha'};A})}[v] \right) f_{\bar{\alpha}'Q} \quad (\text{B.4.30b})$$

$$= \sum_{\alpha'=1,2} \left(u_{\tilde{h}}, \mathbb{1}^{(C_{q_{\alpha'};A})}[v] \right) f_{\bar{\alpha}'Q} \varphi_{\alpha'}^* . \quad (\text{B.4.30c})$$

with $\varphi_{\alpha'}$ as defined in Eq. (B.3.59).

B.4.6.2 Subcase ivb): Rail grouping

This subcase is defined by the TN type



For $\alpha' = 1$ the particle positions are

$$j' = n + \delta_0 + \delta_1 + 1, \quad d' = \delta_2 + 1 \quad (\text{B.4.32a})$$

$$j = n + \delta_0 . \quad (\text{B.4.32b})$$

They result in the phase factor

$$\Phi_1 = e^{+iQ(n+\delta_0+\delta_1+1)-iq'_1(\delta_2+1)} e^{-iQ(n+\delta_0)} \quad (\text{B.4.33a})$$

$$= e^{+iQ(\delta_1+1)+iq'_2(\delta_2+1)} \quad (\text{B.4.33b})$$

$$\Rightarrow \Phi_{\alpha'} = e^{-iQ(\delta_1+1)+iq_{\alpha'}(\delta_2+1)} \quad (\text{B.4.33c})$$

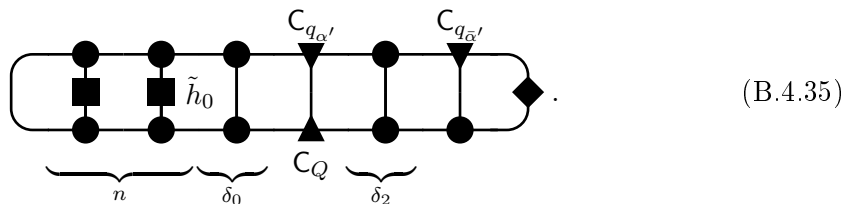
and subsequently, using $v^{\alpha'\bar{\alpha}'}$ from Eq. (B.3.111), in a 3C contribution of

$$H_{3C q'_1}^Q \Big|_{\text{ivb}} := \sum_{\alpha'=1,2} \left(u_{\tilde{h}}, \mathbb{1}^{(A;C_Q)}[v^{\alpha'\bar{\alpha}'}] \right) . \quad (\text{B.4.34})$$

As in the 2QP matrix element calculations, this type of TN does not have non-vanishing factorizations. Therefore, no contributions to C_{η} are needed.

B.4.6.3 Subcase ivc): Transition case

The transition between the previous two subcases is where $C_{q_{\alpha'}}$ and C_Q from a rung, i.e., the TN type



The 3C contribution can immediately be read off the TN to be

$$H_{3Cq'_1}^Q \Big|_{\text{ivc}} := \sum_{\alpha'=1,2} \left(u_{\tilde{h}} \mathbb{1}^{(C_{q_{\alpha'}}, C_Q)} [v^{\bar{\alpha}'}] \right). \quad (\text{B.4.36})$$

This TN type allows the following non-vanishing factorization

$$\text{Diagram 1} \times \text{Diagram 2} \quad (\text{B.4.37})$$

that requires contributions to C_η . As apparent from the factorization, they are given by replacing $\mathbb{1}^{(C_{q_{\alpha'}}, C_Q)}$ with $T \cdot f_{\alpha'Q}$ in the 3C result

$$C_{\eta q'_1}^Q \Big|_{\text{ivc}} := \sum_{\alpha'=1,2} \left(u_{\tilde{h}}, T[v^{\bar{\alpha}'}] \right) f_{\alpha'Q}. \quad (\text{B.4.38})$$

B.4.7 Case v)

This case consists of five subcases, depending on how many and which C tensors the operator acts on.

B.4.7.1 Subcase va)

This is the case of the operator acting on all three C tensors, described by TNs of the type

$$\text{Diagram} \quad (\text{B.4.39})$$

With the restriction $m' > l'$, phase factor and 3C contribution can be read off straight forwardly as

$$H_{3Cq'_1}^Q \Big|_{\text{va}} := \sum_{\alpha'=1,2} \sum_{\ell'=0}^{n-2} \sum_{m'=\ell'+1}^{n-1} \sum_{\ell=0}^{n-1} e^{+iq_{\alpha'}\ell' + iq_{\bar{\alpha}'}m' - iQ\ell} \left(u, \tilde{h}_{\ell', m'; \ell}^{(C_{q_{\alpha'}}, C_{q_{\bar{\alpha}'}, C_Q})} [v] \right). \quad (\text{B.4.40})$$

If either $\ell = \ell'$ or $\ell = m'$ holds, this TN has a factorization that contributes to C_η . Like for the 1QP corrections for case va) of the 2QP matrix element, to describe the corrections, momentum $q_{\alpha'}$ is fixed to the position of the factored out C rung, which is given the site index j . The position ℓ' of the remaining bra-side particle is then summed over values both larger and smaller than j , to account for all possible TN forms. The corresponding phase factor for this summation scheme is

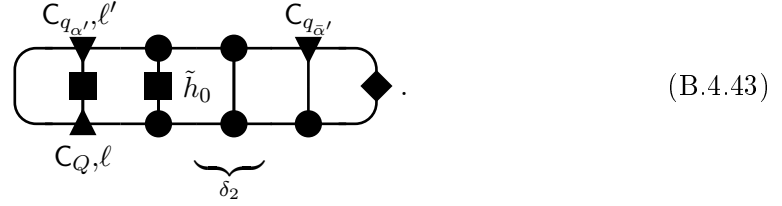
$$\Phi_{\alpha'} = e^{+iq_{\alpha'}j + iq_{\bar{\alpha}'}\ell' - iQj} = e^{+iq_{\bar{\alpha}'}(\ell' - j)}, \quad (\text{B.4.41})$$

which results in the correction

$$C_{\eta q'_1}^Q \Big|_{\text{va}} := \sum_{\alpha'=1,2} \sum_{j=0}^{n-1} \sum_{\ell'=0, \ell' \neq j}^{n-1} e^{+iq_{\bar{\alpha}'}(\ell' - j)} \left(u, \tilde{h}_{\ell'}^{(C_{\bar{\alpha}'}; A)} [v] \right) f_{\alpha'Q}. \quad (\text{B.4.42})$$

B.4.7.2 Subcase vb)

This case deals with the operator acting on one bra-side C and one ket-side C, i.e., TNs of the type



$$(B.4.43)$$

The particle positions for $\alpha' = 1$ are

$$j' = \ell', \quad d' = n - 1 - \ell' + \delta_2 + 1 \quad (B.4.44a)$$

$$j = \ell, \quad (B.4.44b)$$

resulting in a phase factor of

$$\Phi_1 = e^{+iQ(\ell'+n-1-\ell'+\delta_2+1)-iq'_1(n-1-\ell'+\delta_2+1)} e^{-iQ\ell} \quad (B.4.45a)$$

$$= e^{+iq'_1\ell'+iq'_2(n-1+\delta_2+1)-iQ\ell} \quad (B.4.45b)$$

$$\Rightarrow \Phi_{\alpha'} = e^{+iq_{\alpha'}\ell'+iq_{\bar{\alpha}'}(n-1)+iq_{\bar{\alpha}'}(\delta_2+1)-iQ\ell}. \quad (B.4.45c)$$

As expected, the right part of the TN is described by $v^{\bar{\alpha}'}$, which leads to a 3C contribution of

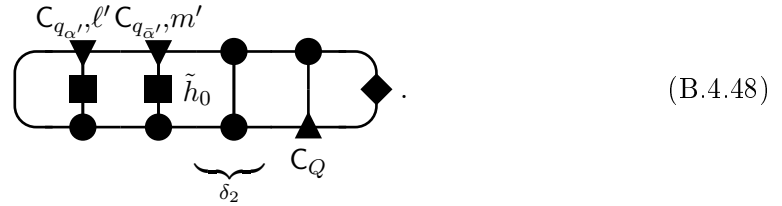
$$H_{3C q'_1}^Q \Big|_{\text{vb}} := \sum_{\alpha'=1,2} \sum_{\ell'=0}^{n-1} \sum_{\ell=0}^{n-1} e^{+iq_{\alpha'}\ell'+iq_{\bar{\alpha}'}(n-1)-iQ\ell} \left(u, \tilde{h}_{\ell';\ell}^{(C_{q_{\alpha'}}, C_Q)} [v^{\bar{\alpha}'}] \right). \quad (B.4.46)$$

This TN type, too, allows a non-vanishing factorization for $\ell' = \ell$, and therefore contributes to C_η . The corrections are readily derived from Eq. (B.4.46), by setting $\ell = \ell' = j$ and factoring out the resulting C rung as $f_{\alpha'Q}$

$$C_{\eta q'_1}^Q \Big|_{\text{vb}} := \sum_{\alpha'=1,2} \sum_{j=0}^{n-1} e^{+iq_{\bar{\alpha}'}(n-1-j)} \left(u, \tilde{h}^{(A;A)} [v^{\bar{\alpha}'}] \right) f_{\alpha'Q}. \quad (B.4.47)$$

B.4.7.3 Subcase vc)

This case is the 3C analog of subcase vg) of the 2QP matrix element, i.e.



$$(B.4.48)$$

Therefore, the phase factor for the operator part of the TN has the same form as Eq. (B.3.155), and the 3C contribution is

$$H_{3C q'_1}^Q \Big|_{\text{vc}} := \sum_{\alpha'=1,2} \sum_{\ell'=0}^{n-1} \sum_{m'=\ell'+1}^{n-1} e^{+iq_{\alpha'}\ell'+iq_{\bar{\alpha}'}m'-iQ(n-1)} \left(u, \tilde{h}_{\ell',m'}^{(C_{q_{\alpha'}}, C_{q_{\bar{\alpha}'}, A})} [v_Q] \right) \quad (B.4.49)$$

where v_Q is defined analogous to $v_{\bar{\alpha}}$ as

$$v_Q := \sum_{\delta_2=0}^{\Xi_T} T^{\delta_2} [\mathbb{1}^{(A;C_Q)} [v]] e^{-iQ(\delta_2+1)}. \quad (B.4.50)$$

No contributions to C_η are needed for this case, since the TN does not have any non-vanishing factorizations.

B.4.7.4 Subcase vd)

This subcase covers TNs where the operator acts one C tensor on the bra-side

$$(B.4.51)$$

For $\alpha' = 1$ the particle positions are

$$j' = \ell', \quad d' = n - 1 - \ell' + \delta_1 + 1 + \delta_2 + 1 \quad (B.4.52a)$$

$$j = n - 1 + \delta_1 + 1, \quad (B.4.52b)$$

yielding a phase factor of

$$\begin{aligned} \Phi_1 &= e^{+iQ(\ell'+n-1-\ell'+\delta_1+1+\delta_2+1)-iq'_1(n-1-\ell'+\delta_1+1+\delta_2+1)} \\ &\quad \times e^{-iQ(n-1+\delta_1+1)} \end{aligned} \quad (B.4.53a)$$

$$= e^{+iq'_1\ell'+i(q'_2-Q)(n-1)} e^{+i(q'_2-Q)(\delta_1+1)+iq'_2(\delta_2+1)} \quad (B.4.53b)$$

$$\Rightarrow \Phi_{\alpha'} = e^{+iq_{\alpha'}\ell'+i(q_{\bar{\alpha}'}-Q)(n-1)} e^{+i(q_{\bar{\alpha}'}-Q)(\delta_1+1)+iq_{\bar{\alpha}'}(\delta_2+1)}. \quad (B.4.53c)$$

The second factor is consistent with the use of $v_Q^{\bar{\alpha}'}$ as defined in Eq. (B.4.29). The 3C contribution is therefore given by

$$H_{3C q'_1}^Q \Big|_{\text{vd}} := \sum_{\alpha'=1,2} \sum_{\ell'=0}^{n-1} e^{+iq_{\alpha'}\ell'+i(q_{\bar{\alpha}'}-Q)(n-1)} \left(u, \tilde{h}_{\ell'}^{(C_{q_{\alpha'};A})} [v_Q^{\bar{\alpha}'}] \right). \quad (B.4.54)$$

Due to the $\delta_2 = -1$ limit case included in $v_Q^{\bar{\alpha}'}$, this subcase does require contributions to C_η , since the TN can then retain a finite value for arbitrarily large δ_1 . Similarly to the correction for the related TN in case iva), the contribution to C_η is given by

$$C_{\eta q'_1}^Q \Big|_{\text{vd}} := \sum_{\alpha'=1,2} \sum_{\ell'=0}^{n-1} e^{+iq_{\alpha'}\ell'+i(q_{\bar{\alpha}'}-Q)(n-1)} \left(u, \tilde{h}_{\ell'}^{(C_{q_{\alpha'};A})} [v] \right) f_{\bar{\alpha}'Q} \varphi_{\alpha'}^*. \quad (B.4.55)$$

B.4.7.5 Subcase ve)

The last subcase is the 3C analog of subcase vh) of the 2QP matrix element

$$(B.4.56)$$

The right part of the TN is therefore described by $v^{\alpha'\bar{\alpha}'}$, and the phase factor for the operator part can easily be derived from Eq. (B.3.156), by dropping the second particle at site m and setting $q_\alpha = Q$. The 3C contribution therefore reads

$$H_{3C q'_1}^Q \Big|_{\text{ve}} := \sum_{\alpha'=1,2} \sum_{\ell=0}^{n-1} e^{-iQ\ell+iQ(n-1)} \left(u, \tilde{h}_\ell^{(A;C_Q)} [v^{\alpha'\bar{\alpha}'}] \right). \quad (B.4.57)$$

Like the analog case vh) of the 2QP matrix element, this TN type does not require contributions to C_η .

Appendix C

Summary of TN calculation results

This appendix contains all the results of the TN calculations of appendix B. It is what needs to be implemented to run actual 2QP computations.

In appendix B, the matrix elements of the Hamiltonian were considered explicitly. However, the results hold for any operator that has a 2QP matrix element of the form Eq. (6.68) or a 2QP-1QP matrix element of the form Eq. (6.61), respectively. Therefore, the results are denoted here with a general operator \hat{O} .

C.1 Shorthand definitions

In order to write down the contributions to the two-particle matrix element more compactly, a number of shorthands is defined. Unless otherwise stated, all sums in these definitions run from 0 to Ξ_T .

Note that they do not only help to write down the results, but many of these quantities occur several times. Therefore, it is also numerically more efficient to compute them once in the beginning of the matrix element computation and use them whenever needed.

C.1.1 Scalars

$$f_{\alpha'\alpha} := \left(u, \mathbb{1}^{(C_{q_{\alpha'}}, C_{q_{\alpha}})} [v] \right) \quad (\text{C.1.1a})$$

$$f_{\alpha'Q} := \left(u, \mathbb{1}^{(C_{q_{\alpha'}}, C_Q)} [v] \right) \quad (\text{C.1.1b})$$

$$\varphi_{\alpha} := \sum_{\delta} e^{+iq_{\alpha}(\delta+1)} \quad (\text{C.1.1c})$$

$$\varphi_{\alpha'\alpha} := \sum_{\delta} e^{+i(q_{\alpha}-q_{\alpha'}) (\delta+1)} \quad (\text{C.1.1d})$$

C.1.2 Summed left boundary matrices

$$u_{\alpha}^{\alpha'} := \sum_{\delta_1} (T^{\dagger})^{\delta_1} [\mathbb{1}^{\dagger(C_{q_{\alpha'}}, C_{q_{\alpha}})} [u]] e^{-i(q_{\alpha}-q_{\alpha'}) (\delta_1+1)} \quad (\text{C.1.2a})$$

$$u_{\alpha}^{\alpha'\bar{\alpha}'} := \sum_{\delta_2} (T^{\dagger})^{\delta_2} [\mathbb{1}^{\dagger(C_{q_{\bar{\alpha}'}, A)} [u_{\alpha'}^{\alpha'}]] e^{+iq_{\bar{\alpha}'} (\delta_2+1)} \quad (\text{C.1.2b})$$

$$u_{\alpha\bar{\alpha}}^{\alpha'} := \sum_{\delta_2} (T^{\dagger})^{\delta_2} [\mathbb{1}^{\dagger(A, C_{q_{\bar{\alpha}}})} [u_{\alpha'}^{\alpha'}]] e^{-iq_{\bar{\alpha}'} (\delta_2+1)} \quad (\text{C.1.2c})$$

$$u_{\alpha, 1Pc}^{\alpha'} := u_{\alpha}^{\alpha'} - u \cdot f_{\alpha'\alpha}^* \varphi_{\alpha'\alpha}^* \quad (\text{C.1.2d})$$

$$u_{\hat{O}} := \sum_{\delta_0} (T^\dagger)^{\delta_0} [O^\dagger^{(A,A)}[u]] \quad (\text{C.1.2e})$$

$$u_{\hat{O}}^{\alpha'} := \sum_{\delta_1} (T^\dagger)^{\delta_1} [\mathbb{1}^{\dagger(C_{q_{\alpha'}}, A)}[u_{\hat{O}}]] e^{+iq_{\alpha'}(\delta_1+1)} \quad (\text{C.1.2f})$$

$$u_{\hat{O}\alpha} := \sum_{\delta_1} (T^\dagger)^{\delta_1} [\mathbb{1}^{\dagger(A, C_{q_\alpha})}[u_{\hat{O}}]] e^{-iq_\alpha(\delta_1+1)} \quad (\text{C.1.2g})$$

$$u_{\hat{O}\alpha}^{\alpha'} := \mathbb{1}^{(C_{q_{\alpha'}}, C_{q_\alpha})}[u_{\hat{O}}] + \mathbb{1}^{(C_{q_{\alpha'}}, A)}[u_{\hat{O}\alpha}] + \mathbb{1}^{(A, C_{q_\alpha})}[u_{\hat{O}}^{\alpha'}] \quad (\text{C.1.2h})$$

$$u_{\hat{O}\ell'}^{\alpha'} := \sum_{\delta_1} (T^\dagger)^{\delta_1} \left[\sum_{\ell'=0}^{n-1} \hat{O}_{\ell'}^{\dagger(C_{q_{\alpha'}}, A)}[u] e^{+iq_{\alpha'}(n-1-\ell')} \right] e^{+iq_{\alpha'}(\delta_1+1)} \quad (\text{C.1.2i})$$

$$u_{\hat{O}\ell\alpha} := \sum_{\delta_1} (T^\dagger)^{\delta_1} \left[\sum_{\ell=0}^{n-1} \hat{O}_\ell^{\dagger(A, C_{q_\alpha})}[u] e^{-iq_\alpha(n-1-\ell)} \right] e^{-iq_\alpha(\delta_1+1)} \quad (\text{C.1.2j})$$

$$u_Q^{\alpha'} := \sum_{\delta} (T^\dagger)^{\delta} [\mathbb{1}^{(C_{q_{\alpha'}}, C_Q)}[u]] e^{-iq_{\alpha'}(\delta+1)} \quad (\text{C.1.2k})$$

C.1.3 Summed right boundary matrices

$$v_{\bar{\alpha}'} := \sum_{\delta_3} T^{\delta_3} [\mathbb{1}^{(C_{q_{\bar{\alpha}'}}}, A)[v]] e^{+iq_{\bar{\alpha}'}(\delta_3+1)} \quad (\text{C.1.3a})$$

$$v_{\bar{\alpha}} := \sum_{\delta_3} T^{\delta_3} [\mathbb{1}^{(A, C_{q_{\bar{\alpha}}})}[v]] e^{-iq_{\bar{\alpha}}(\delta_3+1)} \quad (\text{C.1.3b})$$

$$v_{\bar{\alpha}}^{\alpha'} := \sum_{\delta_2} T^{\delta_2} [\mathbb{1}^{(C_{q_{\bar{\alpha}'}}}, C_{q_{\bar{\alpha}}})}[v] + \mathbb{1}^{(C_{q_{\bar{\alpha}'}}}, A)[v_{\bar{\alpha}}] + \mathbb{1}^{(A, C_{q_{\bar{\alpha}}})}[v_{\bar{\alpha}'}]] e^{+i(q_{\alpha'} - q_{\bar{\alpha}})(\delta_2+1)} \quad (\text{C.1.3c})$$

$$v_{\bar{\alpha}, \text{1Pc}}^{\alpha'} := v_{\bar{\alpha}}^{\alpha'} - v \cdot f_{\bar{\alpha}'\bar{\alpha}} \varphi_{\alpha'\alpha} \quad (\text{C.1.3d})$$

$$v_{\hat{O}} := \sum_{\delta_3} T^{\delta_3} [\hat{O}^{(A,A)}[v]] \quad (\text{C.1.3e})$$

$$v_{\hat{O}}^{\bar{\alpha}'} := \sum_{\delta_2} T^{\delta_2} [\mathbb{1}^{(C_{q_{\bar{\alpha}'}}}, A)[v_{\hat{O}}]] e^{+iq_{\bar{\alpha}'}(\delta_2+1)} \quad (\text{C.1.3f})$$

$$v_{\hat{O}\bar{\alpha}} := \sum_{\delta} T^{\delta} [\mathbb{1}^{(A, C_{q_{\bar{\alpha}}})}[v_{\hat{O}}]] e^{-iq_{\bar{\alpha}}(\delta+1)} \quad (\text{C.1.3g})$$

$$v_{\hat{O}\bar{\alpha}}^{\alpha'} := \mathbb{1}^{(C_{q_{\bar{\alpha}'}}}, C_{q_{\bar{\alpha}}})}[v_{\hat{O}}] + \mathbb{1}^{(C_{q_{\bar{\alpha}'}}}, A)[v_{\hat{O}\bar{\alpha}}] + \mathbb{1}^{(A, C_{q_{\bar{\alpha}}})}[v_{\hat{O}}^{\alpha'}] \quad (\text{C.1.3h})$$

$$v_{\alpha'\bar{\alpha}'} := \sum_{\delta} T^{\delta} [\mathbb{1}^{(C_{q_{\alpha'}}, A)[v_{\bar{\alpha}'}]] e^{+iQ(\delta+1)} \quad (\text{C.1.3i})$$

$$v_{\alpha\bar{\alpha}} := \sum_{\delta} T^{\delta} [\mathbb{1}^{(A, C_{q_\alpha})}[v_{\bar{\alpha}}]] e^{-iQ(\delta+1)} \quad (\text{C.1.3j})$$

$$v_Q := \sum_{\delta} T^{\delta} [\mathbb{1}^{(A, C_Q)}[v]] e^{-iQ(\delta+1)} \quad (\text{C.1.3k})$$

$$v_Q^{\bar{\alpha}'} := \sum_{\delta} T^{\delta} [\mathbb{1}^{(C_{q_{\bar{\alpha}'}}}, C_Q)[v] + \mathbb{1}^{(C_{q_{\bar{\alpha}'}}}, A)[v_Q] + \mathbb{1}^{(A, C_Q)}[v_{\bar{\alpha}'}]] e^{-iq_{\bar{\alpha}'}(\delta+1)} \quad (\text{C.1.3l})$$

C.2 Summary of 2QP matrix element contributions

Case i)

$$V_{q'_1, q_1}^Q \Big|_{\text{i}} := \sum_{\alpha', \alpha=1,2} \left(u_{\alpha, \text{IPc}}^{\alpha'}, v_{\hat{O}_{\bar{\alpha}}}^{\bar{\alpha}'} \right) - \left(u_{\alpha}^{\alpha'}, T[v_{\hat{O}}] \right) f_{\bar{\alpha}'\bar{\alpha}} \quad (\text{C.2.1})$$

Case ii)

$$V_{q'_1, q_1}^Q \Big|_{\text{ii}} = \sum_{\alpha', \alpha=1,2} e^{+i(q_{\alpha} - q_{\alpha'})(n-1)} \left\{ \left(u_{\alpha, \text{IPc}}^{\alpha'}, \hat{O}^{(\text{A}; \text{A})}[v_{\bar{\alpha}'}] \right) - \left(u_{\alpha}^{\alpha'}, \hat{O}^{(\text{A}; \text{A})}[v] f_{\bar{\alpha}'\bar{\alpha}} \varphi_{\alpha'\alpha} \right) \right\} \quad (\text{C.2.2a})$$

$$+ \sum_{\alpha', \alpha=1,2} e^{+iq_{\bar{\alpha}'}(n-1)} \left\{ \left(u_{\alpha\bar{\alpha}}^{\alpha'}, \hat{O}^{(\text{A}; \text{A})}[v_{\bar{\alpha}'}] \right) - \left(u_{\alpha}^{\alpha'}, \mathbb{1}^{(\text{A}; \text{C}_{q_{\bar{\alpha}}})}[v] \right) \cdot \left(u, \hat{O}^{(\text{A}; \text{A})}[v_{\bar{\alpha}'}] \right) \varphi_{\bar{\alpha}'} \right\} \quad (\text{C.2.2b})$$

$$+ \sum_{\alpha', \alpha=1,2} e^{-iq_{\bar{\alpha}}(n-1)} \left\{ \left(u_{\alpha}^{\alpha'\bar{\alpha}'}, \hat{O}^{(\text{A}; \text{A})}[v_{\bar{\alpha}}] \right) - \left(u_{\alpha}^{\alpha'}, \mathbb{1}^{(\text{C}_{q_{\bar{\alpha}}}; \text{A})}[v] \right) \cdot \left(u, \hat{O}^{(\text{A}; \text{A})}[v_{\bar{\alpha}}] \right) \varphi_{\bar{\alpha}}^* \right\} \quad (\text{C.2.2c})$$

Case iii)

$$V_{q'_1, q_1}^Q \Big|_{\text{iii}} := \sum_{\alpha', \alpha=1,2} \sum_{\ell=0}^{n-1} e^{+iq_{\bar{\alpha}'}(n-1) - iq_{\bar{\alpha}}\ell} \left(u_{\alpha, \text{IPc}}^{\alpha'}, \hat{O}_{\ell}^{(\text{A}; \text{C}_{q_{\bar{\alpha}}})}[v_{\bar{\alpha}'}] \right) \quad (\text{C.2.3a})$$

$$+ \sum_{\alpha', \alpha=1,2} \sum_{\ell'=0}^{n-1} e^{-iq_{\bar{\alpha}}(n-1) + iq_{\bar{\alpha}}\ell'} \left(u_{\alpha, \text{IPc}}^{\alpha'}, \hat{O}_{\ell'}^{(\text{C}_{q_{\bar{\alpha}}}; \text{A})}[v_{\bar{\alpha}}] \right) \quad (\text{C.2.3b})$$

$$+ \sum_{\alpha', \alpha=1,2} \sum_{\ell=0}^{n-1} e^{-iq_{\bar{\alpha}}\ell} \left(u_{\alpha}^{\alpha'\bar{\alpha}'}, \hat{O}_{\ell}^{(\text{A}; \text{C}_{q_{\bar{\alpha}}})}[v] \right) - \sum_{\alpha', \alpha=1,2} \sum_{\ell=0}^{n-1} e^{-iq_{\bar{\alpha}}\ell} \left(u_{\alpha}^{\alpha'}, \mathbb{1}^{(\text{C}_{q_{\bar{\alpha}}}; \text{A})}[v] \right) \left(u, \hat{O}_{\ell}^{(\text{A}; \text{C}_{q_{\bar{\alpha}}})}[v] \right) \varphi_{\bar{\alpha}}^* \quad (\text{C.2.3c})$$

$$+ \sum_{\alpha', \alpha=1,2} \sum_{\ell'=0}^{n-1} e^{+iq_{\bar{\alpha}}\ell'} \left(u_{\alpha\bar{\alpha}}^{\alpha'}, \hat{O}_{\ell'}^{(\text{C}_{q_{\bar{\alpha}}}; \text{A})}[v] \right) - \sum_{\alpha', \alpha=1,2} \sum_{\ell=0}^{n-1} e^{+iq_{\bar{\alpha}}\ell'} \left(u_{\alpha}^{\alpha'}, \mathbb{1}^{(\text{A}; \text{C}_{q_{\bar{\alpha}}})}[v] \right) \left(u, \hat{O}_{\ell'}^{(\text{C}_{q_{\bar{\alpha}}}; \text{A})}[v] \right) \varphi_{\bar{\alpha}'} \quad (\text{C.2.3d})$$

$$+ \sum_{\alpha', \alpha=1,2} \sum_{\ell', \ell=0}^{n-1} e^{+iq_{\bar{\alpha}}\ell' - iq_{\bar{\alpha}}\ell} \left(u_{\alpha, \text{IPc}}^{\alpha'}, \hat{O}_{\ell'; \ell}^{(\text{C}_{q_{\bar{\alpha}}}; \text{C}_{\bar{\alpha}})}[v] \right) - \sum_{\alpha', \alpha=1,2} \sum_{\ell'=0}^{n-1} e^{+i(q_{\bar{\alpha}'} - q_{\bar{\alpha}})\ell'} \left(u_{\alpha}^{\alpha'}, \hat{O}^{(\text{A}; \text{A})}[v] \right) f_{\bar{\alpha}'\bar{\alpha}} \quad (\text{C.2.3e})$$

Case iv)

$$V_{q_1^i, q_1}^Q \Big|_{\text{iv}} := \sum_{\alpha', \alpha=1,2} \left\{ \left(u_{\hat{O}\alpha'}^{\alpha'}, v_{\bar{\alpha}, 1\text{Pc}}^{\bar{\alpha}'} \right) - \left(u_{\hat{O}}, T[v_{\bar{\alpha}'}^{\bar{\alpha}'}] \right) f_{\alpha'\alpha} \right\} \quad (\text{C.2.4a})$$

$$+ \sum_{\alpha', \alpha=1,2} \left\{ \left(\mathbb{1}^{\dagger(A; C_{q_{\bar{\alpha}}})} [u_{\hat{O}\alpha'}], v^{\alpha'\bar{\alpha}'} \right) + \left(\mathbb{1}^{\dagger(C_{q_{\bar{\alpha}'}}; A)} [u_{\hat{O}}^{\alpha'}], v_{\alpha\bar{\alpha}} \right) \right\} \quad (\text{C.2.4b})$$

$$+ \sum_{\alpha', \alpha=1,2} \left\{ \left(u_{\hat{O}}^{\alpha'}, \mathbb{1}^{(C_{q_{\bar{\alpha}'}}; C_{q_{\alpha}})} [v_{\bar{\alpha}}] \right) - \left(u_{\hat{O}}, T[v_{\bar{\alpha}}] \right) f_{\bar{\alpha}'\alpha} \right\}$$

$$+ \sum_{\alpha', \alpha=1,2} \left\{ \left(u_{\hat{O}\alpha'}, \mathbb{1}^{(C_{q_{\alpha'}}; C_{q_{\bar{\alpha}}})} [v^{\bar{\alpha}'}] \right) - \left(u_{\hat{O}\alpha'}, T[v^{\bar{\alpha}'}] \right) f_{\alpha'\bar{\alpha}} \right\}$$

$$- \sum_{\alpha', \alpha=1,2} \left(u_{\hat{O}}, \mathbb{1}^{(C_{q_{\alpha'}}; A)} [v] \right) \cdot \left(u, \mathbb{1}^{(C_{q_{\bar{\alpha}'}}; C_{q_{\alpha}})} [v_{\bar{\alpha}}] \right) \varphi_{\alpha'}^*$$

$$- \sum_{\alpha', \alpha=1,2} \left(u_{\hat{O}}, \mathbb{1}^{(A; C_{q_{\alpha}})} [v] \right) \cdot \left(u, \mathbb{1}^{(C_{q_{\alpha'}}; C_{\bar{\alpha}})} [v^{\bar{\alpha}'}] \right) \varphi_{\alpha} \quad (\text{C.2.4c})$$

Case v)

$$V_{q_1^i, q_1}^Q \Big|_{\text{v}} := \sum_{\alpha', \alpha=1,2} \sum_{\ell'=0}^{n-2} \sum_{\ell=0}^{n-2} \sum_{m'=\ell'+1}^{n-1} \sum_{m=\ell+1}^{n-1} e^{+iq_{\alpha'}\ell' + iq_{\bar{\alpha}}m' - iq_{\alpha}\ell - iq_{\bar{\alpha}}m} \\ \times \left(u, \hat{O}_{\ell', m'; \ell, m}^{(C_{q_{\alpha'}}, C_{q_{\bar{\alpha}'}}; C_{q_{\alpha}}, C_{q_{\bar{\alpha}}})} [v] \right)$$

$$- \sum_{\alpha', \alpha=1,2} \sum_{j=0}^{n-1} \sum_{\ell'=0, \ell' \neq j}^{n-1} \sum_{\ell=0, \ell \neq j}^{n-1} e^{+iq_{\alpha}(j-\ell) - iq_{\bar{\alpha}}(j-\ell')} \\ \times \left(u, \hat{O}_{\ell'; \ell}^{(C_{q_{\bar{\alpha}'}}; C_{q_{\bar{\alpha}}})} [v] \right) f_{\alpha'\alpha} \quad (\text{C.2.5a})$$

$$+ \sum_{\alpha', \alpha=1,2} \sum_{\ell'=0}^{n-1} \sum_{\ell=0}^{n-1} e^{+iq_{\alpha'}\ell' - iq_{\alpha}\ell + i(q_{\alpha} - q_{\alpha'})(n-1)} \left(u, \hat{O}_{\ell'; \ell}^{(C_{q_{\alpha'}}; C_{q_{\alpha}})} [v_{\bar{\alpha}, 1\text{Pc}}^{\bar{\alpha}'}] \right) \\ - \sum_{\alpha', \alpha=1,2} \sum_{\ell'=0}^{n-1} e^{i(q_{\alpha} - q_{\alpha'})(n-1-\ell')} \left(u, \hat{O}^{(A; A)} [v_{\bar{\alpha}'}^{\bar{\alpha}'}] \right) f_{\alpha'\alpha} \quad (\text{C.2.5b})$$

$$+ \sum_{\alpha', \alpha=1,2} \sum_{\ell'=0}^{n-2} \sum_{m'=\ell'+1}^{n-1} \sum_{\ell=0}^{n-1} e^{+iq_{\alpha'}\ell' + iq_{\bar{\alpha}}m' - iq_{\alpha}\ell - iq_{\bar{\alpha}}(n-1)} \left(u, \hat{O}_{\ell', m'; \ell}^{(C_{q_{\alpha'}}, C_{q_{\bar{\alpha}'}}; C_{q_{\alpha}})} [v_{\bar{\alpha}}] \right) \\ - \sum_{\alpha', \alpha=1,2} \sum_{j=0}^{n-1} \sum_{\ell'=0, \ell' \neq j}^{n-1} e^{+i(q_{\alpha'} - q_{\alpha})j - iq_{\bar{\alpha}}(n-1) + iq_{\bar{\alpha}}\ell'} \left(u, \hat{O}_{\ell'}^{(C_{q_{\bar{\alpha}'}}; A)} [v_{\bar{\alpha}}] \right) f_{\alpha'\alpha} \quad (\text{C.2.5c})$$

$$+ \sum_{\alpha', \alpha=1,2} \sum_{\ell'=0}^{n-1} \sum_{\ell=0}^{n-2} \sum_{m=\ell+1}^{n-1} e^{+iq_{\alpha'}\ell' + iq_{\bar{\alpha}}(n-1) - iq_{\alpha}\ell - iq_{\bar{\alpha}}m} \left(u, \hat{O}_{\ell'; \ell, m}^{(C_{q_{\alpha'}}, C_{q_{\alpha}}, C_{q_{\bar{\alpha}}})} [v^{\bar{\alpha}'}] \right) \\ - \sum_{\alpha', \alpha=1,2} \sum_{j=0}^{n-1} \sum_{\ell=0, \ell \neq j}^{n-1} e^{+i(q_{\alpha'} - iq_{\alpha})j - iq_{\bar{\alpha}}\ell + iq_{\bar{\alpha}}(n-1)} \left(u, \hat{O}_{\ell}^{(A; C_{q_{\bar{\alpha}}})} [v^{\bar{\alpha}'}] \right) f_{\alpha'\alpha} \quad (\text{C.2.5d})$$

$$+ \sum_{\alpha', \alpha=1,2} \left(u_{\hat{O}_{\ell'}}^{\alpha'}, v_{\bar{\alpha}, 1\text{Pc}}^{\bar{\alpha}'} + \mathbb{1}^{(C_{q_{\bar{\alpha}'}}; C_{\alpha})} [v_{\bar{\alpha}}] - T[v_{\bar{\alpha}}] f_{\bar{\alpha}'\alpha} + \mathbb{1}^{(C_{q_{\bar{\alpha}'}}; A)} [v_{\alpha\bar{\alpha}}] \right) \\ - \sum_{\alpha', \alpha=1,2} \sum_{\ell'=0}^{n-1} e^{-iq_{\alpha'}(n-1-\ell')} \left(\hat{O}_{\ell'}^{\dagger(C_{q_{\alpha'}}; A)} [u], v \right) \cdot \left(u, \mathbb{1}^{(C_{q_{\bar{\alpha}'}}; C_{\alpha})} [v_{\bar{\alpha}}] \right) \varphi_{\alpha'}^* \quad (\text{C.2.5e})$$

$$\begin{aligned}
& + \sum_{\alpha', \alpha=1,2} \left(u_{\hat{O}_\ell \alpha'} \mathbb{1}^{(C_{q_{\alpha'}}; A)} [v_{\bar{\alpha}, \text{IPc}}^{\bar{\alpha}'}] + \mathbb{1}^{(C_{q_{\alpha'}}; C_{\bar{\alpha}})} [v^{\bar{\alpha}'}] - T[v^{\bar{\alpha}'}] f_{\alpha' \bar{\alpha}} + \mathbb{1}^{(A; C_{q_{\bar{\alpha}}})} [v^{\bar{\alpha}' \bar{\alpha}}] \right) \\
& - \sum_{\alpha', \alpha=1,2} \sum_{\ell=0}^{n-1} e^{+iq_\alpha(n-1-\ell)} \left(\hat{O}_\ell^{\dagger(A; C_{q_\alpha})} [u, v] \right) \cdot \left(u, \mathbb{1}^{(C_{q_{\alpha'}}; C_{\bar{\alpha}})} [v^{\bar{\alpha}'}] \right) \varphi_\alpha \quad (\text{C.2.5f})
\end{aligned}$$

$$\begin{aligned}
& + \sum_{\alpha', \alpha=1,2} \sum_{\ell'=0}^{n-2} \sum_{m'=\ell'+1}^{n-1} e^{+iq_{\alpha'} \ell' + iq_{\bar{\alpha}} m' - iQ(n-1)} \left(\hat{O}_{\ell', m'}^{\dagger(C_{q_{\alpha'}}, C_{q_{\bar{\alpha}}}; A)} [u, v_{\alpha \bar{\alpha}}] \right) \quad (\text{C.2.5g})
\end{aligned}$$

$$\begin{aligned}
& + \sum_{\alpha', \alpha=1,2} \sum_{\ell=0}^{n-2} \sum_{m=\ell+1}^{n-1} e^{-iq_\alpha \ell - iq_{\bar{\alpha}} m + iQ(n-1)} \left(\hat{O}_{\ell, m}^{\dagger(A; C_{q_\alpha}, C_{q_{\bar{\alpha}}})} [u, v^{\alpha' \bar{\alpha}'}] \right) \quad (\text{C.2.5h})
\end{aligned}$$

C.3 Summary of 2QP-1QP matrix element contributions

Case i)

$$D_{q_1' |_{\text{ij}}}^Q := \sum_{\alpha'=1,2} \left(u_{Q'}^{\alpha'} \mathbb{1}^{(C_{q_{\bar{\alpha}'}}; A)} [v_{\hat{O}}] \right) \quad (\text{C.3.1})$$

Case ii)

$$D_{q_1' |_{\text{ii}}}^Q := \sum_{\alpha'=1,2} e^{+iq_{\bar{\alpha}'}(n-1)} \left\{ \left(u_{Q'}^{\alpha'} \hat{O}^{(A; A)} [v^{\bar{\alpha}'}] \right) - \left(u, \hat{O}^{(A; A)} [v^{\bar{\alpha}'}] \right) f_{\alpha' Q} \varphi_{\bar{\alpha}'} \right\} \quad (\text{C.3.2})$$

Case iii)

$$D_{q_1' |_{\text{iii}}}^Q := \sum_{\alpha'=1,2} \sum_{\ell'=0}^{n-1} e^{+iq_{\bar{\alpha}'} \ell'} \left\{ \left(u_{Q'}^{\alpha'} \hat{O}_{\ell'}^{(C_{q_{\bar{\alpha}'}}; A)} [v] \right) - \left(u, \hat{O}_{\ell'}^{(C_{q_{\bar{\alpha}'}}; A)} [v] \right) f_{\alpha' Q} \varphi_{\alpha'} \right\} \quad (\text{C.3.3})$$

Case iv)

$$D_{q_1' |_{\text{iv}}}^Q := \sum_{\alpha'=1,2} \left\{ \left(u_{\hat{O}} \mathbb{1}^{(C_{q_{\alpha'}}; A)} [v_{\hat{O}}^{\bar{\alpha}'}] \right) - \left(u_{\hat{O}}, \mathbb{1}^{(C_{q_{\alpha'}}; A)} [v] \right) f_{\bar{\alpha}' Q} \varphi_{\alpha'}^* \right\} \quad (\text{C.3.4a})$$

$$+ \sum_{\alpha'=1,2} \left(u_{\hat{O}}, \mathbb{1}^{(A; C_Q)} [v^{\alpha' \bar{\alpha}'}] \right) \quad (\text{C.3.4b})$$

$$+ \sum_{\alpha'=1,2} \left\{ \left(u_{\hat{O}}, \mathbb{1}^{(C_{q_{\alpha'}}; C_Q)} [v^{\bar{\alpha}'}] \right) - \left(u_{\hat{O}}, T[v^{\bar{\alpha}'}] \right) f_{\alpha' Q} \right\} \quad (\text{C.3.4c})$$

Case v)

$$D_{q_1^Q}^Q \Big|_{(v)} := \sum_{\alpha'=1,2} \sum_{\ell'=0}^{n-2} \sum_{m'=\ell'+1}^{n-1} \sum_{\ell=0}^{n-1} e^{+iq_\alpha \ell' + iq_{\bar{\alpha}} m' - iQ\ell} \left(u, \hat{O}_{\ell', m'; \ell}^{(C_{q_{\alpha'}}, C_{q_{\bar{\alpha}}}, C_Q)} [v] \right) - \sum_{\alpha'=1,2} \sum_{j=0}^{n-1} \sum_{\ell'=0, \ell' \neq j}^{n-1} e^{+iq_{\bar{\alpha}}(\ell' - j)} \left(u, \hat{O}_{\ell'}^{(C_{\bar{\alpha}'}; A)} [v] \right) f_{\alpha' Q} \quad (C.3.5a)$$

$$+ \sum_{\alpha'=1,2} \sum_{\ell'=0}^{n-1} \sum_{\ell=0}^{n-1} e^{+iq_\alpha \ell' + iq_{\bar{\alpha}}(n-1) - iQ\ell} \left(u, \hat{O}_{\ell'; \ell}^{(C_{q_{\alpha'}}, C_Q)} [v^{\bar{\alpha}'}] \right) - \sum_{\alpha'=1,2} \sum_{j=0}^{n-1} e^{+iq_{\bar{\alpha}}(n-1-j)} \left(u, \hat{O}^{(A; A)} [v^{\bar{\alpha}'}] \right) f_{\alpha' Q} \quad (C.3.5b)$$

$$+ \sum_{\alpha'=1,2} \sum_{\ell'=0}^{n-1} e^{+iq_\alpha \ell' + i(q_{\bar{\alpha}'} - Q)(n-1)} \left(u, \hat{O}_{\ell'}^{(C_{q_{\alpha'}}, A)} [v_{\bar{Q}}^{\bar{\alpha}'}] \right) \quad (C.3.5c)$$

$$+ \sum_{\alpha'=1,2} \sum_{\ell'=0}^{n-1} e^{+iq_\alpha \ell' + i(q_{\bar{\alpha}'} - Q)(n-1)} \left(u, \hat{O}_{\ell'}^{(C_{q_{\alpha'}}, A)} [v_{\bar{Q}}^{\bar{\alpha}'}] \right) - \sum_{\alpha'=1,2} \sum_{\ell'=0}^{n-1} e^{+iq_\alpha \ell' + i(q_{\bar{\alpha}'} - Q)(n-1)} \left(u, \hat{O}_{\ell'}^{(C_{q_{\alpha'}}, A)} [v] \right) f_{\bar{\alpha}' Q} \varphi_{\alpha'}^* \quad (C.3.5d)$$

$$+ \sum_{\alpha'=1,2} \sum_{\ell=0}^{n-1} e^{-iQ\ell + iQ(n-1)} \left(u, \hat{O}_\ell^{(A; C_Q)} [v^{\alpha' \bar{\alpha}'}] \right) \quad (C.3.5e)$$

Bibliography

- [1] P. Monthoux and D. Pines. Spin-fluctuation-induced superconductivity and normal-state properties of $\text{YBa}_2\text{Cu}_3\text{O}_7$. *Phys. Rev. B*, 49:4261, 1994.
- [2] C. C. Tsuei, J. R. Kirtley, Z. F. Ren, J. H. Wang, H. Raffy, and Z. Z. Li. Pure $d_{x^2-y^2}$ order-parameter symmetry in the tetragonal superconductor $\text{TI}_2\text{Ba}_2\text{CuO}_{6+\delta}$. *Nature*, 387:481–483, 05 1997.
- [3] Nobelprize.org. The Nobel Prize in Physics 2016. http://www.nobelprize.org/nobel_prizes/physics/laureates/2016/, 2016. Accessed: 29 Jan 2018.
- [4] J. M. Kosterlitz and D. J. Thouless. Long range order and metastability in two dimensional solids and superfluids. (Application of dislocation theory). *J. Phys. C*, 5(11):L124, 1972.
- [5] J. M. Kosterlitz and D. J. Thouless. Ordering, Metastability and Phase Transitions in Two-Dimensional Systems. *J. Phys.*, C6:1181, 1973.
- [6] D. J. Thouless, M. Kohmoto, M. P. Nightingale, and M. den Nijs. Quantized Hall Conductance in a Two-Dimensional Periodic Potential. *Phys. Rev. Lett.*, 49:405–408, Aug 1982.
- [7] F. D. M. Haldane. Continuum Dynamics of the 1-D Heisenberg Antiferromagnet: Identification with the $O(3)$ Nonlinear Sigma Model. *Phys. Lett.*, 93A:464, 1983.
- [8] F. D. M. Haldane. Nonlinear Field Theory of Large-Spin Heisenberg Antiferromagnets: Semiclassically Quantized Solitons of the One-Dimensional Easy-Axis Néel State. *Phys. Rev. Lett.*, 50:1153, 1983.
- [9] G. Jotzu, M. Messer, R. Desbuquois, M. Lebrat, T. Uehlinger, D. Greif, and T. Esslinger. Experimental realization of the topological Haldane model with ultracold fermions. *Nature*, 515(7526):237–246, 11 2014.
- [10] Richard P. Feynman. Simulating physics with computers. *International Journal of Theoretical Physics*, 21(6):467–488, Jun 1982.
- [11] D. P. DiVincenzo. Quantum Computation. *Science*, 270(5234):255–261, 1995.
- [12] B. Fauseweh and G. S. Uhrig. Multiparticle spectral properties in the transverse field Ising model by continuous unitary transformations. *Phys. Rev. B*, 87:184406, 2013.
- [13] L. Vanderstraeten, F. Verstraete, and Jutho Haegeman. Scattering particles in quantum spin chains. *Phys. Rev. B*, 92:125136, Sep 2015.
- [14] B. Fauseweh, J. Stolze, and G. S. Uhrig. Finite-temperature line shapes of hard-core bosons in quantum magnets: A diagrammatic approach tested in one dimension. *Phys. Rev. B*, 90:024428, 2014.

- [15] Benedikt Fauseweh and Götz S. Uhrig. Effects of interactions on dynamic correlations of hard-core bosons at finite temperatures. *Phys. Rev. B*, 96:115150, Sep 2017.
- [16] R. J. Baxter. Dimers on a Rectangular Lattice. *J. Math. Phys.*, 9:650, 1968.
- [17] S. R. White. Density Matrix Formulation for Quantum Renormalization Groups. *Phys. Rev. Lett.*, 69:2863, 1992.
- [18] K. G. Wilson. The Renormalization Group: Critical Phenomena and the Kondo Problem. *Rev. Mod. Phys.*, 47:773, 1975.
- [19] S. Östlund and S. Rommer. Thermodynamic Limit of Density Matrix Renormalization. *Phys. Rev. Lett.*, 75:3537, 1995.
- [20] S. Rommer and S. Östlund. Class of ansatz wave functions for one-dimensional spin systems and their relation to the density matrix renormalization group. *Phys. Rev. B*, 55:2164, 1997.
- [21] M. Fannes, B. Nachtergaele, and R. F. Werner. Exact Antiferromagnetic Ground States of Quantum Spin Chains. *Europhys. Lett.*, 10:633, 1989.
- [22] M. Fannes, B. Nachtergaele, and R. F. Werner. Finitely Correlated States on Quantum Spin Chains. *Commun. Math. Phys.*, 144:443, 1992.
- [23] U. Schollwöck. The density-matrix renormalization group in the age of matrix product states. *Ann. of Phys.*, 326:96, 2011.
- [24] M. A. Cazalilla and J. B. Marston. Time-dependent density-matrix renormalization group: A systematic method for the study of quantum many-body out-of-equilibrium systems. *Phys. Rev. Lett.*, 88(25), Jun 24 2002.
- [25] S. R. White and A. E. Feiguin. Real-Time Evolution Using the Density Matrix Renormalization Group. *Phys. Rev. Lett.*, 93:076401, 2004.
- [26] T. Xiang. Density-matrix renormalization-group method in momentum space. *Phys. Rev. B*, 53:R10445–R10448, Apr 1996.
- [27] S. Nishimoto, E. Jeckelmann, F. Gebhard, and R. M. Noack. Application of the density matrix renormalization group in momentum space. *Phys. Rev. B*, 65:165114, Apr 2002.
- [28] A. E. Feiguin and S. R. White. Finite-temperature density matrix renormalization using an enlarged Hilbert space. *Phys. Rev. B*, 72:220401, Dec 2005.
- [29] A. C. Tiegeler, S. R. Manmana, T. Pruschke, and A. Honecker. Matrix product state formulation of frequency-space dynamics at finite temperatures. *Phys. Rev. B*, 90:060406, Aug 2014.
- [30] E.M. Stoudenmire and S. R. White. Studying Two-Dimensional Systems with the Density Matrix Renormalization Group. *Ann. Rev. Condens. Matter Phys.*, 3(1):111–128, 2012.
- [31] F. Verstraete and J. I. Cirac. Renormalization algorithms for Quantum-Many Body Systems in two and higher dimensions. *eprint arXiv:cond-mat/0407066*, July 2004.
- [32] V. Murg, F. Verstraete, and J. I. Cirac. Variational study of hard-core bosons in a two-dimensional optical lattice using projected entangled pair states. *Phys. Rev. A*, 75:033605, Mar 2007.

- [33] J. Jordan, R. Orús, G. Vidal, F. Verstraete, and J. I. Cirac. Classical Simulation of Infinite-Size Quantum Lattice Systems in Two Spatial Dimensions. *Phys. Rev. Lett.*, 101:250602, Dec 2008.
- [34] D. Porras, F. Verstraete, and J. I. Cirac. Renormalization algorithm for the calculation of spectra of interacting quantum systems. *Phys. Rev. B*, 73:014410, Jan 2006.
- [35] G. Vidal. Entanglement Renormalization. *Phys. Rev. Lett.*, 99:220405, Nov 2007.
- [36] M. Rizzi, S. Montangero, and G. Vidal. Simulation of time evolution with multiscale entanglement renormalization ansatz. *Phys. Rev. A*, 77:052328, May 2008.
- [37] H. J. Liao, Z. Y. Xie, J. Chen, Z. Y. Liu, H. D. Xie, R. Z. Huang, B. Normand, and T. Xiang. Gapless Spin-Liquid Ground State in the $S = 1/2$ Kagome Antiferromagnet. *Phys. Rev. Lett.*, 118:137202, Mar 2017.
- [38] C. Knetter and G. S. Uhrig. Perturbation theory by flow equations: dimerized and frustrated $S = 1/2$ chain. *Eur. Phys. J. B*, 13:209, 2000.
- [39] S. Kehrein. *The Flow Equation Approach to Many-Particle Systems*, volume 217 of *Springer Tracts in Modern Physics*. Springer, Berlin, 2006.
- [40] H. Krull, N. A. Drescher, and G. S. Uhrig. Enhanced perturbative continuous unitary transformations. *Phys. Rev. B*, 86:125113, 2012.
- [41] S. Dusuel, M. Kamfor, K. P. Schmidt, R. Thomale, and J. Vidal. Bound states in two-dimensional spin systems near the Ising limit: A quantum finite-lattice study. *Phys. Rev. B*, 81:064412, 2010.
- [42] M. Moeckel and S. Kehrein. Interaction Quench in the Hubbard Model. *Phys. Rev. Lett.*, 100:175702, 2008.
- [43] F. J. Dyson. General Theory of Spin-Wave Interactions. *Phys. Rev.*, 102:1217, 1956.
- [44] S. V. Maleev. Scattering of slow neutrons in ferromagnets. *Sov. Phys. JETP*, 6:776, 1958.
- [45] M. Powalski, G. S. Uhrig, and K. P. Schmidt. Roton Minimum as a Fingerprint of Magnon-Higgs Scattering in Ordered Quantum Antiferromagnets. *Phys. Rev. Lett.*, 115:207202, Nov 2015.
- [46] M. Powalski, K. P. Schmidt, and G. S. Uhrig. Mutually attracting spin waves in the square-lattice quantum antiferromagnet. *ArXiv e-prints*, January 2017.
- [47] T. Fischer, S. Duffe, and G. S. Uhrig. Adapted continuous unitary transformation to treat systems with quasi-particles of finite lifetime. *New J. Phys.*, 10:033048, 2010.
- [48] M. Wortis. Bound States of Two Spin Waves in the Heisenberg Ferromagnet. *Phys. Rev.*, 132:85–97, Oct 1963.
- [49] H. Bethe. Zur Theorie der Metalle. I. Eigenwerte und Eigenfunktionen der linearen Atomkette. *Z. Phys.*, 71:205, 1931.
- [50] P.G. de Gennes. Collective motions of hydrogen bonds. *Solid State Commun.*, 1(6):132 – 137, 1963.
- [51] H. G. Vaidya and C. A. Tracy. *Physica A*, 92:1, 1978.

- [52] C. J. Hamer, J. Oitmaa, and W. Zheng. One-particle dispersion and spectral weights in the transverse Ising model. *Phys. Rev. B*, 74:174428, Nov 2006.
- [53] P. Pfeuty. The One-Dimensional Ising Model with a Transverse Field. *Ann. of Phys.*, 57:79, 1970.
- [54] J. B. Parkinson and D. J. J. Farnell. *An Introduction to Quantum Spin Systems*. Springer, Berlin, 2010.
- [55] E. Lieb, T. Schultz, and D. Mattis. Two Soluble Models of an Antiferromagnetic Chain. *Ann. Phys.*, 16:407–466, 1961.
- [56] A. J. A. James, W. D. Goetze, and F. H. L. Essler. Finite-temperature dynamical structure factor of the Heisenberg-Ising chain. *Phys. Rev. B*, 79:214408, 2009.
- [57] B. Fauseweh. *Analysis of the transverse field Ising model by continuous unitary transformations*. Master Thesis, available at <http://t1.physik.uni-dortmund.de/uhrig/master.html>, TU Dortmund, 2012.
- [58] G. D. Mahan. *Condensed Matter in a Nutshell*. Princeton University Press, Princeton, NJ, 2011.
- [59] M. B. Hastings and T. Koma. Spectral Gap and Exponential Decay of Correlations. *Commun. Math. Phys.*, 265:781, 2006.
- [60] K. Okunishi, Y. Akutsu, N. Akutsu, and T. Yamamoto. Universal relation between the dispersion curve and the ground-state correlation length in one-dimensional antiferromagnetic quantum spin systems. *Phys. Rev. B*, 64:104432, 2001.
- [61] W. Marshall and S. W. Lovesey. *Theory of Thermal Neutron Scattering*. The International Series of Monographs on Physics. Clarendon Press, Oxford, 1971.
- [62] O. Derzhko, T. Verkholyak, T. Krokhumalskii, and H. Büttner. Dynamic probes of quantum spin chains with the Dzyaloshinskii-Moriya interaction. *Phys. Rev. B*, 73:214407, 2006.
- [63] R. Orús. A practical introduction to tensor networks: Matrix product states and projected entangled pair states. *Ann. of Phys.*, 349:117, 2014.
- [64] F. Keim. *Effective One-Dimensional Models from Matrix Product States*. Master Thesis, available at <http://t1.physik.uni-dortmund.de/uhrig/master.html>, TU Dortmund, 2012.
- [65] F. Keim and G.S. Uhrig. Effective One-Dimensional Models from Matrix Product States. *Eur. Phys. J. B*, 88(6):154, 2015.
- [66] J.D. Bekenstein. Black Holes and Entropy. *Phys. Rev. D*, 7:2333–2346, Apr 1973.
- [67] M. Srednicki. Entropy and area. *Phys. Rev. Lett.*, 71:666–669, Aug 1993.
- [68] C. Callan and F. Wilczek. On geometric entropy. *Phys. Lett. B*, 333(1-2):55–61, Jul 28 1994.
- [69] M. B. Plenio, J. Eisert, J. Dreißig, and M. Cramer. Entropy, Entanglement, and Area: Analytical Results for Harmonic Lattice Systems. *Phys. Rev. Lett.*, 94:060503, Feb 2005.

- [70] J. Eisert, M. Cramer, and M. B. Plenio. Colloquium: Area laws for the entanglement entropy. *Rev. Mod. Phys.*, 82(1):277–306, Jan 2010.
- [71] U. Fano. Description of States in Quantum Mechanics by Density Matrix and Operator Techniques. *Rev. Mod. Phys.*, 29:74–93, Jan 1957.
- [72] K. Okunishi, Y. Hieida, and Y. Akutsu. Universal asymptotic eigenvalue distribution of density matrices and corner transfer matrices in the thermodynamic limit. *Phys. Rev. E*, 59:R6227–R6230, Jun 1999.
- [73] M.-C. Chung and I. Peschel. Density-matrix spectra for two-dimensional quantum systems. *Phys. Rev. B*, 62:4191–4193, Aug 2000.
- [74] M.-C. Chung and I. Peschel. Density-matrix spectra of solvable fermionic systems. *Phys. Rev. B*, 64:064412, Jul 2001.
- [75] G.K.L. Chan, P.W. Ayers, and E.S. Croot. On the distribution of eigenvalues of grand canonical density matrices. *J. Stat. Phys.*, 109(1-2):289–299, Oct 2002.
- [76] J. Motruk, M. P. Zaletel, R. S. K. Mong, and F. Pollmann. Density matrix renormalization group on a cylinder in mixed real and momentum space. *Phys. Rev. B*, 93:155139, Apr 2016.
- [77] D. Poulin, A. Qarry, R. Somma, and F. Verstraete. Quantum Simulation of Time-Dependent Hamiltonians and the Convenient Illusion of Hilbert Space. *Phys. Rev. Lett.*, 106:170501, Apr 2011.
- [78] I. Peschel, X. Wang, M. Kaulke, and K. Hallberg. *Density-Matrix Renormalization*, volume 528 of *Lecture Notes in Physics*. Springer, Heidelberg, 1998.
- [79] F. Fröwis, V. Nebendahl, and W. Dür. Tensor operators: Constructions and applications for long-range interaction systems. *Phys. Rev. A*, 81:062337, Jun 2010.
- [80] L. Onsager. Crystal Statistics. I. A Two-Dimensional Model with an Order-Disorder Transition. *Phys. Rev.*, 65:117, 1944.
- [81] R. Orús and G. Vidal. Infinite time-evolving block decimation algorithm beyond unitary evolution. *Phys. Rev. B*, 78:155117, Oct 2008.
- [82] I. Affleck, T. Kennedy, E. H. Lieb, and H. Tasaki. Rigorous Results on Valence-Bond Ground States in Antiferromagnets. *Phys. Rev. Lett.*, 59:799, 1987.
- [83] N. Metropolis, A. W. Rosenbluth, M. N. Rosenbluth, A. H. Teller, and E. Teller. Equation of State Calculations by Fast Computing Machines. *J. Chem. Phys.*, 21(6):1087–1092, 1953.
- [84] G. Vidal. Classical Simulation of Infinite-Size Quantum Lattice Systems in One Spatial Dimension. *Phys. Rev. Lett.*, 98:070201, 2007.
- [85] A. Milsted, J. Haegeman, T.J. Osborne, and F. Verstraete. Variational matrix product ansatz for nonuniform dynamics in the thermodynamic limit. *Phys. Rev. B*, 88:155116, Oct 2013.
- [86] V. Zauner-Stauber, L. Vanderstraeten, M. T. Fishman, F. Verstraete, and J. Haegeman. Variational optimization algorithms for uniform matrix product states. *Phys. Rev. B*, 97:045145, Jan 2018.
- [87] LAPACK. - Linear Algebra PACKage. <http://www.netlib.org/lapack/>.

- [88] Ö. Legeza and G. Fáth. Accuracy of the density-matrix renormalization-group method. *Phys. Rev. B*, 53:14349–14358, Jun 1996.
- [89] G. Vidal, J. I. Latorre, E. Rico, and A. Kitaev. Entanglement in Quantum Critical Phenomena. *Phys. Rev. Lett.*, 90:227902, Jun 2003.
- [90] J. Haegeman, B. Pirvu, D. J. Weir, J. I. Cirac, T. J. Osborne, H. Verschelde, and Frank Verstraete. Variational matrix product ansatz for dispersion relations. *Phys. Rev. B*, 85:100408(R), 2012.
- [91] S. Sachdev and R. N. Bhatt. Bond-operator representation of quantum spins: Mean-field theory of frustrated quantum Heisenberg antiferromagnets. *Phys. Rev. B*, 41:9323, 1990.
- [92] J. Haegeman, T.J. Osborne, and F. Verstraete. Post-matrix product state methods: To tangent space and beyond. *Phys. Rev. B*, 88:075133, Aug 2013.
- [93] J. Zak. Berry’s phase for energy bands in solids. *Phys. Rev. Lett.*, 62:2747–2750, Jun 1989.
- [94] L. Vanderstraeten, J. Haegeman, T. J. Osborne, and F. Verstraete. S Matrix from Matrix Product States. *Phys. Rev. Lett.*, 112:257202, Jun 2014.
- [95] L. Vanderstraeten, J. Haegeman, F. Verstraete, and D. Poilblanc. Quasiparticle interactions in frustrated Heisenberg chains. *Phys. Rev. B*, 93:235108, Jun 2016.
- [96] B. Fauseweh. Private communication. 2015.
- [97] C. Knetter, K. P. Schmidt, and G. S. Uhrig. The structure of operators in effective particle-conserving models. *J. Phys. A: Math. Gen.*, 36:7889, 2003.
- [98] L. Vanderstraeten, J. Haegeman, T. J. Osborne, and F. Verstraete. S Matrix from Matrix Product States. *Phys. Rev. Lett.*, 112:257202, Jun 2014.
- [99] H. Ueda, I. Maruyama, and K. Okunishi. Uniform Matrix Product State in the Thermodynamic Limit. *J. Phys. Soc. Jpn.*, 80:023001, 2011.
- [100] C. K. Majumdar and D. K. Ghosh. On Next-Nearest-Neighbor Interaction in Linear Chain. I. *J. Math. Phys.*, 10:1388, 1969.
- [101] C. K. Majumdar and D. K. Ghosh. On Next-Nearest-Neighbor Interaction in Linear Chain. II. *J. Math. Phys.*, 10:1399, 1969.
- [102] C. K. Majumdar. Antiferromagnetic Model with Known Ground State. *J. Phys. C*, 3:911, 1969.

List of Figures

2.1	Ground states and excitations of the TFIM	9
2.2	TFIM, exact ground state magnetization	13
3.1	Bipartition $A B$ of a 2D system.	18
4.1	TFIM, correlation length	45
4.2	TFIM, Schmidt coefficients	46
4.3	TFIM, correlation length as function of bond dimension	47
4.4	FMHC, ground state energy	48
4.5	TFIM, ground state energy	49
4.6	TFIM, von Neumann entropy	50
4.7	TFIM, M_x ground state magnetization	51
4.8	TFIM, M_x ground state magnetization, double logarithmic plot	52
5.1	FMHC, energy spectrum, $\Gamma = 2$ and $J_2 = 0$	69
5.2	FMHC, energy spectrum, $\Gamma = 1.0$ and $J_2 = 0.5$	70
5.3	TFIM, dispersion at $\lambda = 0.8$	71
5.4	TFIM, dispersion at $\lambda = 1.2$	72
5.5	TFIM, dispersion at $\lambda = 1.0$	72
5.6	TFIM, excitation gap	73
5.7	Creation operator extension analysis	75
5.8	Error matrix element η	77
5.10	Examples of eigenvector components corresponding to the dispersion	79
5.11	Symmetry of Hamiltonian in momentum space	80
5.12	TFIM, S^{xx} spectral weight, $\lambda = 0.5$	81
5.13	TFIM, S^{xx} spectral weight, $\lambda = 0.99$	82
6.1	2QP real space overlaps	89
6.2	TFIM, metric tensor for $D = 2$ at $\lambda = 0.5$	95
6.3	TFIM, metric tensor for $D = 3$ at $\lambda = 0.5$	95
6.4	TFIM, 2QP spectral weight at $\lambda = 0.5$	98
6.5	TFIM, 2QP spectral weight at $\lambda = 0.5$, error analysis	99
6.6	TFIM, 2QP spectral weight at $\lambda = 0.9$	100
6.7	TFIM, quasi-particle decay amplitude, low D	107
6.8	TFIM, quasi-particle decay amplitude, medium D	108
6.9	FMHC, S -matrix at $\Gamma = 2$, $J_2 = 0.5$	111
6.10	TFIM, S -matrix for $Q = 0$ at $\lambda = 0.5$, $D = 2$	112
6.11	TFIM, S -matrix for $Q = 0$ at $\lambda = 0.5$, $D = 2$	113
6.12	TFIM, S -matrix for $Q = \pi$ and $Q = \frac{\pi}{2}$ at $\lambda = 0.5$, $D = 2$	113
6.13	TFIM, S -matrix for $Q = 0$ at $\lambda = 0.9$, $D = 2$	114
6.14	TFIM, S -matrix for $Q = \pi$ and $Q = -\frac{\pi}{2}$ at $\lambda = 0.9$, $D = 2$	114
6.15	TFIM, S -matrix for $Q = 0$ at $\lambda = 0.5$, $D = 3$	115

List of Tables

3.1	Examples of tensor network notation	18
4.1	Ground state search algorithm	43
4.2	Extrapolated results for TFIM correlation length	48

List of Acronyms

CUT	continuous unitary transformation
DMRG	density matrix renormalization group
EV	eigenvalue
EVP	eigenvalue problem
FMHC	ferromagnetic Heisenberg chain
iMPS	infinite system matrix product state
MPS	matrix product state
MPO	matrix product operator
NRG	numerical renormalization group
OBC	open boundary conditions
ONB	orthonormal basis
PBC	periodic boundary conditions
PEPS	projected entangled pair states
QCP	quantum critical point
QP	quasi-particle
QPT	quantum phase transition
SVD	singular value decomposition
TDL	thermodynamic limit
TEBD	time evolving block decimation
TFIM	transverse field Ising model
TI	translation invariance
TN	tensor network
TNS	tensor network states
uMPS	uniform matrix product state

Danksagung

An dieser Stelle möchte ich allen danken, die dazu beigetragen haben, dass diese Arbeit entstehen konnte. Zuallererst möchte ich mich bei Prof. Dr. Götz Uhrig für seine jederzeit hervorragende Betreuung und seine schier unendliche Geduld bedanken.

Prof. Dr. Frithjof Anders danke ich für die Erstellung des zweiten Gutachtens über die Arbeit.

Außerdem danke ich der gesamten T1-Arbeitsgruppe für das angenehme Arbeitsklima und insbesondere meinen gegenwärtigen und ehemaligen Bürokollegen Mona Kalthoff, Philip Schering, Sebastian Sohn, Jens Winkelmann und Mohsen Yarmohammadi.

Besonderer Dank gilt Benedikt Fauseweh, Lars Gravert, Philip Schering und Joachim Stolze für viele anregende und hilfreiche Diskussionen.

Für das Korrekturlesen bis zur letzten Minute möchte ich mich auch besonders bei Laura Möller bedanken. Ich danke außerdem Benedikt Fauseweh für viele hilfreiche Anmerkungen zum Manuskript, und Philip Schering und Mohsen Yarmohammadi für weiteres Korrekturlesen.

Zuletzt, aber deshalb nicht weniger, danke ich meiner Familie und meinen Freunden die mich die ganze Zeit unterstützt haben.